Intelligent
Automotive Thermal Comfort Control

by

Jürgen Kranz

A thesis submitted in compliance with the full requirements for the

Philosophiae Doctor: Engineering (Mechatronics)

in the

FACULTY OF ENGINEERING, THE BUILT ENVIRONMENT AND INFORMATION TECHNOLOGY

of the

Nelson Mandela Metropolitan University in Port Elizabeth

Promoter:	Prof TI van Niekerk
Co-Promoters:	Prof HFG Holdack-Janssen
	Prof G Gruhler

January 2011

Acknowledges

This research project would not have been possible without the contributions from many students and academics. I want to express my gratitude to everyone who has assisted and contributed to this research.

Especially I want to thank the following:

- Prof TI van Niekerk, Prof HFG Holdack-Janssen and Prof G Gruhler for their excellent guidance and support,
- The whole teams of the VWSA-DAAD Chair in Automotive Engineering, Mechanical Engineering and ACTS,
- Dr HG Kaiser for initiating the research project,
- Volkswagen South Africa Ltd for providing assistance with the research vehicle and components, especially Mr C Kennedy and Mr H Pillay,
- Mr C Wachsmuth and Mr G Homann from Ostfalia University for assisting with technical documentation and components,
- Mr L Grimbeek, Mr K du Preez, Mrs M Brown and Ms B Moodaley for providing organizational assistance,
- Prof W Kessler for providing assistance with methods of exploratory data analysis,
- Prof P Mercorelli for the fruitful discussions concerning theoretical aspects of AI,
- All the South African and German students who have been involved in this project, especially Mr M Boepple, who has designed the PCB layouts,
- Ms S Oliver for assisting with language editing,
- My parents, Adolf and Roswitha for their understanding, support and encouragement.

I also want to thank the German Academic Exchange Service (DAAD), NMMU's Research Capactity Development (RCD), Ostfalia University, the Baden-Württemberg-Stiftung and the Frank-Goltermann Stiftung for providing financial support.

Finally, I appreciate the vital academic co-operation between NMMU and Reutlingen University, which gave me the opportunity to conduct my research at NMMU.

Declaration

Jürgen Kranz hereby declares that:

- This thesis has not been previously submitted in full or partial fulfillment of the requirements for an equivalent or higher qualification at any other educational institution,

- The work done in the thesis is his own,

- All sources used or referred to have been documented and recognized.

Date: 25th March 2011

Signature

Abstract

Mobility has become a substantial part in our society. Since we spend a lot of our available time on the road, we expect the automotive environment to provide similar comfort levels than residential buildings. Within this context, this research thesis especially focuses on automotive thermal comfort control. The automotive cabin is a very special environment, which is characterized by extreme inhomogeneity and overall transient behavior. Thermal comfort is a very vague and a very subjective term, which depends on physiological and psychological variables. Theories for thermal comfort in transient environments have not been fully established yet and researchers are still busy with its investigation. At present, automotive industry relies on extensive thermal comfort models, manikins and powerful simulation tools to assess and control thermal comfort. This thesis studies the application of artificial intelligence and proposes a blackbox approach which aims for extracting thermal comfort knowledge directly from human's interaction with the HVAC controls. This methodology avoids the use of human physiological and psychological thermal comfort models and does not require any a-priori knowledge. A novel comfort acquisition tool has been developed and has been integrated into a research vehicle in order to gather the required data for system learning. Data has been collected during spring, autumn and summer conditions in Southern Africa. Methods of data mining have been applied and an intelligent implementation using artificial neural networks has been proposed. The achieved results are promising and allow for about 87% correct classification. It is concluded that methods of artificial intelligence perform well and are far superior compared to conventional approaches. These methods can be used as a powerful tool for the development process of vehicle air-conditioning controls and have great potential for time and cost reduction.

Table of Contents

Abbreviations

A/C	Air Conditioning
ACC	Automatic Climate Control
AI	Artificial Intelligence
ANN	Artificial Neural Network
ASHRAE	American Society of Heating Refrigeration Air-Conditioning Engineers
BVP	Best Validation Performance
CAD	Computer Aided Design
CAN	Controller Area Network
CFD	Computational Fluid Dynamics
ECU	Electronic Control Unit
EEPROM	Electronic Erasable Programmable Read Only Memory
FNN	Feed Forward Neural Network
HMI	Human Machine Interface
HVAC	Heating Ventilation Air Conditioning
IR	Infrared Radiation
ISO	International Organization for Standardization
ISOS	Intelligent Solar Sensor
LCD	Liquid Crystal Display
MCU	Micro Computing Unit
MRT	Mean Radiant Temperature
MSE	Mean Square Error
NC	Not Connected
NMMU	Nelson Mandela Metropolitan University

NN	Neural Network
PC	Principle Component
PCA	Principle Component Analysis
PCB	Printed Circuit Board
PD	Percentage of Dissatisfied
PMV	Predicted Mean Vote
PPD	Predicted Percentage of Dissatisfied
PWM	Pulse Width Modulation
RAM	Random Access Memory
SVM	Support Vector Machine
TSV	Thermal State Vote
VW	Volkswagen AG
VWSA	Volkswagen of South Africa Ltd

Nomenclature

Θ_j^n:	Bias term of the j[th] neuron in the n[th] layer
f_j^n:	Activation function of the j[th] neuron in layer n
w_{ji}^n:	Weight linking the i[th] neuron in the (n-1)[th] layer with the j[th] neuron in the n[th] layer
$\bar{x}$:	General: Arithmetic mean of variable x
$x'_{m,i}$:	Min-max transformed variable
$x'_{s,i}$:	General: Sigmoid transformation
$x'_{z,i}$:	Z-core transformed variable
y_j^n:	output of the j[th] neuron in layer n
σ_x:	Standard deviation of general variable x
A:	General: Surface
b:	Beta weight vector
b	Blower level
f	Flap position
f():	General: Function
H, h:	Relative humidity
h_{cs}:	Cumulative sum
I:	Solar radiation intensity
L:	Thermal load.
M:	Rate of metabolic heat production
net:	Weighted sum
N^{n-1}:	Number of neurons in layer n-1
N_s:	Number of required training samples
N_v	Degrees of freedom in an FANN
Θ:	Bias term
PD:	Percentage of Dissatisfied
PMV:	Predicted Mean Vote
PPD:	Predicted Percentage of Dissatisfied
Q:	Body heat loss
r_{ab}:	Bivariate correlation of variables a and b.
$r_{ab \cdot c}$:	Partial correlation coefficient between a and b, without c.
$r_{c,12\ldots k}$:	Multiple correlation coefficient between variable c and variables 1…k
$\mathbf{R_x}$:	Inter-correlation matrix
$\mathbf{r_{xc}}$:	Correlation vector of predictor and criterion variable
S:	Heat storage in the skin/core compartment
T_k	Temperature knob
TR:	Function that indicates traffic volume
t_s:	Sampling time
V, v:	Vehicle speed
v_a:	Air velocity
w:	Weight vector
W:	Rate of external work
x	General: Input vector
y	General: Output vector
y'	Actual output vector
η:	External mechanical efficiency of the body
ϑ_1, T1:	Air outlet temperature
ϑ_2, T2,:	In-cabin temperature
ϑ_3, T3:	Driver feet temperature

$\vartheta_{4,}$ T4: Driver head temperature i
ϑ_5, T5: Cabin roof temperature
ϑ_6, T6: Passenger feet temperature
ϑ_7, T7: Dashboard temperature
ϑ_8, T8: Passenger head temperature
ϑ_a: Air temperature
ϑ_{Am}, Am: Ambient temperature
ϑ_c: Human core temperature
ϑ_{cl}: Clothing surface temperature
ϑ_{ec}: Engine coolant temperature
ϑ_{eq}: Equivalent temperature
ϑ_{et}: Effective temperature
ϑ_{FAm}, FAm: Filtered ambient temperature
ϑ_i: Surface temperature i
ϑ_o: Operative temperature
ϑ_r: Mean radiant temperature
ϑ_{sk}: Human skin temperature
λ: General: Eigenvalue
ξ: General: Interval
Φ, A: Solar azimuth angle
Ψ, E: Solar elevation angle

List of Figures

List of Tables

Chapter 1

Introduction

1.1 Automotive Air-Conditioning

In the early stage of automotive history, the vehicle was just seen as an auxiliary tool for locomotion and for the transport of heavy goods [10]. The cabin spaces were open to the environment, requiring the passengers to choose their clothing according to the weather conditions. In the further automotive development and with increasing expectations of the customers in terms of comfort, closed passenger compartments were introduced which required heating and cooling of the interior. The first heating ventilation and air conditioning (HVAC) units consisted of some heat-able clay bricks and ice blocks for heating-up and cooling-down the passenger compartment. The ventilation was implemented by tilting windscreens or vents [24].

Nowadays the role of vehicles in our society has totally changed. They are no longer considered as a simple tool for locomotion. Mobility has become a substantial part in our society and advancements in technology have arose new appealing opportunities concerning automotive HVAC systems. Automotive HVAC units cannot be seen exclusively as luxury equipment, but have also a significant influence on road safety. Thermal discomfort can be a physical strain and leads to fatigue. Therefore, only a thermal balanced driver is considered to be observant [23]. Investigations in the US have shown that thermal discomfort is the third most common reason for road accidents [130].

The proportion of vehicles with air-conditioning has dramatically increased in recent years. The air-conditioning penetration on new vehicles in the UK has increased from 50.7% in 1999, to about 76.5% in 2004 [24].

An automotive HVAC unit has to provide the most possible amount of comfort under all environmental situations [121]. They can consist of up to 20 electrical motors to control the air flow inside the passenger compartment and take into account the environmental information of up to a dozen sensors [22]. However, this enormous amount of environmental data as well as the fact, that thermal comfort is a complex interaction between those and additional physiological variables, complicates the control and development strategy.

At present, during the engineering process of an air-conditioning unit, the effects of environmental parameters, temperature- and air distribution inside the passenger compartment, as well as the cabin properties on thermal comfort are determined. This approach implies the use of powerful computer aided design (CAD) and computational fluid dynamics (CFD) software.

These obtained results, in combination with appropriate comfort models, are then used to predict the passenger's comfort level. Thermal comfort models can be considered as mathematical representations of the human's internal metabolism. Latest approaches even simulate the whole thermo-regulatory process of the human body.

The development process is iterative since design alternations have to be implemented, unless the desired system response has been achieved. This approach is called virtual comfort engineering and is illustrated in Figure 1-1, which has been adopted from Delphi[1].

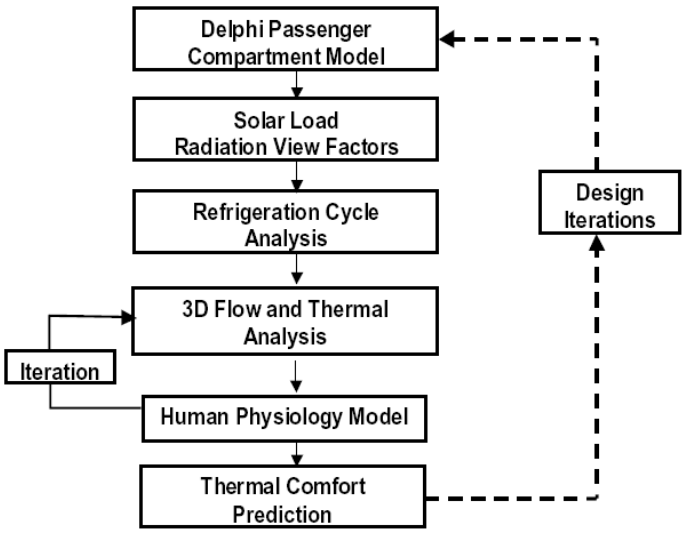

Figure 1-1: Typical virtual comfort engineering process [45]

The quality of prediction depends on the model, which is used for thermal comfort evaluation. 1972 Fanger[2] developed the first thermal comfort model, which is known as predicted mean vote (PMV) and allows thermal sensation prediction in five steps from cold to hot. Since it is based on statistical investigations, the predicted percentage of dissatisfied scale (PPD) was introduced. The PPD index shows, that in a statistical mean about 5% of the probands are not complying with the PMV and are therefore experiencing thermal discomfort. Recently, it has been shown that the PPD is even higher and has its global minimum at about 15% [45].

Over the last three decades, researchers all over the world have been busy with the investigation of further models, which has resulted in an enormous amount of models and manikins available at present [81].

A second possible approach for HVAC development assumes the properties of the passenger compartment to be fixed and therefore as independent variables. Thermal comfort is then measured as an objective function of air-flow and temperature distribution inside the vehicle

[1] Delphi is an American supplier for automotive products, inter alia HVAC systems

[2] P. Ole Fanger (†2006) was an University professor at Syracuse University, New York. He made substantial contributions to the field of HVAC research.

compartment. Since no models are involved, this approach eliminates the need of investigating the complex air flow and temperature distribution inside the cabin. However, this approach is currently not very popular among scientists, because the gained results allow little contribution to the field of human thermal comfort research and are highly vehicle specific [128].

The author agrees that for latter approach, little contribution towards the knowledge of human's thermo-regularity system will be achieved. However, in an era of productivity and global competitiveness, costs as well as time reduction in system development play a crucial role in engineering processes. Therefore, this approach might be an interesting field for research on intelligent systems. These systems are often associated with qualities known from human beings and incorporate functions like learning and decision making under a large degree of uncertainty. It has also been proven that some methods, summarized under artificial intelligence (AI), are capable of approximating any nonlinear function [63].

1.2 Problem

The established development cycle of automotive HVAC units is very complex and implies the use of powerful software tools. This, in combination with possible iterative design alternations, increases the development time and the costs. Furthermore, the performance of the final system depends on the quality of the comfort model and the assumptions made for the simulation of the cabin properties.

1.3 Sub-problems

The following sub-problems have to be considered:

- The relationship between thermal comfort and the environmental variables is inherently nonlinear,
- Thermal comfort levels may vary in time and location,
- A passenger cabin is a very inhomogeneous and transient environment,
- Environmental variables related to human thermal comfort are not independent from each other and some of them can hardly be measured,
- Thermal comfort is a highly subjective term and may also depend on psychological parameters.

1.4 Hypothesis

It is assumed that the most important parameters influencing human thermal comfort sensation can be roughly measured through some finite discrete measurement points inside the vehicle cabin. This means that the information is already roughly contained in the environment, can be

described with certain measurable variables and is linked to thermal comfort through an unknown function in some statistical sense. In other words, the issue can also be addressed as an approximation problem in a multidimensional feature space. Figure 1-2 illustrates the principle, using a blackbox approach to estimate the output variables. The blackbox shall approximate human behavior.

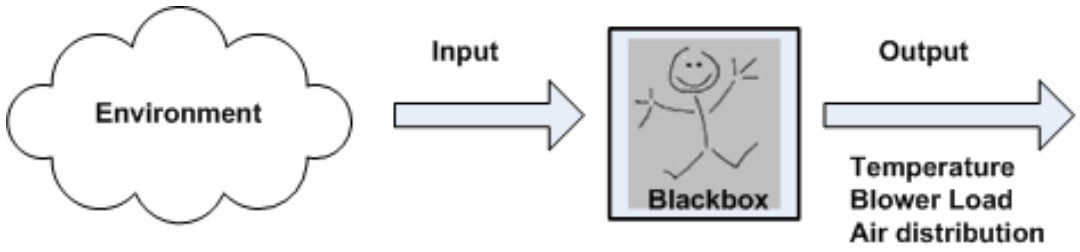

Figure 1-2: Blackbox approach to predict HVAC parameters

It is well known, that structures with artificial intelligence are highly suitable in those field of application and may have considerable advantages against conventional technologies. Therefore, it should be possible to use some concepts of AI for this kind of problem. Furthermore it is assumed that necessary vehicle system parameters, which cannot be determined directly, are accessible via the controller area network (CAN) of the vehicle's internal bus system and are log-able with appropriate software tools like Vector[3] CANoe.

Finally, it is assumed that powerful microprocessors can be used to develop a human machine interface (HMI), in order to connect the vehicle, the sensor elements, as well as the passenger feedback directly to the data logging unit.

1.5 Delimitation

The following delimitations have been defined for this research project:

- Only concepts of AI will be considered,
- The research will be based on a Volkswagen (VW) Polo platform,
- Modelling and verification will be restricted to Mathworks Matlab®.

This research shall be regarded as individual part oriented. An implementation in a real vehicle is however far beyond this research.

[3] Vector is a German automotive supplier specialised on automotive bus systems.

1.6 Significance of the Research

1.6.1 Within the University

This project can serve to expand NMMU's research activities in the automotive sector. It can also serve as initiation of further research projects in the field of automotive air-conditioning.

1.6.2 General

The major goal is to reduce costs in the development cycle of automotive air-conditioning units. Complex and time consuming simulations on air-flow and temperature distributions might be no longer required.

The envisaged research is also preliminary work for self-learning automatic climate control (ACC) systems. If one was capable of reliably learning an HVAC system with collected data, there would only be a little step in substituting that collected data with data collected directly from the passenger's interaction with the control panel. This would be a completely new generation of ACC systems, which are capable of adapting themselves during operation.

Furthermore South Africa is highly suitable for HVAC research since it accommodates a plurality of climate zones.

1.7 Research methodology

In order to accomplish with the goals of the research the following steps are necessary:

- Detailed literature research on thermal comfort,
- Detailed literature research on intelligent systems,
- Identification of thermal comfort relevant parameters,
- Development of a HMI for data logging and interfacing to the vehicle's peripheral components,
- Installation of the experimental setup into the research vehicle,
- Field measurement in order to obtain the necessary amount of data, needed for system learning,
- System modelling in Matlab,
- System learning with collected data,
- System verification in Matlab.

1.8 Summary

This chapter has briefly introduced the field of automotive air-conditioning, the problem statement, the hypothesis, the delimitation as well as the significance of the research.

Chapter 2 presents the relevant concepts of human thermal comfort sensation and thermal comfort measurement technologies. Furthermore it shows the state of art in application of AI towards thermal comfort engineering.

Chapter 3 presents the overall system and describes the experimental setup in detail.

Chapter 4 deals with methods of data mining, feature extraction and dimensionality reduction and applies them to this research project.

Chapter 5 shows an exemplary implementation using neural networks and verifies the model in Matlab.

Chapter 6 discusses the results and gives ideas for future research.

Chapter 2

Concepts for Intelligent Automotive Climate Control

2.1 Automotive HVAC systems

The following sub-sections outline the basic architecture of automotive HVAC systems and describe the fundamental control techniques concerning this research.

2.1.1 Cooling circuit

Air-conditioning systems are closed installations based on the theory of thermodynamic cyclic processes. The pressure-temperature dependency of a suitable refrigerant is used to absorb environmental heat at a designated point and to release it to the ambient environment at another local point. Currently and most often, a R134a[4] vapour compression cycle is used in automotive application. Figure 2-1 illustrates the process.

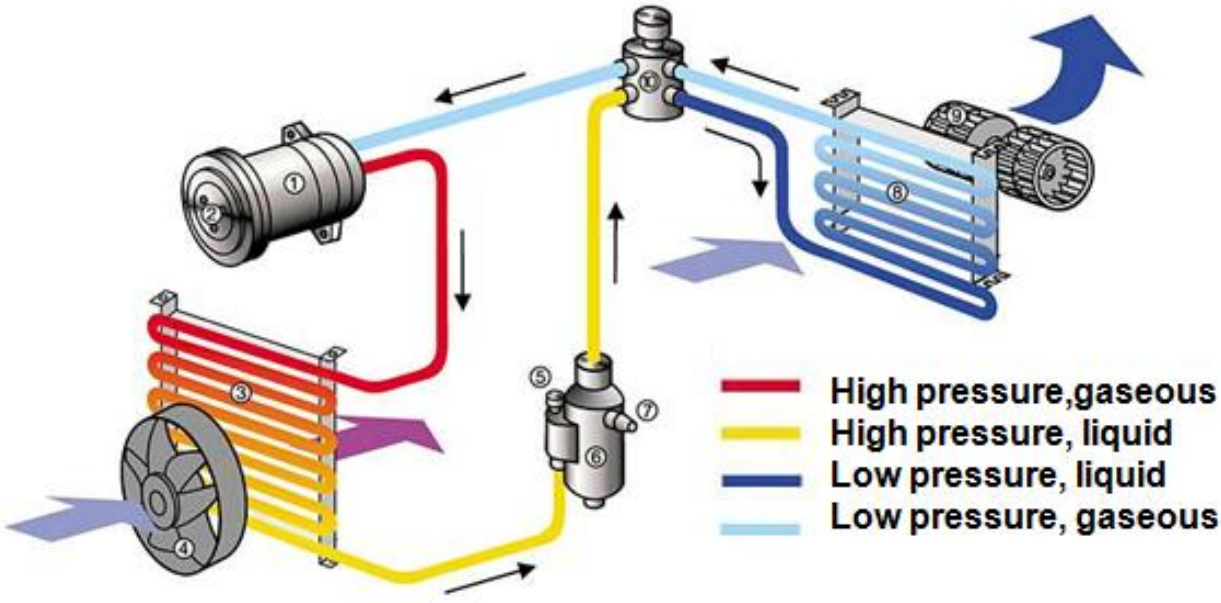

Figure 2-1: Automotive HVAC Cooling Circuit [103]

The compressor (1) induces low pressure gaseous refrigerant. The refrigerant is being compressed and leaves the compressor as a high pressurized, heated up gas. It is then pumped into the condenser (3) where it is condensed into a high pressure liquid. This is achieved by

[4] R134a is a haloalkane refrigerant with a boiling temperature of -26,3ºC at sea level. It is was introduced in the early 1990s as a substitute for R12 which was replaced due to its high ozone depletion potential.

leading air over the condenser's numerous cooling fins. If the vehicle's ambient airstream is not sufficient to bring the refrigerant below its boiling point, additional air flow will be provided by an electrical blower (4). The sub-cooled liquid refrigerant then flows into the receiver (6) where it is being filtered from moisture and dirt. The receiver also serves as a refrigerant reservoir to compensate fluctuations resulting from varying operating conditions. The expansion valve (10) causes the refrigerant to vaporize through a sudden drop in pressure. The low pressurized liquid/vapor mixture is then fed into the evaporator (8) where it absorbs heat through vaporization from the evaporator's surface. This heat is taken from ambient air temperature, which is led over the evaporator's surface using a blower (9).

2.1.2 Heater box

The heater box is generally located under the vehicle's instrument panel. It contains the heat exchanger and the evaporator for heating and cooling the vehicle cabin. Additionally, it incorporates numerous flaps to distribute the air inside the automobile compartment. Figure 2-2(a) shows the principle.

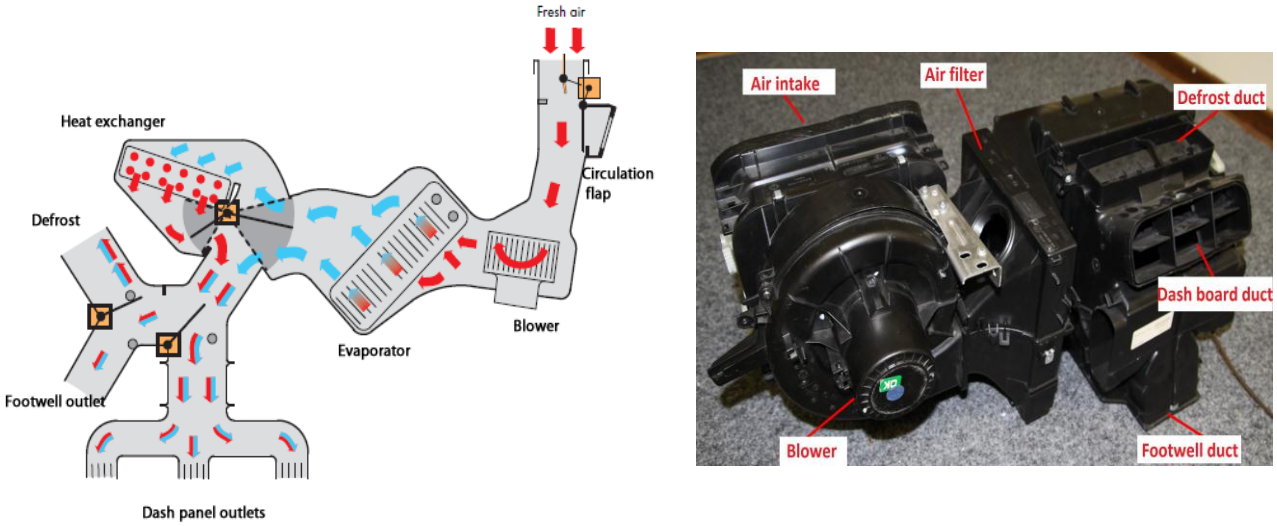

(a) **(b)**

Figure 2-2: Heater box; (a) schematic [127], (b) Volkswagen Polo heater box (2006)

In Figure 2-2(a), air is induced by a blower and is being led over the evaporator. Dependent of the operating mode, ambient air is drawn from the outside environment or from the inside of the passenger cabin in recirculation mode. In dependence of the environmental conditions and the passengers' temperature setup, the air stream will be split off and some air will be led over the heat exchanger and will be afterwards mixed with the main airflow again. The heat exchanger is fed with the engine's coolant water. Dependent on the HVAC design, air temperature and air

distribution is controlled electrically or mechanically via Bowden cables. Figure 2-2(b) shows the type of heater box, which was used for this research.

2.1.3 HVAC control systems

At present there are three different types of automotive HVAC systems available on the market:

- Manual A/C systems,
- Semi-automatic A/C systems,
- Automatic A/C systems.

Manual A/C systems require the occupant to use switches and Bowden cables to set up temperature and air distribution in order to maintain thermal comfort inside the passenger cabin. This kind of control is the simplest one, because it doesn't adjust the control strategy to compensate for environmental changes. Manual systems are predominantly used in low cost vehicles.

Semi-automatic systems incorporate electronic control of the in-cabin temperature, which is commonly measured at one position in the center console. The control unit actuates the temperature door motor, shown in Figure 2-2(a), to automatically adjust the temperature according to the occupant's reference value. Control of the air distribution flaps, as well as the blower level, must still be manually set up by the passenger.

Automatic HVAC systems autonomously control in cabin temperature, air flow and air distribution. All actuators inside the heater box are controlled electronically. Automatic HVAC systems take into account various environmental parameters and continuously adjust the cabin output parameters in order to provide a comfortable climate. However, due to a lack of sensory environmental information and because of the use of simplified control algorithms, the potential to control the interior climate is often limited. Additionally, often only in-cabin temperature is controlled in a feedback loop. Air distribution and blower load are open loop systems [60].

2.2 Principles of thermal comfort

Thermal comfort is a very subjective term since its perception to people has enormous variations in environmental and physiological parameters. This makes it difficult to describe it in terms of clear defined parameters and variables. In 1970, the American Society of Heating, Refrigeration and Air-Conditioning Engineers (ASHRAE) defined thermal comfort as "*That condition of mind which expresses satisfaction with the thermal environment*". This vague definition is still part of thermal comfort standards like ISO 7730 and ASHRAE Standard 55P [2], [28].

In the past decades there has been much effort to describe and measure thermal comfort. However, human thermal comfort is still far from fully understood and is therefore still under

investigation [70]. The most important findings will be summarized in the following sub-sections.

2.2.1 Human thermoregulation

The human body continuously produces heat due to its metabolic activities. This heat must be dissipated in order to prevent hyperthermia. Reversely, excessive heat loss to the environment may results in hypothermia. The hypothalamus is the central control organ for body temperature control. Human's internal core temperature is about ϑ_c=36.8ºC in resting state and about ϑ_c=37.9ºC at high metabolic activities [1]. Skin temperatures are more variable and are a function of the surrounding conditions. They decrease with increasing activity. Thermal information is transferred to the hypothalamus by electrical impulses from various thermal receptors in the brain and the skin. Skin receptors are mostly cold sensitive while core sensors are mainly sensitive to heat [17], [80]. Human's thermal sensory system does not incorporate heat flux receptors [94]. According to the sensory information, the hypothalamus triggers various mechanisms to maintain the body's thermal equilibrium. These mechanisms can be divided into behavioural and physiological actions.

Behavioural responses are adaptive actions, like clothing changes and opening/closing of windows but also include reflexive protective behaviour, e.g. when skin temperature drops suddenly. Physiological responses to a given environment occur as internal body regulation processes. When core temperature rises above a set point, vasodilatation of skin blood vessels is initiated. This mechanism changes the blood flow rate from deep in the body to the skin and the consequent adjustment of heart rate rise may increase skin blood flow by up to 15 times, in order to dissipate more internal heat to the environment [1], [17], [40]. Sweating occurs at elevated core temperatures and is an effective way to cool down the skin. Internal heat is reduced by evaporation of sweat from the skin. Sweating occurs at ϑ_c>37ºC and follows the impulse rate of the warm receptors. At skin temperatures ϑ_{sk}<34ºC, sweating is suppressed. When the body temperature drops below a set point, vasoconstriction occurs. Thereby skin blood flow and heart rate are reduced while muscle tension is increased to produce internal heat (shivering). An increase in metabolism is initiated at ϑ_{sk}<34ºC and follows the rate of the cold receptors in the skin. An increase in metabolism is suppressed at ϑ_c>37ºC.

Figure 2-3 summarizes these principles again.

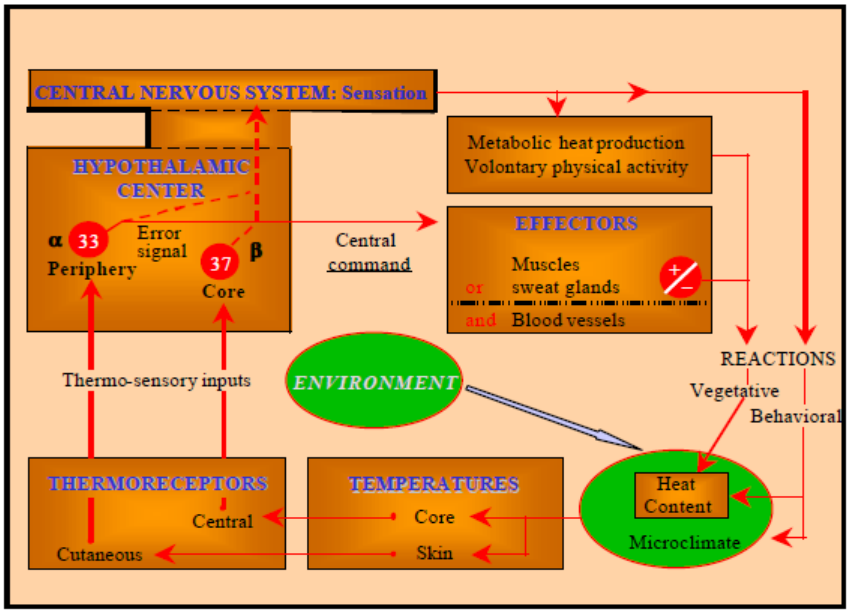

Figure 2-3: Human's thermo-regularity system [17]

2.2.2 Conditions for overall thermal comfort

In general three conditions must be fulfilled to establish overall thermal comfort [33], [70] and [75]:

- Combinations of skin and core temperatures must provide a sensation of thermal neutrality.
- The body must be in thermal equilibrium. That implies that the heat produced by internal metabolism must be equal to the amount of heat dissipated to the environment by conduction, convection, radiation, evaporation and respiration.
- No occurrence of local discomfort.

Thermal acceptability is given when ϑ_{sk}>34ºC and ϑ_{c}<37ºC [70], [115]. However, these threshold values for cold and warm sensations undergo individual as well as daytime variations [94], [80]. Local discomfort may arise due to inhomogeneous environments, as well as due to draft and asymmetrical radiation fields.

2.2.3 Primary thermal comfort parameters

There are six primary parameters which influence thermal comfort [2]. Those parameters mainly influence body's heat exchange with the environment and will be summarized below.

2.2.3.1 Air temperature

Air temperature ϑ_a is the time- and location-averaged temperature of the occupant's surrounding compound. Although it is well known that human's body is not able to feel air temperatures but

rather the heat loss to the environment, air temperature still greatly influences the body's heat exchange and thermal equilibrium [98], [122].

2.2.3.2 Mean radiant temperature

Mean radiant temperature (MRT) is a hypothetical parameter and is defined as [2]:

'*The temperature of a uniform black enclosure that exchanges the same amount of thermal radiation with the occupant as the actual enclosure*'.

Radiation plays an important role in the heat exchange of the human body with the environment. According to [74], radiation may contribute up to 30% to the whole heat exchange of the subject. For example, cold walls or windows may cause a person to feel cold even though the surrounding air temperature may be at a comfortable level. Likewise warm surfaces may cause a person to feel warmer than the surrounding air temperature would indicate [5].

Provided a high emittance of the surrounding materials, the radiant temperature ϑ_r can be estimated from measured values of the temperature of the surrounding surfaces and their positions with respect to the occupant [28].

$$\vartheta_r^4 = \sum_{i=1}^{N} \vartheta_i^4 F_{p-i}, \qquad \textbf{(1)}$$

with

ϑ_i Temperature of surface i [˚C],

$F_{p\text{-}i}$: Angle factor between a person and surface i,

N: Number of surfaces surrounding the occupant.

2.2.3.3 Humidity

Humidity refers to the moisture content of the air. It affects evaporation of water from sweating surfaces and its diffusion through the skin [9]. Provided an environment close to thermal comfort, humidity plays a minor role since heat dissipation through sweat evaporation can be neglected [33]. According to [96], a 10% increase in humidity h is equivalent to only $\Delta\vartheta_a$=0.3ºC. At low air temperatures, thermal sensation can be even considered as independent of humidity [115].

However, humidity is a contributing factor towards indirect comfort influences like skin moisture, tactile sensation of fabrics, health and air quality. It is well known that too low levels of humidity can affect health and cause complaints like dry noses and throats as well as irritated skin and eyes. On the other hand too high levels of humidity can lead to sensation of stickiness and increased discomfort arising from wet clothing.

Some literature sources recommend 35%<h<75% [114]. However in general, literature holds off providing clear margins for acceptable humidity limits. It is generally accepted that cooler, drier air is perceived as being freer of contaminants and less stale. At a given temperature, decreased humidity therefore results in occupants feeling cooler, drier and more comfortable.

2.2.3.4 Metabolic rate

The metabolic rate quantifies the transformation of chemical energy into heat and mechanical work within an organism. Metabolic rate varies over a wide range and is expressed with the unit 'met'. 1 met is defined as the metabolic rate of a sedentary person.

$$1\,met = 58.1\frac{W}{m^2} \quad \textbf{(2)}$$

Table 1 shows exemplary characteristic metabolic rates for some selected activities. The values have been taken from [2], [28] and [80].

Table 1: Examples of metabolic rates associated with some exemplary activities

Activity		Metabolic rate [met]
Resting		
	Sleeping	0.7
	Seated	1.0
	Standing	1.2
Working		
	Cooking	1.6 - 2.0
	House cleaning	2.0 – 3.4
	Pick and shovel work	4.0 – 4.8
Leisure		
	Dancing	2.4 – 4.4
	Basketball	5.0 – 7.6
Driving		
	On a paved road	1.2
	On a gravel road	1.37
	Off-road	1.54
	Driving a heavy vehicle	3.2

An adult has an average surface of A=1.8m^2 [1]. Substituted in equation (2), this results in an internal heat production M=104.58W for an average adult at sedentary level. The generated heat must be dissipated to the environment in order to maintain heat balance. Metabolic rates for each individual depend on activity, age, gender and vary over a wide range.

The table may however only serve as an indication for typical ranges and represents empirical values. Measurement of metabolic rates is very intensive and is dealt with in standards like ISO 8996 [29].

2.2.3.5 Clothing insulation

Clothing influences the heat transfer from the human body to the environment. According to [1], the intrinsic clothing insulation R_{cl} can be calculated as:

$$R_{cl} = \frac{\vartheta_{sk} - \vartheta_o}{Q} - \frac{1}{hf_{cl}}, \quad \textbf{(3)}$$

with

ϑ_{sk}: Skin temperature [˚C],

ϑ_o: Operative temperature [˚C],

Q: Body heat loss $\left[\frac{W}{m^2}\right]$,

h: Radiative heat transfer coefficient $\left[\frac{W}{m^2K}\right]$,

f_{cl}: Clothing area factor.

Clothing insulation I_{cl} which is expressed in 'clo' values can be calculated from R_{cl} as:

$$I_{cl} = \frac{R_{cl}}{0.155}, \quad \textbf{(4)}$$

with

$$1\ clo = 0.155\,\frac{m^2K}{W}. \quad \textbf{(5)}$$

Establishing the insulating properties of clothing is a time-consuming and complicated process that is usually conducted in laboratory experiments. As it is not practical to directly measure clothing insulation, researchers generally estimate these values using tables that have been developed from clothing insulation studies. An example of such a table is shown in Figure 2-4.

Garment Description[a]	$I_{clu,i}$, clo[b]	Garment Description[a]	$I_{clu,i}$, clo[b]	Garment Description[a]	$I_{clu,i}$, clo[b]
Underwear		Long-sleeved, flannel shirt	0.34	Long-sleeved (thin)	0.25
Men's briefs	0.04	Short-sleeved, knit sport shirt	0.17	Long-sleeved (thick)	0.36
Panties	0.03	Long-sleeved, sweat shirt	0.34	**Dresses and skirts[c]**	
Bra	0.01	**Trousers and Coveralls**		Skirt (thin)	0.14
T-shirt	0.08	Short shorts	0.06	Skirt (thick)	0.23
Full slip	0.16	Walking shorts	0.08	Long-sleeved shirtdress (thin)	0.33
Half slip	0.14	Straight trousers (thin)	0.15	Long-sleeved shirtdress (thick)	0.47
Long underwear top	0.20	Straight trousers (thick)	0.24	Short-sleeved shirtdress (thin)	0.29
Long underwear bottoms	0.15	Sweatpants	0.28	Sleeveless, scoop neck (thin)	0.23
Footwear		Overalls	0.30	Sleeveless, scoop neck (thick)	0.27
Ankle-length athletic socks	0.02	Coveralls	0.49	**Sleepwear and Robes**	
Calf-length socks	0.03	**Suit jackets and vests (lined)**		Sleeveless, short gown (thin)	0.18
Knee socks (thick)	0.06	Single-breasted (thin)	0.36	Sleeveless, long gown (thin)	0.20
Panty hose	0.02	Single-breasted (thick)	0.44	Short-sleeved hospital gown	0.31
Sandals/thongs	0.02	Double-breasted (thin)	0.42	Long-sleeved, long gown (thick)	0.46
Slippers (quilted, pile-lined)	0.03	Double-breasted (thick)	0.48	Long-sleeved pajamas (thick)	0.57
Boots	0.10	Sleeveless vest (thin)	0.10	Short-sleeved pajamas (thin)	0.42
Shirts and Blouses		Sleeveless vest (thick)	0.17	Long-sleeved, long wrap robe (thick)	0.69
Sleeveless, scoop-neck blouse	0.12	**Sweaters**		Long-sleeved, short wrap robe (thick)	0.48
Short-sleeved, dress shirt	0.19	Sleeveless vest (thin)	0.13	Short-sleeved, short robe (thin)	0.34
Long-sleeved, dress shirt	0.25	Sleeveless vest (thick)	0.22		

[a]"Thin" garments are summerweight; "thick" garments are winterweight. [b]1 clo = 0.155 (m²·K)/W [c]Knee-length

Figure 2-4: Clothing insulation [1]

However, those values can only be considered as indicative, since body motion, posture and air movement have a great influence on clothing insulation. Some researchers therefore doubt the reliability of clothing tables due to enormous measurement problems [49]. Reference [32] especially emphasizes the impact of body posture on 'clo' values because clothes are compressed while sitting. Seat isolation must be also considered, because it has a considerable impact on overall clothing insulation. A standard car seat may increase overall clothing insulation by up to 0.27 clo [93].

2.2.3.6 Air velocity

Air velocity influences heat loss from the skin. Convective heat transfer is roughly proportional to the square root of mean air velocity [72]. A clear link between air velocity and thermal comfort has not been established yet [2], [98].

However, it is generally accepted that a rise in air velocity can be used to compensate for higher air temperatures, in order to produce the same heat loss from the skin. Air motion can for example be considered as a pleasant breeze when the body is warm, but can also produce draft effects when the overall body sensation is cool or neutral [72], [3]. Draft is hereby defined as an unwanted local cooling of the body by air motion and is known to be the one of the most annoying factors [1].

The most promising approach to quantify draft effects was done by P.O. Fanger. 1989 he investigated the effects of draft sensation and developed an empirical model taking into account the air temperature ϑ_a, the air velocity v_a and the turbulence intensity T_u. The percentage of dissatisfied (PD) is given in the following equation:

$$PD = (34 - \vartheta_a:)(v_a - 0.05)^{0.62}(0.37 v_a T_u + 3.14)$$

$$T_u = 100 \frac{\sigma_v}{v_a}, \qquad \textbf{(6)}$$

with

σ_v: Standard deviation of air velocity within a 0.2s time period.

Equations (6) show that PD increases with:

- Decreasing air temperature,
- Increasing air speed,
- Increasing air turbulence intensity.

Heat loss from skin is dependent on the turbulence intensity of the airflow, the air velocity and the air temperature. For illustration a similar effect can be observed with noise. Most people consider intermittent noise more annoying than noise with a constant amplitude.

Equation (6) is presently part of established comfort standards [18]. However, there are various researchers who doubt the model's predictions due to various reasons. According to [72], Fanger's experiments only include air flow towards the neck and the model's predictions can hardly be adapted for other body parts. There might be also a chance that positive effects of air movement in warm environments are underrated [3]. According to his research 92% of the people predicted to be exposed to the risk of draft demanded even more air.

2.2.4 Secondary thermal comfort parameters

Basic research was done and published by P.O. Fanger concerning secondary parameters influencing thermal comfort [37]. These parameters include:

- Day to day variations,
- Age,
- Body build,
- Geographical differences,
- Thermal acclimatization.

Essentially his research showed that there is no statistically significant correlation between thermal comfort and these parameters. Most of the research available today generally confirms these findings [8], [18]. However, Fanger indicated that women may tend to prefer slightly higher neutral temperatures than males. This was confirmed by a Finnish study with 3094 subjects which showed, that females are less satisfied with room temperatures than males, prefer higher room temperatures and feel both uncomfortably cold and uncomfortably hot more often than males [61].

There might also be differences in perception of thermal comfort during the day, because it is known that human's thermo-receptor threshold values fluctuate in dependence of the time of the day [115]. According to [15], thermal comfort sensation of test engineers during road testing may change during the day. Although there may be only little effects of thermal acclimatization, thermal comfort perception may also be dependent of the time of the year [77].

2.2.5 Psychological behaviour

Some researchers argue that thermal comfort is also dependant from economic, ecologic, ergonomic and physiologic criteria in order to cover regional, financial, cultural and individual boundary conditions [7], [86], [93]. To some extent, thermal comfort is also an individual state of mind and cannot be only explained with physical variables. It is therefore also linked to contextual variables such as local climate, occupants' expectations, available control over the environment and the processes by which the indoor environment is controlled, perceived,

experienced, and interacted with [8]. The ability to control the own thermal environments may make the automotive subjects feel more positive about their overall thermal comfort [134]. For example, knowledge of air temperature contributes to human's perception of thermal comfort [105]: Subjects were seated in a climate chamber whose environment was controlled electronically. A heater was placed in the chamber and half of the subjects were informed that the heater is switched off. The other half was misinformed and was told that the heater is switched on. Although the heater was actually off and could therefore not thermally influence the environment in the climate chamber, it was found out that those subjects, who were told that the heater was on, reported higher thermal sensations than those who were told the opposite.

Similarly, occupants would be more tolerant against draft, if they have personal control over air delivery devices [18].

Some researchers report psychological and behavioral adaption effects [131]. Psychological adaption is thereby an altered perception of the environment due to past experience, accompanied with a relaxation of expectations. Behavioral or 'adaptive' adjustments will induce a change in heat balance and are known as the adaptive theory of thermal comfort, which will be described in Chapter 2.3.4.

2.2.6 Transient and non-uniform environments

Thermal comfort theory in uniform, steady state environments is nowadays widely accepted and measurement methodologies exist, which have been defined in standards like ISO 7730 or ASHRAE Standard 55 [28], [3]. Most of thermal comfort knowledge available today has been gained in the in the past 30 years. However, this knowledge is mainly based on research conducted under the assumption of homogeneous and steady-state laboratory conditions. In practice, there is hardly any steady-state or homogeneous hypothetical environment. For example, local discomfort may arise due to local convective cooling by draught, cooling and heating by radiation, as well as cold feet and warm head caused by vertical temperature differences [5], [75]. Assessment of thermal non-uniform environments is difficult due to a lack of general knowledge about the superposition and influence of multiple thermal sources [26]. Today thermal comfort in transient and non-uniform environments is far from fully understood and researchers are still arguing about the exact interrelationships [122]. Therefore a general theory cannot be presented in this thesis, however some findings of the latest research will be summarized.

In uniform and steady state environments, there is a linear relationship between whole body thermal sensation, thermal acceptability and thermal comfort. On the ASHRAE thermal sensation scale (Chapter 2.4.1.1), overall thermal comfort is assumed to occur between -1

(slightly cool) and +1 (slightly warm) [2], [28]. These linear correlations are not applicable to non-uniform and transient environments. According to [136], subjects report more discomfort, the more the non-uniformity of thermal sensation they perceive, even if they are in overall thermal neutrality. Overall thermal comfort is strongly influenced by single body parts. Thermal sensation across the body depends on [134]:

- The body's local thermo regularity mechanism,
- Asymmetry in clothing insulation,
- Thermal sensitivity of the individual body parts,
- Rate of change in body's skin and core temperatures.

Feet adapt very slowly to the environment. Long adaption times up to 5 hours may occur due to poor blood circulation [36]. It is well known that cold feet are less comfortable than warm feet. This may be justified due to low core temperatures at feet level. It could be possible that the body therefore reacts more sensitive to further decrease in temperature.

The opposite applies to the head which prefers cooler ambient temperatures. Thermal comfort standards therefore point out that increasing temperature from the foot to the head may be less acceptable than increasing temperature level from head to feet area [1], [2], [28]. The head is crucial for thermal comfort sensation and less importance is accounted for hands and feet [36]. According to [134], the back, chest and pelvis are the most dominant body parts and the brain seems to be more sensitive to cooling changes in parts near the body core than to changes in extremities. These parts were found to show preference for warm sensation [133].

If skin temperature is in a middle range, the correlation between skin temperature and thermal sensation will be close to linear. Small decreases in skin temperature of chest, back, neck and head induce a large cooling sensation whilst other body parts like face, hands and arms have less sensitive cooling [132]. The higher the face skin temperature, the more the sensitivity. The lower the face skin temperature, the less the thermal sensitivity [77].

However, local sensation does not only depend on skin temperatures, but also on the overall thermal state of the body. This means that for a given overall thermal state, different output sensations may exist for the same input stimuli. Local thermal sensation is much warmer during cold tests when the whole body is cold and much colder during warm tests when the whole body is warm [132].

According to [134], overall body thermal sensation is a complaint-driven process. The strongest local sensations tend to dominate overall sensation and whole body sensation tends to follow the cooler local body sensations [41]. A study investigated human responses to local cooling with air jets in warm conditions and found that the air jet velocity preferred by the subjects was not

the one corresponding to thermal neutrality, but the one that decreased the sensation of warmth without causing too much discomfort due to draft [136].

Similar observations have been made for local thermal comfort. Local thermal comfort assessment is affected when the whole body thermal sensation is different from the local thermal state. In general, any action that leads to a decrease in whole body's heat stress is felt as pleasant. In hypo-thermic states, warm stimuli are felt as pleasant and unpleasant in hyper-thermic states. If the subject is in neutral state, neither warm nor cold stimuli are felt as pleasant. However, there are also exceptions to these findings. Independent from the body's thermal state a warm pelvis is found to be comfortable when the body is cold, but a preference for a cold pelvis in overall warm body state can't be observed [133].

Analogous, cool breathing air is felt pleasant if the whole body is warm, but warm breathing air is still felt unpleasant when the whole body is cold. Additionally, extreme local cold-warm sensations are felt to be uncomfortable independent of the body's thermal state.

Overall thermal comfort is better specified with local comfort votes than local sensation votes. Under stable conditions overall thermal comfort is, similar to overall thermal sensation, a complaint driven process. When two body parts are strongly uncomfortable, the whole body comfort sensation will be close to the most uncomfortable part, independent of the comfort level of the other parts. However, in transient conditions, overall thermal comfort is better than predicted by the two most uncomfortable body parts. This may be due to physiological reasons or because comfort levels are varying all the time, a decisive judgment might therefore be less definite [134].

According to [137], thermal sensation change with time has significant effect on thermal comfort. According to [138], persons were seated in a Room with ϑ_a=+25˚C, were asked to enter a room with ϑ_a>+30˚C and to report their thermal state. It was noticed that skin temperatures and thermal state vote (TSV) increased gradually. When the subjects returned to the cooler room, the TSV changed immediately whilst skin temperatures decreased gradually. It is therefore concluded that the body reacts more sensitive to sudden cold changes than to sudden exposure to hot environments and skin temperatures can only be of limited use. This is confirmed by [122], which states that thermal comfort in transient environments can be predicted more precisely from air temperature than from skin temperature.

2.2.7 Vehicular environment

Comfort in a vehicle is an interaction of many sources and can be divided into different aspects [40], [97]:

- Dynamic factors as vibration, shocks,
- Ambient factors like thermal comfort,
- Air quality,
- Ergonomics.

An automotive passenger compartment is a very special environment and distinguishes inherently from architectural environments. It can be best classified as an inhomogeneous, transient and non-steady environment [21]. Comfort predictions in vehicles are very complex due to non-uniformities of temperature and air flow, high localized air velocities and many radiation sources. Many parameters are not independent from each other and their interrelationship is not known exactly, which makes an experimental study nearly impossible [45]. So far there has been little research on vehicle thermal comfort and many researchers tried to adapt principles of existing literature to the automotive environment [72]. However, some researchers argue that due to the enormous differences to architectural environments, existent standards and methods can hardly be adapted [33]. Since an average adult dissipates about M=100W of energy to the environment and the space in a vehicle compartment is limited, occupation rate per volume and per area is very large and passengers will have an influence on the vehicle interior [33], [40]. Air flow within a passenger compartment is highly asymmetric and of three-dimensional nature [40], [45], [97]. Temperature- and velocity differences between head and feet level, as well as between front and rear compartment, are high [41]. The ventilation flow from the HVAC unit to the passenger compartment can be affected by many properties of the passenger compartment, including parameters such as location of the air vents and passenger occupancy [4], [62]. Figure 2-5 shows an example of an inherently non-uniform air velocity field from the middle of a vehicle compartment, using the method of particle image velocimetry.

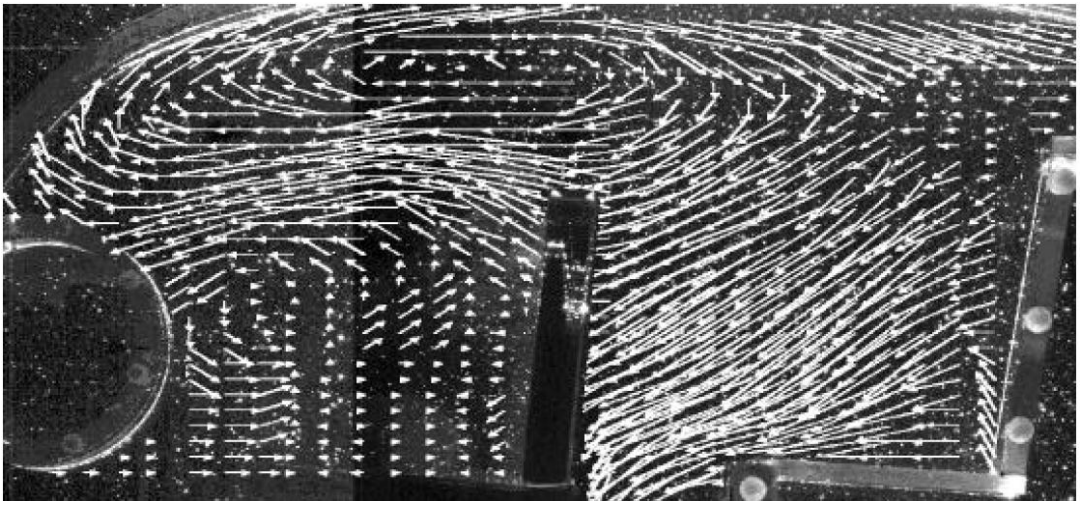

Figure 2-5: Air velocity field inside a passenger cabin [4]

An aggravating factor is the passenger's ability to select between various ventilation profiles, the air flow direction as well as the nozzle opening ratio of each vent independently. This results in an unmanageable large number of possible flow patterns.

External environmental conditions have a strong influence on the vehicle cabin due to limited insulation material as well as a large glazing ratio [40], [97]. Mean radiant temperature normally differs far more from air temperature than in buildings and air velocity is also higher than in buildings and less uniform [96]. Unlike to buildings, the position of a vehicle is not fixed in space and parameters suffer from strong temporal and local variability, resulting in complex non-uniform and transient interior conditions. To compensate for these disturbances, air has to be locally provided. This increases the chance of unwanted local cooling or heating on some parts of the body [21], [53]. In heated rooms air temperature normally increases with height away from the floor. This is unacceptable in vehicles, where heated air should be directed to the bottom area, whereas cooled air should be directed to the head region [33], [88]. In a vehicle cabin, passengers can hardly adapt to extreme climate conditions through changing clothing, opening and closing blinds, or changing location.

Solar radiation has a strong influence on thermal comfort in a vehicle cabin [32]. 70% of the solar load in a vehicle arises due to sunlight through glazing areas [33], [34]. The actual solar load on vehicles is dependent of the glass properties, solar incident angle and the solar spectrum. Short-wave radiation is based on skin or clothing absorbency and long-wave radiation is absorbed, based on the skin and clothing emittance [45]. A window influences thermal comfort in three ways [72]:

- Long wave radiation from the warm or cold interior glass surface,
- Transmitted solar radiation,
- Induced air motion caused by differences between glass surface temperatures and adjacent air temperatures.

Latter one can reach values up to v_a=1m/s [72]. Whether disturbances are perceived as pleasant or annoying also depends on the overall situation. For example, in winter sun radiation on the skin may be felt as pleasant, while additional warming through sun radiation in summer will most probably be perceived as discomfort. There are also secondary factors which may influence the thermal comfort perception in a vehicle cabin, such as interior and exterior colors, upholstery and vehicle size [33].

2.3 Thermal comfort models

Thermal comfort modelling basically started in the 1960s mainly for use in military and aerospace applications. As a consequence, oodles of thermal comfort models have been

developed and published in the past decades and an overview is extremely in transparent. In addition, much research has been conducted by private companies and has not been published due to confidentiality reasons.

Available research concerning modelling approaches can be distinguished in:

- Thermal comfort indices,
- Virtual models,
- Manikins.

The major advantage of the use of models is their reliability. For identical conditions, they will give 'identical' responses. Especially automotive industry has adopted the modelling approach in order to reduce costs arising from vehicle test involving subjects. However, a disadvantage of models can be given in terms of validity, because no mathematical or physical model will accurately represent human response [100]. Some researchers mention that models are used in part to diminish the variability subject to human judgments and perceptions. Different underlying theories are used for different modelling approaches, which makes an objective comparison very difficult [33].

2.3.1 Thermal comfort indices

A thermal index is a tool which is used for designing and assessing thermal environments in terms of individual parameters that correspond to thermal comfort. A thermal index is a single number that represents the degree of thermal comfort. Many attempts have been made to describe thermal comfort with only one index. One can distinguish between rational and direct indices. First ones are primarily based on mathematical relationships and use the equation of heat balance to predict human response, while latter ones incorporate direct measurement of physical parameters that respond to thermal comfort [33]. Direct indices often combine two or more parameters in one variable to simplify the description of the thermal environment. Literature reveals vast of proposed indices. However, most of them have only little meaning in practical applications. An overview is given in [93]. The most important ones will be introduced in the following subsections.

2.3.1.1 PMV & PPD index

The pioneer of thermal comfort modelling was P.O. Fanger. His work in the early 1970s to predict thermal comfort has been considered as the most valuable and important approach in thermal comfort research history. Fanger's work is based on the principle of energy balance, which means that internal heat produced by internal metabolism must be equal to the amount of heat dissipated to the environment. Mathematically this means:

$$M - W = q_{sk} + q_{res} + S, \quad \textbf{(7)}$$

with

M: Rate of metabolic heat production $\left[\frac{W}{m^2}\right]$,

W: Rate of external work $\left[\frac{W}{m^2}\right]$,

q_{sk}: Total heat loss from skin $\left[\frac{W}{m^2}\right]$,

q_{res}: Total heat loss through respiration $\left[\frac{W}{m^2}\right]$,

S: Heat storage in the skin/core compartment $\left[\frac{W}{m^2}\right]$.

Through laboratory tests with college aged subjects, Fanger could derive a linear relationship for activity level and sweat rate as well as for activity level and mean skin temperature. Heat loss from skin and respiration rate was expressed with physical variables and was substituted in equation (7). However, there are infinite combinations that will satisfy equation (7). Fanger therefore noticed that satisfaction of the heat balance equation alone is not a sufficient condition for thermal comfort and concluded that:

'*Man's thermoregulatory system is quite effective and will therefore create heat balance within wide limits of the environmental variables, even if comfort does not exist*' [37].

However, there is only a narrow interval that ensures thermal comfort, meaning that mean skin temperature and sweat rate must be within narrow limits. After statistical analysis and investigation of those limits, Fanger presented a modified heat balance equation and called it 'Comfort equation':

$$\frac{M}{AD_u}(1-\eta) - 0.35\left[0.43 - 0.061\frac{M}{AD_u}(1-\eta) - p_a\right] - 0.42\left[\frac{M}{AD_u}(1-\eta) - 50\right] - 0.0023\frac{M}{AD_u}(44 - p_a) - 0.0014\frac{M}{AD_u}(34 - \vartheta_a) \quad \textbf{(8)}$$

$$= 3.4 \cdot 10^{-8} f_{cl}[(\vartheta_{cl} + 273)^4 - (\vartheta_r + 273)^4] + f_{cl} h_c(\vartheta_{cl} - \vartheta_a)$$

with

M: Metabolic rate $\left[\frac{W}{m^2}\right]$,

A_{Du}: Dubois area (surface of the nude body) [m^2],

η: External mechanical efficiency of the body,

p_a: partial pressure of water vapour in the room air [Pa],

ϑ_a: Air temperature [˚C],

ϑ_{cl}: Mean temperature of outer surface of clothed body [˚C],

ϑ_r: Mean radiant temperature [˚C],

f_{cl}: Ratio of surface area of the clothed body to the surface area of the nude body,

h_c: Convective heat transfer coefficient $\left[\frac{W}{m^2K}\right]$.

Equation (8) allows the calculation of reasonable combinations of variables which ensure thermal comfort. When the comfort equation is satisfied, a large group of persons will show a thermal sensation close to neutral. However, equation (8) cannot be used to evaluate a given environment and to express the level of comfort probably experienced by occupants.

To overcome this limitation, Fanger extended his comfort equation. Under the assumption of narrow ranges for thermal comfort, he concluded that the level of discomfort is higher, the more the load on the effector mechanisms deviates from the comfort condition. The correlation to the predicted mean vote (PMV) is then a function of the body's thermal load L and the internal heat production M. It can be described as the remainder of equation (8) when heat balance is not fulfilled. Equation (9) represents this relationship mathematically.

$$PMV = f\left(L, \frac{M}{A_{Du}}\right) = \left(a \cdot e^{k\frac{M}{A_{Du}}} + b\right) L \qquad \textbf{(9)}$$

The PMV output is calibrated to the seven point ASHRAE scale, ranging from -3 (cold) to +3 (hot). The parameters a, k and b have been statistically determined by Fanger through extensive tests with subjects. After insertion of a, b, k and equation (8) into equation (9) and after some simplifications, the PMV can be written as:

$$\begin{aligned} PMV = {} & [0.303e^{-0.036M} + 0.028] \\ & \cdot \{M - W - 3.05 \cdot 10^{-3}[5733 - 6.99(M - W) - p_a] \\ & - 0.42[(M - W) - 58.15] - 1.7 \cdot 10^{-5} M(34 - \vartheta_a) - 3.96 \\ & \cdot 10^{-8} f_{cl}[(\vartheta_{cl} + 273)^4 - (\vartheta_r + 273)^4] - f_{cl} h_c(\vartheta_{cl} - \vartheta_a)\} \end{aligned}$$

and:

$$\begin{aligned} \vartheta_{cl} = {} & 35.7 - 0.028(M - W) \\ & - I_{cl}\{3.96 \cdot 10^{-8} f_{cl}[(\vartheta_{cl} + 273)^4 - (\vartheta_r + 273)^4] + f_c h_c(\vartheta_{cl} - \vartheta_a)\} \end{aligned} \qquad \textbf{(10)}$$

$$h_c = \begin{cases} 2.38|\vartheta_{cl} - \vartheta_a|^{0.25} \; for \; 2.38|\vartheta_{cl} - \vartheta_a|^{0.25} > 12.1 \cdot \sqrt{v_a} \\ 12.1\sqrt{v_a} \; for \; 2.38|\vartheta_{cl} - \vartheta_a|^{0.25} < 12.1 \cdot \sqrt{v_a} \end{cases}$$

$$f_{cl} = \begin{cases} 1 + 1.29 I_{cl} \; for \; I_{cl} \leq 0.078 m^2 \cdot \dfrac{K}{W} \\ 1 + 0.645 \; for \; I_{cl} > 0.078 m^2 \cdot \dfrac{K}{W} \end{cases}$$

with:

M: Metabolic rate $\left[\frac{W}{m^2}\right]$,

W: External, mechanical work $\left[\frac{W}{m^2}\right]$,

I_{cl}: Clothing insulation $[m^2 \frac{K}{W}]$,

f_{cl}: Clothing ratio,

ϑ_r: Mean radiant temperature [°C],

ϑ_a: Air temperature [°C],

v_a: Air velocity $[\frac{m}{s}]$,

p_a: Partial water vapour pressure [Pa],

h_c: Convective heat coefficient $[\frac{W}{m^2 K}]$,

ϑ_{cl}: Clothing surface temperature [°C].

The PMV model was developed for steady state and uniform environments. It addresses the body as a whole and its output doesn't allow for conclusions about the thermal sensation of single body parts. Clothing insulation is assumed to cover the body entirely and uniformly. Clothing values from tables affect the PMV calculation additively. Fanger states that the PMV model is only able to address statistically the thermal response of a large group of people and is not valid to predict the response of the individual [37].

Fanger recognized that due to individual differences a climate that satisfies everybody does not exist. This conclusion has enormous meaning for the implementation of HVAC controls:

Regardless of the complexity and the performance of the underlying control algorithms, we are never able to design a product that satisfies the whole entirety of people.

To estimate the proportion of people which are thermally dissatisfied with a given environment, the predicted percentage of dissatisfied (PPD) was introduced. Under the assumption that single votes are normally distributed around the mean, the PPD can be found as:

$$PPD = 100 - 95e^{(-0.03353 \cdot PMV^4 - 0.2179 \cdot PMV^2)} \quad \textbf{(11)}$$

Figure 2-6 represents the PPD in dependence of the PMV. It is noteworthy that Fanger identifies the minimum amount of dissatisfied people for a given climate under optimal conditions as 5%.

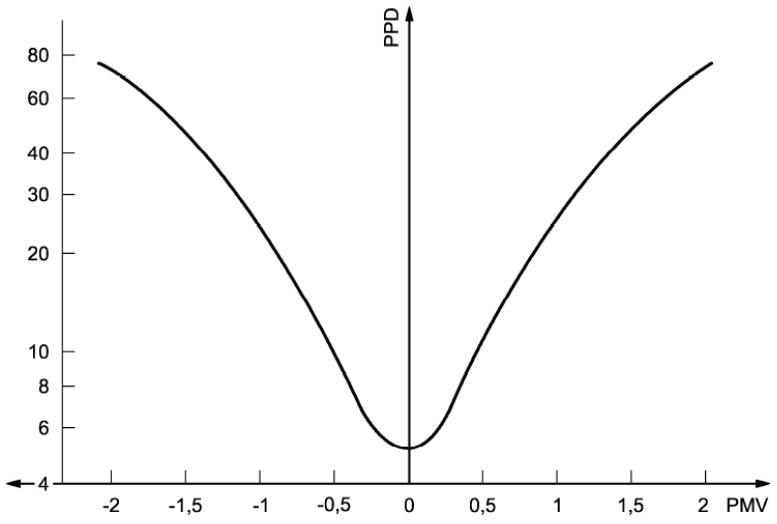

Figure 2-6: PPD Index [28]

Presently, the PMV index is the most established and best understood method to evaluate indoor thermal comfort. It is therefore substantial part of established thermal comfort standards like ASHRAE 55P or ISO 7700 [2], [28].

Much research has been conducted in the last decades to verify the PMV and PPD models. Most researchers support Fanger's theory. However, there are also some researchers who critically question Fanger's findings. In studies, [8] found that most respondents reported a much warmer thermal sensation than predicted by the standard model and concludes that PMV underestimates the actual thermal sensation, which is probably affected by additional factors such as available control over the environmental conditions, the annual outdoor climate and culturally related expectations. PMV is not always a good predictor of actual thermal sensation, because of difficulties in obtaining accurate measures of clothing insulation and activity level [18]. This is confirmed by [49], which mentions that the 'clo' values described in tables are not accurate enough to classify comfort within 0.3 PMV steps.

There is consensus that the PMV model cannot be used in transient and non-uniform environments and is not applicable to the individual [40], [55], [76], [96]. PMV is only suitable for minor fluctuations of the input variables, provided that the time averaged values of the previous one hour period are applied [75]. The PMV evaluation method treats the entire body as one object and therefore does not distinguish between different parts of the body. If one body side is warm and the other cold, the PMV calculation would result in a mean zero thermal load and would therefore indicate a neutral thermal sensation. Obviously, the local effects of asymmetric conditions, such as an environment with a hot or a cold window, or local air motion around a person's face provided by a fan, are lost in this whole-body model. A person may

perceive local discomfort although the whole body is within comfort ranges [48]. It is known that the PMV equation has not been verified against various kinds of clothing and activity. Therefore, with the same clothing, activity and thermal environmental parameters, some people may still feel discomfort although a thermal sensation of neutrality is predicted by the PMV index. The validity of the PPD model has also been argued. According to Fanger the PPD constitutes of 2.5% dissatisfied persons due to cool sensation and 2.5% dissatisfied persons due to warm sensation. It is thereby assumed that subjects who report a thermal sensation of slightly cool, neutral and slightly warm are satisfied with their environment, while subjects who report a thermal sensation of cold, cool, warm and hot are dissatisfied with their environment. Some researchers argue that the PPD and PMV indices were therefore determined by definition and not by interview [79]. Different PPDs have been proposed in literature [126]. Figure 2-7 compares some suggestions for PPD.

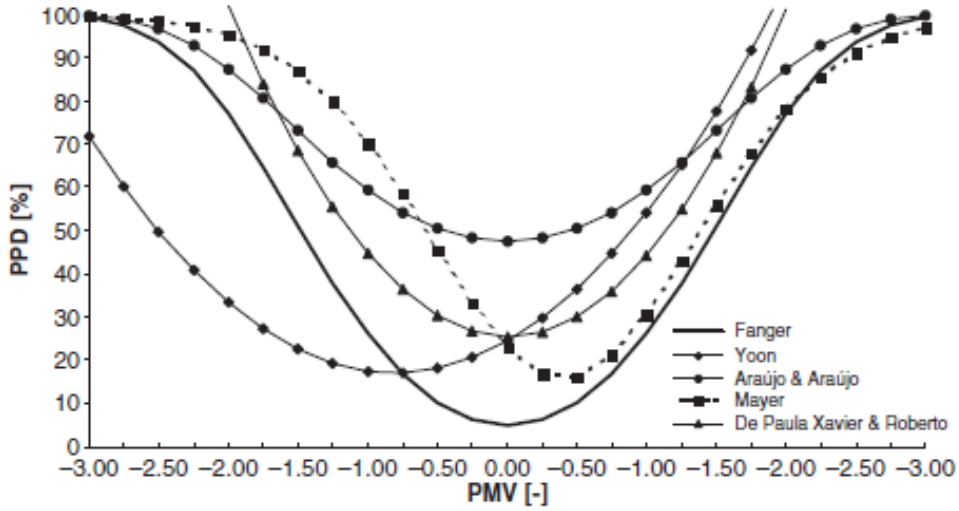

Figure 2-7: PPD comparison [126]

2.3.1.2 Operative temperature

The operative temperature ϑ_o is defined as the weighted average of air temperature and mean radiant temperature. It can be represented as

$$\vartheta_o = \frac{h_r \vartheta_r + h_c \vartheta_a}{h_r + h_c}, \qquad \textbf{(12)}$$

with:

ϑ_r: Mean radiant temperature [˚C],

ϑ_a: Air temperature [˚C],

h_r: Radiative heat coefficient [$\frac{W}{m^2 K}$],

h_c: Convective heat coefficient [$\frac{W}{m^2 K}$].

For sedentary persons who are not exposed to direct sun light and when v_a<0.2m/s, equation (12) can be approximated as the arithmetic mean of ϑ_a and ϑ_r [2].

2.3.1.3 Equivalent temperature

The equivalent temperature is a measure of the effects of non-evaporative heat loss from the human body. It is derived from the operative temperature and also includes the effect of air velocity on a heated body. The equivalent temperature does not account for subjective variations or human sensitivity [32]. According to [92], it is defined as the

'*Uniform temperature of an imaginary enclosure with air velocity equal to zero in which a person will exchange the same dry heat by radiation and convection as in the actual non uniform environment*'.

The effects on human body are best known for whole body heat exchange. Limited experience exists for local heat exchange. It is supposed that the sum of radiative and convective heat exchange R and C is equal to the total heat exchange. Introducing the equivalent temperature ϑ_{eq}, it can be mathematically described as:

$$\begin{aligned} R + C &= F_{cl} f_{cl} h_r (\vartheta_{sk} - \vartheta_r) + F_{cl} f_{cl} h_c (\vartheta_{sk} - \vartheta_a) \\ &\stackrel{\text{def}}{=} F_{cl} f_{cl} h_r \left(\vartheta_{sk} - \vartheta_{eq}\right) + F_{cl} f_{cl} h_c \left(\vartheta_{sk} - \vartheta_{eq}\right). \end{aligned} \quad \textbf{(13)}$$

Solving equation (13) for ϑ_{eq} yields:

$$\vartheta_{eq} = \vartheta_{sk} - \frac{R + C}{h_r + h_c}. \quad \textbf{(14)}$$

Equivalent temperature can be also calculated using the comfort equation or through empirical relationships. There is no direct method to determine the real equivalent temperature for the whole body and local body parts. The standard definition for the equivalent temperature in equation (14) only applies to the whole body. However, in inhomogeneous environments whole body equivalent temperature is not sufficient to perform accurate measurements. Therefore four different equivalent temperatures have been defined [40], [93] and [52]:

- Whole body equivalent temperature, which refers to the heat exchange of the whole body,
- Segmental equivalent temperature, which refers to the heat exchange of single body parts,
- Directional equivalent temperature, which refers to the heat exchange within the half space in front of the infinitesimal space,
- Omnidirectional equivalent temperature, which refers to the heat exchange around the body, or to a part of the body.

These equivalent temperatures differ in terms of properties and measurement methodologies. More detailed information can be found in literature, e.g. [32].

In transient and inhomogeneous environments like a vehicle compartment, the evaluation and association of local equivalent temperatures is important. Standards like ISO 14505, which deals with comfort measurement in vehicles, recommend a representation like Figure 2-8.

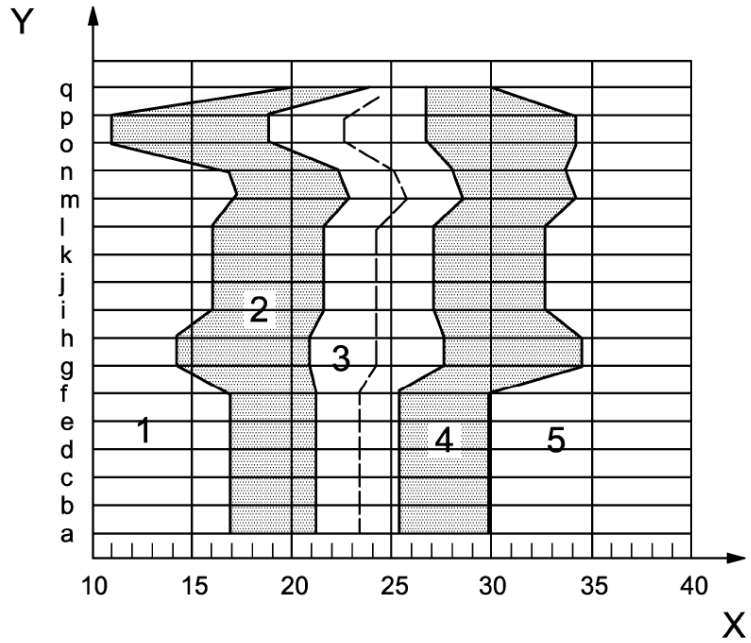

Figure 2-8: Equivalent temperature [32]

In this case the y- axis of Figure 2-8 represents 16 different body parts (a-q). The x- axis represents ϑ_{eq}. The sections 1-5 represent ranges of thermal sensation, such as:

1 Too cold,

2 Cold, but comfortable,

3 Neutral,

4 Warm, but comfortable,

5 Too warm.

That means a representation like Figure 2-8 defines thermally acceptable levels for different body parts. According to different clothing insulations for different seasons of the years, thermal comfort sections may vary over the year and sections in Figure 2-8 will be offset.

Some researchers argue that human sense of thermal comfort is very complex and doubt that the application of equivalent temperature is the appropriate index for thermal comfort assessment [39], [135]. Other scientists mention that equivalent temperature only covers dry heat loss and doesn't account for humidity, clothing insulation and metabolic rate. Local equivalent temperature just quantifies the thermal sensation of individual body parts. However, it does not

give any indication about individual comfort levels [72]. For instance, when some body parts are (slightly) cool whilst other body parts are warm, the concept of equivalent temperature is not able to quantify overall body comfort. According to [106], local equivalent temperature is a good, but not a fully sufficient indicator for thermal comfort.

2.3.1.4 Effective temperature

The effective temperature ϑ_{et} combines operative temperature and humidity in one single index. It is defined as [1]:

"*The temperature of an environment at 50% relative humidity that results in the same total heat loss from the skin as in the actual environment*"

Mathematically it can be written as:

$$\vartheta_{et} = \vartheta_o + wi_m LR(p_a - 0.5p_{et}), \quad \textbf{(15)}$$

with

- w Skin wetness,
- i_m: Total vapor permeation efficiency,
- ϑ_o: Operative temperature [˚C],
- LR: Lewis ratio, ratio of evaporative heat transfer coefficient to convective heat transfer coefficient [K/kPa],
- p_{et}: Saturated vapor pressure at [kPa].

2.3.2 Virtual thermal comfort models

The occupant's thermal interaction with the environment involves physiological and psychological responses. Models shall quantify those responses and allow for making predictions even if, in case of automotive engineering, a vehicle prototype is not yet available. Hereby the mathematical representation of the human's thermo-regularity system and the psychological response to the environment is modeled. Models incorporate data acquired from experiments with human subjects, theoretical as well as empirical relationships. Established models are normally multi-node models, where a thermal system has been simplified into a series of nodes which shall represent various segments of the human body. Nowadays there is a plurality of thermal comfort models available. Industry, especially automotive companies and suppliers, often rely on their own in-house developed approaches. Documentation about the state of the art and trends in research is therefore often only limited available.

Reference [85] describes a model to assess thermal comfort inside a vehicle cabin in dependence of the climatic conditions and the materials that compose the vehicle. However, the model uses hardly measurable variables like sky temperature and the amount of radiation on each external

surface of the vehicle. Reference [101] shows a model to predict human thermal comfort and concludes that for analysing local thermal comfort, local skin temperatures have to be considered with high accuracy. Reference [113] describes a modern automotive HVAC development cycle using virtual technologies for HVAC design. Reference [69] introduces an INCA model to simulate the vehicle compartment, which has been connected to a Matlab model, for simulating the human thermo-regularity system. The model consists of 14 body segments with each segment consisting of four concentric layers, namely core, muscles, adipose tissue and skin. Skin is further divided in four sub regions. Reference [82] has developed a thermal comfort evaluation package consisting of three predictive software tools:

1. A three-dimensional model for simulating human's internal physiological system, incorporating responses like shivering, sweating, heart rate and local blood flows,
2. A psychological model for predicting human thermal comfort,
3. A thermal comfort manikin for vehicle testing and verification.

The combination of thermal comfort models and manikins will be discussed in Chapter 2.3.3.
Some available models also consider variables like height, weight, age, gender, skin color and body fat [45]. Reference [44] uses a model that incorporates 16 body segments. Each segment is modeled as four body layers (core, muscle, fat, and skin tissues) including a clothing layer. The comfort model has the ability to predict local thermal comfort level of an occupant in a highly non-uniform thermal environment as a function of air temperature, surrounding surface temperatures, air velocity, humidity, direct solar flux, activity and clothing type. Combined with a physical model of the vehicle compartment including the geometrical configuration of the passenger compartment like glazing surfaces, physical and thermal properties of the enclosure, glass properties and knowledge of external loads, thermal comfort can be predicted. This approach is called virtual comfort engineering, since a real vehicle and test panels of subjects are not necessary. Further information about modelling can be found in literature like [93], [128].
However, computational models are often limited due to low resolution of temperature field calculations, inadequate modelling of human's thermo-regularity system, insufficient information about the clothing worn, and a lack of agreement between calculated and measured results [93].

2.3.3 Manikins

Human testing is normally considered as expensive and time consuming. In extreme environments it is also considered as unethical to use humans as test subjects. Those problems shall be overcome by the use of manikins. Manikins are complex instruments with a human shape, which shall measure convective, radiative and conductive heat losses over the whole

body surface and any direction. A summary of human heat exchange with the environment is illustrated in Figure 2-9(a) and an example of a real thermal manikin with clothes is given in Figure 2-9(b).

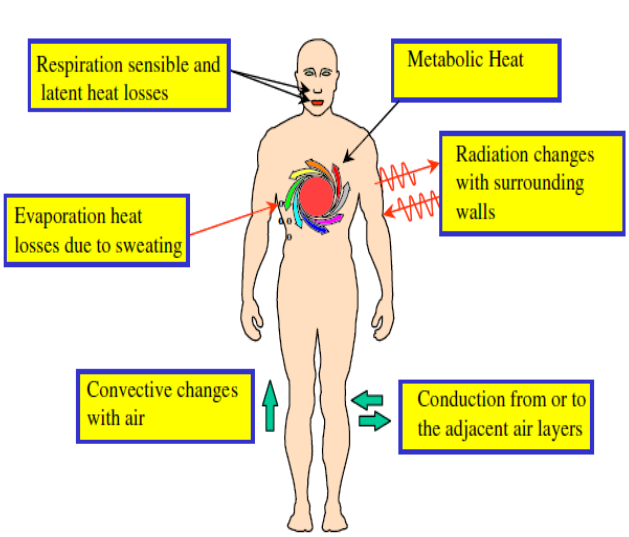

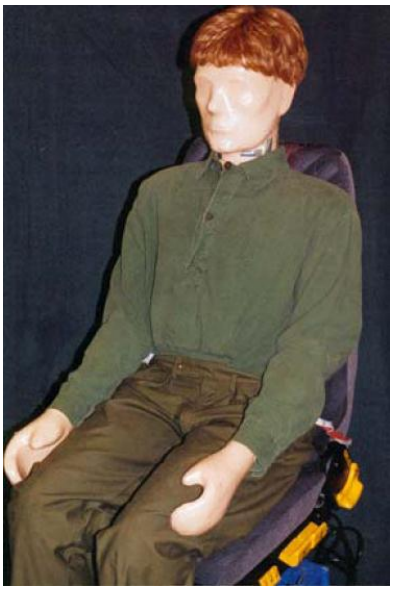

(a) **(b)**

Figure 2-9: Thermal manikins; (a) Sources of human heat exchange [40], (b) Example of a clothed thermal manikin [93]

Thermal manikins are especially suitable for the automotive environment since in vehicle compartments, thermal comfort cannot be always simulated without the presence of a human body, due to its thermal interaction with the environment and due to changes in air flow pattern [40].

Manikins of the latest generation are supposed to imitate the human body as in many aspects as possible and consist of more than hundred individually controlled segments, including functions like respiration, blood circulatory and perspiration systems [93].

Reference [15] shows a manikin with 21 heated sensors which exchanges energy with the environment by convection and radiation. Sensors measure the resultant surface temperature (RST) and correlate it to thermal comfort. There are also manikins available, which incorporate breathing functionalities [128].

Some manikins can be even coupled with physiological and psychological models. For example, [109] introduces a suite of thermal comfort tools to assist in the development of smaller and more efficient climate control systems in automobiles. These tools which include a 126-segment sweating manikin, a finite element physiological model of the human body and a psychological model based on human subject testing, are designed to predict human thermal comfort in automotive environments. The principle is illustrated in Figure 2-10.

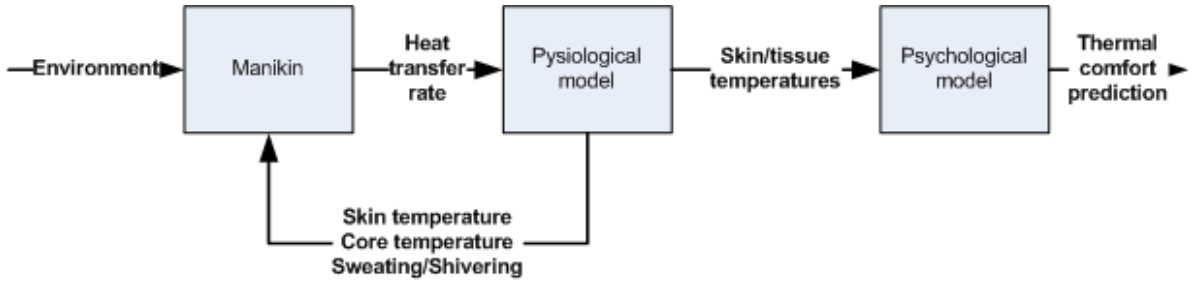

Figure 2-10: Feedback loop of manikin and comfort models

The manikin measures the heat loss from the human body in the vehicle environment and sends the heat flux from each segment to the physiological model. The physiological model predicts the body's response to that environment, determines 126 segment skin temperatures as well as sweat rates, breathing rate and re-transmits this data back to the manikin. The manikin uses this information to adjust itself and provides the updated data to the physiological model. The psychological model evaluates the data from the physiological model to predict the local and global thermal comfort, as a function of local skin and core temperatures and their rates of change. Similar work was published by [108], which developed a psychological model consisting of a 120 zones thermal manikin, linked to a physiological and psychological model, in order to predict comfort in transient non-homogenous environments.

Due to advances in simulation technology and CFD technologies, there is a trend towards virtual manikins in order to achieve further cost reductions.

2.3.4 Adaptive approach

The adaptive theory of thermal comfort has its origin in field studies from the late 1970s, when researchers discovered that environmental conditions and parameters, like clothing insulation and metabolic rate, can only be hardly measured in field testing. It was also observed that people show a tendency to adapt themselves to changing environmental conditions and well known indices like PMV did not deliver the expected results. The PMV considers the human being as a passive recipient of the environment. However, in some areas of application occupants are not considered as inert recipients of the environment, because they are supposed to interact with their environment in order to optimize their conditions.

This behaviour was especially observed in naturally ventilated housings where well known indexes like PMV do often not correlate very well and comfort ranges are wider than rational ranges predict. Researchers therefore suggested that there must be a feedback between comfort and the subjects' behaviour and that they must have adapted themselves to the environment.

The adaptive theory postulates: If an environmental change occurs, such as to produce discomfort, people react in ways which tend to restore their comfort [91]. An example of this

may be the opening or closing of windows, changing of clothing, making use of window blinds, etc. The adaptive principle therefore links thermal comfort to the people's behaviour. Based on the assumption that there is a feedback between the environment and human's interaction with his environment, the adaptive theory proposes that indoor comfort temperature only depends linearly from outdoor temperature.

In the author's opinion the term adaptive might be misleading in this context. From an engineering point of view 'Adaption' normally refers to a learning process rather associated with machines than humans. In the further course of this thesis, terms like 'learning' and 'adaption', will be solely used with respect to soft computing principles.

2.4 Measurement of thermal comfort

Due to the complexity and the transient nature of the automotive environment, comfort indices and simulation methods are often limited in validity [41], [32]. Additionally, many parameters cannot be simply derived from fundamental relationships [87]. Therefore, methods for measuring thermal comfort, including instruments as well as human testing, have to be defined. These methods can be divided in subjective, behavioral and objective methods.

2.4.1 Subjective methods

The only direct method of measuring thermal comfort is to use human subjects [100]. Subjective methods shall quantify the subject's response to a given environment with use of subjective scales. These scales are based on psychological continua that are relevant to the phenomenon of interest. Subjective methods are also required for validating various comfort models and comfort indices. At present there are five types of subjective scales [32]:

- Thermal sensation,
- Thermal emotion,
- Thermal preference,
- Thermal acceptance,
- Thermal tolerance.

Some examples of relevant concepts will be discussed in the following subsections.

2.4.1.1 ASHRAE scale

The ASHRAE scale is an example for a thermal sensation scale. Thermal sensation is a measure of the subject's thermal state. It quantifies an abstract psychological measure of feeling. It refers to how a subject feels at the moment. No information is given on how the subject's may evaluate the environment nor how he/she would like the environment to be [122]. The thermal state of the

body determines the thermal sensation. Some researchers therefore strictly distinguish between thermal sensation and thermal state evaluation [111]. The term “I feel cold” is for example a thermal state response whereas the term “the air feels cold” is considered to be a thermal sensation response. In this thesis the terms thermal sensation and thermal state will however be used interchangeably.

Thermal state evaluation is most often used in HVAC research. A popular thermal sensation scale is the ASHRAE scale, presented in Table 2.

Table 2: ASHRAE scale

Numerical value	Linguistic value
+3	Hot
+2	Warm
+1	Slightly warm
0	Neutral
-1	Slightly cold
-2	Cool
-3	Cold

It is often implicitly assumed that thermal sensation is somehow correlated to thermal comfort and people who feel neither warm nor cold are supposed to be comfortable. Some researchers therefore argue that with the ASHRAE scale, thermal comfort is not measured directly [105]. It might also be possible that subjects are comfortable even if they rate themselves not in a neutral thermal state (see Chapter 2.2.6).

Studies show, that there is significant difference between thermal sensation and thermal preference. In research conducted by [86], in 57% of the occasions the desired thermal sensation was different to neutral. People often tend to prefer slightly warm environments [86] and [79].

2.4.1.2 Uncomfortable/Sticky scale

Another concept of thermal evaluation is given in Table 3 and Table 4.

Table 3: Stickiness scale

Numerical value	Linguistic value
+4	Very sticky
+3	Sticky
+2	Slightly sticky
+1	Not sticky

Table 4: Uncomfortable scale

Numerical value	Linguistic value
+4	Very uncomfortable
+3	Uncomfortable
+2	Slightly uncomfortable
+1	Not uncomfortable

Both scales have a similar layout with an absence of effect at the base and an increasing strength of effect up the scale. Psychologically, it is considered as important to use the consistent wording 'sticky/uncomfortable', which presents psychological continuum and ensures that the scale is uni-dimensional [100]. Both scales should be used together to complement each other. An example makes this clear:

If a person votes 'Uncomfortable' according to Table 4, no information is given about the source of discomfort. It could be either too humid, too hot but also too cold. However, if the subject adds 'Not sticky' according Table 3, one can conclude that discomfort is present due to cool/coldness. It is rather unlikely that a subject feels uncomfortable, too hot and the environment is assessed to be not sticky.

2.4.1.3 Thermal preference scale

Preferences scales like Table 5 include an evaluation of the environment. Compared to thermal state evaluation, preference scales allow conclusions about the subject's preferred environment.

Table 5 Thermal preference scale

Numerical value	Linguistic value
+7	Much warmer
+6	Warmer
+5	Slightly warmer
+4	No Change
+3	Slightly cooler
+2	Cooler
+1	Much cooler

2.4.1.4 General conclusions

There are many more scales available in literature, e.g. [93], [111]. Scales can also be modified and details may be added. Binary scales (Yes/No) might also be helpful for evaluation of a given environment.

In general, evaluation scales must be carefully identified to meet the requirements of the specific application, because the way a scale is represented or handled may influence the results [32]. Often a combination of scales is recommended to be integrated into a questionnaire in order to complement each other and to provide a comprehensive measure of thermal comfort [100], [32]. To demonstrate this, two examples with a combined thermal state scale, an uncomfortable scale and a thermal preference scale will be given:

Example 1:

The simultaneous statements are given:

a) I feel slightly warm,
b) I feel not uncomfortable,
c) I could feel warmer.

According to a) the subject's thermal state is slightly warm. However, he/she does not mention discomfort (b), although he/she even prefers a warmer climate (c). However, it cannot be concluded that a warmer environment would not result in discomfort.

Example 2:

The simultaneous statements are given:

a) I feel slightly warm,
b) I neither feel comfortable nor uncomfortable,
c) I would like to be warmer.

According to (a) the subject's thermal state is slightly warm. He/she explicitly expresses the request to feel warmer (c). This suggests that the subject might feel uncomfortable. However, discomfort is not mentioned by (b).

Scales are relatively easy to use because no special instrumentation is needed. An advantage is that they directly address the phenomena of interest. A disadvantage is that human sensation of thermal comfort is individual and linguistic terms, as well as the semantics of language, may be interpreted differently by a panel of test subjects. The scales are supposed to be of cardinal nature. For instance a thermal sensation vote on the ASHRAE scale of 1.5 is supposed to be an evaluation exactly in the middle of slightly warm and warm. However, it is not proven that human's thermal sensation is also linearly spaced within this range. This might be especially a

problem when statistically evaluating the results of questionnaires. A weak point for some applications may also be the lack of explanation for the reaction of the subject [32].

It must be carefully considered that humans vary in their thermal sensitivity, which means the ability to distinguish between different thermal states. This means that a person with a high thermal sensitivity may be able to evaluate a given climate more precisely and with more details than a thermal less sensitive subject. This is especially important in designing questionnaires and choosing the number of the scale's linguistic terms. It must be pointed out, that most scales solely refer to whole body thermal sensation. In the majority of cases, they do not take into account local sensations. However, in vehicles local thermal discomfort may arise from various different sources. For instance, insulation of an automotive seat may prevent drying of a perspired back, which may also lead to thermal discomfort, although the other thermal parameters are within comfort ranges.

In terms of completeness it must be mentioned that there might be groups of people who are not able to fulfill the task of thermal evaluation, like babies and certain groups of disabled persons.

2.4.2 Behavioral methods

Behavioral methods quantify or represent human behavior as response to an environment. The particular aspect of observed human behavior is related to the human condition of interest. In terms of thermal comfort, a behavioral response might be a change of clothing, a change in seat, etc. Advantages of behavioral methods include minimum interference with what is being measured and a direct 'active' measurement of discomfort. Disadvantages include the difficulty in establishing validity and reliability of the method and direct interpretation of the results in terms of thermal comfort. For the example, changing a seat could be also the result of other environmental or psychological factors. Behavioral methods may deliver valuable knowledge to an external observer in a specific situation. However, they are not suitable for this thesis, because observations cannot be acquired automatically.

2.4.3 Objective methods

Objective measures aim to quantify the physical or mental condition of a person by the use of instrumentation or measurements of relevant variables, according to the phenomena of interest. An example is measurement of mean body skin temperature, or skin wetness, which both correlate to thermal comfort sensation. However, the measured values might be influenced by measurement errors and might be superimposed by distortions. Since thermal comfort is a condition of mind, correlation to physical variables might not be complete. Some objective

measures, like change in heart rate may also arise from other factors like nervosas, excitement, etc. [93].

An advantage of objective measures is that they are often independent from subjective methods and deliver consistent outputs for given input variables. However, measurement difficulties may arise. For instance in transient and inhomogeneous environments, localized phenomena can affect temperature and air velocity making it impossible to measure them accurately [32], [129].

2.4.4 Instruments for thermal comfort measurement

In buildings, which are normally considered as stationary and homogeneous, it is often sufficient to evaluate the room climate at only one position [21]. It is also comparatively easy to install measurement equipment and to measure single environmental variables [40]. Methods and instruments for measuring and evaluating the thermal environment are defined in standard ISO 7726 [27]. For buildings there has also been some research to develop sensor elements which incorporate more than one environmental physical variable and directly predict thermal comfort. Reference [58] proposes a silicon integrated sensing device based on a simplified PMV equation. Clothing and metabolic rates have to be inputted and are considered to be constant. Reference [124] introduces a similar concept based on a look-up table for PMV values. Assumption is made that all variables, with exception of mean radiant temperature, can be easily obtained. Metabolic activity and clothing insulation were chosen as constants for a typical office environment.

As pointed out in Chapter 2.2.7, the vehicle environment inherently differs from those of architectural buildings. Due to inhomogeneity, many sensors had to be installed in the vehicle compartment. To interpret the results with rational and direct comfort indices, measurement values must be accurate and according to their exact definition. ISO 14505 does not recommend indices like PMV and PPD for comfort evaluation in automotive environments [32]. Automotive industry has therefore developed a different strategy of assessment of thermal comfort [21] and focuses predominantly on the use of equivalent temperature to assess the climate in a vehicle compartment [40], [92], [32]. There are three possible methods to determine equivalent temperature in a vehicle cabin.

2.4.4.1 Measurement of single physical variables

Theoretically, it is possible to determine equivalent temperature through measurement of single variables like air temperature, mean radiant temperature and air velocity. However, this approach is not recommended since compartment space is limited and due to the cabin's properties, equivalent temperature has to be measured at many locations [32]. Additionally,

errors arise because the sensors cannot be installed at exactly the same positions [40], [93], [97]. Due to the extremely inhomogeneous environment, it is therefore possible that environmental conditions may vary strongly within a small radius.

2.4.4.2 Heated sensors

A method to assess equivalent temperature is to use heated sensor elements, which respond to the combined influence of environmental variables. Heated sensors are based on the principle of deriving the equivalent temperature from measurement of dry heat loss from the sensor surface. Examples of such sensors are described in [35], [96] and [94]. The sensors are loaded with a constant heat flux according to the desired metabolic rate. The RST is measured and can be calculated with a linear relationship to the equivalent temperature. According to [94], the equivalent temperature ϑ_{eq} can be determined as:

$$\vartheta_{eq} = 1.09 \cdot RST - 15.08℃. \quad \textbf{(16)}$$

There are different possible designs. Heated sensors in a flat package can be used to measure directional heat fluxes. However, there are also sensors with an ellipsoid shape available, as illustrated in Figure 2-11. These have the advantage to have a similar ratio to horizontal and vertical projected areas in order to simulate the shape of a human being.

Figure 2-11: Ellipsoid thermal comfort transducer [96]

These sensors are predominantly used to measure omni-directional heat flux. To assess thermal comfort in a vehicle, flat heated sensors can be mounted at characteristic positions on an unheated manikin or omni-directional sensors can be mounted on a frame. The principles are shown in Figure 2-12(a) and Figure 2-12(b)

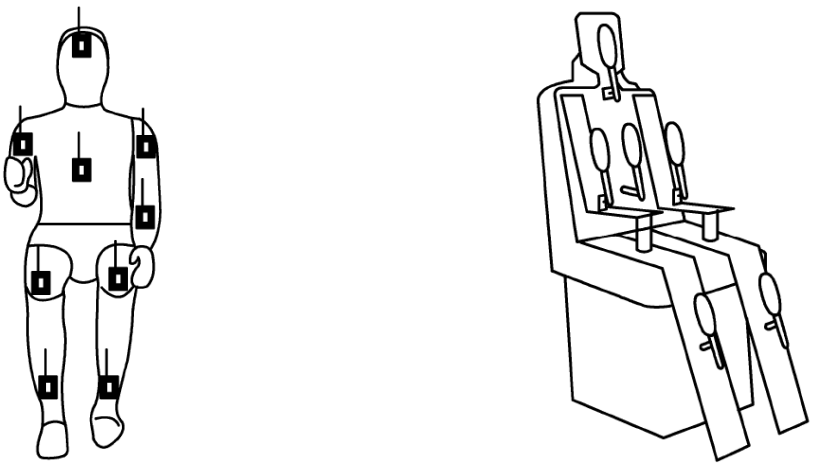

(a) **(b)**

Figure 2-12: Thermal evaluation in automotive with sensors [32]; (a) Unheated manikin with attached flat sensors, (b) Frame with omni-directional transducers

2.4.4.3 Manikins for thermal comfort measurement

Automotive industry prefers manikins to assess thermal comfort. Thermal manikins are the only instrument capable of simultaneously measuring the effects of air temperature, radiant heat exchange, air velocities, solar gains, clothing properties and including the presence of a physical body.

Manikins consist of many individually controlled segments which can be further separated in zones. Figure 2-13 shows an illustration of a manikin which is divided into 16 zones.

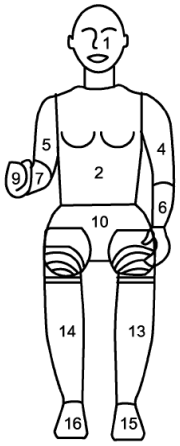

Figure 2-13: Thermal manikin divided in 16 zones [32]

Voltage is pulsed to each segment at a rate that allows maintaining surface (skin) temperature. Power consumption is then a measure of radiative, convective and conductive heat loss which can be mathematically described as:

$$Q_{meas} = h_c(\vartheta_{sk} - \vartheta_a) + h_r(\vartheta_{sk} - \vartheta_r) + h_k(\vartheta_{sk} - \vartheta_i). \quad \textbf{(17)}$$

The direct measurement of total heat loss Q eliminates the determination of the single parameters in equation. However, there is no method available which accounts for single measurements of the right side of equation (17).

Manikins have to be calibrated in climate chambers under well-defined conditions with use of equation (18). Radiative and convective heat coefficients have been thereby summarized to h_{cal}.

$$\vartheta_{eq} = \vartheta_{sk} - \frac{Q}{h_{cal}} \quad \textbf{(18)}$$

To measure the heat flux for the whole human body plural zones should be used in order to account for asymmetries [32]. For instance, temperature asymmetries on the manikin's surface may arise due to sun radiation or parts being in direct contact with the vehicle.

Thermal manikins can be operated in different operating modes:

- Constant surface temperature,
- Constant heat flux,
- According to a comfort equation.

Those methods should be chosen according to the application and differ in terms of stability, speed, surface temperature and in measurement range. More details can be found in appropriate literature, such as [32].

2.4.4.4 General conclusions

Results obtained from different measurements methodologies cannot be compared with each other [32]. To measure the local equivalent temperature, the heat flux of the individual segments (which may be further separated in heated zones) is determined. According to [84], the differences for whole body equivalent temperature between different manikins could differ up to $\Delta\vartheta_{eq} = 4$°C and the more non-uniform the environment, the more the differences in measured equivalent temperature. The differences mainly depend on the surface shape, surface size and the surface temperature of the sensors. Reference [12] states, that the repeatability of determination of the equivalent temperature according to the heat-integrating sensors and the basic climatic measurements is better than that according to thermal manikin measurements.

However, none of the methods can mimic the exact heat exchange of a human body. The final interpretation of the equivalent temperature still requires extensive comparison to subjects.

2.5 Technical realizations using intelligent concepts

The electronic circuitry of automotive HVAC ECUs is often divided into two subsystems. This is shown in Figure 2-14.

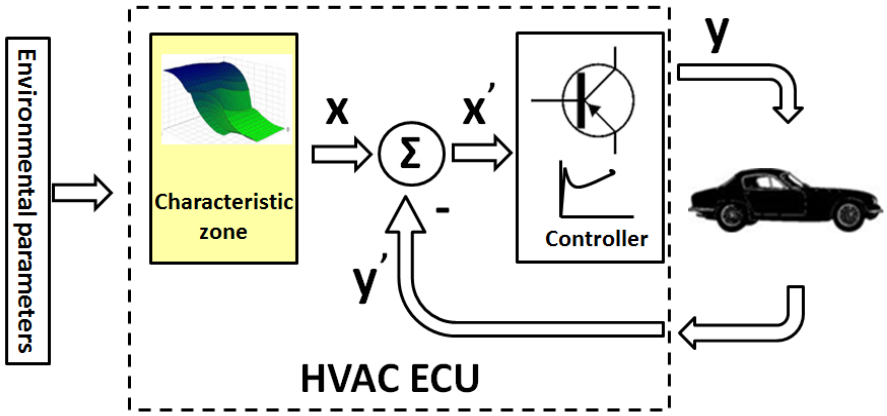

Figure 2-14: Simplified HVAC ECU layout

For clear illustration, only one single feedback control unit is assumed to control all HVAC actuators. The output vector **y** is therefore continuously adjusted, according to the difference of the reference vector **x** and the actual vector $\mathbf{y}'$. The reference vector is determined by a multidimensional characteristic zone, which has been yellowly marked in Figure 2-14. It also contains thermal comfort parameters, which have been determined with methods described in Chapters 2.3 and 2.4.

These comfort parameters are stored in an electrically erasable programmable read-only memory (EEPROM) as parametric characteristic zones or multiple 'if-else' statements. The application engineer has the opportunity to adapt the reference block, in order to fit the HVAC behaviour to the vehicle. However, due to the high dimensionality of the problem and existing interrelationships between parameters, this is often a matter of luck and does not guarantee success at all. The researcher feels that this procedure is not optimal and suggests substituting the characteristic zone block in Figure 2-14 through a blackbox approach. This blackbox will be trained with collected measurement data using methods of artificial intelligence.

Artificial intelligence is predominantly used in fields of research, where it is difficult to obtain exact mathematical knowledge about the process or when knowledge is even unavailable. Many approaches using methods of artificial intelligence have been proposed in literature with respect to thermal comfort. On the one hand this may be justified with the fuzzy definition of thermal comfort and on the other hand due to the enormous difficulties in measuring and assessing thermal comfort. The following subsections will summarize some existing concepts of intelligent strategies with application to thermal comfort.

2.5.1 Fuzzy logic

Due to the nonlinear relationships between system variables and thermal comfort, [25] proposes fuzzy to control thermal comfort in a similar way as a human would do. He therefore uses heuristic terms to describe the level of comfort. Input variables are ambient temperature, engine coolant temperature, interior temperature, an one-dimensional image of the sun load and the set-point of user temperature. The system outputs were defined as intake air mode, discharge air mode, blend position and blower speed.

Reference [99] models the electrical system of a vehicle and proposes two fuzzy controllers in order to control blower speed and temperature inside the vehicle cabin. The emphasis on the research was not primarily based on thermal comfort, but rather on compensating the non-linear characteristics in the temperature and blower control process.

Reference [130] claims that temperature feedback in an automobile is not sufficient to achieve thermal comfort. An optimized fuzzy controller, based on Fanger's PMV index, is therefore proposed as automotive controller feedback. To simplify the system, only air temperature and air velocity are used as input variables. Metabolic rate is assumed to be constant at a rate of 1 met, relative humidity as h=50%, and clothing is assumed to be constant at 0.7 clo. Mean radiant temperature is defined to be equal to air temperature.

Reference [16] proposes a PID fuzzy controller and aims to control indoor PMV. To measure the PMV, a thermal comfort meter was used.

Reference [112] proposes a fuzzy logic controller to predict human thermal sensation in an automobile. Input variables are air temperature, various vehicle parameters as well as skin temperatures taken from thermocouples. The vehicle was however kept stationary during the tests and during data acquisition and passenger's desired air temperature value was tied.

Reference [73] aims to avoid iterative calculations for Fanger's PMV model and therefore suggests fuzzy logic to determine the PMV index. Input variables are air temperature, mean radiant temperature, air velocity, relative humidity, clothing insulation as well as activity level.

Reference [42] argues that it is impossible to use mathematical models for the design process of HVAC systems due to the complexity of calculations, human's vague and subjective sensation of thermal comfort and the difficulties to measure all variables in low cost. A fuzzy controller using air temperature, relative humidity, air velocity, radiant temperature, clothing insulation and metabolic rate is proposed. A similar concept has been published by [119].

2.5.2 Neural networks

With a similar argumentation, [139] proposes a neural network to predict the PMV index. Input variables are air temperature, mean radiant temperature, air velocity, relative humidity, clothing insulation as well as activity level. Similar work was done by [67], which incorporates human learning with a neural network to approximate PMV.

Reference [6] states that real-time calculation of the PMV model is necessary to use it in HVAC control systems and therefore suggests a neural network to estimate PMV. Input variables are air temperature, relative humidity, air velocity, globe temperature, wet bulb temperature and wall temperature.

Due to enormous technical efforts to measure operative temperature, [118] proposes a neural network to estimate the operative temperature in buildings. The concept is based on the assumption that the operative temperature can be estimated by knowledge of other variables which can be acquired more easily, for instance indoor and outdoor temperatures, the electrical power consumption in the room, wall temperatures, ventilation flow rates as well as the time of day.

Reference [89] presents a fuzzy logic network combined with a neural network which uses average air temperature and average humidity to predict thermal comfort. Similar research was done by [19].

Reference [59] optimizes the blower pattern and temperature distribution inside a vehicle cabin using three neural networks. The neural networks are used to control air flow volume, air outlet temperature and air outlet position.

Reference [65] suggests a neural network to predict automobile seat comfort using pressure sensors.

In order to predict clothing thermal comfort, [71] suggests a fuzzy neural network taking into account only body core and skin temperatures as well as their deviations.

Reference [125] proposes a neural network to predict the automotive passenger's thermal sensation. Input variables are limited to four skin temperatures.

Reference [39] suggests a neural network in order to estimate whole body thermal comfort, whole body thermal sensation, partial thermal sensation of face, left forearm, left hand and left foot. Input variables were 15 skin temperatures taken from different body parts.

Reference [68] proposes a neural network to predict occupant's thermal sensation. Input data was air temperature, air velocity, humidity and mean radiant temperature. Training data came from a thermal comfort survey. The neural network was verified for a number of situations

including fixed clothing and metabolic rates, as well as variable clothing, metabolic activities and different subjects.

2.5.3 Support vector machines

Reference [66] demonstrates the application of least square support vector machines (SVM) to estimate the PMV index as well as psychometric variables like humidity ratio, dew point temperature and enthalpy of air.

Reference [83] uses SVMs to predict thermal comfort indices like PMV, PPD and ET for vehicle application. As modelling data, air temperature, mean radiant temperature, relative humidity, air velocity, metabolism and clothing is used. Evaluation was done in an environmentally controlled climate chamber, using the seven-point ASRAHE thermal sensation scale.

2.6 Summary

There are three different concepts for automotive HVAC units available today. Automatic ones are supposed to control the cabin environment autonomously and compensate for all perturbations. However, in practice there is often only measured the in-cabin temperature and a simplified one dimensional image of the solar load is used. Systems therefore suffer from a lack of environmental sensory information and a deficient correlation to thermal comfort.

It is concluded that thermal comfort is a complicated factor involving various physical, physiological, as well as psychological variables. This is in contrary to the generally established opinion, that thermal comfort can be determined and modeled only by knowledge of air temperature. The involvement of physiological and psychological aspects considerably complicates the development of models and the assessment of thermal comfort. The next chapter will deal with these problems in detail and will propose solutions.

Theories dealing with thermal comfort in steady state and uniform environments have been available since the early 1970s. The most important contribution was done by P.O. Fanger, whose work is still the basis of present thermal comfort standards. Fanger recognized that due to individual differences, a climate that satisfies everybody does not exist. This is a very important conclusion, which affects the implementation and performance of control strategies for HVAC units. Conversely however, it should be possible to develop a HVAC control strategy, which is specially adapted to the individual.

There are many further indices and models available to predict and assess thermal comfort. The applicability of indices and models to the automotive environment is controversial, because most of them have been developed and verified in uniform and steady-state laboratory environments.

Some researchers claim, that the assumptions for those tests can't be transformed to real situations. In terms of this research, it is therefore suggested to evaluate thermal comfort in a real car incorporating real driving/traffic situations.

Thermal comfort in transient and inhomogeneous environments is still far from understood. Comprehensive theories and standards dealing with those environments do not exist and researchers are still busy with investigations. The vehicle cabin can be classified as such an environment, however of a much more dynamical nature and with more perturbations, than known from architectural structures.

In terms of this project, this means that one is hardly capable of extracting information from previous research and that the layout of the experimental setup can hardly be verified against existing literature. Methods for measuring thermal comfort can be distinguished in subjective, behavioral and objective methods.

Automotive industry predominantly adopts the concept of equivalent temperature, virtual thermal comfort models and thermal manikins to assess the automotive environment. However, it is concluded that no mathematical model can exactly represent human's behavior. A detailed argumentation, why thermal manikins and the principle of equivalent temperature are only applicable in a vehicle's design process, will be given in the following chapter.

Methods of artificial intelligence have been successfully applied in many engineering areas. In thermal comfort engineering, efforts have however been especially made in the approximation and simplification of existent thermal comfort indexes like PMV. It is noteworthy, that some researchers have applied those concepts also to the automotive environment, although it is well known that their underlying theories only apply to uniform and steady-state environments and may not be valid in automotive application. Little research has been done so far in thermal comfort evaluation using human test subjects, in combination with methods of artificial intelligence. Theoretically, strategies of artificial intelligence are capable of approximating any given non-linear function. It is therefore concluded, that artificial intelligence is a suitable concept to model thermal comfort in automotive applications.

However again, any technical implementation of thermal comfort, regardless of the quality and the complexity of involved control algorithms, cannot account for the individual differences in terms of thermal comfort perception. It is therefore considered as impossible to design a static system that satisfies all people simultaneously.

Chapter 3

Experimental Setup

Humans have preferences and judgments about their environment, which they have learnt from past experience. It seems straightforward to apply this methodology also to technical engineering processes. Reference [105] states:

'If people say that they like something or that they prefer something, it should be fed into the design process even if it cannot be proven with rational models.'

This is in contrast to the commonly established scientific approach. Engineers ideally investigate a problem in order to gather knowledge about a given unknown process in advance. This knowledge is then used to develop a model, or to propose a solution to the problem. This approach works well in cases where a human is able to clearly identify the problem and the system's performance depends on the researcher's knowledge about the modeled process. However, hardly any engineer will be able to solve a problem, or to suggest a solution to a problem, if he/she does not understand the process or its underlying theory.

In terms of this research, knowledge about the system 'human' is prevalently unknown. Information can only be gathered through measurements of the environment, in terms of an input vector, and human's behavior as corresponding output vector. In order to learn the underlying functionality from data implies the existence of a comprehensive data base, containing the necessary knowledge to which the system should adapt to. In terms of this research, this means:

- Information about the ambient environment,
- Information about the vehicle environment,
- Information about the correlation of thermal comfort to those parameters.

Data sets from field studies in architectural environments have been collected by various researchers over the last four decades. However, due to the peculiarities of the vehicular environment, this knowledge can't be utilized for this research. It is therefore necessary to develop a suitable framework for data collection in order to evaluate the thermal environment in an automobile. Data acquisition is followed by a data mining process to ensure consistency and a final modelling phase for system learning. This cycle is illustrated in Figure 3-1.

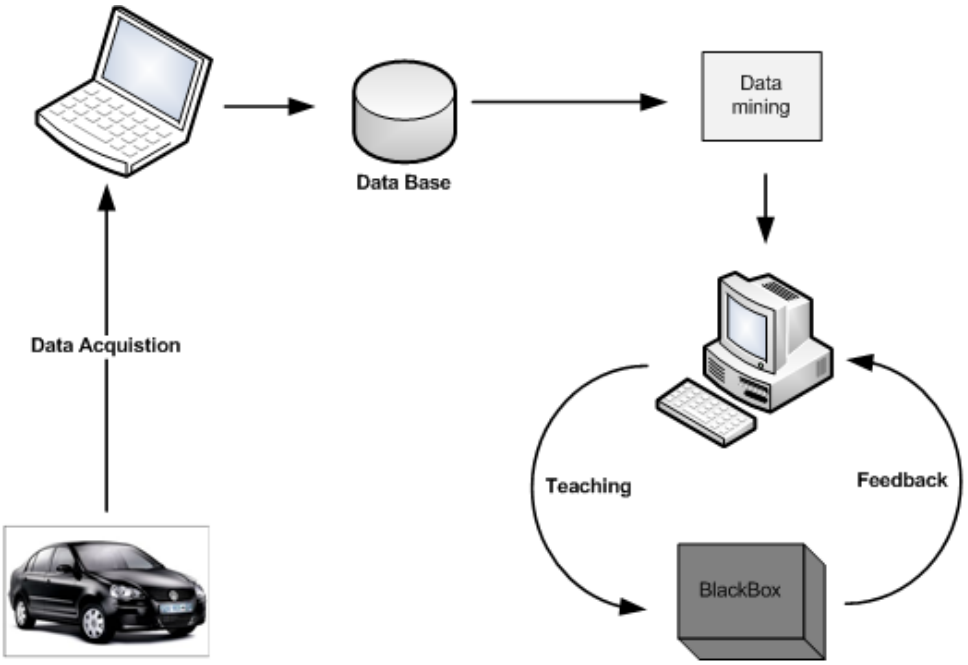

Figure 3-1: Procedure and architecture for data acquisition

Adequate tools have therefore to be developed and integrated to an experimental setup. This chapter will list the requirements and will describe the experimental setup in detail. Data mining and system learning methods will be described in Chapter 4 and Chapter 5.

3.1 Initial situation

In Chapter 2.2.7, the vehicle compartment was found to be of considerably more complex nature than architectural buildings. The state of the art in assessment of automotive thermal comfort is the use of heated sensors and manikins. These principles have been presented in Chapter 2.4.4.

The use of this methodology is theoretically absolutely justifiable due to the principle of human's perception of the environment. Chapter 2.2 points out, that humans are predominantly sensitive to heat exchange with the environment. It is therefore consequent to conclude that heat flux measurements may, theoretically, deliver more comprehensive results than just measurements of single physical variables. However in real world situations, apart from climate chamber tests, it is often not convenient or even impossible to use heated sensors or manikins for thermal comfort assessment. This is justified due to various secondary aspects which are of technical, economical and ergonomic nature. These include:

- Measurement of equivalent temperature from different instruments and different control strategies are not comparable to each other and are, due to complex environmental interactions, often hardly repeatable. In this context, it shall be mentioned, that for example, heat flux measurements are dependent of clothing insulation. However,

clothing properties themselves are a complex function of various other ergonomic factors, also including body posture [30],

- Instruments for measuring equivalent temperature have to be regularly calibrated. For long measurement series, a weekly calibration procedure is recommended [32]. In the author's opinion, this seems to be inappropriate for automotive application.
- Heated sensors must be installed at characteristic positions on the human body in order to obtain meaningful results. This is acceptable in laboratory environments. However, physically attaching any sensors to the passenger in everyday life is unpractical and will considerably influence his/her overall comfort sensation and satisfaction,
- During road tests manikins can hardly be used to evaluate driver's thermal comfort sensation [106]. Due to the same reasons, they can't be used as a HVAC controller feedback either,
- The integration of heated sensors in the vehicle's final design is considered to be difficult. This especially applies to omni-directional sensors, like those presented in [96],
- Sensor response to transient environments is slow and instruments often require recovery times of several minutes [32],
- Heated sensors and manikins are quite costly. 2008, quotations indicated a price range of about 13000€ for one heated sensor element including the appropriate control electronics. To cover the inhomogeneity of the vehicle compartment more sensors would be needed and would have to be installed.

It is noteworthy that during a vehicle's design process automotive manufacturers often simulate the environmental conditions in climate chambers using the principle of equivalent temperature to assess thermal comfort. However, in the final vehicle's design the interior vehicle climate is only controlled by in-cabin temperature in the majority of cases. It is therefore disputable, if present automotive HVAC units can cope with the specifications, which were identified for them during the vehicle's design process.

The author concludes that the use of thermal manikins and heated sensors is therefore limited applicable to measurement of thermal comfort in automotive environments. This may be less justified in today's existing sensor technology, but rather in the definition of equivalent temperature and its measurement requirements.

3.2 Specifications

During road testing, the vehicle is exposed to an extended range of environmental conditions and mechanical forces, like shocks and vibrations. Therefore specifications have to be defined in order to ensure that the equipment operates reliably under all circumstances.

3.2.1 Test procedures

Established test procedures for automotive HVAC units can be divided into three categories [21]:

- Transient conditions,
- Short transient conditions,
- Stationary conditions.

Transient testing conditions refer to heating and cooling of the passenger compartment under extreme environmental conditions. An example may be a cooling down process of a passenger vehicle, which has been previously soaking in the sun. This scenario is often simulated in climate chambers with the purpose of verifying the maximum cooling power of the HVAC system. These results are especially important in the design phase of a vehicle, because HVAC units are presently designed and verified against extreme and harsh environmental conditions [120]. The measured quantity is usually in-cabin air temperature, which gives an indication about the time to cool down or heat up the vehicle compartment. Nevertheless, due to the presence of high thermal asymmetries and air velocities during these tests, a very poor correlation is achieved in terms of thermal comfort perception and environmental parameters.

Short transient testing conditions aim to simulate small variations of interior and exterior climate. An example may be a change in cabin set-temperature, vehicle speed or sun load. Short transient conditions consolidate the overwhelming majority of conditions in every-day driving situations.

Stationary conditions rarely occur in automobiles. Steady-state conditions may be present in a truck cabin during the sleeping period of the driver [21]. However, nearly stationary conditions may also occur when for instance driving on a highway on a cloudy day, with no change in speed and ambient temperature.

This research mainly focuses on short transient and steady state conditions. In terms of transient conditions, it is postulated that extremes in environmental conditions with deactivated HVAC unit also induce extreme interior conditions. Therefore the correlation between input vector and output vector might not be consistent, because any arbitrary HVAC setting that helps to reduce thermal discomfort would be perceived as pleasant by the occupants.

However, the measurement equipment must still be able to distinguish between all three testing categories. Even in non-extreme environments, there is still a transient phase beginning with the start of each measurement. An example may be the gradually increasing coolant temperature from the point of starting the vehicle. This directly influences the temperature in the mixing chamber of the heater box and therefore also the vehicle interior. Additional influence is exercised by the occupants. The thermal state of the body, before entering the car, affects the response of a person during initial testing [41]. It is therefore important for the measurement equipment to be able to distinguish between testing categories, in order to produce consistent outputs.

3.2.2 Functional requirements

Measurement equipment is required to operate under a variety of environmental conditions. It must be insensitive to shocks, vibrations and it is required to continuously monitor the periphery, in order to prevent corrupt sensor recordings.

In terms of thermal comfort evaluation, literature points out, that questionnaires are time consuming and may put stress on the test subjects. This might influence the objective measure [32], [106]. It is therefore suggested to use computers for thermal comfort evaluation. This is especially true for automotive thermal comfort evaluation, where subjects are required to evaluate their comfort levels several times per minute, due to the overall transient conditions in the vehicle cabin.

Humans quickly feel a change in their environment and will immediately react to this change. It is therefore important that the instruments have small response times, in order for being able to recognize transient changes.

The following functional requirements have been identified for the experimental setup:

- Operation within a wide range of environmental conditions and resistivity against shocks and vibrations,
- Short response time to changes in environmental conditions,
- Continuous self-diagnosis of all peripheral components,
- Automatic thermal comfort evaluation using a computer,
- Synchronization of all data sources,
- Tools must be able to communicate with each other in a lossless, integrated way and must be flexible enough for customization.

3.3 Design framework

3.3.1 Relevant parameters

In Chapter 2.2.3, relevant comfort variables have been identified and another explicit experimental design is therefore not needed. In practice however, some of those parameters are nearly impossible to measure in terms of reasonably expense. This research is a trade-off between costs and accuracy, in order to keep the project as industry-related as possible.

3.3.1.1 Air temperature

In-cabin air temperature is the most frequent measured parameter in HVAC systems. This might be justified by the fact, that it can be obtained relatively easy and often people associate thermal comfort mainly with air temperature. There are many different methods to measure air temperature. ISO 7726 proposes three categories of instruments:

- Expansion thermometers,
- Electrical thermometers,
- Thermo anemometers.

However in practice, only thermometers with electrical output interface have significance. This is most probably because of economic reasons and convenient use in HVAC feedback control systems. The response time of the sensor element is predominantly dependent of its size and its heat exchange with the environment. The smaller the sensor element and the less its specific heat capacity, the less its response time. When measuring air temperature, special care must be taken to minimize the influence of radiation from surrounding surfaces [40]. According to [27], this can be achieved with:

- Reducing the emission coefficient of the sensor's surface. This can be done with polishing the sensor's surface or applying reflective paint,
- Reducing the temperature gradient between the air and surrounding surfaces,
- Shielding the sensor element against radiation,
- Using fan aspirated sensors in order to increase heat convection between the surrounding air and the sensor element.

In the major vast of automotive applications, fan aspirated sensors are used to measure in-cabin air temperature. Sometimes also infrared (IR) sensors are used, which aim to measure the average surface temperature in the sensor's field of view [47]. Both types of sensors are often integrated into the HVAC ECU. In terms of thermal comfort, [46] claims that fan-aspirated sensors may suffer from high response times. It has been proposed, that thermal comfort might be better correlated to breath temperature. Therefore an ultrasonic sensor, capable of measuring

bulk air temperature, has been proposed. However, the speed of sound is influenced by many other variables and [47] concludes, that in some cases, there is a shift of up to $\Delta\vartheta = 5℃$, compared to measurements with thermocouples.

3.3.1.2 Mean radiant temperature

Mean radiant temperature has major influence on thermal comfort perception and might cause discomfort, even if air temperatures are in acceptable ranges [33]. Some researchers believe, than it can have up to the same influence on thermal comfort than air temperature [45]. Sources of radiation are manifold and include for example dashboard and roof temperatures in extreme summer or winter conditions. Mean radiant sources can be measured with instruments being capable of integrating the radiation of an environment's surface to a mean value. Examples are black globe thermometers and two-sphere radiometers [74]. In terms of thermal comfort, ISO 7726 recommends ellipsoid shaped sensor elements, in order to account for the body shape of a human being. The response time of the instrument is dependent of its sensor diameter. Due to high response times, globe thermometers can hardly be used in transient environments [27]. The mean radiant temperature is often approximated using the temperatures of the surrounding surfaces as well as the corresponding angle factors. Latter approach was found to be also convenient for this research and has been described in Chapter 2.2.3.2.

3.3.1.3 Air velocity

Air velocity effects human heat exchange in terms of convection and evaporation. Air streams can be represented as vectors in a three-dimensional space. There exist various tools to measure directional and non-directional air velocity:

- Impeller anemometers,
- Hot-wire anemometers,
- Pulsed-wire anemometers,
- Thermistor anemometers,
- Ultrasonic anemometers,
- Laser Doppler anemometers.

Thermistor anemometers are often used to determine the air velocity in rooms [27]. In vehicle compartments, the small air outlets generate high air velocities and air fluctuations in the cabin. Air velocity is additionally often affected by localized phenomena, making it impossible to measure it accurately [129].

Air flow in the vehicle cabin also changes with infiltration rate which is a function of vehicle speed. At high speed, more air is forced into the passenger compartment due to increased air

pressure levels at air intake level. This effect was verified with a measuring setup illustrated in Figure 3-2.

(a) **(b)**

Figure 3-2: Air velocity measurements; (a) Front air outlet, (b) Passenger head

An impeller anemometer was installed at one front air outlet as well as at head position. This is shown in Figure 3-2(a) and Figure 3-2(b) respectively. Experiments were conducted with a constant blower load of 50% while the aperture ratios of the air outlets were kept constant. The results for the air velocity v_a, measured at nozzle level in dependence of the vehicle speed v_v, are presented in Table 6.

Table 6: Air velocity in dependence of vehicle speed at nozzle level

v_v [km/h]	v_a [m/s]
0	4.8
60	5.1
110	5.6

The results of the measurements, taken at head level, are shown in Table 7.

Table 7: Air velocity in dependence of vehicle speed at head level

v_v [km/h]	v_a [m/s]
0	0.6
50	0.7
80	0.9

It is therefore evident that the vehicle's dynamic condition has an influence on the air velocity and most probably also on the air distribution inside the vehicle compartment. According to Table 7, this effect might probably be perceived by the occupants.

Due to the enormous non-uniformity of air distribution and the variety of possible air-flow patterns inside the vehicle cabin, the author considers it as impossible to measure air velocity with one, or more single discrete sensors, at all comfort relevant positions.

In this research it is rather assumed, that air velocity and air distribution inside the vehicle cabin is a function of mainly

- Vehicle speed v_v,
- Flap position f,
- Blower load b.

This dependence can be mathematically expressed as

$$v_a = f(v_v, f, b). \quad \textbf{(19)}$$

It is assumed, that the system can internally reveal the thermal comfort relevant correlation. Real measurement of air velocity and exact knowledge of air distribution is therefore not explicitly needed.

Adjustability of the air outlets can additionally inherently influence air velocity and air distribution within the vehicle compartment [60]. In terms of this research, nozzle position as well as nozzle direction have therefore been permanently fixed in the vehicle.

3.3.1.4 Humidity

Humidity can be measured in different denotations. Absolute humidity represents the actual amount of vapor content in the air. Relative humidity refers to the vapor content of the air according to the theoretical maximum possible amount, air is able to absorb at the given air temperature and atmospheric pressure. There are various instruments available to determine absolute and relative humidity:

- Dew point hygrometers,
- Lithium-chloride hygrometers,
- Capacitive hygrometers,
- Absorption hygrometers,
- Psychometers.

Detailed descriptions of the instruments can be found for instance in [27]. However, for automotive application only capacitive hygrometers are applicable due to economic and maintenance reasons. For human heat exchange with the environment, only absolute humidity is of relevance [27] and vapor pressure can be considered as constant within the vehicle cabin [32]. Measurements of relative humidity can be converted to absolute humidity with knowledge of local air temperature. Literature claims, that due to the positive effect of humidity in heat stress, heat exchange via evaporation in the automobile cabin can be neglected [32]. However, Chapter

2.2.3.3 pointed out that even if humidity had no primary influence on thermal comfort, it might still influence thermal comfort perception secondly, on an air's freshness point of view. Measurement of relative humidity has therefore also been implemented in this research.

3.3.1.5 Metabolic rate

Human metabolic activity is extremely difficult to measure. Available methods are summarized in ISO 8996 [29]. Presently, there are four principles to estimate or measure human energy expenditure:

- Screening methods,
- Observation methods,
- Analysis methods,
- Expertise methods.

Screening methods refer to the estimation of typical metabolic rates according to various business professions, or to classify different activities into discrete categories.

Observation methods use external experts to estimate metabolic rates. Thereby activity is estimated due to observations of work load at individual body parts and body posture. It is also possible to establish a correlation using tables for specific activities. An example of such tables has been presented in Chapter 2.2.3.4.

Analysis methods refer to measurements of heart rate and its correlation to metabolic rate. Heart rate H can be composed as:

$$H = H_0 + \Delta H_M + \Delta H_S + \Delta H_T + \Delta H_N + \Delta H_E, \quad \textbf{(20)}$$

with:

H_0 Heart rate in idle state,

ΔH_M: Rise in heart rate due to dynamic muscular work,

ΔH_S: Rise in heart rate due to static muscular work,

ΔH_T: Rise in heart rate due to thermal stress,

ΔH_N: Rise in heart rate due to psychological stress,

ΔH_E: Rise in heart rate due to other factors.

Heart rate can be considered as linear in a range from 120 beats/minute up to about 20 beats/minute below the person's maximum heart rate [29], [49]. In this range, the psychological term of equation (20) can be neglected. The equation also shows that heart rate is dependent of many other factors, which are primarily not correlated to metabolic activity. Additional factors that may influence human's heart rate are for instance gender, age and body weight.

Expertise methods refer to measurements of metabolic activity in terms of the subject's oxygen consumption. It is also possible to use chemical methods and samples of urine to estimate an

average metabolic rate for a given period of time. Other methods determine whole body heat loss or measure the body's total mass loss over a period of time. Additionally, it is possible to estimate metabolic activity with knowledge of core temperature. [109] developed and verified an empirical human thermal comfort model using subjects, who had to swallow wireless temperature sensors, in order to measure the temperature of the distractive tract.

All existent methodologies to measure human's activity rate are quite extensive and impractical for the use in automotive applications. Any attachment of sensors or insertion of sensors in body orifices is considered to be inadequate for this research.

In case of automotive applications, it is assumed that internal activity is predominantly linked to the driving situation. For instance, it is considered that driving on a busy road with many stop-and-go conditions may put more stress on the subject than driving on an empty highway at constant speed. It is therefore assumed that metabolic activity W can be related to variables, which provide information about the dynamic behavior of the vehicle, as well as the traffic situation. Information about the traffic situation can be best derived from the driver's interaction with the vehicle.

It is therefore suggested to analyze the frequency of alternating changes T of acceleration and brake pedal, in combination with the standard deviation of the vehicle speed σ_v. Mathematically, this means:

$$W \sim f(T, \sigma_v). \quad \textbf{(21)}$$

The number of alternating changes in acceleration and brake pedal is determined according to the following time-discrete 'traffic' function TR[n]:

$$TR[n] = \sum_{k=1}^{k=b} T[n-k] \;\; with \;\; \{T[n-k] = 0 \; for \; (n-k) < 0, \quad \textbf{(22)}$$

with:

n: Sample time,

b: Number of observation intervals.

In terms of this research, the constant b was chosen to be 15. With t_s=10s, equation (22) allows for a total observation interval of 150s. With changes in traffic volume, TR[n] will gradually increase or decrease with time. This is thoroughly a correct assumption, since human stress level is considered to show a similar characteristic.

3.3.1.6 Clothing insulation

Measurement of clothing insulation is extremely difficult [55]. ISO 9920 describes three methods to determine clothing insulation:

- Estimation of clothing insulation with tables for single pieces of clothing,
- Estimation of clothing insulation with tables for entire clothing combinations,
- Measurement of clothing insulation with heated manikins.

However, neither of these methods is suitable for application in automotive feedback control systems. The estimation of clothing insulation is vague and measurements are often imprecise. Therefore methods for measurement will not be described in this context and further details can be found in literature, such as [31].

For completeness it is mentioned that clothing insulation also depends on:

- Body posture,
- Automotive seat contact,
- Atmospheric air pressure,
- Humidity,
- Washing cycles of fabrics.

However, clothing insulation plays an important role in assessment of thermal comfort. In this research, it is assumed that subjects have consistent clothing habits while driving a car. It is considered as implausible, that a person chooses different clothing insulations for thermally identical environments. However, it must be considered that basic clothing insulation may vary during the year. By trend, basic clothing insulation is considered to be higher during winter than in summer. This will most probably cause variations in measurements results, according to the season of the year.

3.3.1.7 Solar load

Solar load has significant influence on thermal comfort in a vehicle compartment. It is estimated, that 50% of the HVAC unit's cooling load in recirculation mode is due to solar heat gain [128]. Any exterior and interior surface absorbs and reflects solar energy and any surface that absorbs solar energy will increase its temperature as a consequence. About half of the solar energy consists of UV, V and IR rays, whereas IR contributes about 50% towards the total solar spectrum [33]. The effect of the solar spectrum on thermal comfort is controversial. References [72] and [51] cite studies emphasizing the influence of visible and middle infrared spectra towards thermal comfort, while others put the emphasis on long wavelength IR radiation. Reference [51] doubts the expressiveness of those studies with respect to thermal comfort, because they were conducted with high spectral-separated radiation levels. Based on testing, [51] concludes that in real life situations only radiation level, and not its spectral composition, is relevant for the thermal response of subjects. Due to large glazing areas and asymmetric cabin geometry, sun radiation may project complex patterns onto the human body. Some examples are

shown in Figure 3-3, which have been taken at different times of day and different positions of the vehicle relative to the sun. Radiated areas have been yellowly intensified. The azimuth- and elevation angles have been marked with ‘A’ and ‘E’ respectively.

(a) **(b)** **(c)**

Figure 3-3: Sun radiation on human body; (a) -10˚A/40˚E, (b) +20˚A/15˚E, (c) -60˚A/40˚E

Sun intensity is normally measured with pyranometers, which produce a linear thermo-voltage in dependence of the sun intensity. Due to economic reasons, automotive industry applies photodiodes instead. There are mainly three kinds of automotive solar sensors available today:

- Single zone solar sensors,
- Dual zone solar sensors,
- Quad zone solar sensors.

First ones consider the whole passenger compartment as one single zone. This type of sensor is usually used in combination with single zone HVAC units. Plural zone units allow passengers to set up individual climatic settings. For those systems, dual zone sensors or even quad zone sensors are installed. Latter ones are predominantly used in premium vehicles, where the rear passengers are required to have also the possibility to set-up an individual climate. Figure 3-4 illustrates the principle layout and shows an example of a dual zone solar sensor. Diffusers are thereby attached to impress the sensor with a specific characteristic. The sensor’s cover is usually transparent for IR radiation. The problem with those conventional sensors is the ambiguity of the output signals [90]. For instance, a low sun with a strong radiation may cause the same sensor output as a high sun with low solar radiation.

(a) **(b)**

Figure 3-4: Dual zone solar sensor [82]; (a) Schematic, (b) Example of implementation

To overcome this limitation a novel three-dimensional sensor is used for this research. This allows for detailed differentiation of various radiation patterns, like those illustrated in Figure 3-3.

3.3.2 Sampling rate

Thermal comfort standards like ISO 7730 or ASHRAE do not give any indication how often environmental variables should be sampled in order to obtain meaningful results. This might be justified by comparatively slow ramps, which occur in architectural buildings. However, for draught determination it is recommended to monitor the mean values for air temperature and air velocity for a period of three minutes with a sampling rate of 5 Hz [75].

Choosing a reasonable sampling time is of immense importance for the measurement of thermal comfort parameters. For instance, if sampling rate is chosen too low, transient conditions will not be detected. This may result in loss of valuable information. On the other hand, if sampling rate is chosen too high, a hypersensitivity to transients and distortions may occur. This can influence system stability and additionally results in an overload of data.

Literature reveals different sampling rates for similar concepts. Reference [20] analyses the airflow in a vehicle compartment with 72 temperature sensors which are sampled with 0.2Hz. Similar research has been conducted by [135], which has chosen a sampling rate of 0.1Hz. This is confirmed by [32] who recommends a sampling time t_s of 10s for heating up and cooling down measurements in a vehicle cabin. Reference [41] evaluates thermal comfort in a vehicle with ballots every two minutes in the first 30 minutes and afterwards at five minute intervals.

To determine an optimal sampling rate for this research, some experiments in a car have been conducted. The basic idea is that the sampling rate should be as low as possible, but high enough for being able to detect the most transient source, influencing thermal comfort. This source was determined to be sun radiation. Subjects were therefore placed in a pre-conditioned vehicle, which was parked in the shadow. It was ensured that the subjects felt comfortable inside the car before the test started. After that, the vehicle was directly moved into the sun at a sun intensity of roughly I=1000 W/m^2. It was thereby ensured, that some body parts were directly exposed to sun radiation. The subjects were asked to report discomfort immediately and that time was measured. It was paid attention, that during the tests similar body parts were radiated and the subjects wore similar clothing. The subjects reported discomfort after periods ranging from 5s to 15s. The differences in response times can be explained with individual differences of thermal sensitivity.

According to these results, t_s=10s has been chosen for this research.

3.3.3 Human response

Measuring the human response to the thermal environment is the closest information researchers can obtain [33]. An established principle to evaluate thermal comfort is therefore the use of subjective methods, which have been summarized in Chapter 2.4.1. However, those scales have some disadvantages like imprecise wordings and plurality of meaning to the subjects. This can be explained with the semantic properties and variety of languages, whose effects cannot be easily compensated for. It can also not be assumed that steps within scales are equally spaced [93]. As a rule of thumb, evaluation scales should be as detailed as necessary but as simple as possible. Both effects are of opposite nature and a trade-off must be found. Too detailed evaluation scales might exceed the subject's thermal sensitivity and might lead to inconsistent data acquisition. With application to the automotive environment there are mainly two difficulties with regards to evaluation scales:

The transient environment in an automobile requires comfort evaluation within short time intervals. For this research, the intervals are equal to the sampling rate, meaning that subjects are required to evaluate their environment every ten seconds. This would probably overstrain the subjects.

Secondly from a driver's point of view, it is considered to be irresponsible and unpractical to demand filling questionnaires with a frequency of 0.1Hz during road testing. It is therefore required to develop an evaluation system which can be used intuitively without reducing driver's ability to focus on traffic situations. For this research, two approaches have been developed to correlate measurements to thermal comfort:

- Electronic evaluation using a thermal preference scale in combination with a draught preference scale,
- Indirect evaluation of thermal comfort using the HVAC controller's settings.

The second approach avoids direct thermal comfort evaluation and assumes that the occupant interacts with the HVAC controls in such a way, that thermal comfort will always be maintained in the vehicle cabin. According to the magnitude of change, it is possible to estimate the degree of comfort or discomfort. This principle will be used in the further course of this thesis.

3.3.4 Preliminary investigations

Since there is no instrument available that ideally fulfills all the specifications for this research, it was investigated if different tools can be combined to an integrated experimental setup. Initial testing was therefore done using standard measurement and data acquisition equipment, kindly provided by Volkswagen South Africa Ltd.

Several NiCr-Ni thermocouples have been connected to a Thermo-Scan®[5] interface. The Thermo-Scan interface and the NiCr-Ni thermocouples are shown in Figure 3-5(b) and Figure 3-5(c) respectively. A top-up interface was additionally developed, in order to assess thermal comfort and to serve as a gateway for the solar sensor. This is shown in Figure 3-5(a).

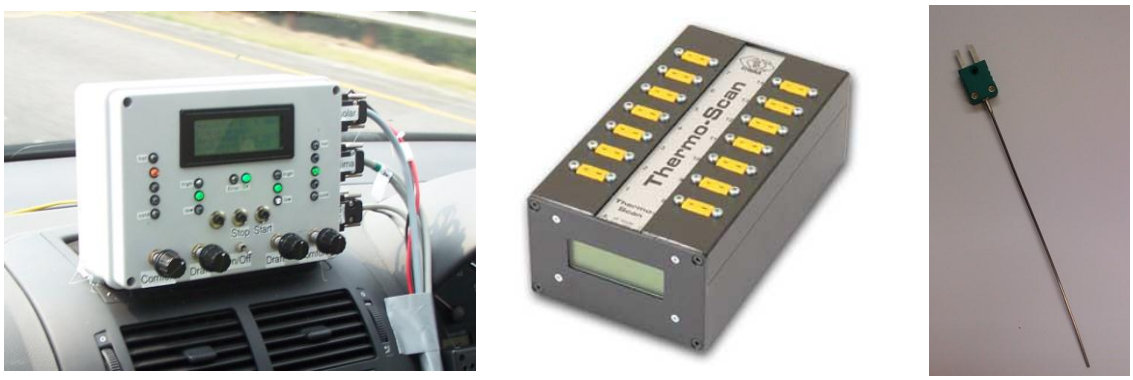

(a) **(b)** **(c)**

Figure 3-5: Preliminary experimental setup; (a) HMI, (b) Thermo-Scan, (c) NiCr-Ni thermocouple (Type K)

The software package INCA[6] was used as superior instance to control and synchronize all data sources. A connection to the comfort interface and to the vehicle's Powertrain CAN has been established with a dual channel CAN card. The Thermo-Scan has been connected to a Laptop PC via RS232 interface. This configuration is shown in Figure 3-6.

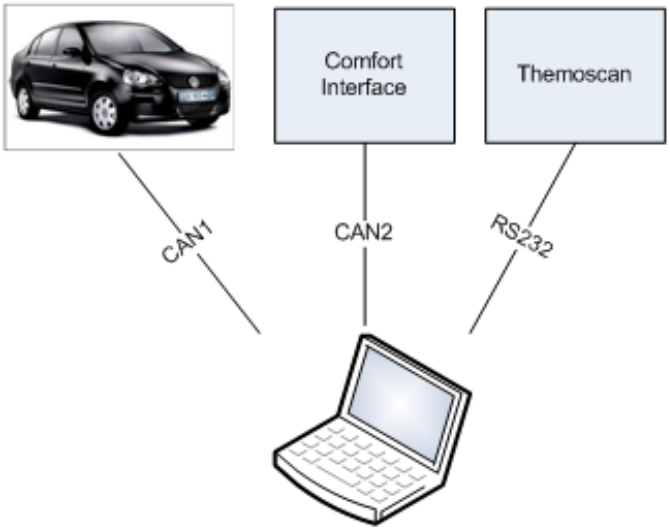

Figure 3-6: Distributed measurement system

[5] An interface from CSM GmbH, for the connection of up to 14 NiCr-Ni thermocouples
[6] A commercial calibration, measurement and application software package for automotive applications developed by ETAS GmbH

After some initial testing, is has been observed that some of the thermocouples failed unpredictably during road testing, which resulted in irrationally high in in-cabin temperature readings. This problem was found to be the consequence of connectors coming loose sporadically due to vibrations during road-testing. INCA does not implement any fault detection and does not offer any diagnostic services. Data acquisition takes place irrespective of sensor readings being plausible or not. Information taken from bugged sensors is hardly correctable after measurement. Faulty data induces complications during system learning and probably affects the system's performance.

Secondly, it was observed that data from different sources cannot be synchronized properly with the available equipment. Data is being recorded with time stamps and would have to be synchronized thereafter manually. This is a complex, time consuming and error-prone process, which may also result in faulty correlations. In terms of this research, INCA was considered not to be flexible enough for customization. Particularly, the system's sampling rate could not be freely adapted to meet the requirements of this research.

Additionally, a hard wired prototype of the comfort interface turned out to be inadequate for road-testing, because connections came loose during road testing. This problem can be avoided by the use of a printed circuit board (PCB) design.

Finally, it was concluded that some of the requirements in Chapter 3.2.2 cannot be met with the available tools. Due to the lack of alternative systems, it was therefore decided to develop a novel comfort acquisition system, incorporating all functions and requirements which have been identified for this research.

3.4 Hardware design

This section will discuss the hardware concept of the experimental setup and will also address the integration into the research vehicle. For the rest of this thesis, the term 'blower level' refers to the setting of the in-cabin air vent, which has discrete values of 'one', 'two', 'three' and 'four'. Similarly the term 'flap position' refers to the position of the air distribution flaps within the heaterbox and specifies the direction of the provided air flow. Latter domain is limited to 'feet', 'feet-head', 'breast', 'breast-head' and 'head'.

3.4.1 Concept

For this research, a Volkswagen Polo was used as an experimental platform. The exterior color of the vehicle was chosen to be black, in order to maximize the effects of sun radiation and energy absorbance. The vehicle is shown in Figure 3-7.

Figure 3-7: Research vehicle

The experimental setup serves as integrated platform for measurement, data acquisition, thermal comfort evaluation and HAVC emulation. It therefore incorporates various analog and digital interfaces to connect periphery. Vehicle parameters are directly obtained from the vehicle's powertrain bus through a high-speed CAN link. A Liquid Crystal Display (LCD) has been implemented for visualization of measurement variables as well as for monitoring the system status. Two four-way joysticks allow for comfort/draught evaluation for driver and passenger as well as setting up the interface. Data logging to a laptop PC is done via high-speed CAN link. The comfort acquisition unit is controlled by Atmel ATMEGA8 MCU via background debug mode (BDM). This allows easy inline re-programming of the comfort acquisition unit's firmware. For software development, ATMEL AVRStudio® has been used. In detail, the experimental setup consists of:

- Nine digital temperature sensors,
- One analog humidity sensor,
- One digital three-dimensional solar sensor,
- One interface to the HVAC controller,
- One fan aspirated temperature sensor,
- Two 4-way joysticks,
- One 500kbs high-speed CAN connection to the vehicle's powertrain bus,
- One 125kbs high-speed CAN connection to laptop PC,
- One 125kbs low-speed CAN connection to the vehicle's comfort Bus,
- One 240x128 dot matrix LCD.

The overall concept is presented in Figure 3-8.

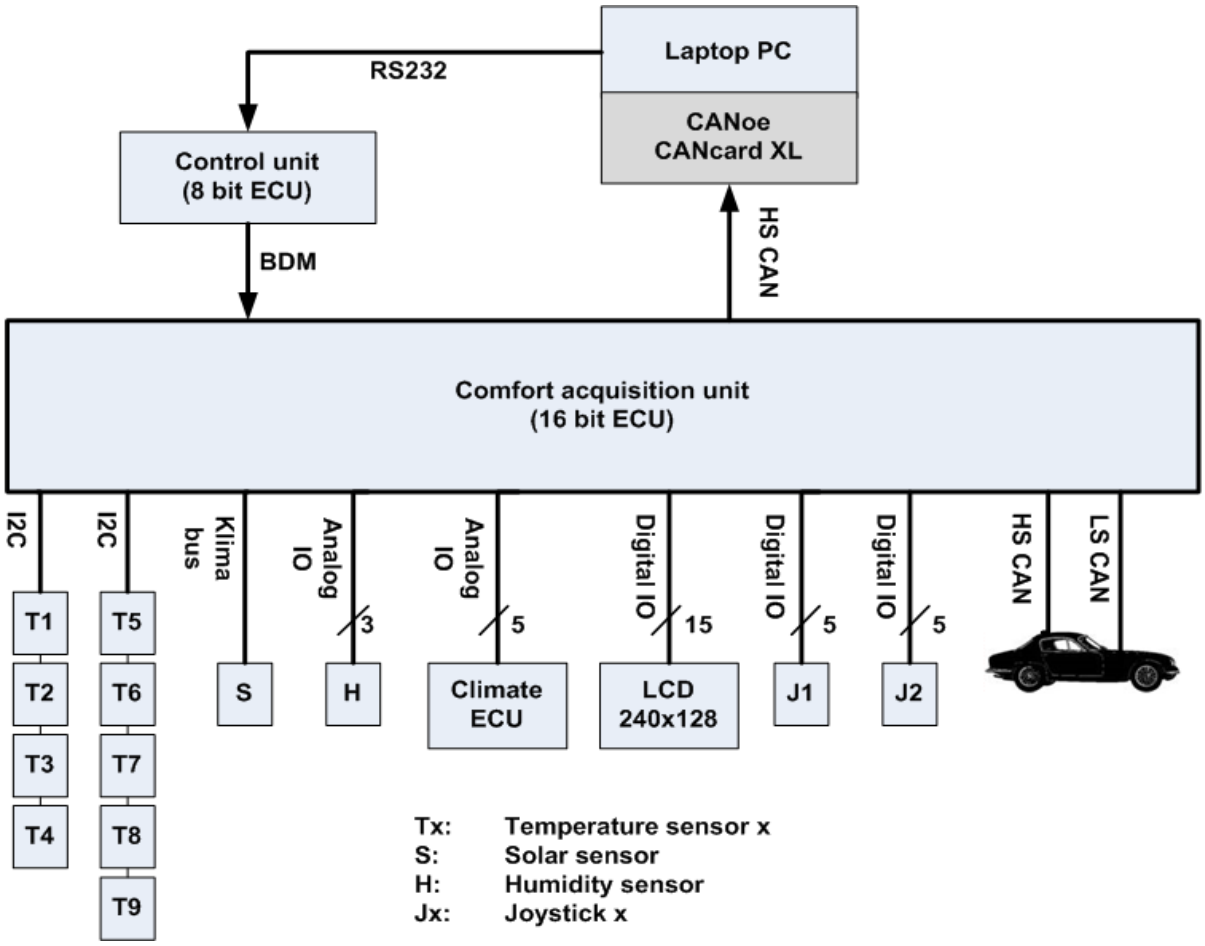

Figure 3-8: Experimental setup overview

The computing core is based on a 16-bit Freescale MC9S12DP512 MCU rated at 48MHz. This controller family was developed for automotive applications and includes a large variety of on-chip peripherals. More specification details can be found in [38]. For software development in ANSI-C, the Metrowerks Codewarrior® development suite has been used. The comfort acquisition equipment was installed in the boot of the research vehicle. This is shown in Figure 3-9.

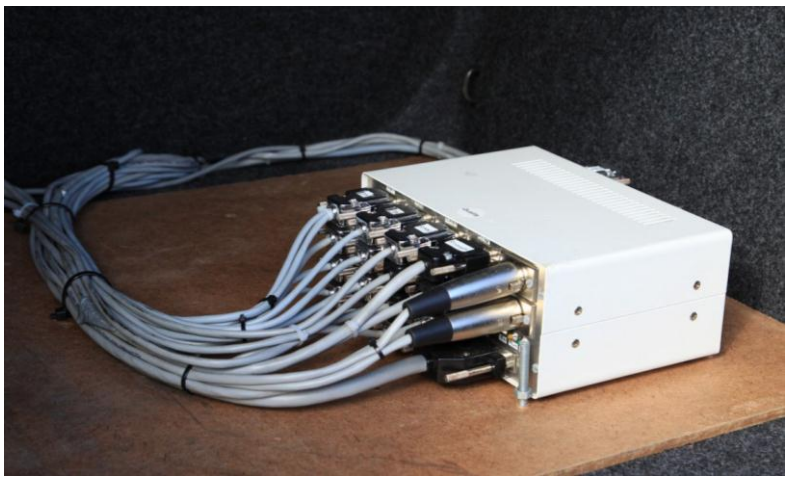

Figure 3-9: Installation of measurement equipment

Shielded cables were used for all electrical in- and outgoing connections in order to minimize the influence of electrical distortions and to avoid interventions with the vehicle's internal electronics. Figure 3-10 shows the installation of the HMI and the LCD in the real vehicle.

Figure 3-10: HMI and display installation

The system integration is shown in Figure 3-11.

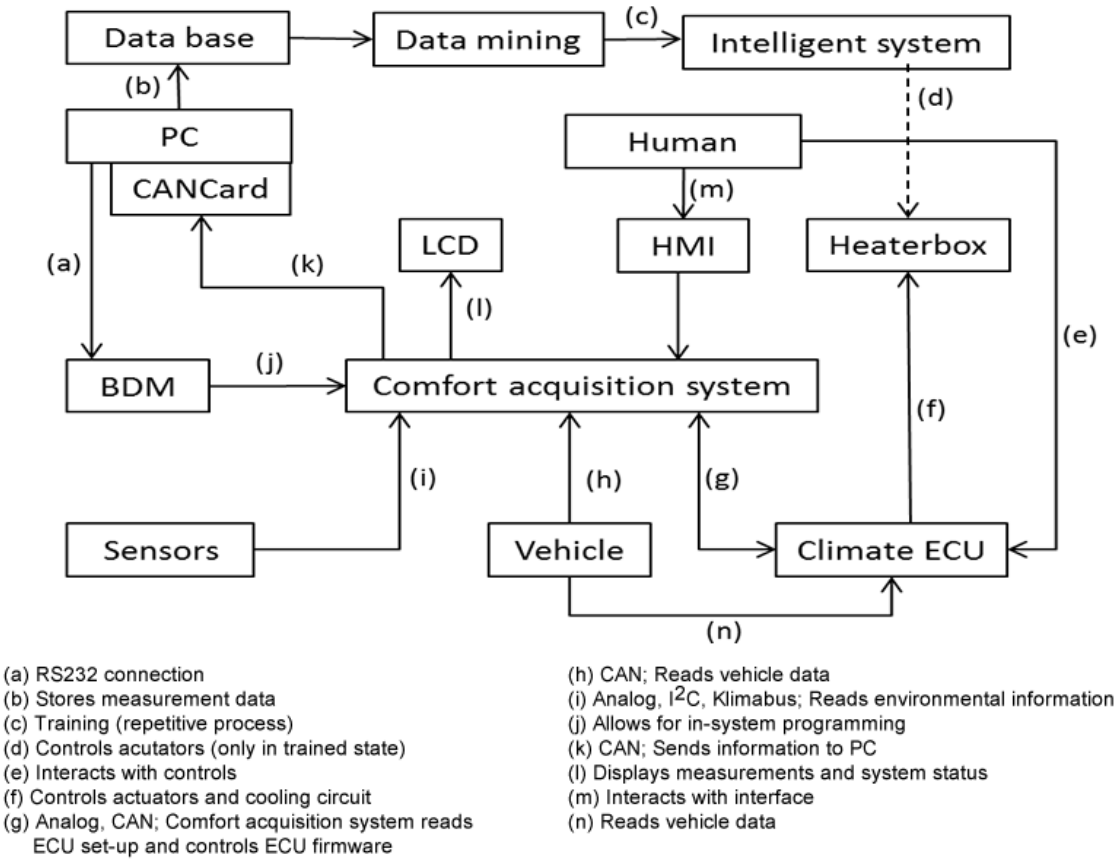

Figure 3-11: Components of thermal comfort acquisition and system control

3.4.2 Temperature sensors

Nine digital DS1631 high-precision digital temperature sensors, manufactured by Maxim Integrated Products Inc., have been installed in the vehicle compartment to measure temperature at distinctive locations. The sensors have been connected via I^2C bus. This bus system was introduced by Philips Electronics N.V. in 1992. Originally, it was developed for the use in consumer products, in order to link a small number of devices on a single electronics card. Nowadays, the I^2C protocol has been established as a universal interface for periphery connections. Communication is done with one clock and one data wire. The bus connection principle is illustrated in Figure 3-12(a). The format of a typical Read/Write sequence is shown in Figure 3-12(b).

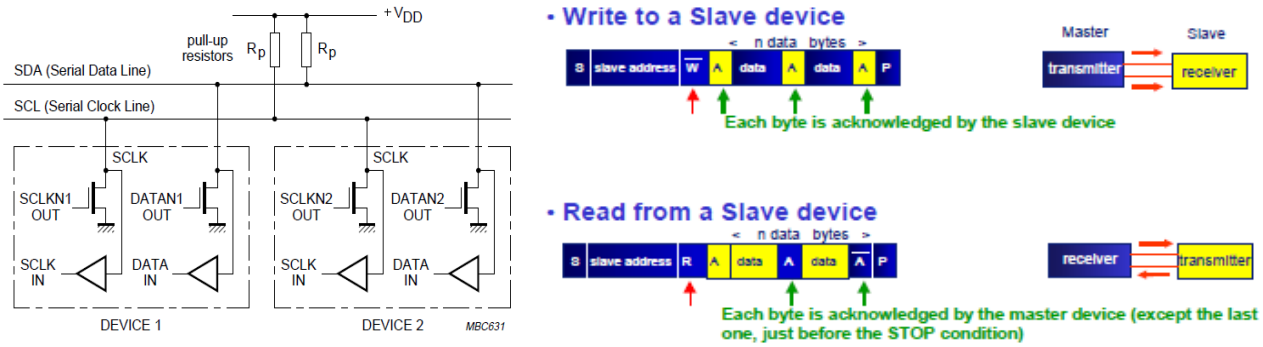

(a) **(b)**

Figure 3-12: I2C Bus Structure [95]; (a) Bus connection, (b) Data flow

Further information about the I^2C bus can be found in appropriate literature, such as [95]. The DS1631 thermostats were chosen because of:

- High accuracy of $\Delta\vartheta = \pm 0.5℃$ in a wide temperature range from $0 \leq \vartheta \leq +70℃$,
- Reliable MCU connection due to a digital interface,
- Low drift rates over time ($\Delta\vartheta$ =± 0.2˚C/30 years at ϑ = +40˚C).

Digital signals are more robust against electrical interferences, since there is no need of leading and amplifying small analog voltage levels. This is of special importance in harsh environments like automobiles. Additionally, digital transmission protocols make it possible to easily implement basic diagnostic functions. The sensor's resolution can be variably programmed from 9 to 12 bits. For this research, the resolution was set to 11 bits, which is equivalent to a maximum temperature resolution of $\Delta\vartheta = \pm 0.25℃$. The pinning of the DS1631 thermostat is shown in Figure 3-13(a). More detailed technical specifications can be found in [78]. In order to facilitate the installation inside the vehicle cabin, a PCB was developed to carry the sensor. This is shown in Figure 3-13(b).

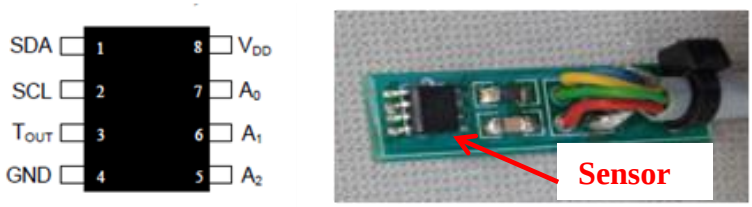

(a) **(b)**

Figure 3-13: DS1631 Digital temperature sensor; (a) Footprint (b) Installation on carrier PCB

3.4.2.1 Instrument panel

Figure 3-14 shows the locations of temperature sensors, which have been installed in the center console of the vehicle compartment.

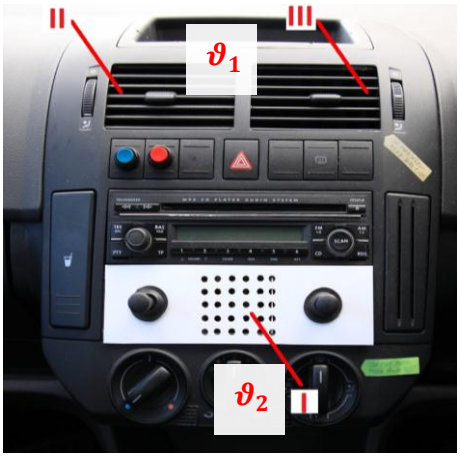

Figure 3-14: Temperature sensor locations

To estimate the vehicle's cabin mean air temperature ϑ_2, an air aspirated sensor was installed behind the perforated white cover at position 'I'. A conventional 12Vdc fan from a desktop computer was used to draw air from the interior, passing the sensor element. However, in order to reduce airflow, the fan was powered down and was supplied with V=8Vdc. The current was kept in a narrow range allowing only I=70mA (±2.5mA). This is continuously monitored by software. In case of violation, data acquisition is stopped immediately and an error message is produced. The configuration is shown in Figure 3-15.

Figure 3-15: Installation of fan-aspirated sensor element

At positions ‘II’ and ‘III’ in Figure 3-14, two temperature sensors have been installed to estimate the mixing chamber’s air temperature ϑ_1. For installation, the controls and instruments had to be removed. The air-distribution inside the heaterbox is strongly stratified and the flow field is considered to be quite turbulent. A better measurement location is therefore in between the heaterbox and the connection pipes to the dash board’s side windows air outlets. This is shown in Figure 3-16(a).

(a) **(b)**

Figure 3-16: Temperature sensors at front air outlet; (a) Overview, (b) Enlarged frontal air outlet section

Figure 3-16(b) shows an enlarged section of the frontal air outlet. It shows the location of the sensors, as well as the permanent openings, which are independent of the flap position. These openings always lead some air to the side windows in order to prevent misting. This ensures that always some air is being led across the DS1631 thermostats.

3.4.2.2 Dashboard

In general, the dashboard is the largest continuous part of plastic in vehicles. It is located behind the windscreen and is directly exposed to sunlight. The effect of radiation absorptivity is additionally intensified due to its black color. The dashboard temperature may rise up to $\vartheta_7 = +80℃$ during summer season [107]. Reference [21] even indicates a range of up to $\vartheta_7 = +100℃$. It is assumed that the dashboard is therefore the most intense radiation source in the vehicle. It is therefore suggested to measure the temperature of the dashboard as an approximation for the mean radiant temperature inside the vehicle cabin. Figure 3-17(a) shows the measurement of the dashboard temperature ϑ_7.

(a) **(b)**

Figure 3-17: Measurement of dashboard temperature; (a) Sensor position, (b) Sensor installation

Figure 3-17(b) shows the sensor attachment at the dashboard's body. To improve conduction from the dashboard surface to the sensor element, heat conduction paste was used. The sensor itself was additionally reinforced with cable ties and epoxy glue, to make it insensitive against shocks and vibrations.

3.4.2.3 Vehicle cabin

Literature does not clearly indicate at which and at how many locations inside the vehicle compartment, in-cabin temperature should be measured. In buildings, ASHRAE Standard 55P specifies three measurement heights for sitting persons at 0.1m, 0.6m and 1.1m above floor level. However, in the automotive environment such a standard would not deliver meaningful results due the extreme inhomogeneity of the cabin. Chapter 2.2.6 emphasizes the importance of head and feet for thermal comfort sensation. It was therefore decided to install temperature sensors at head and feet level for each driver and front passenger. This approach seems to be compliant with studies from other researchers [21], [37]. However, there are also other concepts available in literature. For instance, [62] assesses thermal comfort during the heating period of a vehicle and installed sensors at feet, knee, breast and head positions. For this research, thermostats were placed at head and feet level. The sensor locations for head level are shown in Figure 3-18.

Figure 3-18: Temperature sensor positions at head level

Figure 3-19 indicates the sensor positions at feet level.

Figure 3-19: Temperature sensor positions at feet level

It is important to note, that neither the sensors at head level nor those at feet level have been shielded against radiation. This means that the sensors are also sensitive to radiation to some extent. Due to general limited roof insulation in vehicles, this may have advantages for extreme ambient conditions. On the other hand, the plastic parts at feet level may gradually heat up due to their closeness to the heater box's heat exchanger and might therefore also cause radiation discomfort at feet level. The black colored package of the temperature sensors enhances the sensors' sensitivity to radiation.

3.4.3 Humidity sensor

The absolute vapor pressure is approximately constant within the vehicle cabin [88]. It is therefore sufficient to measure relative humidity in combination with temperature at only one location inside the vehicle compartment. The measurement position of both, relative humidity h and cabin roof temperature ϑ_5, is shown in Figure 3-18.

For this research project, a HIH 4000 sensor manufactured by Honeywell C&S was chosen, because of:

- High accuracy (Δh = ± 3.5%),
- Linear output voltage,
- Low drift over time (Δh = ± 0.5% per year at ϑ_a =+25˚C).

More technical specifications can be found in [54]. Figure 3-20(a) shows the sensor element. For easy installation, the humidity sensor has been also mounted on a PCB. This is shown in Figure 3-20(b).

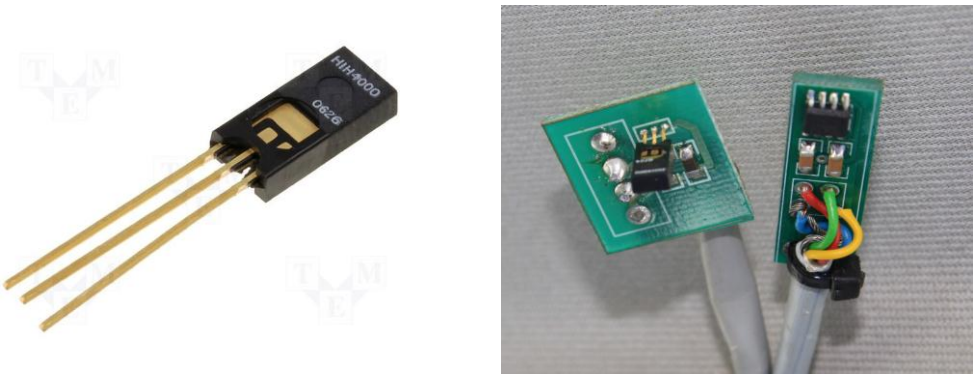

(a) **(b)**

Figure 3-20: Humidity sensor; (a) Sensor element; (b) Installation on PCB

The sensor is supplied with V=5Vdc and produces an output voltage, closely linear in dependence to relative humidity. The precision can be improved by using a second order polynomial. However for this research, approximation through a straight line is considered to be sufficient. The humidity can be calculated according to:

$$h = \frac{V_o - 0.16V_S}{0.0062V_S}, \quad [\%] \qquad \textbf{(23)}$$

with:

V_0: Sensor output voltage [V],

V_s: Sensor supply voltage [V].

3.4.4 Solar sensor

In Chapter 2.2.7, the influence of the sun on thermal comfort in vehicles has been pointed out. For this research, an innovative, custom-programmed three-dimensional solar sensor has been used, which is capable of measuring the sun's intensity I, azimuth angle φ and elevation angle Ψ. Figure 3-21(a) shows the principle.

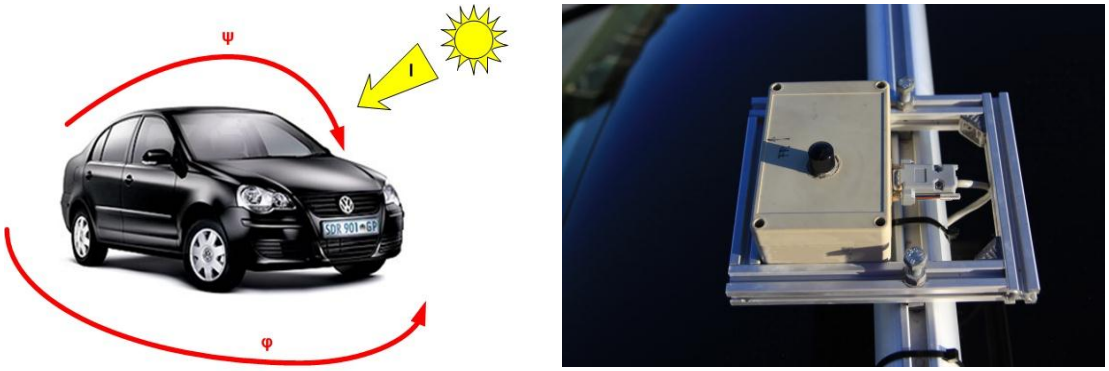

(a) **(b)**

Figure 3-21: Solar Sensor; (a) Sun angle definitions, (b) Sensor position on vehicle

The solar sensor was mounted on the vehicle's roof, as illustrated in Figure 3-21(b). The sensor is mainly sensitive to the range of near infrared radiation. The spectral sensitivity is shown in Figure 3-22.

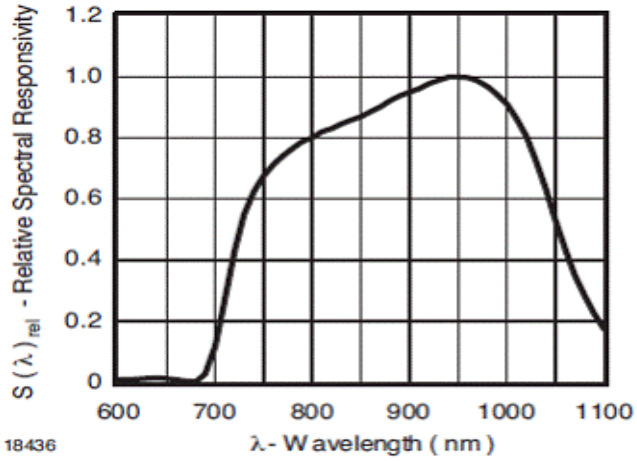

Figure 3-22: Spectral sensitivity of the solar sensor [11]

The sensor uses the 'Klimabus' protocol to communicate with external hardware. In principle, this is based on a master-slave system with the MCU acting as master and the solar sensor as slave. The protocol is similar to RS232 communication. However, signal levels are unipolar, timing specifications differ and output impedances must be within defined ranges. Data is being transmitted and received via one bidirectional data line. More information about the 'Klimabus' can be found in [11].

An adaption interface is necessary, in order to connect the solar sensor to a standard serial communication interface. The schematic is shown in Figure 3-23.

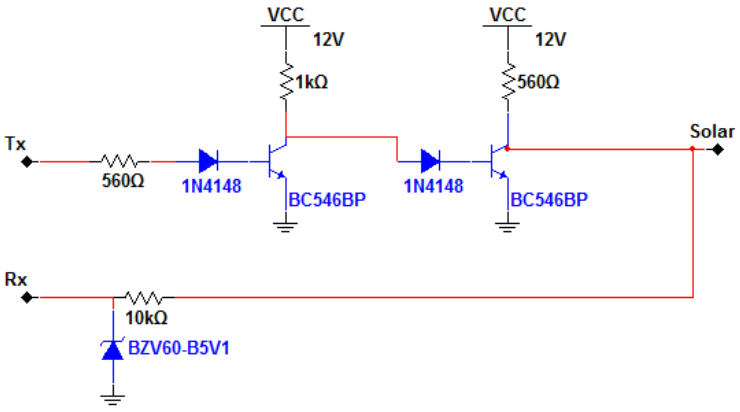

Figure 3-23: Solar adaption Interface

Data has to be requested from the sensor with a request frame. The sensor then replies with a response frame containing the solar information. Request and response block have the same structure, differ however in terms of address and frame length. Data length is coded implicitly in

the address byte and each frame is terminated by two bytes of checksum. The principle is shown in Figure 3-24.

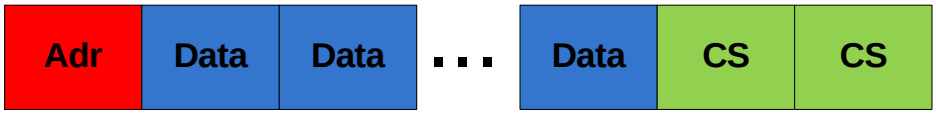

Figure 3-24: Solar sensor data frame (bytes)

Solar intensity, azimuth- and elevation angles are coded with two bytes each. The possible maximum resolution of the solar angles is $\Delta\varphi, \Psi = 0.015625$ degrees. However, such a high resolution is only of theoretical benefit. The solar intensity has to be calibrated. This was done with a calibrated pyranometer as reference and a solar tracker. The pyranometer was therefore mounted on the solar tracker and was permanently adjusted to the sun. The solar sensor was placed on the ground. This is shown in Figure 3-25.

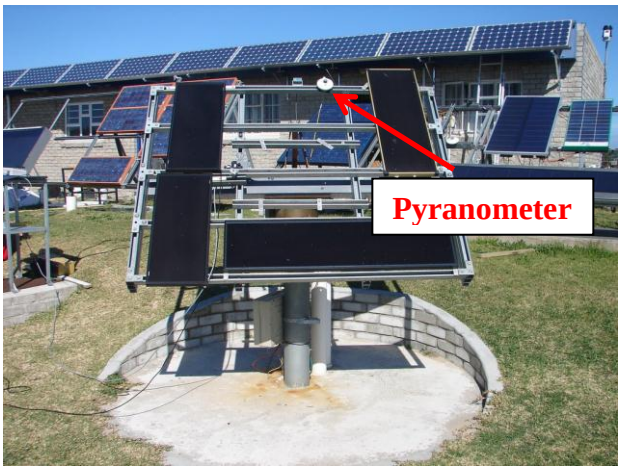

Figure 3-25: Solar tracker at NMMU

Figure 3-26 shows the pyranometer output and ISOS output.

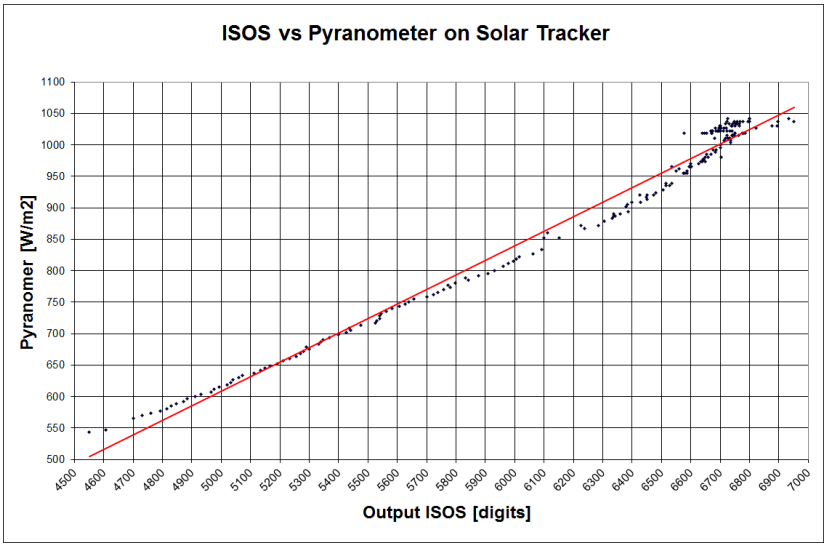

Figure 3-26: Solar sensor calibration

The sun intensity was therefore correlated to the solar sensor output through approximation with a straight line:

$$E \cong 0.1415 \frac{W}{m^2} \cdot S_o, \quad \textbf{(24)}$$

with:

S_0: Solar sensor output [digits].

3.4.5 Manual HVAC ECU and heaterbox

Chapter 2.1.3 pointed out, that there are three types of HVAC units available today. However, for this research a manual HVAC control unit and a corresponding manual heater box is required. Semi-automatic or automatic control units cannot be used due to two reasons:

- Internal control strategy,
- Low frequency of human intervention.

Both, semi-automatic and automatic control systems, aim to autonomously control parameters of the interior cabin environment. This would intervene with the user's individual setup and would therefore affect data acquisition. Secondly it is assumed that human's number of interactions with the control unit decreases with increasing level of control algorithms. With the use of (semi-)automatic HVAC units, one might not being able to collect a comprehensive data set. This means that user votes might be just considered as indicative, but not detailed enough for system learning.

The research vehicle's factory-fitted configuration is either an automatic or a semi-automatic unit. Manual HVAC systems are not available for this type of vehicle. It was therefore decided, to adapt and to integrate a manual HVAC unit from another type of vehicle. The manual control unit, as well as the appropriate heaterbox, were kindly provided by Volkswagen South Africa Ltd. The installation procedure of the heater-box was already shown in Figure 3-16.

Figure 3-27 show the prototype version of the manual HVAC control unit.

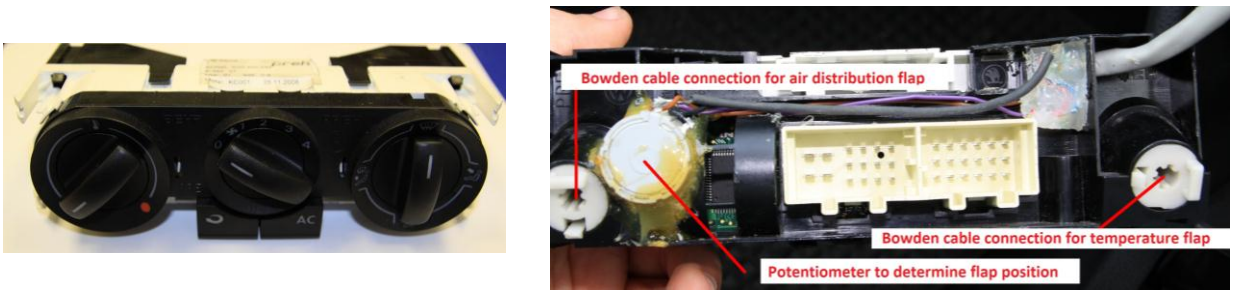

(a) **(b)**

Figure 3-27: Manual climate ECU; (a) Front side; (b) Back side

The following ECU parameters have been identified to be relevant for this research:

- Blower level b,
- Temperature knob value T_k,
- Flap position f.

The blower level can be directly derived from the vehicle's Comfort CAN bus. However, the temperature knob's value and the flap positions are not needed by any other ECU in the vehicle and are therefore not available on any internal bus. Therefore a potentiometer was mechanically integrated into the manual HVAC control unit, in order to determine the flap position. This extension is shown in Figure 3-27(b). The temperature knob value is directly read from the internal potentiometer of the HVAC ECU.

Although manual HVAC units are not able to autonomously control the interior cabin climate, they still influence it indirectly due to control of the cooling circuit. Because of permanent changes in environmental conditions and driving situations, the required cooling load is adjusted continuously. This mainly affects the set-up value of the evaporator temperature. However, this research requires a constant evaporator temperature, irrespective of the mode of operation and irrespective of changing environmental conditions. The HVAC control unit must therefore be limited in its functionality and scope of operation. This is achieved by accessing its firmware and forcing it into a special engineering operating mode during testing, which allows for individual set-up of various control parameters[7].

A constant evaporator temperature of $\vartheta_{ev} = +5℃$ has been set up for this research.

3.4.6 CAN Link

The CAN protocol was developed by Robert Bosch GmbH in the 1980s in order to provide a common platform for inter-ECU communication. In regular operating mode, it uses two wires for communication. These wires are called CAN_High and CAN_Low and allow for differential data transmission. CAN is a multi-master topology and is categorized as a message based protocol. High-speed CAN systems are normally terminated with two 120Ω resistors. A CAN data frame can consist of up to eight data bytes. There are standard and extended identifiers to address messages. These predominately distinguish in their possible address range. The CAN protocol has a large overhead ratio of control information to actual data. This makes CAN extremely fault tolerant. Figure 3-28(a) shows the bus connection principle. The format of a CAN frame is shown in Figure 3-28(b).

[7] The HVAC unit's control algorithms are considered to be confidential property of Volkswagen AG. It is trusted that the reader is aware that neither control algorithms nor methods to override the ECUs firmware can be presented in detail in this thesis.

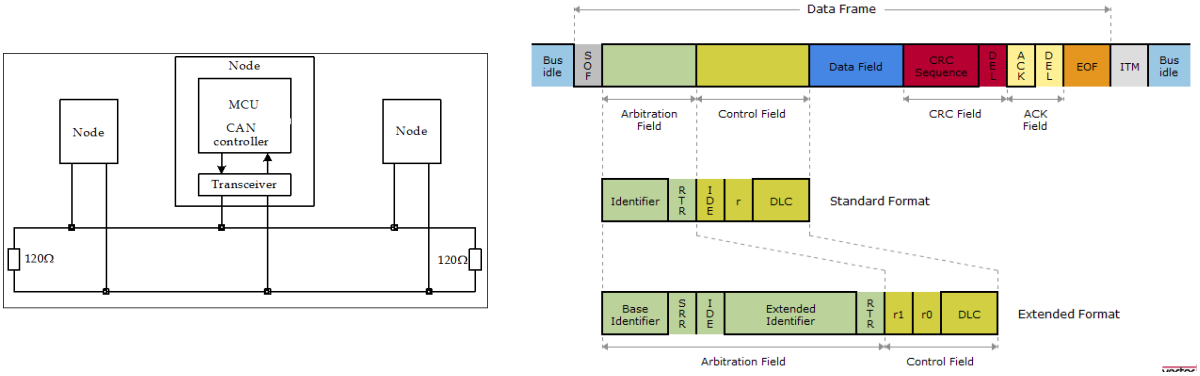

(a) **(b)**

Figure 3-28: CAN bus; (a) Bus connection, (b) Data frame format [Vector Informatik GmbH]

Further information about the CAN protocol can be found in literature, like [104].

For this research, two high-speed and one low-speed CAN connections were integrated in the comfort acquisition interface. The connections to the vehicle are shown in Figure 3-29.

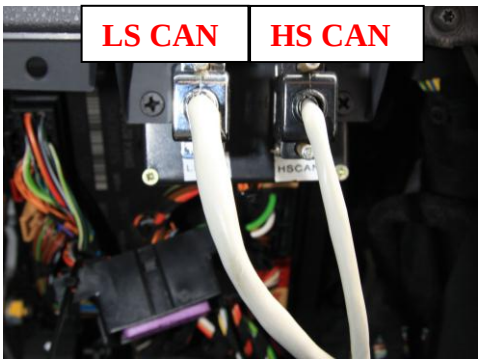

Figure 3-29: High-speed and low-speed CAN connection

In this context it must be mentioned that the terms ‘high-speed’ and ‘low-speed’ do not necessarily refer to the transmission speed, but rather on the properties of the physical signal layer. Differences in voltage levels of CAN_High and CAN_Low are shown in Figure 3-30.

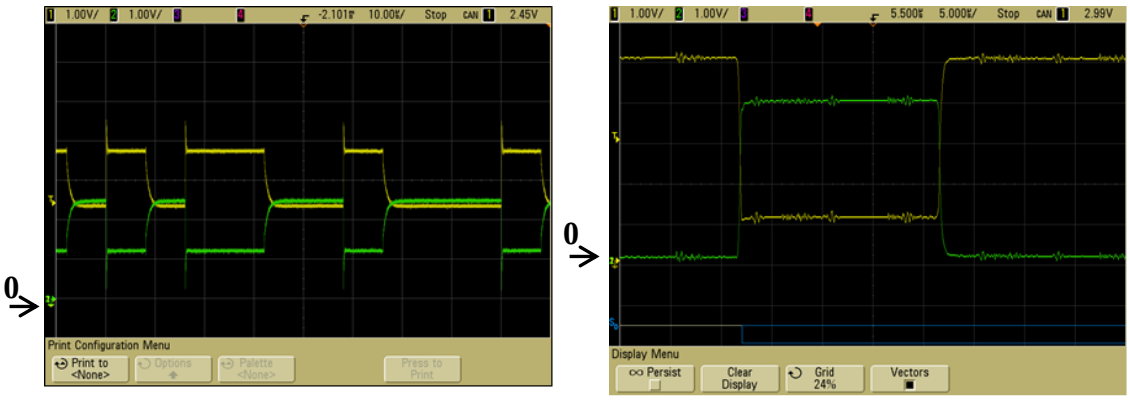

(a) **(b)**

Figure 3-30: CAN signal levels; (a) High-speed CAN, (b) Low-speed CAN

Therefore different transceivers have been integrated into the comfort acquisition unit. Low speed CAN additionally requires termination of each node. This is in contrast to high-speed CAN, where the bus is globally terminated at its ends.

The following information is being obtained from the vehicle's powertrain bus:

- Blower load b,
- Coolant temperature ϑ_{ec},
- Vehicle speed v,
- Compressor status AC,
- Refrigerant pressure p_{ref},
- Brake and gas pedal information TR,
- Ambient temperature ϑ_{Am},
- Filtered ambient temperature ϑ_{FAm}.

3.4.7 Display

A 240x128 dot matrix LCD has been integrated in the experimental setup to monitor all measurement variables as well as the system status. This is shown in Figure 3-31.

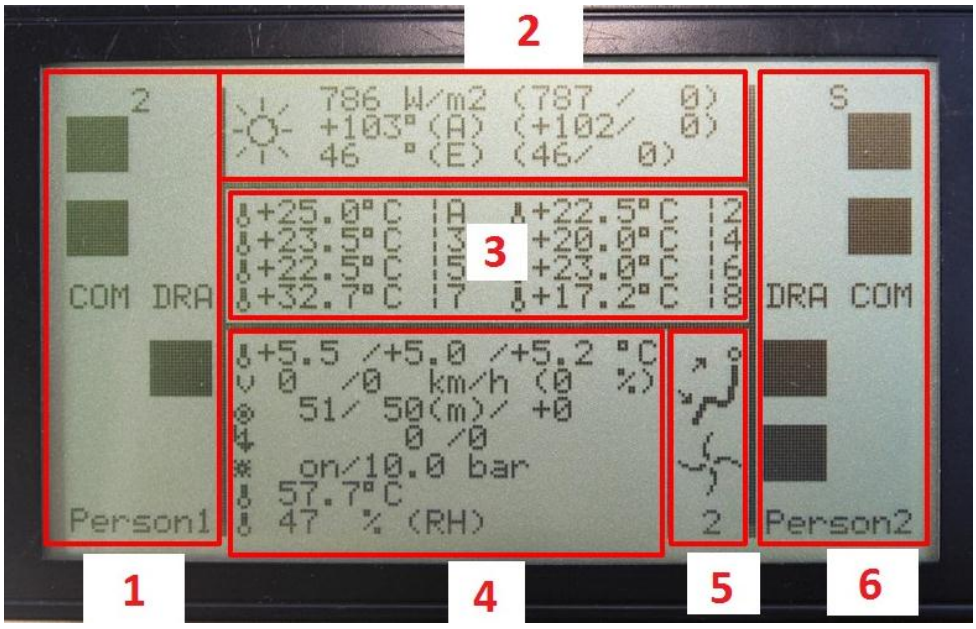

Figure 3-31: Measurement screen

The following sub-sections will describe the inscriptions in detail.

3.4.7.1 Labels 1 and 6

The comfort interface allows for overall comfort and draught assessment for driver and front passenger. This is indicated with ‘COM’ and ‘DRA’. Comfort evaluation is done with a five-step preference scale:

- Warmer,
- Slightly warmer,
- No change,
- Slightly cooler,
- Cooler.

A similar concept was chosen for draft evaluation:

- More air,
- Slightly more air,
- No change,
- Slightly less air,
- Less air.

Evaluation is done with using the joysticks on the HMI. This is shown in Figure 3-32.

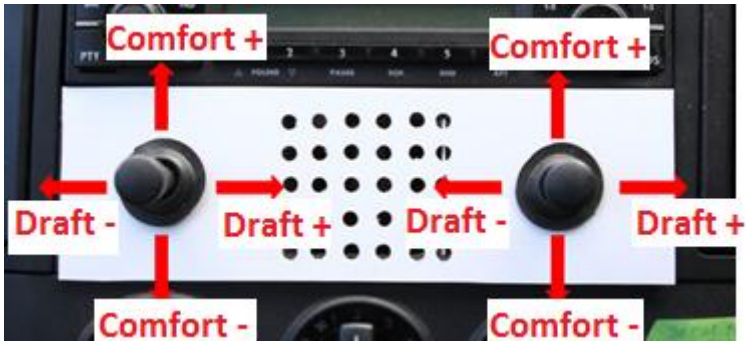

Figure 3-32: HMI

The number in the upper middle of field ‘1’ in Figure 3-31 displays the mode of operation. The coding is:

‘1’ Transient and stationary mode,

‘2’ Stationary mode,

‘3’ Transient mode.

The digit in the middle top of field ‘6’ displays the mode of operation:

‘S’ Stationary data acquisition,

‘T’ Transient data acquisition.

This information is especially useful in operating mode ‘1’, when the user is required to switch from transient to stationary mode. This is done with the driver joystick, pushing and holding it for at least three seconds in any direction.

3.4.7.2 Label 2

This field displays the solar properties.

1. Row: Sun Intensity I, mean sun intensity $\bar{I}$, standard deviation σ_i,
2. Row: Azimuth angle φ, resultant azimuth angle $\bar{\varphi}$, standard deviation σ_{az},
3. Row: Elevation angle Ψ, resultant elevation angle $\bar{\Psi}$, standard deviation σ_{elev}.

3.4.7.3 Label 3

This field shows the in-cabin temperatures as well as the ambient temperature taken from the vehicle bus.

A: Filtered ambient temperature ϑ_{Am},
2: Cabin air temperature ϑ_2,
3: Driver feet temperature ϑ_3,
4: Driver head temperature ϑ_4,
5: Cabin roof temperature ϑ_5,
6: Passenger feet temperature ϑ_6,
7: Dashboard temperature ϑ_7,
8: Passenger head temperature ϑ_8.

Filtered ambient temperature is a parameter which is calculated internally in the instrument cluster, from the actual ambient temperature sensor reading. The algorithm adjusts the ambient temperature sensor’s raw values according to the vehicle’s operating condition. In the research vehicle, the filtered temperature shows a PT1 characteristic. Details about the filtering algorithms cannot be presented in this context, due to confidentiality reasons.

3.4.7.4 Label 4

This field displays various vehicle parameters.

1. Row: Mixing chamber air temperature (left sensor), mixing chamber air temperature (right sensor), mean mixing chamber air temperature ϑ_1,
2. Row: Vehicle speed v, mean vehicle speed $\bar{v}$, standard deviation v_v,
3. Row: Temperature knob setup, mean temperature knob setup T_k, difference to previous interval ΔT_k,
4. Row: Number of alternating brake/gas cycles, total number of the previous 15 intervals TR,

5. Row: AC status (on/off), refrigerant pressure p_{ref},
6. Row: Coolant temperature ϑ_{ec},
7. Row: Relative humidity h.

3.4.7.5 Label 5

This field displays the flap position f as well as the blower level b.

3.4.8 Data logging

The comfort acquisition box has been programmed to transfers all synchronized and filtered data via 125kbps high-speed CAN link. A Vector CANCardXL® and an Opto251® cab for physical bus connection were used as interface to a laptop computer. The CAN hardware is shown in Figure 3-33.

Figure 3-33: CAN card and CAN cab

Vector CANoe® software was used for data logging. To decode and display the physical information, a CAN definition 'dbc' file has been additionally developed. Figure 3-34 shows a CANoe logging file in raw format.

```
date Sat May 1 07:51:06 am 2010
base hex  timestamps absolute
no internal events logged
// version 7.0.1
  18.642352 1  200             Rx   d 7 10 4C 00 00 AA 90 89
  18.643303 1  201             Rx   d 8 00 56 00 55 00 54 00 56
  18.644254 1  202             Rx   d 8 00 56 00 4E 00 53 00 55
  18.644917 1  203             Rx   d 4 5D 05 AF 00
  18.645724 1  204             Rx   d 6 01 BB FB BD 05 D6
  18.646267 1  207             Rx   d 2 00 00
  18.646810 1  206             Rx   d 2 00 00
  18.939880 1  200             Rx   d 7 10 4E 00 00 AA 90 89
  18.940831 1  201             Rx   d 8 00 55 00 55 00 54 00 56
  18.941782 1  202             Rx   d 8 00 56 00 4E 00 53 00 55
  18.942445 1  203             Rx   d 4 5D 05 AF 00
  18.943252 1  204             Rx   d 6 01 BB FB BD 05 D6
  18.943795 1  207             Rx   d 2 00 00
  18.944338 1  206             Rx   d 2 00 00
  19.243528 1  200             Rx   d 7 10 4E 00 00 AA 90 89
  19.244479 1  201             Rx   d 8 00 55 00 55 00 54 00 56
  19.245430 1  202             Rx   d 8 00 56 00 4E 00 53 00 55
  19.246093 1  203             Rx   d 4 5D 05 AF 00
  19.246900 1  204             Rx   d 6 01 BB FB BD 05 D6
  19.247443 1  207             Rx   d 2 00 00
  19.247986 1  206             Rx   d 2 00 00
```

Figure 3-34: CANeo logging text file

Figure 3-35 shows a screenshot of the measurement variables during data acquisition.

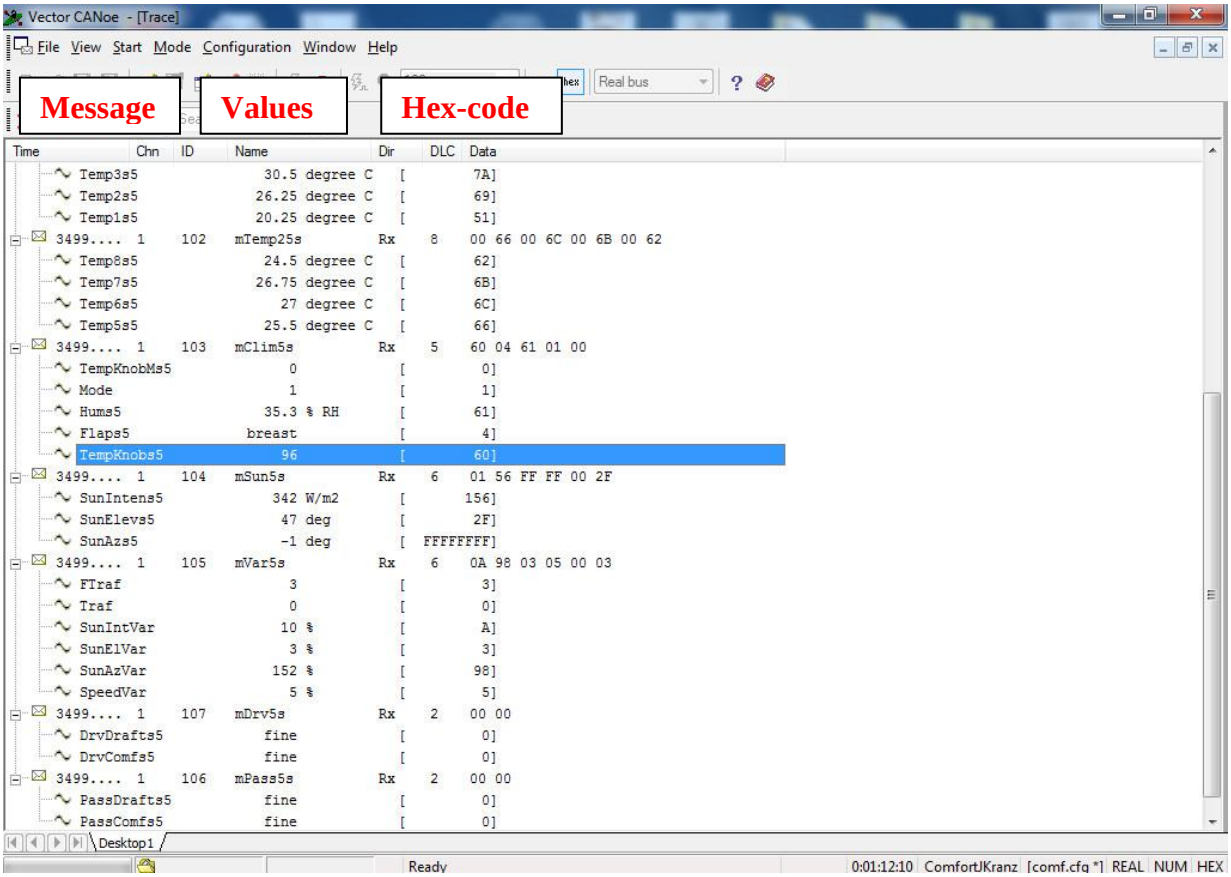

Figure 3-35: Vector CANoe screenshot during data acquisition

The first column in Figure 3-34 contains an absolute time stamp. The second column shows that Channel 1 of the CAN card is connected. The third column shows the CAN identifiers. The mnemonic ‘Rx’ in the fourth column indicates, that data is being read from the bus. This is followed by the data length code and the data itself. With the CAN definition .dbc file, these values can be decoded to their physical meanings. Appendix A.1 shows all defined CAN messages.

3.5 Software design

The following sub-sections will shortly describe the software structure of the Comfort interface. For illustration purposes, the operational sequences will be presented strongly simplified. However, the complete source code will be available from the author, in order to allow the interested reader a deep analysis of the functionality.

3.5.1 Initialization

Before start of measurement, the comfort acquisition unit needs to be set up and forced into a well-defined state. This sequence and the involved processes are shown in Figure 3-36.

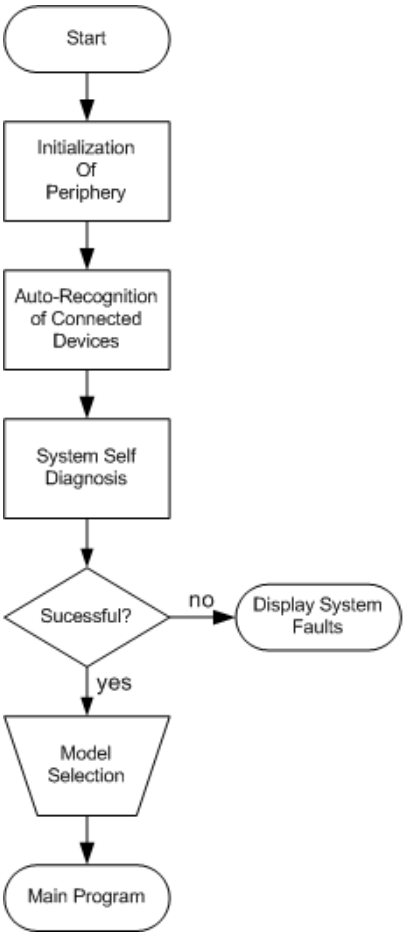

Figure 3-36: Initialization sequence

The connected periphery is automatically detected, set-up and diagnosed. Self-diagnosis include functional as well as plausibility verification. The diagnosis screen is shown in Figure 3-37.

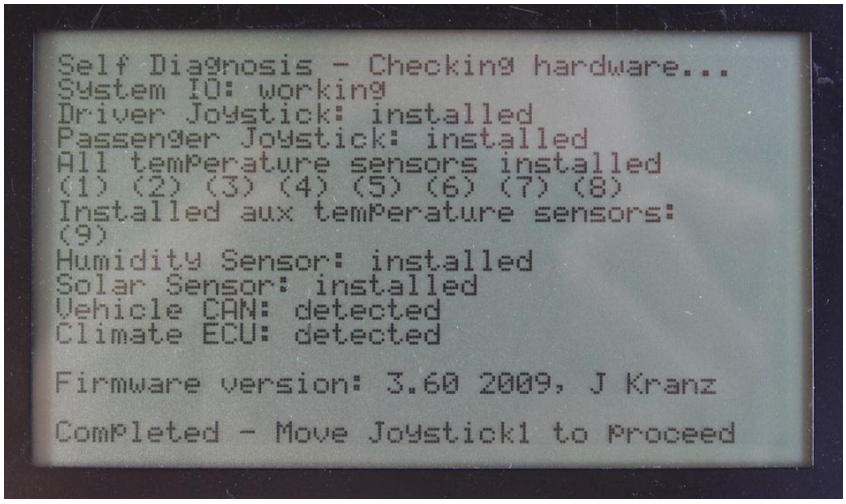

Figure 3-37: Initialization screen

The diagnostic screen makes it possible to check required hardware prior to the start of measurement. Not connected periphery does not influence program flow. However, later failure

of any previously detected device causes an exception and immediate stop of program execution. Mode selection makes it possible to select between three operating modes:

- Transient and stationary testing,
- Transient testing,
- Stationary testing.

The mode selection screen is shown in Figure 3-38.

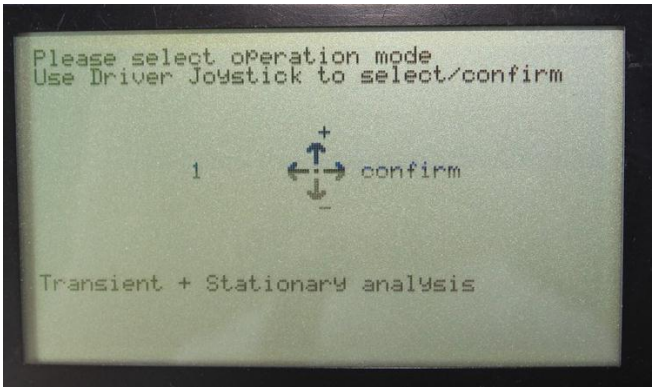

Figure 3-38: Mode selection screen

Selection is done via HMI. Combined transient and stationary testing requires a change in operating mode, as soon as stationary conditions have been achieved in the vehicle cabin. This is also done via HMI. Additionally, a status message is cyclically displayed in the LCD.

3.5.2 Main loop

After successful initialization procedure, the main program is entered, consisting of five parallel concurrent tasks. This is indicated in Figure 3-39.

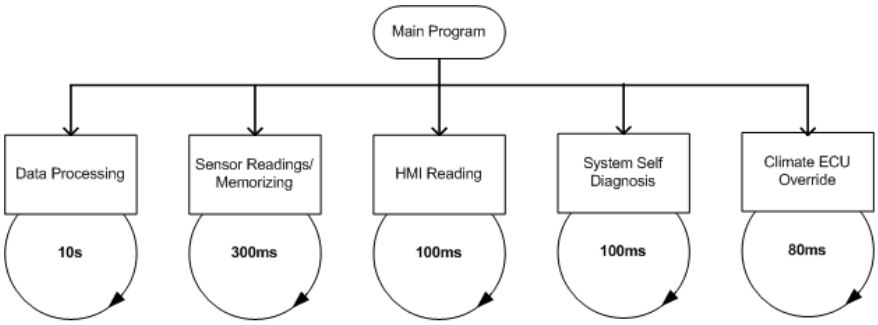

Figure 3-39: Cyclic main processes

The priority of the processes increases from the right to the left side.

3.5.2.1 Climate ECU Override

In order to ensure a constant evaporator temperature, the firmware of the HVAC controller must be forced into a special mode, which allows to setup up the desired system behavior. This is

done periodically with a frequency of 12.5Hz. Since this process is essential in terms of providing consistent measurement conditions, it was assigned to the highest priority. It can therefore not be interrupted by any process, but can interrupt all other processes.

3.5.2.2 System Self Diagnosis

In order to prevent corrupt data acquisition due to failure of previously recognized periphery during data acquisition, hardware must be monitored periodically. This is done with a frequency of 10Hz. Any detected failure will result in an immediate stop of data acquisition and will produce an error message on the LCD, in combination with an acoustic alarm signal. Additionally all peripheral interfaces and ports are deactivated, to protect the system hardware. Presently, the system is capable of detecting 32 system faults. An example of system failure is shown in Figure 3-40.

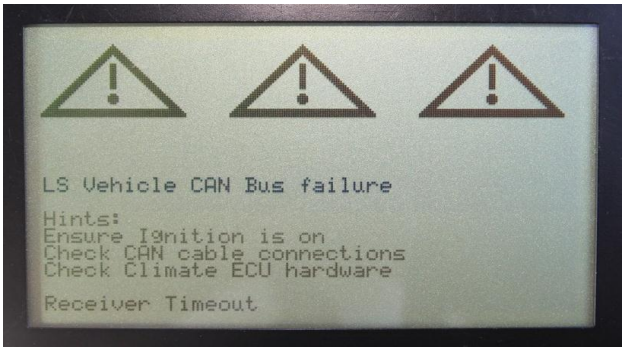

Figure 3-40: Comfort CAN failure ($1A)

This error message indicates that connection to the vehicle's Comfort CAN bus was lost and the CAN receiver reported a timeout. In this example, the error was intentionally provoked by switching of ignition during data acquisition. This results in deactivation of the vehicle's internal bus systems and therefore in an absence of required CAN messages.

Identifying and displaying information about the source of failure is valuable especially during road testing, when laboratory equipment is not readily available. Having detailed information about the problem may reduce system downtimes, as well as losses in data acquisition. The error codes and their corresponding meanings are summarized in Table 8.

Table 8: System fault listings

Code	Description	Code	Description
$01	Data logger link failure	$11	I^2C multiplexer failure
$02	Powertrain CAN receiver failure	$12	Humidity sensor failure
$03	Powertrain CAN filter failure	$13	CAN0 module intiliazation failure
$04	Solar sensor hardware failure	$14	CAN1 module intiliazation failure

$05	Solar Sensor checksum incorrect	$15	CAN4 module intiliazation failure
$06	Temperature sensor 1 failure	$16	CAN3 module intiliazation failure
$07	Temperature sensor 2 failure	$17	Climate ECU emulation failure
$08	Temperature sensor 3 failure	$18	Refrigerant pressure too low
$09	Temperature sensor 4 failure	$19	Comfort CAN filter failure
$0A	Temperature sensor 5 failure	$1A	Comfort CAN receiver failure
$0B	Temperature sensor 6 failure	$1B	Temperature sensor 9 failure
$0C	Temperature sensor 7 failure	$1C	Reference temperature failure
$0D	Temperature sensor 8 failure	$1D	Undefined solar value
$0E	Heater box flap detection error	$1E	Fan current below limit
$0F	Joystick 1 failure	$1F	Fan current over limit
$10	Joystick 2 failure	$20	Unknown event handler

3.5.2.3 HMI

The HMI is sampled with a frequency of 10Hz in order to ensure immediate response to any user input. Comfort and draught sensations cannot be evaluated simultaneously and must therefore be done sequentially. If software detects a change in any direction of driver and passenger joysticks, the appropriate CAN message is temporarily deactivated from the CAN map. This prevents sampling of comfort and draught values in between or during user inputs. The corresponding CAN message is activated again shortly after user interaction. This is done when no joystick change is detected for at least two seconds. This time span is optically displayed with two blue LEDs on the LCD, for driver and passenger respectively. This methodology additionally allows for easy correction of accidentally wrong entered data.

3.5.2.4 Sensor readings

All sensor peripheries are periodically read and stored at intervals of t=300ms. Figure 3-41 shows the procedure.

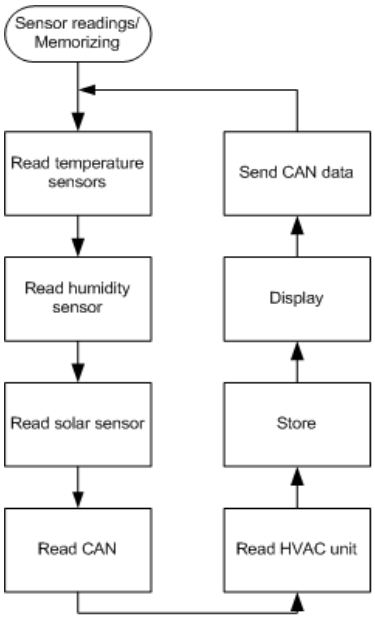

Figure 3-41: Reading/Storing process

Internal Random Access Memory (RAM) memory is allocated to store all measured information for at t_s=10s. The updated sensor information is sent to the LCD afterwards. For optional review this information is also transmitted to the Laptop via CAN link. These CAN messages have been defined with identifiers $2xx.

3.5.2.5 Data processing

According to the system's thermal comfort sampling rate t_s, internal data has to be filtered and processed every 10s. This sequence is shown in Figure 3-42.

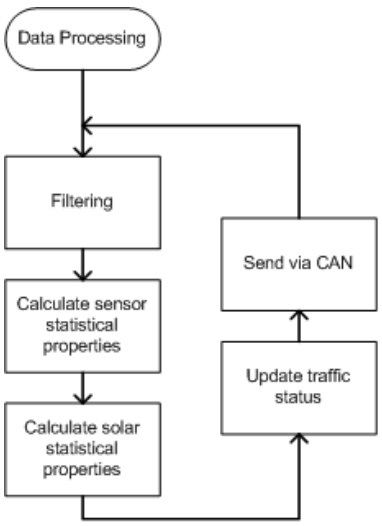

Figure 3-42: Data processing task

Human interaction with the HMI or the HVAC control unit must be treated separately, compared to other sensory information. This shall be explained with the following hypothetical example for the flap position, assuming an observation interval from 0.0s to 10.0s.

Table 9: Example for average flap position determination

Time [s]	Flap position f	Δt [s]
0.0	Head	1.5
1.5	Breast-head	7.8
9.3	Feet	0.7

The discrete domain F for 'flap position' f can be represented as:

$$f \in F \; and \; F = \{x | x \subset \mathbb{N}\} . \quad \textbf{(25)}$$

In this example, Table 9 shows that within the observation interval three different air distributions have been selected by the subject. Hereby, the setting 'head' has been selected for 1.5s, 'breast-head' for 7.8s and 'feet' for 0.7s.

It would be straightforward to consider the setting 'breast-head' as a representative for the chosen interval. Sampling the value flap position once per interval at any arbitrary position, would probably not result in representative results. Calculation of the arithmetic mean of 'f' does not guarantee agreement with equation (25).

It was therefore decided to calculate the cumulative sums of flap position per observation interval. A similar approach was chosen for:

- Driver/passenger comfort/draught levels,
- Blower level.

For all other sensor data x, the arithmetic mean is calculated according to:

$$\bar{x} = \frac{1}{n} \sum_{i=0}^{n} x_i, \quad \textbf{(26)}$$

with n being the number of samples per observation interval (n=33). For variables with high dynamic behavior, the standard deviation σ_x was additionally calculated:

$$\sigma_x = \sqrt{\frac{1}{n} \sum_{i=0}^{n} (x_i - \bar{x})^2} \quad \textbf{(27)}$$

This was done for:

- Vehicle speed,
- Solar parameters.

However, equation (26) cannot be used for calculating the arithmetic mean of the solar angles. This is justified due to their periodic properties. It was decided to calculate the resultant angles for each interval. The solar sensor's output must therefore be transformed to spherical

coordinates. This coordinate system, including the corresponding angle definitions, is shown in Figure 3-43.

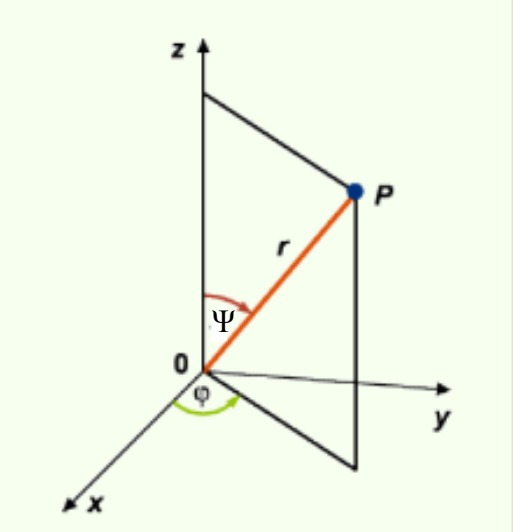

Figure 3-43: Spherical coordinate system [14]

The solar sensor output is therefore considered as vector $\vec{r}$ in a three-dimensional space. The sun intensity I is considered as the magnitude of that vector. The vector is transformed to its unity components. For n vectors in one measurement interval, the resultant elevation angle $\bar{\Psi}$ can be calculated using vector addition:

$$\bar{\Psi} = \tan^{-1} \frac{\sqrt{\sum_{i=0}^{n} {I_i}^2 \sin^2 \Psi_i \cos^2 \varphi_i + \sum_{i=0}^{n} {I_i}^2 \sin^2 \Psi_i \sin^2 \varphi_i}}{\sum_{i=0}^{n} I_i \cos \Psi_i}, \tag{28}$$

with:

$$\bar{\Psi} = \begin{cases} \dfrac{\pi}{2} & for \quad \sum_{i=0}^{n} I_i \cos \Psi_i = 0 \\ & \quad \sum_{i=0}^{n} {I_i}^2 \sin^2 \Psi_i \cos^2 \varphi_i = 0 \; and \\ not\ defined & for \quad \sum_{i=0}^{n} {I_i}^2 \sin^2 \Psi_i \sin^2 \varphi_i = 0 \; and \\ & \quad \sum_{i=0}^{n} I_i \cos \Psi_i = 0 \end{cases} \tag{29}$$

Similarly, the resultant azimuth angle $\bar{\varphi}$ is:

$$\bar{\varphi} = \tan^{-1} \frac{\sum_{i=0}^{n} I_i \sin \Psi_i \sin \varphi_i}{\sum_{i=0}^{n} I_i \sin \Psi_i \cos \varphi_i}. \tag{30}$$

Due to the definition of the azimuth angle, equation (30) is only valid for the frontal half-plane of Figure 3-43, which is in case for $\sum_{i=0}^{n} I_i \sin\Psi_i \sin\varphi_i \geq 0$. The rear half-plane, as well as special cases must be considered separately. This has been summarized in equation (31).

$$\bar{\varphi} = \begin{cases} \tan^{-1}\dfrac{\sum_{i=0}^{n} I_i \sin\Psi_i \sin\varphi_i}{\sum_{i=0}^{n} I_i \sin\Psi_i \cos\varphi_i} + \pi & for \quad \sum_{i=0}^{n} I_i \sin\Psi_i \cos\varphi_i < 0 \\ +\dfrac{\pi}{2} & for \quad \sum_{i=0}^{n} I_i \sin\Psi_i \cos\varphi_i = 0 \; and \; \sum_{i=0}^{n} I_i \sin\Psi_i \sin\varphi_i > 0 \\ -\dfrac{\pi}{2} & for \quad \sum_{i=0}^{n} I_i \sin\Psi_i \cos\varphi_i = 0 \; and \; \sum_{i=0}^{n} I_i \sin\Psi_i \sin\varphi_i < 0 \\ not\ defined & for \quad \sum_{i=0}^{n} I_i \sin\Psi_i \cos\varphi_i = 0 \; and \; \sum_{i=0}^{n} I_i \sin\Psi_i \sin\varphi_i = 0 \end{cases} \tag{31}$$

An undefined azimuth angle may occur in practice, when the sun is in exact zenith relative to the vehicle. In this case, the comfort acquisition tool outputs the hexadecimal error code $FFFF for elevation angle $\bar{\Psi}$ and $7FFF for azimuth angle $\bar{\varphi}$.

3.6 Data acquisition procedure

Data acquisition has been conducted in Southern Africa during spring, summer and autumn on a total distance of 20.000km. In advance, test subjects have been trained in using the HVAC unit's controls. This was to ensure that subjects are familiar with the system and their environment, in order to provide knowledge, which specific setting of the HVAC unit will fit best to a given source of thermal discomfort. To ensure repeatability and consistency for each measurement session, all equipment remained in the car and the position of the sensors was kept constant.

The air outlets have been permanently fixed with respect to both axes.

During all tests, subjects were asked to wear clothing with similar clothing insulation. Clothing color was kept constant, in order to produce similar radiation effects. Clothing was therefore dictated for blue jeans in combination with a black shirt. All subjects were in a general good

state of health during the tests. When entering the car, it was taken care that subjects were relaxed and were not influenced from previous activities. Chapter 2.2.7 emphasized the importance of human occupation in vehicle cabins. Tests were therefore only conducted with a constant occupation rate of two people.

3.7 Summary

It is concluded that available measurement equipment can only be partly used for this type of research. This was shown to be due to functional, as well as economic aspects. A thermal comfort acquisition system was developed, taking into account various environmental parameters, vehicle information, as well as data from a three-dimensional solar sensor. Thermal comfort evaluation for driver and front passenger, as well as draught level evaluation, can be done via two separate four-way joysticks. Alternatively, thermal comfort has been estimated with knowledge of the user's interaction with the HVAC ECU. It has been recognized that in most cases driver and front passenger simultaneously reported different levels of thermal comfort. This might be due to variations in individual comfort perception as well as due to the inhomogeneity of vehicle cabin. Since a single zone HVAC unit was used for this research, the problem could not be accounted for. To ensure data consistency, only the driver was therefore allowed to change the HVAC settings. To increase the efficiency and to double the amount of data, it is therefore suggested to use a dual zone manual HVAC unit for future testing. Road testing and data collection has been conducted during spring, autumn and summer conditions in Southern Africa at moderate to hot environmental conditions.

Chapter 4

Data Mining

Data mining has emerged during the 1980s and is considered as an ensemble of tools and methods for knowledge extraction from large amounts of data. In business, it has gained considerable importance with respect to data warehouses, which are repositories of heterogeneous data sources, organized under a uniform scheme, aiming to help business executives to make strategic decisions. Data mining is a multidisciplinary field including database technology, artificial intelligence, machine learning, statistics, pattern recognition, knowledge-based systems, knowledge acquisition, information retrieval, high-performance computing and data visualization [43].

Data mining has also great importance with respect to engineering sciences. Continuous advances in computer and sensor technology allow the collection of massive data sets. In practice, it is common to connect measurement equipment to an unknown process, in order to draw conclusions about its underlying functionality. Often, due to a lack of knowledge about the process itself, much more sensor devices and higher sampling rates are applied, than might actually be needed. Especially if field testing is expensive in terms of labor and operational costs, engineers tend to connect vast amounts of measurement equipment, in order to gather as most as prospective valuable information as possible and to reduce the risk of repeated measurements. This often results in an enormous amount of data, which makes it difficult to search for relevant information and functional relationships.

In literature, this dilemma is sometimes called ‘data rich but information poor situation’.

4.1 Strategy

For this research project, the previously given definition of data mining won’t be completely adapted. In this context, data mining will be restricted to methods of data preprocessing, feature selection and data transformation. The terms ‘artificial intelligence’ and ‘machine learning’ will be detached from the original definition and will be rather associated with modelling, which will be dealt with in Chapter 5. This classification is shown in Figure 4-1.

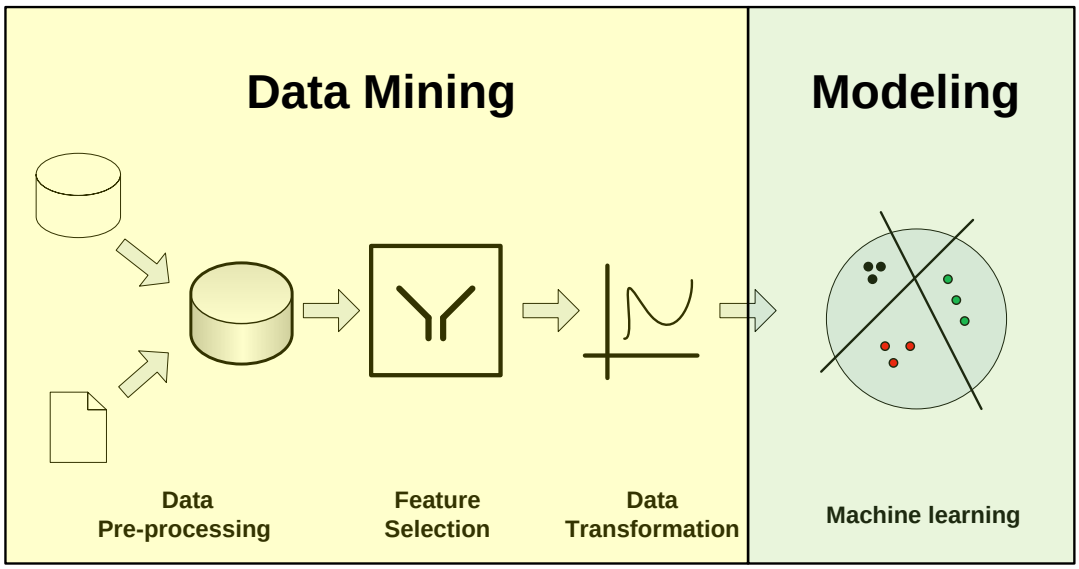

Figure 4-1: Data mining and modelling

In terms of this research, data mining can be seen as a preliminary stage for the modelling process.

4.2 Data preprocessing

Real world data tend to be incomplete, noisy and inconsistent. Additionally, data are often stored in multiple locations and must be combined for further processing. Data preprocessing therefore mainly refers to:

- Data integration,
- Data cleaning.

In the following sub-sections, these methods will be applied to automotive thermal comfort research.

4.2.1 Data integration

Data has been intermittently collected in field testing on several days during spring, autumn and summer conditions. The software tool Vector CANoe® has been connected to the comfort acquisition interface and has been used for data acquisition. For each measurement session M_i, a separate CANoe .blf file has been created automatically. For the subsequent modelling phase, these data files have to be converted and combined to Matlab format. The raw data files contain data with a sample frequency of 0.33Hz as well as 3Hz. First ones will be used for the modelling process while latter ones have been additionally recorded for the case, that some more detailed information might be needed in a later design stage. Table 10 shows those two groups of CAN messages. For the exact CAN definitions, the reader is referred to Appendix A.1.

Table 10: CAN identifiers

CAN Identifier (hex)	Description
$200 - $206	Data sampled with a frequency of 3Hz.
$100 - $106	Data sampled with a frequency of 0.1Hz

The CAN identifiers $200 - $206 have been therefore removed from the data set and the contents of messages $100 - $106 have been converted to Matlab .mat format. Matlab is also used to merge the data to an $\mathbb{R}^{m \times n}$ measurement matrix M. The row space of M thereby defines the number of sample vectors and the column space represents the dependent and independent variables. This process is shown in Figure 4-2.

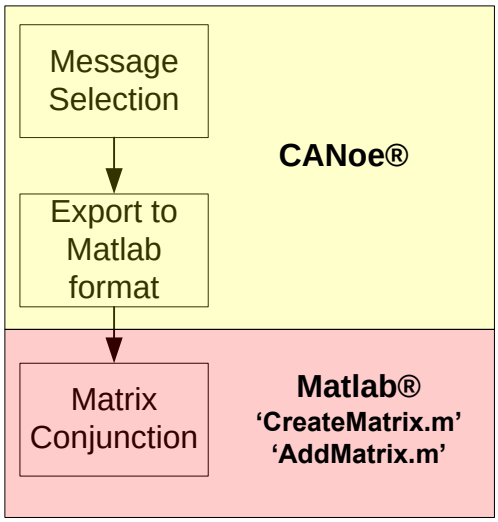

Figure 4-2: Data integration

The function 'CreateMatrix.m' is used to remove any timestamps in the i^{th} session's n column vectors (variables) and re-synchronizes them to a session matrix $M_i \in \mathbb{R}^{l_i \times n}$. The function 'AddMatrix.m' combines all k data set matrices M_i to one global measurement matrix M, with $\sum_{i=1}^{k} l_i = m$.

4.2.2 Data cleaning

According to [43], data cleaning incorporates processes for:

- Smoothing out of noise,
- Removal of disturbances,
- Removal of inconsistencies.

To some extent, data cleaning has been already implemented within the experimental setup. For example, averaging of samples predominantly attenuates high frequencies in measurements and can be considered as primitive low-pass filter. Additionally, external hardware low-pass filters

have been connected to each analog input and algorithms have been implemented to reduce the risk of corrupt input-output mappings. Continuously monitoring the hardware and immediately stopping data acquisition at failure, prevents corrupt sensor recordings. Errors in data transmission can be neglected, since the CAN protocol offers a wide variety of error recognition mechanisms. The statistical probability of an undetected error can be calculated as $p = 10^{-11}$ [104].

In terms of this research, data cleaning primarily refers to the separation of useful information from status parameters. Status parameters are required to allow conclusions about the operating mode in order to ensure valid testing conditions, but do not directly carry any thermal comfort relevant information.

4.2.2.1 Samples from transient conditions

This research focuses on thermal comfort prediction in short-transient and stationary environments. Non-stationary measurement vectors have therefore to be removed from the data set. Transient conditions include:

- Low engine coolant temperature ϑ_{ec},
- Transient interior climate evaluation by the test engineer,
- Samples with deactivated air-conditioning unit.

Figure 4-3 shows the curve of the vehicle's coolant temperature ϑ_{ec} for the whole data set. It is apparent that in the vast majority of samples, fairly stationary conditions are present. However, in some cases the operator has obviously started/re-started data acquisition shortly after a cold or a warm start of the vehicle, before steady-state coolant temperature has been achieved.

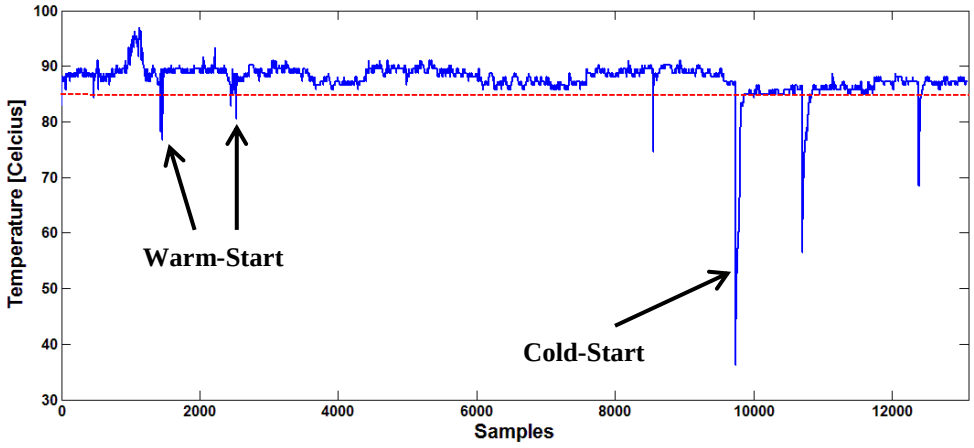

Figure 4-3: Coolant temperature

Coolant temperature directly affects the inflation temperature and has therefore considerable impact on the vehicle interior. The red dashed line in Figure 4-3 was therefore identified as the

lower steady-state boundary for coolant temperature. Samples with $\vartheta_{ec} < +86°C$ have to be removed from the data set. An upper limit is abdicated, because coolant temperature is a function of engine load as well as ambient temperature and is always subject to some variation. Limiting the range towards higher ordinates, might result in loss of valuable environmental information.

Transient conditions in the vehicle interior may also occur when the vehicle is parked and the air conditioner is switched off. The vehicle cabin interior might therefore be in a thermal state far away from thermal comfort levels. When starting or restarting data acquisition, the test engineer has therefore the opportunity of distinguishing between operating modes and is capable of marking the data as transient or non-transient. In case of non-stationary initial conditions, the operator has to remove the marker, as soon as stationary comfortable conditions have been re-established. A case of typical application is the cooling down procedure of the interior, when the car has been unattended soaking in the sun for some time. In Figure 4-4, this separation of operating modes is shown for the whole data set. Operating mode '0' refers to non-stationary and operating mode '1' refers to stationary in-cabin conditions. Data vectors with operating mode '0' have to be removed from the data set. It is apparent that there are a considerable high number of transient measurement vectors.

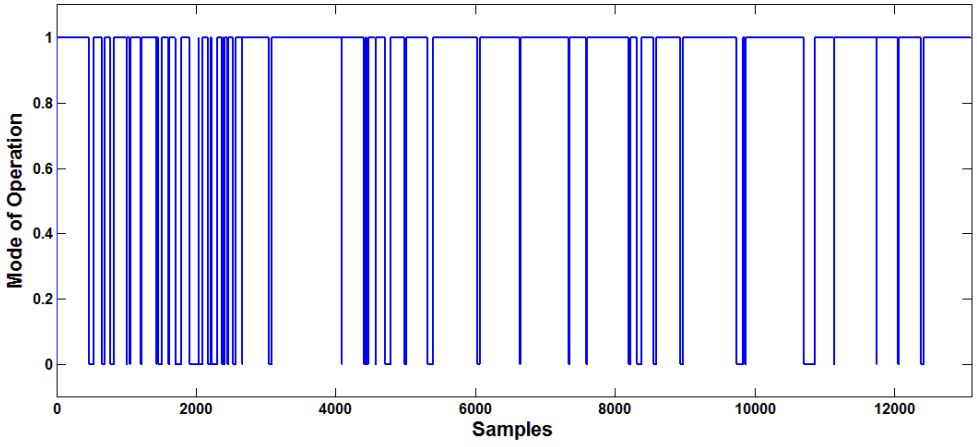

Figure 4-4: Operating mode distribution

4.2.2.2 Solar data

Measurement of sun properties ideally implies sensor exposure to direct sun light. In terms of measurement of solar angles, diffuse radiation cannot be handled by the solar sensor, used in this research. Sources of diffuse radiation are manifold and may include clouds, shadings, etc. Additionally, evaluating sun angles after sunset or at night drives is without meaning. Critical situations may also occur at the presence of large lighting gradients. Such situations may occur when the sun is covered by a barrier, e.g. a building, and the vehicle is located within its sphere

of influence. The solar sensor therefore evaluates the brightest contrast in the sky and may therefore output solar angles, which are far from reality.

It was recognized that in case of diffuse radiation, the solar angles were not stable and were subject to sudden changes, which seemed not to be predictable at all.

After sunset, this problem can be easily dealt with by the exclusion of samples with low radiation levels for the calculation of the solar resultant angles. According to the author's investigations, sun radiation level $I < 300$ W/m^2 seemed to be appropriate as lower boundary and have only little influence on human's thermal comfort sensation. In these cases, knowledge of the exact sun position is not necessary. However, this results in missing values for the solar angles. According to [43], there are different methodologies to handle missing data:

- Ignoring the sample vector,
- Filling manually in the missing value,
- Using a global constant to fill the missing value,
- Using the attribute mean,
- Using the most probable value.

Ignoring samples with low radiation levels would result in the loss of valuable environmental information. Filling in values manually is not possible due to data post-processing and due to violation of physical fundamental principles, like system causality. Substitution with attribute mean is also not possible, because of the unpredictability of the angle behavior. Prediction of a most probable value is not wise, because of the angle's dependency with respect to the vehicle's position.

Instead of the actual solar angles, the measurement equipment was therefore programmed to output error constants, if:

- $I < 300$ W/m^2 for all samples within the observation interval,
- Equations (28) and (29) in Chapter 3 are undefined.

These error codes are $FFFF in case of the sun elevation angle and $7FFF for the azimuth angle. However, one must be aware that through this modification the data set is biased. Solely evaluation of the sun intensity might be not a sufficient condition, because radiation levels might also be high at diffuse radiation. The author suspects that diffuse radiation can be detected by an unknown function, taking only into account the variation of solar intensity, azimuth angle and elevation angle. This requires further research and is beyond the scope of this thesis. However, in Chapters 4.5 and 4.6 it will be shown that the sun intensity can be used as a first approximation to separate classes of diffuse and direct sun radiation.

Figure 4-5 shows the course of the sun elevation angle.

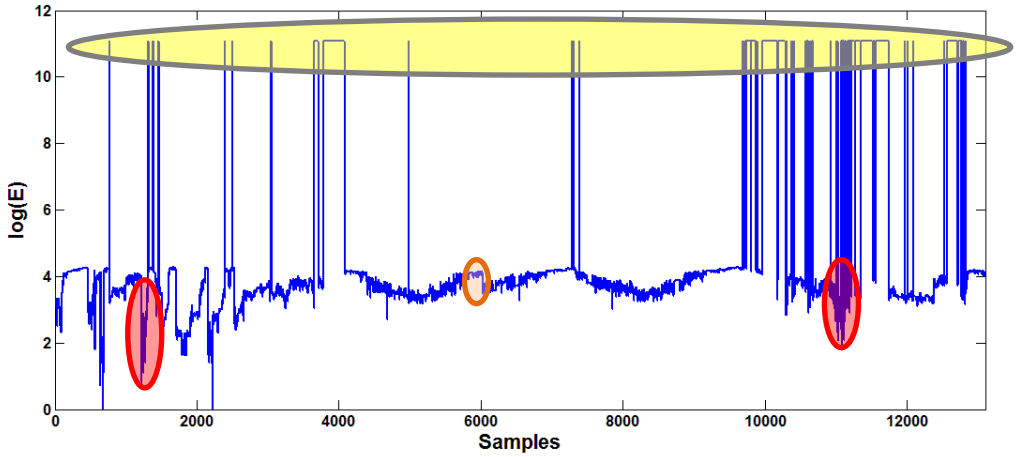

Figure 4-5: Sun elevation angle (log)

The ordinate axis has been logarithmized, in order to account for visualization of the large arithmetic distance of measurement vectors and error codes.

The yellow-shaded ellipse shows the samples with error codes. The red-shaded ellipses show samples with a high gradient of change in elevation angle within short periods of time. Physically this appears to be unrealistic. This means, the red shaded samples show examples where solely evaluation of sun intensity fails to detect corrupt solar angles. In these cases, the diffuse radiation level was about I = 700W/m^2. The orange shaded sample shows an example for a start and re-start of measurement at different times of the day. Despite the step within the course of the angle, it can be considered as a valid sample.

However, choosing an error constant of $FFFF and $7FFF turned out to be inappropriate for the modelling phase, because mathematical measures of distance may pretend a high variance in the data structure and may therefore confuse the training algorithms. It was therefore decided to substitute the error constants with values of '0'. In terms of the elevation angle, this can be physically interpreted as the sun, being in zenith relative to the vehicle.

4.2.2.3 Rounding

A high resolution of most sensory information is not needed for this kind of research. The variable's accuracy was therefore reduced to:

- Temperatures: $\Delta\vartheta = \pm 0.5°C$,
- Vehicle speed: $\Delta v = \pm 10km/h$,
- Sun Intensity: $\Delta I = \pm 100W/m^2$,
- Solar Angles: $\Delta\Psi$, $\Delta\varphi = \pm 10°$,
- Humidity: $\Delta h = \pm 5\%$ RH,
- Variances: $\Delta\sigma_i = \pm 10\%$.

Rounding can be also considered as a technique for data reduction. Lowering the resolution and summarizing samples, will result in dimensionality reduction of the sample space.

4.2.2.4 Consistency

Human beings are fuzzy in their decision space. Therefore when measuring human response for a given thermal environment, inconsistencies may occur. However, from a technical point of view, a unique mapping of input and output vector is essential for a successful learning strategy. Given a Cartesian product of two sets X x Y, this requirement can be written as

$$R \subseteq X \text{ x } Y, \quad \forall x \in X, \quad \forall y_1, y_2 \in Y,$$
$$(x, y_1) \in R \ \wedge (x, y_2) \in R \ \Rightarrow \ y_1 = y_2. \tag{32}$$

If statement (32) fails, meaning $\forall (x, y_i) \in R \; with \; (y_i \neq y_j) \; for \; \forall (i \neq j)$, consistency is not present. In this case, the distributive frequency for all $y_i \, , i = 1,2,..,k$ is computed and the domain is divided into k+1 intervals ξ

$$[\xi_1, \xi_2], [\xi_2, \xi_3], \dots, [\xi_k, \xi_{k+1}],$$
$$with$$
$$A = \{y_1 \dots y_k\} \text{ and} \tag{33}$$
$$\xi_1 \leq \min_{y \in A} y, \xi_{k+1} \geq \max_{y \in A} y \, .$$

The cumulative sums h_c can be calculated as

$$h_c(Y, k) = \|\{\xi \in Y | \xi_c \leq \xi \leq \xi_{c+1}\}\|, c = 1, \dots, k. \tag{34}$$

A discrete distribution implies

$$\sum_{c=1}^{k} h_c(Y) = k. \tag{35}$$

To enforce data consistency, the inconsistent sets will be substituted with

$$y = \max_{c=1 \dots k} h_c(Y, k) \; with \; (x, y) \in R \, . \tag{36}$$

Figure 4-6 shows the implementation of equations (32) to (36) in Matlab. The Matlab function 'SortConsistency.mat' searches for samples, where equation (32) is not fulfilled. The following three functions 'EnsureBlowerConsistency.m', 'EnsureFlapConsistency.m' and 'EnsureTempConsistency.m' implement statements (33) - (36) for blower level, flap position and temperature knob respectively.

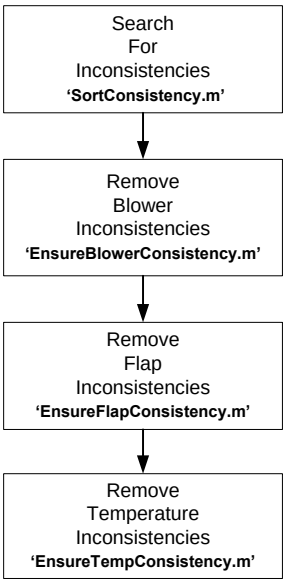

Figure 4-6: Process to enforce data consistency

4.3 Feature Selection

Pareto's principle states that only 20% of the data accounts for 80% of the information [123]. In literature, there are various methods available to specify the similarity of a set of variables.

4.3.1 Variance- and correlation analysis

Given two vectors[8] $\mathbf{a} \in \mathbb{R}^m, \mathbf{b} \in \mathbb{R}^m$, the co-variance $cov(\mathbf{a},\mathbf{b})$ can be calculated as

$$cov(\mathbf{a},\mathbf{b}) = \frac{\sum_{i=1}^{m}(a_i - \bar{a})\left(b_i - \bar{b}\right)}{m}. \quad \textbf{(37)}$$

The co-variance is a measure of how two variables (vectors) change together. If $\mathbf{a} \equiv \mathbf{b}$, equation (37) results in

$$cov(\mathbf{a},\mathbf{a}) = var(\mathbf{a}) = \frac{\sum_{i=1}^{m}(a_i - \bar{a})^2}{m}. \quad \textbf{(38)}$$

Equation (38) is called variance of vector **a**. The standard deviation of vector **a** is defined[9] as

$$\sigma_a = \sqrt{var(\mathbf{a})} = \sqrt{\frac{\sum_{i=1}^{m}(a_i - \bar{a})^2}{m}}. \quad \textbf{(39)}$$

Variance and co-variance are linear measures of similarity. Large differences from the sample mean result in large values for variance/co-variance. In terms of covariance, the values are positive, if higher than average values of **b** correspond to higher than average values of **a**. If lower than average values of **a** correspond to higher than average values of **b**, the co-variance is

[8] Vectors and matrices are printed with bold letters.

[9] In literature often m-1 instead of m is used. This is based on the assumption, that the available set is only a sub-sample out of the entire population. For these cases, it has been proven that m-1 is advantageous.

negative. Zero variance is achieved, if no central tendency can be determined, for example for a circular shaped data cloud.

However, due to its domain, the co-variance is not suitable to compare relationships [13]. The Bravais-Pearson coefficient r overcomes this difficulty and is defined as:

$$r_{ab} = \frac{cov(\mathbf{a},\mathbf{b})}{\sigma_a \sigma_b} = \frac{m\sum_{i=1}^{m} a_i b_i - (\sum_{i=1}^{m} a_i)(\sum_{i=1}^{m} b_i)}{\sqrt{[m\sum_{i=1}^{m} a_i^2 - (\sum_{i=1}^{m} a_i)^2][m\sum_{i=1}^{m} b_i^2 - (\sum_{i=1}^{m} b_i)^2]}}. \quad \textbf{(40)}$$

The definition range of r is limited to the interval [-1,+1]. With r = 0, there is no linear correlation between **a** and **b**. A value r = +1 indicates a strong positive correlation whilst r = -1 indicates a strong negative correlation of vectors **a** and **b**. Correlations solely specify similarity and do not specify causality. One can therefore not investigate, if a change in attribute is caused by change of another attribute.

The validity of equations (37) - (40) is not limited to vectors and can also be transferred to matrices. Given a matrix $\mathbf{A} \in \mathbb{R}^{m\,x\,n}$, the co-variance matrix can be defined[10] as

$$cov(\mathbf{A}) = \frac{1}{n}\mathbf{A}^{\mathrm{T}}\mathbf{A} \text{ with } cov(\mathbf{A}) \in \mathbb{R}^{nxn}. \quad \textbf{(41)}$$

Equation (41) is symmetric and contains $\frac{n!}{(n-2)\cdot 2}$ interrelationships along the off-diagonal elements. The diagonal elements contain the n measures of variance. The correlation matrix can be calculated as:

$$cor(\mathbf{A}) = \mathbf{S}^{-1} cov(\mathbf{A}) \mathbf{S}^{-1}, \quad \textbf{(42)}$$

with **S** being a diagonal matrix containing $1/\sigma_i$.

4.3.2 Partial, semi-partial and multiple correlation analysis

Co-variance and correlation methods specify the similarity between two attributes. This is a potential source for spurious correlations, whose interpretations may mislead the researcher. Spurious bivariate correlations may occur, when two attributes are correlated with a third attribute which is the actual reason for their change.

Partial and semi-partial correlation methods offer the opportunity to remove the influence of one or more variables on prospective predictor variables. Mathematically, this is achieved with methods of regression analysis. Partial correlation is considered as bivariate correlation between regression residuals. In case that a bivariate correlation r_{ab} of two variables a and b, shall be relieved from the influence of variable c, one can state

[10] Provided average-centered matrix elements.

$$r_{ab\cdot c} = \frac{r_{ab} - r_{ac}r_{bc}}{\sqrt{1 - r_{ac}^2}\sqrt{1 - r_{bc}^2}}. \quad \textbf{(43)}$$

Multiple correlation determines the correlation between one criterion variable and more than one predictor variables. In case that 1,2,…,k predictor variables should be used for correlation analysis with one criterion variable c, one can write

$$r_{c,12..k} = \sqrt{\sum_{i=1}^{k} b_i r_{ic}}. \quad \textbf{(44)}$$

Hereby the b_i coefficients are called 'beta' weights and can be calculated according to

$$\mathbf{b} = \mathbf{R_x^{-1}}\mathbf{r_{xc}}, \quad \textbf{(45)}$$

where $\mathbf{b} \in \mathbb{R}^k$ is a column vector containing the unknown beta weights, $\mathbf{R_x} \in \mathbb{R}^{k\,x\,k}$ the inter-correlation matrix of the predictor variables and $\mathbf{r_{xc}} \in \mathbb{R}^k$ the column vector containing the correlations between the predictor variables and the criterion variable.

With equations (44), (45) and B being a set of k variables, a partial correlation of order k can be written as:

$$r_{xy\cdot B}^2 = \frac{r_{y,(xB)}^2 - r_{y,B}^2}{1 - r_{y,B}^2}. \quad \textbf{(46)}$$

To determine the correlation between the criterion variable y and a predictor variable x, whereas x has been removed by the influence of the k-ordered variable set B, one can write

$$r_{y(x\cdot B)}^2 = r_{y,(xB)}^2 - r_{y,B}^2. \quad \textbf{(47)}$$

Equation (47) is called multiple semi-partial correlation between y and x, whereas x is removed by the influence of variable set B.

4.3.3 Principle component analysis

Methods described in the previous chapters allow investigation of similarity between two components. With large data sets, however, the number of data pairs increases dramatically. With 20 variables for example, one has already to deal with 190 inter-correlations. Partial- and semi-partial correlation may deliver deceptive results, if variables are highly correlated with each other. Especially for large data sets, it is therefore often desirable to have a method that transforms variables into a new feature space, in order to facilitate visualization of their properties. Such a methodology is principle component analysis (PCA).

PCA is a statistical technique of multivariate data analysis, which is often used for data visualization, dimensionality reduction and data compression. It is also known as Karhunen-Loève transform or Hotelling transform [13], [56]. PCA is based on the premise that salient

information in a given feature space lies in those features that have the largest variance. Rigor mathematical disquisition of PCA and its properties can be found in literature, like [56] and [57]. The author rather chooses a descriptive way to show the principles of PCA, according to [116].

PCA aims to linearly[11] transform the original data matrix **X** into a new data matrix **Y**. Given a matrix **X** with $\mathbf{X} \in \mathbb{R}^{m\,x\,n}$, this rotational operation can be defined as

$$\boldsymbol{Y} = \boldsymbol{PX}, \tag{48}$$

where **P** is an orthonormal matrix, which maximizes the variance of **Y** and minimizes its co-variance. Mathematically, this means that **P** diagonalizes *cov*(**Y**). The matrix **P** shall only rotate but not stretch the elements of **X**. This implies

$$\mathbf{P}\mathbf{P}^{\mathbf{T}} = 1 \text{ and } |\boldsymbol{P}| = 1. \tag{49}$$

The co-variance matrix of **Y** is can be written as[12]

$$\boldsymbol{cov}(\mathbf{Y}) = \frac{1}{n}\mathbf{Y}^{\mathrm{T}}\mathbf{Y} = \frac{1}{n}(\mathbf{Y}^{\mathrm{T}}\mathbf{Y})^{\mathrm{T}} = \frac{1}{n}\Big((\mathbf{PX})^{\mathbf{T}}(\mathbf{PX})\Big)^{\mathbf{T}} = \mathbf{P}cov(\mathbf{X})\mathbf{P}^{\mathrm{T}}. \tag{50}$$

To diagonolize *cov*(**Y**) in equation (50) including conditions (49), the Lagrange function L can be used [110]:

$$\mathrm{L} = \mathbf{P}cov(\mathbf{X})\mathbf{P}^{\mathbf{T}} - \lambda(\mathbf{P}\mathbf{P}^{\mathbf{T}} - \mathbf{1}). \tag{51}$$

The problem therefore reduces to extreme value determination of L, meaning finding the solution of $\frac{\partial L}{\partial P} = 0$. This results in

$$cov(\mathbf{X})\mathbf{P} = \lambda\mathbf{P} \Rightarrow\ (cov(\mathbf{X}) - \lambda)\mathbf{P} = 0. \tag{52}$$

Mathematically, equation (52) constitutes an eigenvalue problem. The eigenvectors of *cov*(**X**) therefore represent the elements of the rotational matrix **P**. Every eigenvector and its corresponding eigenvalue constitute a principle component. There are various methodologies available to solve equation (52). Statistical software normally uses singular value decomposition (SVD) or sometimes iterative solutions, like the NIPALS algorithm. Details can be found in literature like [57] and [64].

The result can be verified by using the theorem, that any symmetric matrix **C** can be represented by $\mathbf{C} = \mathbf{E}\mathbf{D}\mathbf{E}^{\mathrm{T}}$, with **D** being a diagonalized matrix and **E** being the Eigenvector matrix of **C**. With substitution into (50), one can verify that *cov*(**Y**) is being diagonalized.

The elements of each eigenvector are called 'loadings', which quantify the relation of the variables with the factors. The eigenvalues indicate the variance of the corresponding factors

[11] Nonlinear PCA is also possible and is known as Kernel PCA or Independent PCA.
[12] Valid for symmetric matrices **Y**

with respect to the data set. The coordinates of the original vectors, with respect to the new factor coordinates, are called 'scores'. For convenient interpretation of scores and loadings, it might be useful to calculate the correlation r_{ka} between a variable vector $\mathbf{x_k}$ and a principle component $\mathbf{t_a}$. This is done with equation (53).

$$r_{ka} = \frac{\sum_{i=1}^{N}(x_{ik} - \overline{\mathbf{x_k}})(t_{ia} - \overline{\mathbf{t_a}})}{\sqrt{\sum_{i=1}^{N}(x_{ik} - \overline{\mathbf{x_k}})^2 \sum_{i=1}^{N}(t_{ia} - \overline{\mathbf{t_a}})^2}}. \quad \textbf{(53)}$$

4.3.4 Dimensionality reduction

The purpose of PCA is to reduce a number of n variables to a smaller number k < n principle components (PCs), whilst retaining as much as possible of variation in the original n variables. These PCs are arranged in order of decreasing eigenvalues and explain successive variance. Dimensionality reduction can be therefore considered as selection of an adequate subset of PCs or variables. However, in literature there are only little objective formal criteria to choose the number of meaningful components. Those few criteria are generally based on formal test of a hypothesis and make distribution assumptions, which are often unrealistic in real world data [57]. Therefore the following subsections will be restricted to empirical methods, which are based on experience and have turned out to perform well in practice.

4.3.4.1 Kaiser-Guttman criterion

This method assumes that PCA is predominantly used in terms of data reduction. It is therefore only meaningful to keep factors, which explain more variance than the original variables. This is the case for PCs with eigenvalues larger than one. This means, that for a set $P = \{p_1, \dots, p_n\}$ with p_i components, the subset P_1

$$P_1 \subseteq P, for\ \forall\ p_i \in P_1\ with\ \lambda_i \geq 1, \quad \textbf{(54)}$$

will be chosen. However, the Kaiser-Guttman criterion is controversial in literature. Some researchers argue that with many factors, the number of relevant components will be often overestimated [13]. In contrary to that, it might be sometimes advisable to choose a lower cut-off eigenvalue than '1' [57].

4.3.4.2 Scree test

The scree test was developed by RB Cattell[13] in 1966. It is a graphical representation of the eigenvalues in dependence of the PCs. It shows at which PC k, the slopes of the lines, joining

[13] Raymond Bernard Cattel (†1998) was an American psychologist.

the plotted eigenvalues, are steep to the left of k and not steep to the right of k. This value k often appears as an ‘elbow’ in the scree plot. An exemplary scree plot is shown in Figure 4-7.

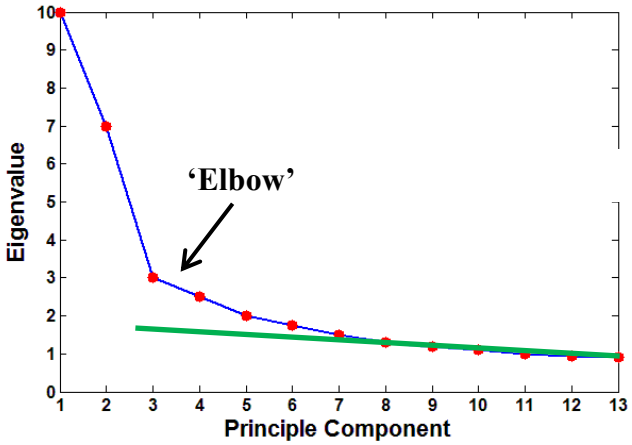

Figure 4-7: Scree plot

However, there are various interpretations of the scree plot available today. Common practice is to look for the sharp bend (‘elbow’). Then the components down to that one, immediately following the elbow, or the last components before the elbow, are taken into consideration [13], [57]. Cattell suggested searching for the point, beyond which the scree graph defines a more or less straight line. This line does not necessarily need to be horizontal. The first point on that straight line is then taken, to be the last factor to be retained [57].

The actual number of components to choose therefore depends on the observer’s interpretation of the scree plot. For the example in Figure 4-7, one could identify an elbow at PC3, indicating that three or four components should be retained. The approximation through a straight line is indicated by the green line and suggests retaining eight components. Dependent on the observer’s picture of a straight line, the line could also be approximated up to PC5, suggesting five components to retain.

4.3.4.3 Cumulative percentage of total variation

This method is based on the selection of a ‘sufficient’ large percentage k of total variation. However, there is no clear definition of the term ‘sufficient’, and the decision falls to the user. With the eigenvalues λ_i, this method can be expressed as

$$\frac{\sum_{i=1}^{p} \lambda_i}{\sum_{i=1}^{q} \lambda_i} \cdot 100 > k, \qquad \textbf{(55)}$$

with q being the total number of PCs and p being the number of ‘sufficient’ PCs. The choice of an appropriate value for k depends on the application. For example, when one or two PCs dominate the vast majority of variety, a high percentage might be desirably to account additional

information on less ordered components. However, if there are many factors, choosing a high percentage might cause an impractical high number of components for further analysis.

4.3.4.4 Variable selection

Finding the number p of PCs that account for most of the variation in the data set, can also be interpreted as finding the effective dimensionality p of the data set. This means that often p, or some few more variables, can then be chosen form the data set. Two approaches have proven to perform well in practice [57]:

1. One variable x is assigned to each of the first p relevant components. The remaining q-p variables are deleted from the data set.
2. One variable x is assigned to each of the q-p least relevant factors. These variables are then deleted from the data set.

These procedures can be applied iteratively.

4.4 Data Transformation

Many variables differ in scale and domain. Sometimes it is therefore desirable to ensure, that all variables have a similar domain. This is called data normalization which will be used interchangeably with the term 'data transformation' in this thesis. In PCA data normalization is generally an implicit step. Otherwise the components would be successively aligned according to the variables with the largest domain. In case of thermal comfort data, this would result in being PC1 to be aligned to sun intensity, followed by azimuth angle and vehicle speed. Variables with a small domain, like humidity, would be only considered on higher components. In most cases, this seems not to be acceptable. Also in machine learning theory, it is especially important to minimize the bias of one feature over another. Adequate normalization of the input data, can reduce the estimation errors in neural networks by a factor of five to ten and calculation times in the training process can be reduced in one order of magnitude [117].

There are many normalization techniques available. A well-established normalization method is the z-core normalization $x'_{z,i}$:

$$x'_{z,i} = \frac{x_i - \bar{x}}{\sigma_x}, \tag{56}$$

with $\sum_{i=1}^{n} x'_{z,i} = 0 \ \ and \ \ \sigma_z = \frac{\sum_{i=1}^{n}(x'_{z,i} - \bar{x}'_{z,i})}{n} = 1.$

The domain of z-core transformed values is normally between -3 and +3 [64]. Another linear transformation is called min-max normalization $x'_{m,i}$. Min-Max normalization rescales the range of each input variable to a new predefined range. As with the z-score normalization, the transformation is linear and does not change the distribution of the data. It can be written as:

$$x'_{m,i} = \left(max_{target} - min_{target}\right)\frac{x_i - min_{value}}{max_{value} - min_{value}} + min_{target}, \quad \textbf{(57)}$$

with

max_{target}: new maximum value,

min_{target}: new minimum value,

max_{value}: maximum value in the data set,

min_{value}: minimum value in the data set.

If outliers need to be reduced, data can be non-linearly transformed by using a sigmoid function. Equation (58) puts the normalized data into the range of 0 to +1, whilst equation (59) transforms the data to a range of -1 to +1.

$$x'_{s,i} = \frac{1}{1 + e^{-\left(\frac{x_i - \bar{x}}{\sigma}\right)}} \quad \textbf{(58)}$$

$$x'_{s,i} = \frac{1 - e^{-\left(\frac{x_i - \bar{x}}{\sigma}\right)}}{1 + e^{-\left(\frac{x_i - \bar{x}}{\sigma}\right)}} \quad \textbf{(59)}$$

In terms of this research, the author has decided to use z-core transformation for further processing, mainly due to its convenient statistical properties.

4.5 Application to Climatic Test Data

This subsection applies the methods of Chapter 4.3 to thermal comfort research. The author thereby follows an intuitive approach, which is described in [64]. This approach is sometimes called exploratory data analysis. PCA will be used, in combination with classical correlation analysis, to reduce the dimensionality of the feature space. To visualize the results, the software package TheUnscrambler® from Camo has been used. In order not to overload the plots with variable names, abbreviations given in Table 11 will be used for the rest of the text. Calculations obtained from equations (40), (53) and (55) are imprinted in tables in appendices A.2 - A.5. This information, like percentages of correlation, loadings and explained variances, will be used freely in the discussions without further reference. The domain of all the relevant input variables, which specifies the ranges of environmental conditions during data acquisition, can be found in Appendix A.7.

Table 11: Variable abbreviations

Code	Meaning	Code	Meaning
A	Sun azimuth angle φ	**T2**	Cabin Air temperature ϑ_2
Am	Ambient temperature ϑ_{Am}	**T3**	Driver feet temperature ϑ_3
AV	Standard deviation azimuth angle σ_{az}	**T4**	Driver head temperature ϑ_4
E	Sun elevation angle Ψ	**T5**	Cabin roof temperature ϑ_5
EV	Standard deviation elevation angle σ_{elev}	**T6**	Passenger feet temperature ϑ_6
FAm	Filtered ambient temperature ϑ_{FAm}	**T7**	Dashboard temperature ϑ_7
H	Humidity h	**T8**	Passenger head temperature ϑ_8
I	Sun intensity I	**TR**	Traffic information TR
IV	Standard deviation sun intensity σ_i	**V**	Vehicle speed v
T1	Air outlet temperature ϑ_1	**VV**	Standard deviation vehicle speed σ_v

Furthermore, the whole dataset does not contain flap position feet. An explanation might be that testing has only been conducted in moderate to hot environments and situations of perceived cold feet did not occur at any time. T3 has therefore been removed upfront from the dataset. The variables T6 and T8 have been also removed, because thermal comfort has only been set up by the driver, due to a manual single zone HVAC ECU.

4.5.1 Dataset containing all variables

Figure 4-8 shows the Scree and Pareto plot for the original data set.

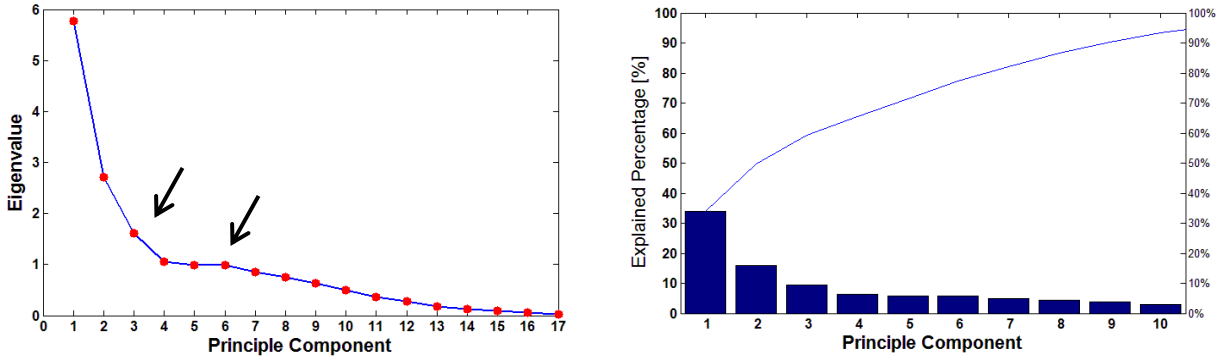

(a) **(b)**

Figure 4-8: Scree and Pareto plot for all variables; (a) Scree plot, (b) Pareto plot

The Pareto plot in Figure 4-8(b) indicates the explained percentage of variation for each PC. It is apparent, that the data set contains high redundancy. Ten PCs account for 94% of the total

variance. Chapter 4.3.4.4 suggests that therefore about 10 variables should be sufficient to account for the data sets variation. This means, PCs 11-17 can be considered as noise. The Scree plot in Figure 4-8(a) shows one distinctive ‘elbow’ between PC3 and PC4. A second ‘elbow’, with a less gradient occurs between PC6 and PC7. The scree criterion would therefore suggest keeping three or four factors. The eigenvalues for PC4 and PC5 are 1.063 and 0.988 respectively. According to the Kaiser-Guttman criterion, only PC1 to PC4 would be relevant. The blue line in Figure 4-8(b) shows the cumulative sums of the explained variances. It is apparent, that the first three components already account for about 59.5% of the dataset’s variance. If PC4 is added, about 65% of variance can be explained. The second elbow in Figure 4-8(a) occurs at PC6 which explains 77.2% of total variance. The Kaiser-Guttman criterion suggests retaining four factors, explaining 65% of total variance. Considering the second ‘elbow’ in Figure 4-8(a), six components should be retained, accounting for a total explained variance of 77.2%. This interpretation is fairly confirmed by Cattell’s straight line approximation. The researcher therefore recommends considering six PCs for further processing.

Figure 4-9 shows the PCA results for PC1 and PC2. The inner circle in Figure 4-9(b) indicates 50% correlation and the outer circle indicates 100% correlation of factors and variables. The circles can be mathematically expressed as

$$r^2 = r_a^2 + r_{a+1}^2, \qquad \textbf{(60)}$$

with a being the factor of interest. The variables in the inner circle of Figure 4-9(b) are badly accounted for by PC1 and PC2. Interpretations are therefore statistically not expressive. Variables within the inner and outer circle have a fairly high correlation with PC1 and PC2 and can be used for interpretation. PC1 and PC2 explain 87.7% of T5, 74.8% of T4, 79.28% of Am, 78.1% of FAm, 73.4% of I, 73.45% of E, 75.19% of T1, 71.76% of AV and 88.51% of EV. It is therefore not meaningful to consider further factors for the description of these variables. The red shaded circle in Figure 4-9(a) shows scores, which have higher than average values for the variables Am, FAm, T4 and T5. The opposite is true for those scores, which appear reflected at the origin. The yellow shaded circle in Figure 4-9(a) shows an interesting grouping of scores, which have lower than average values on I, E and higher than average values on AV, EV and T1. It is apparent, that this group is linearly separable from the rest of the data cloud. Figure 4-9(b) suggests, that the variables FAm and Am are very similar.

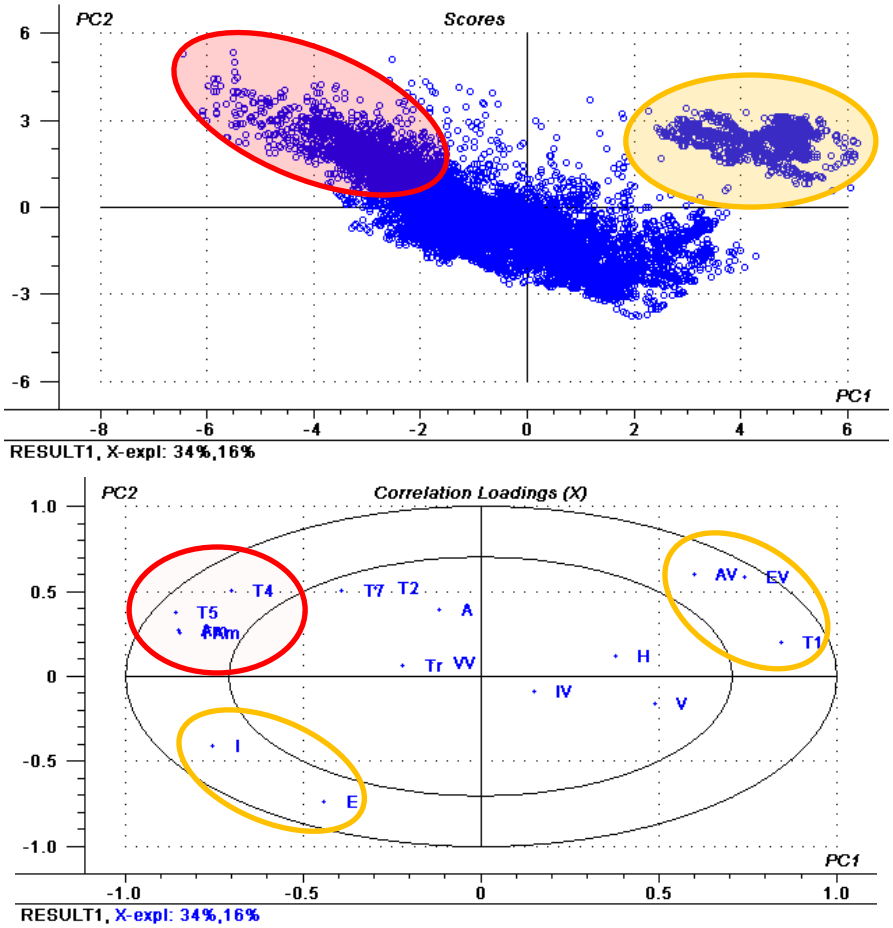

(a)

(b)

Figure 4-9: PCA results all variables (PC1, PC2); (a) Score plot, (b) Correlation-loading plot

This is confirmed by Figure 4-10(a), which shows the loadings of FAm and Am for the first six PCs. High redundancy is also confirmed by a bivariate correlation coefficient of r=0.98.

The correlation-loading plot additionally suggests that variables EV, AV are highly negatively correlated to I and E. Figure 4-10(b) shows the loadings for I, EV and AV. It is apparent that, with exception of PC4, I is in opposite direction to EV and AV. However, the influence of PC4 is not significant, since it only contributes 0.3% towards I, 0.01% towards EV and 0.77% towards AV. The researcher furthermore suspects, that the yellow shaded circle in Figure 4-9(a) mainly contains samples with diffuse solar radiation. This is because of their higher than average values for AV and EV.

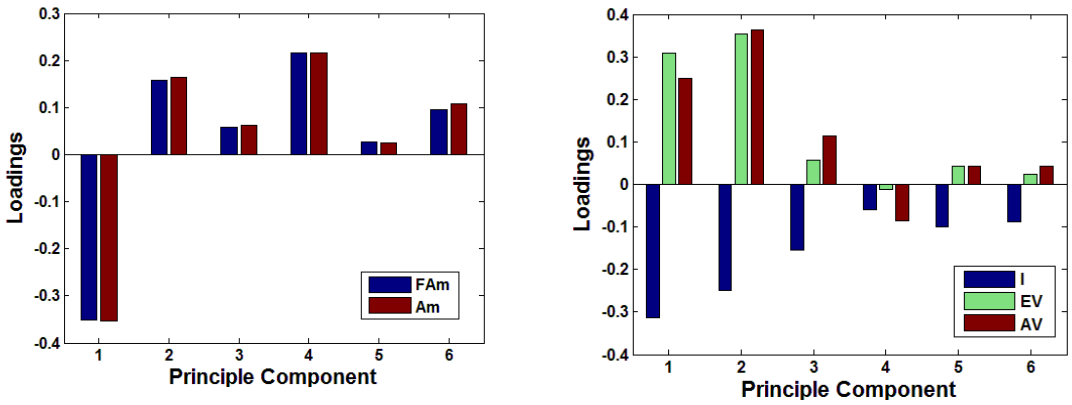

(a) **(b)**

Figure 4-10: Variable loadings; (a) FAm, Am, (b) I, EV, AV

The assumptions from Chapter 4.2.2.2 have therefore been confirmed. As a first approximation, the variables AV and EV can therefore be deleted from the data set, without significant loss of information.

At first glance, one could also assume that I and E share the same information and are therefore also redundant. However, this is not the case since they significantly distinguish on PC1 and PC2.

4.5.2 Dataset removed from the influence of FAm, EV and AV

The variables FAm, EV and AV have been removed from the dataset and a PCA has been recalculated. The corresponding Scree and Pareto plots are shown in Figure 4-11. In comparison to Figure 4-8, one can see that the first PCs explain less variance. This is not amazing, since some highly correlated variables and common variance have been removed from the data set. However, the findings from the previous section are still valid and the interpretation of Figure 4-11 leads to the same interpretations.

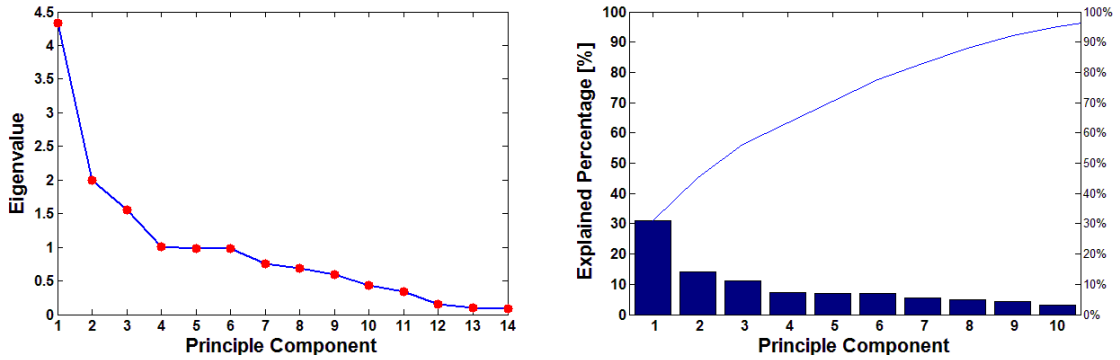

(a) **(b)**

Figure 4-11: Scree and Pareto plot without Fam, EV, AV; (a) Scree plot, (b) Pareto plot

Therefore, the number of necessary PCs is still identified as six, because only little information has been lost through the deletion of those highly correlated variables. Figure 4-12 shows the recalculated PCA results. It confirms that the information content did not change significantly. The yellow-shaded samples in Figure 4-12(a) are still grouped together and have lower than average values of E, I and higher than average values for T1. Similarly the red-shaded samples still have higher than average scores in Am, T4 and T5. Due to the removal of FAm, EV and AV, the variables T2 and T7 have received more influence on PC1 and PC2. This appears in the Score plot in Figure 4-12(b), where the grey shaded area indicates higher than average scores in T2 and T7. A clear visual separation between red and grey shaded samples is however not possible.

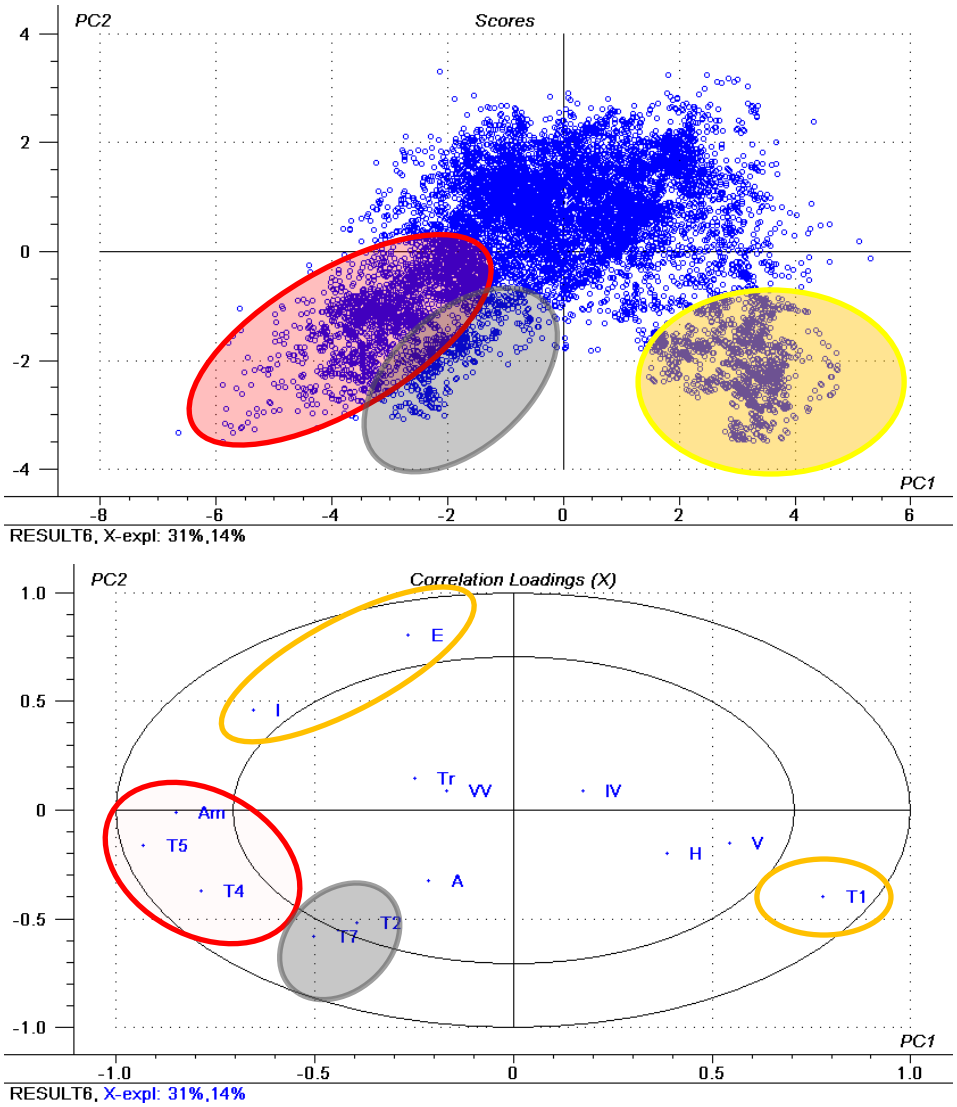

(a)

(b)

Figure 4-12: PCA results without FAm, EV, AV (PC1, PC2); (a) Score plot, (b) Correlation-loading plot

Figure 4-12(a) indicates that Am, T4 and T5 share similar variance with PC1 (72.2%, 62.1%, 86.7%) but only moderately differ on PC2 (0.0%, 14%, 2.6%). Figure 4-13 shows the loadings of Am, T4 and T5. The researcher assumes that they are similar in effect.

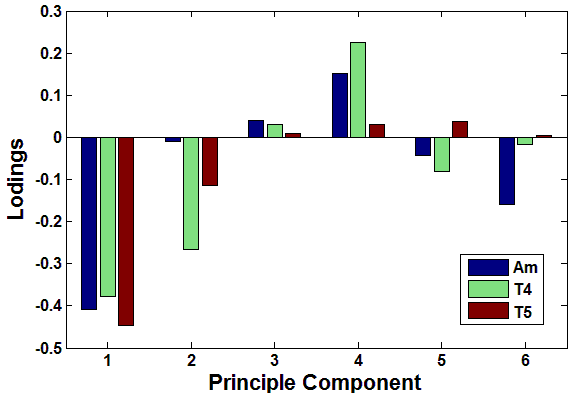

Figure 4-13: Loadings Am, T4, T5

Figure 4-13 suggests that these temperatures share most of their common variance on PC1. However, this only indicates some rough similarity but no clear redundancy.

In Figure 4-14, the variables Am, T4, T5 are plotted in dependence of all samples. It is obvious, that T4 and T5 fairly share the same tendency. It can also be seen, that T4 and T5 approximately follow the course of Am. T4 and T5 measure temperatures at the roof interior and at head position. According to Chapter 2.4, the head area is especially sensitive to climatic extremities. The clear influence of Am to T4 and T5 is an amazing insight, which suggests that thermal comfort perception inside the vehicle cabin is considerably influenced by the ambient temperature, even if the cabin interior is air-conditioned and decoupled from the exterior environment. In this context, it shall be mentioned again, that temperature sensors T4 and T5 have not been shielded against radiation. That means that they are not only sensitive to air temperature, but also to radiation. The research vehicle's black color might have intensified this effect.

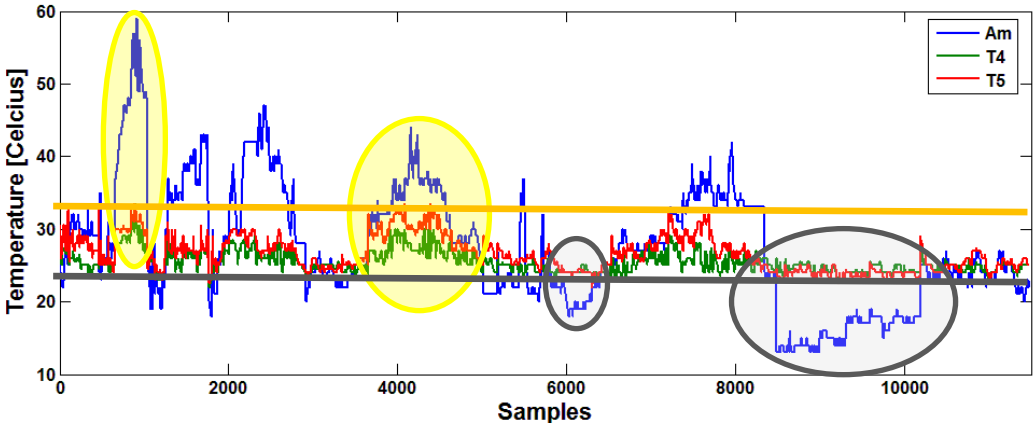

Figure 4-14: Distribution of Am, T4, T5

However, it is apparent, that this dependency is not linear. The grey circled areas in Figure 4-14 suggest that there seems to be a saturation effect in T4 and T5 towards lower ambient temperatures. This lower saturation level has been marked by the grey line. The same applies to higher ambient temperatures, which are represented by the yellow shaded areas. The yellow line marks the upper saturation limit towards high ambient temperatures. These non-linear saturation effects may limit the expressiveness of the bivariate correlation coefficient and the PCA results and might also be the reason that Am, T4 and T5 share most of their common variance on PC1, but distinguish moderately on PC2. For this research, linear correlation is not a necessary requirement for modelling. Methods presented in Chapter 5 are capable of theoretically realizing any non-linear mapping. Therefore, T4 and T5 can be considered to be redundant to Am and can be removed from the dataset.

Figure 4-12(b) indicates, that 76.7% of T1's variance is explained by PC1 and PC2. PC1 thereby explains 60.7%. This suggests that T1 might be highly negatively correlated to Am. However, Am is not correlated to PC2, while PC2 adds additional 16% variance towards T1. Figure 4-15 shows a scatter plot of Am and T1. For $\vartheta_{Am} \leq +36℃$, Am and T1 are fairly negatively linearly correlated. This is indicated by the red line on the left-hand side of the plot. For $\vartheta_{Am} > +36℃$, T1 seems to be fairly positively linearly correlated to ambient temperature.

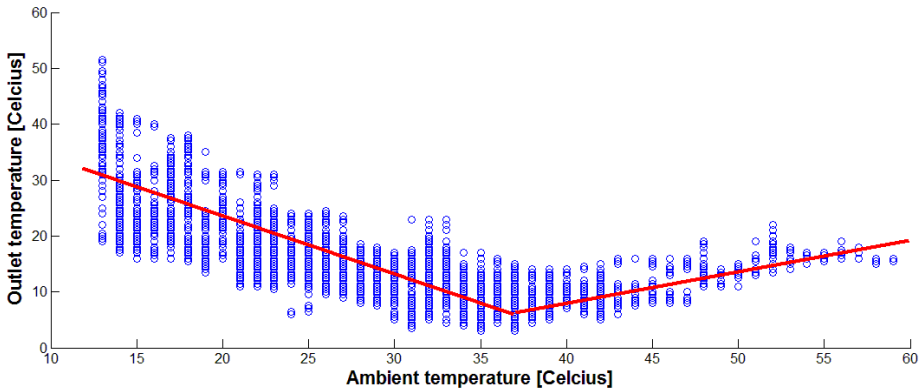

Figure 4-15: Scatter Plot Am, T1

An explanation of this effect might be that for increasing ambient temperatures the required cooling load must increase, in order to maintain in-cabin comfort levels. This means, that the air outlet temperature must decrease. At a certain point, when the available cooling power is exhausted, or the maximum setup point of the HVAC unit has been reached, a further increase in ambient temperature forces the outlet temperature to rise as well. With a reasonable degree of accuracy, T1 can therefore be removed from the dataset, because its information can be described with variable Am.

4.5.3 Dataset without T1, T4 and T5

IV is highly correlated to PC4 (72.8%) and moderately to PC5 (9.3%). This means, its variation can be explained by 82.1% with PC4 and PC5. Figure 4-16(b) shows that IV dominates the correlation-loading plot of PC4 and PC5 in the fourth quadrant. All other variables are far within the inner 50% circle and have therefore only little influence. Figure 4-16(a) shows the corresponding score plot. The grey shaded ellipse shows samples with higher than average values for IV. No distinctive interpretation can be given for samples with lower than average scores for IV.

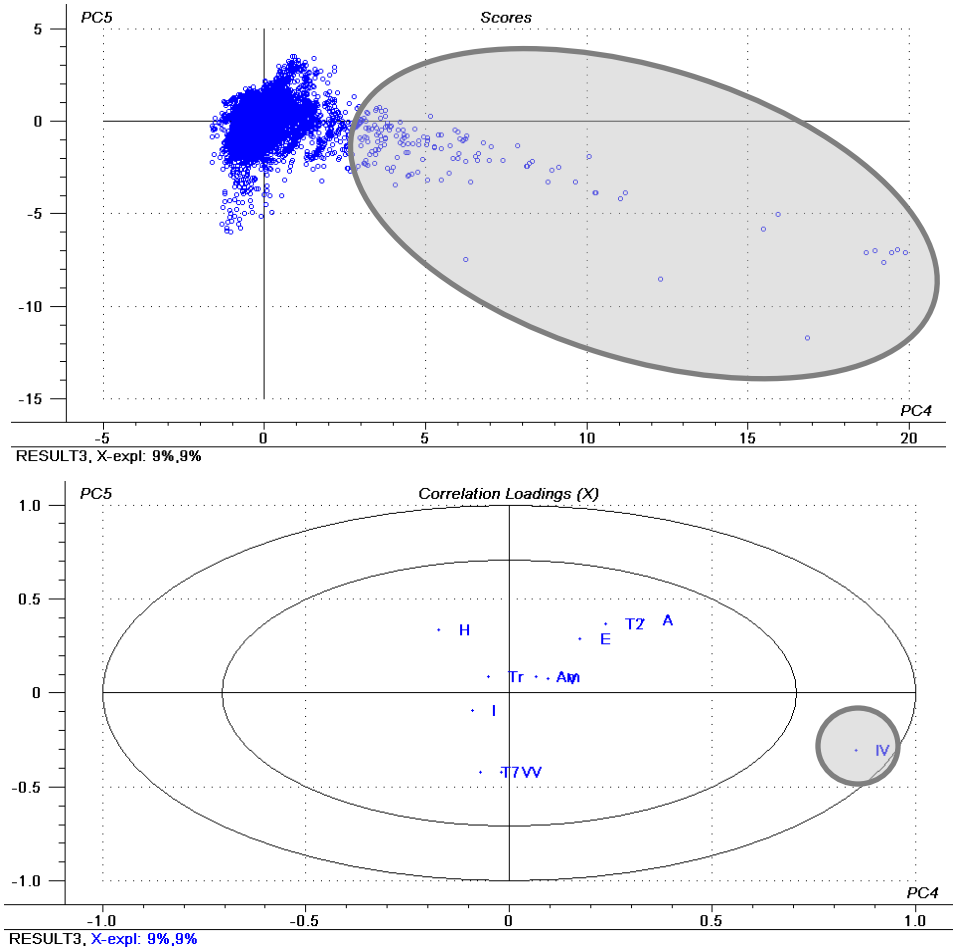

(a)

(b)

Figure 4-16: PCA results without T1, T4, T5 (PC4, PC5); (a) Score plot, (b) Correlation-loading plot

Most of the data acquisition has been conducted on sunny and cloudy days, including night drives. The number of scores in Figure 4-16(a) proposes little statistical expressiveness. Additionally, the scattered scores cannot be assigned to a specific flap or blower value. It is therefore suggested omitting the variable IV from the data set, due to a lack of statistical confidence. Testing procedures with alternating cycles of sun and cloudiness have not been conducted. This may imply further testing.

4.5.4 Dataset without IV

Figure 4-17 shows the Scree and the Pareto plot. The Scree plot shows one elbow at the third, as well as at the fifth PC. The first elbow is more distinctive than the second one. However, a straight line approximation appears more appropriate for PC5 to PC10. PC1 to PC4 explain 65.5% of the total variance and PC5 adds another 9.4%. This is shown in Figure 4-17(b). It is therefore suggested to retain PC1 to PC5 for further investigations.

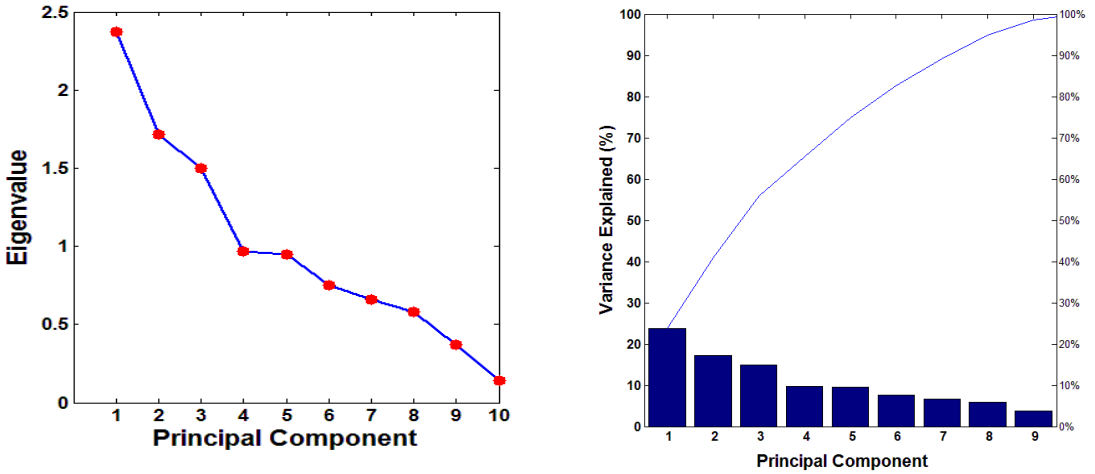

(a) **(b)**

Figure 4-17: Scree and Pareto plot without IV; (a) Scree plot, (b) Pareto plot

V is largely explained by PC1 (39.1%) and PC3 (24.4%). The remaining loadings are insignificant. The first three components explain 41.59% of VV's and 51.9% of TR's total variance. Figure 4-18 shows a loading plot for V, TR, and VV. It is apparent, that on the first three factors, V is in opposite direction of VV and TR. For a first approximation, the author therefore suggests omitting the variables TR and VV from the dataset, since a large proportion of their common variance is negatively correlated.

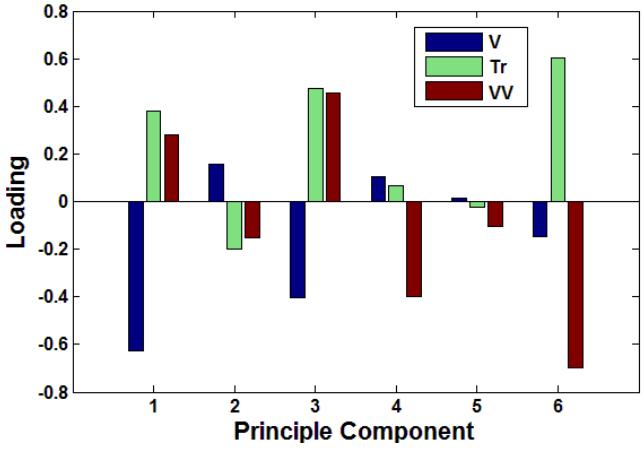

Figure 4-18: Loadings V, TR, VV

There is a logical explanation for these findings. When the vehicle speed is high, the vehicle is most probably driving on a highway. Changes in vehicle speed and variations in frequency of gas and brake pedal activity probably occur less frequent. At low vehicle speed, the vehicle is most likely driving under urban traffic conditions. Therefore chances in speed, due to acceleration and deceleration, may occur more frequently. Differences on higher factors can be explained with the memory effect of TR.

4.6 Interpretation

The dimensionality of the input space data set has been reduced from $\mathbb{R}^{20} \rightarrow \mathbb{R}^{8}$, only containing the variables A, Am, E, H, I, T2, T7 and V. The following subsection will try to reveal the variable's influence on blower level and flap position. Therefore, the following color codes will be used:

I. Blower score plot:

'blue'	Blower level '1',
'red'	Blower level '2',
'green'	Blower level '3',
'light blue'	Blower level '4'.

II. Flap score plot:

'blue'	'Breast' position,
'red'	'Breast-head' position,
'green'	'Head' position.

4.6.1 Ambient temperature, dashboard temperature and sun intensity

Figure 4-19 shows the correlation-loading plot for PC1 and PC2.

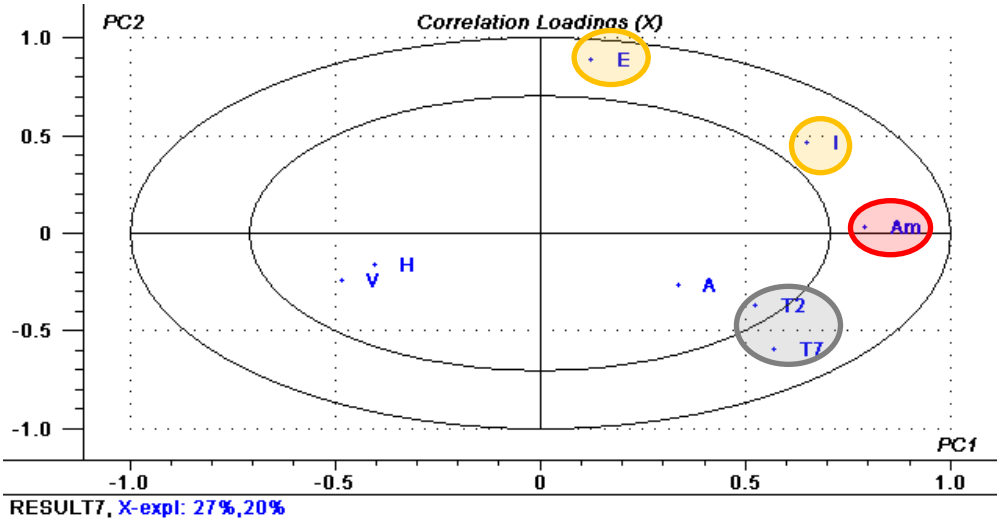

Figure 4-19: Correlation-loading plot PC1-PC2

It is apparent that the first and the second factor explain 47% of the dataset's total variance and explain 80% of E's, 63.7% of I's, 67.8% of T7's and 62.7% of Am's variance.

Figure 4-20(a) shows the corresponding blower score plot. In combination with Figure 4-19, it is apparent that samples in the yellow shaded ellipse have lower than average values for E and I. This data cloud contains the samples with diffuse radiation and high values in AV and EV. This tendency is enforced for lower than average values of E. It is apparent, that in the vast majority of cases, blower level '2' has been chosen. The red shaded ellipse indicates that higher than average values for the ambient temperature predominantly correspond to blower level '4'. It is evident that for lower than average values of Am, predominantly blower level '2' has been chosen. However, there also seems to be sporadic appearance of blower level '1'. Blower level '3' seems to be predominantly positively correlated to higher than average values of Am, T2 and T7, although a clear separation cannot be given. Lower than average values for T2 and T7 frequently correspond to blower levels '2' and '1'. Higher than average values on these variables correspond to blower levels '1', '3' and '4', whereas there is no clear distinction between blower levels '3' and '4'.

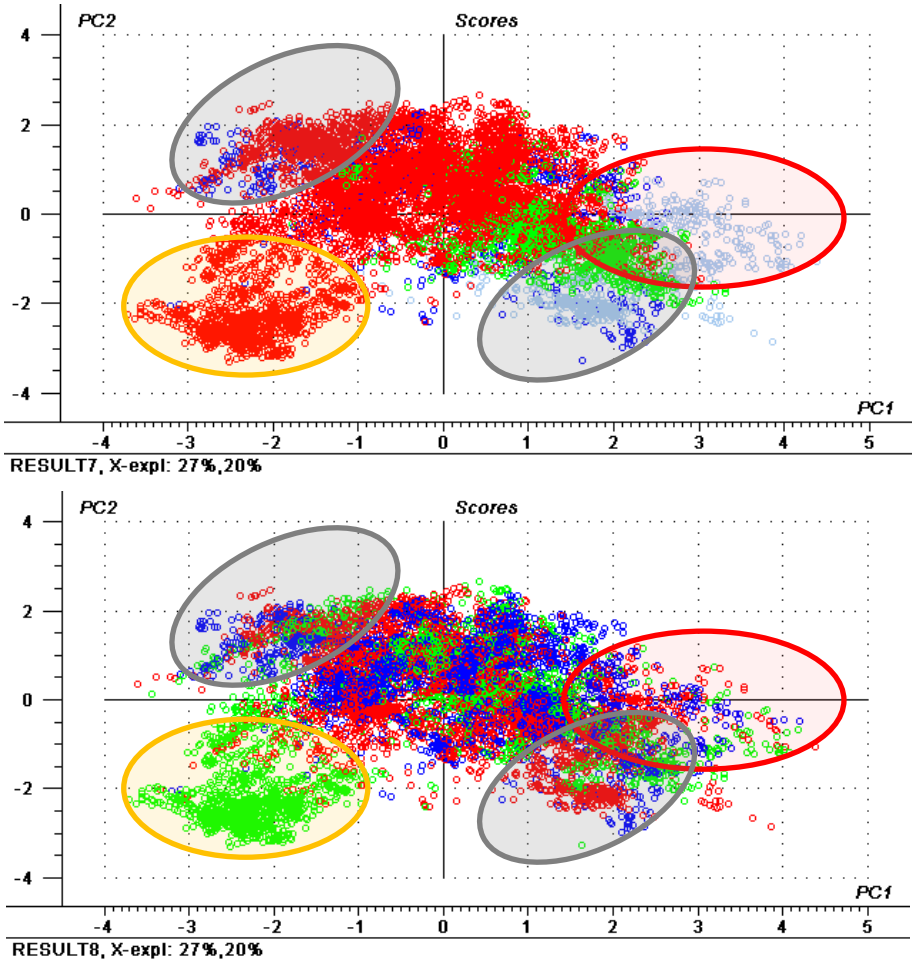

(a)

(b)

Figure 4-20: Score plots PC1-PC2; (a) Blower, (b) Flaps

At first glance blower level ‘1’ appears to be misaligned in this group. However, it shows out that blower levels ‘1’ and ‘4’ in this group clearly separate on PC5. A more detailed interpretation seems to be difficult, since all variables only load moderately on this factor. Figure 4-20(b) shows the score plot for the flap positions. It is apparent that lower than average values of I and E predominantly correspond with flap position ‘head’. In contrary to the previous score plot, one can hardly recognize any further structure in the data cloud. All flap positions seem to be distributed over the whole range.

4.6.2 Humidity

Humidity moderately correlates with PC1, PC3, PC4 and PC6. However, with PC3 and PC4 60% of its variance can be explained. This is shown in Figure 4-21.

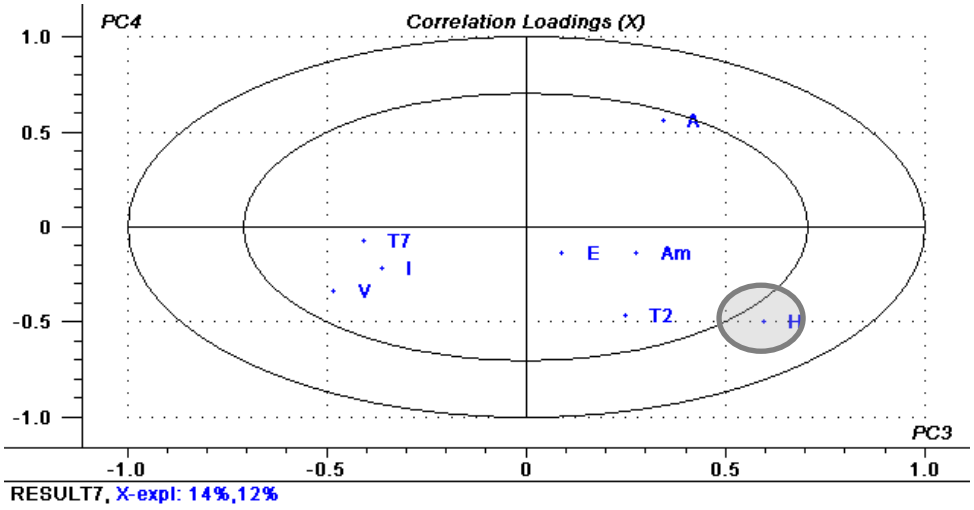

Figure 4-21: Correlation-Loading Plot PC3-PC4

The corresponding score plots for blower level and flap position are shown in Figure 4-22. Figure 4-22(a) suggests that higher than average values of H predominantly correspond to blower level ‘4’. There is also some indication that lower than average values of H may correspond to blower level ‘1’. In Figure 4-22(b), no distinctive preferences for flap position can be given for higher than average values of H. For lower than average values, one can recognize an increased occurrence of flap position ‘breast’. The score plot reveals that there seems to be a concentration of flap position ‘head’ towards positive scores of PC3 and PC4. This might be caused by higher than average values for A. However, interpretation is chancy, because A loads less than 50% on PC3 and PC4.

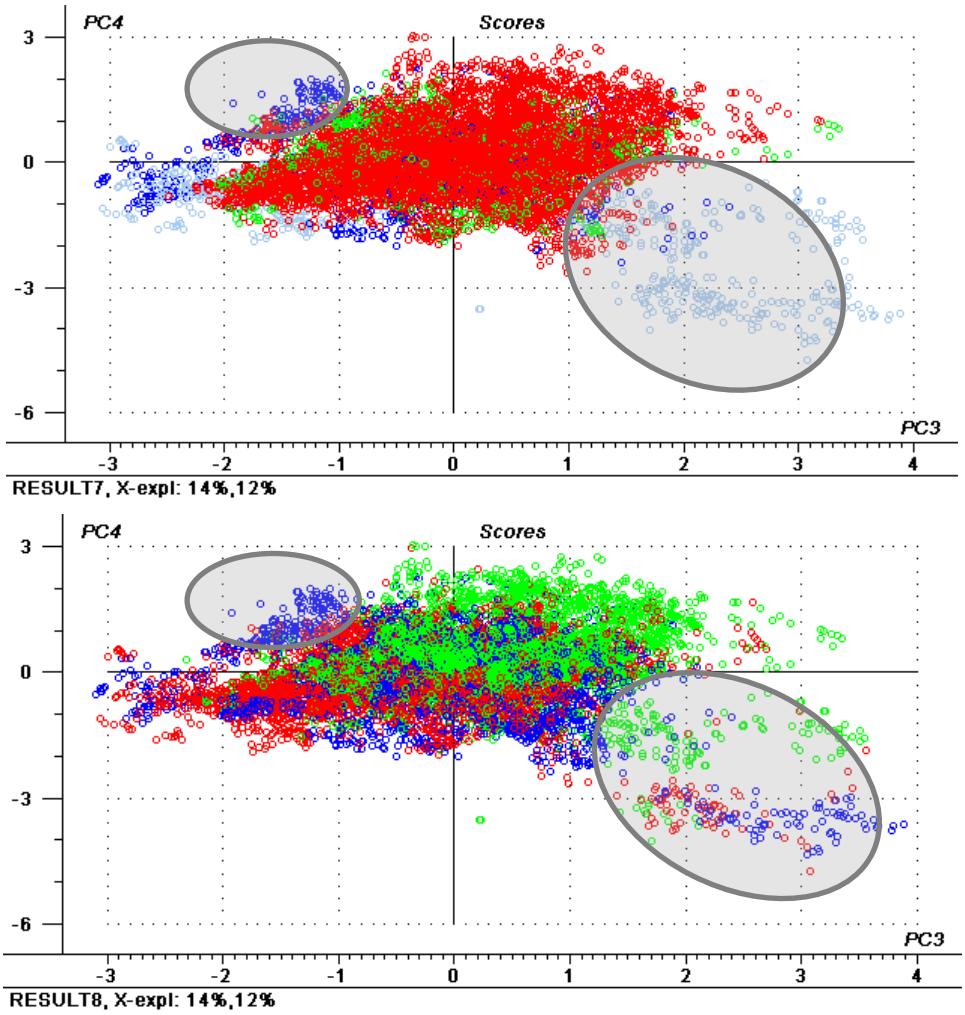

(a)

(b)

Figure 4-22: Score plots PC3-PC4; (a) Blower, (b) Flaps

4.6.3 Sun elevation angle

PC2 and PC5 explain 89.4% of E's variance. This is shown in in the correlation-loading plot in Figure 4-23.

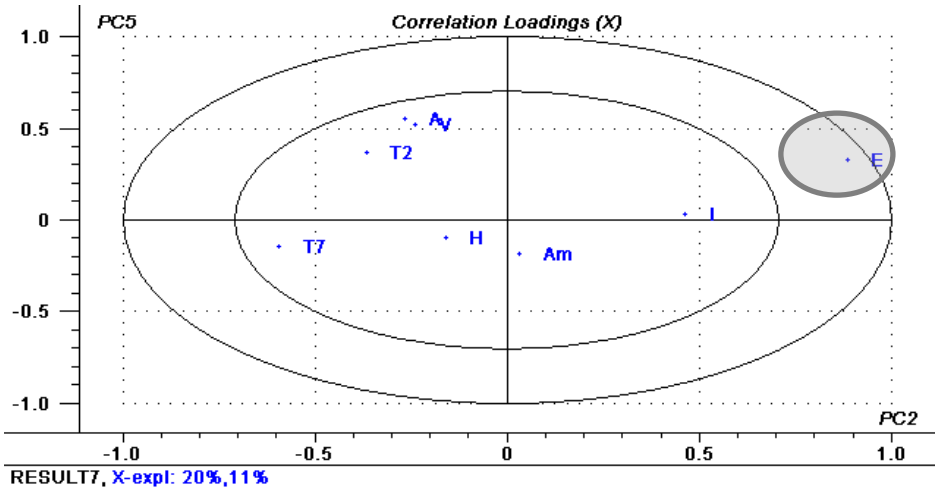

Figure 4-23: Correlation-Loading plot PC2-PC5

Figure 4-24(a) suggests, that higher than average values of E correspond to blower level ‘2’ and blower level ‘1’. However, a distinct separation seems not to be possible. Lower than average values for E predominantly correspond to blower level ‘2’. The superposition of blower levels ‘3’ and ‘4’ at negative scores of PC5 may be caused by higher than average values for T7, which correlates with 35.2% towards PC2.

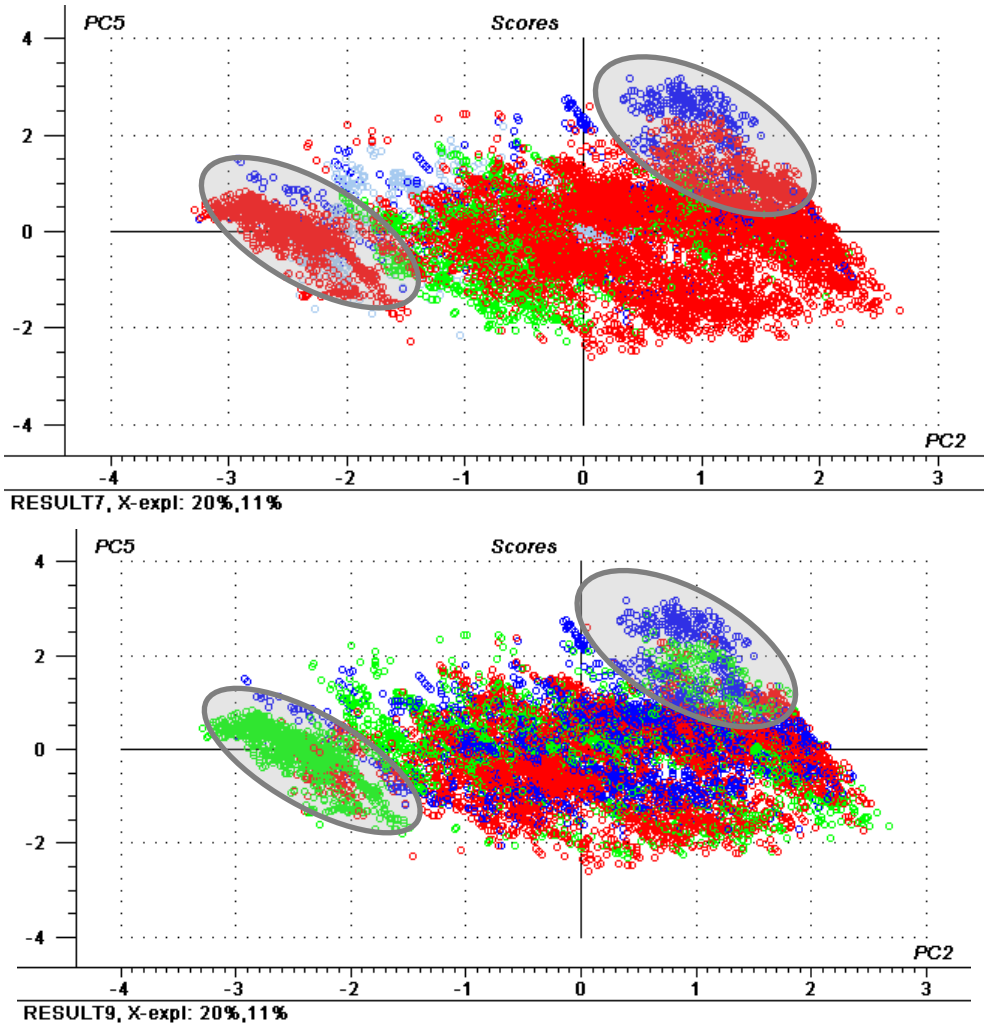

Figure 4-24: Score plots PC2-PC5; (a) Blower, (b) Flap

Figure 4-24(b) suggests that lower than average values for E correspond to flap position ‘head level’. Interpretation of the remaining scores is extremely vague. One could interpret higher than average values for E with an above-average occurrence of flap positions ‘breast’ and ‘head’. However, this seems to be contradictorily.

4.6.4 Sun azimuth angle

PC4 and PC5 contribute with 62.3% towards A’s variance. Figure 4-25 shows the correlation-loading plot.

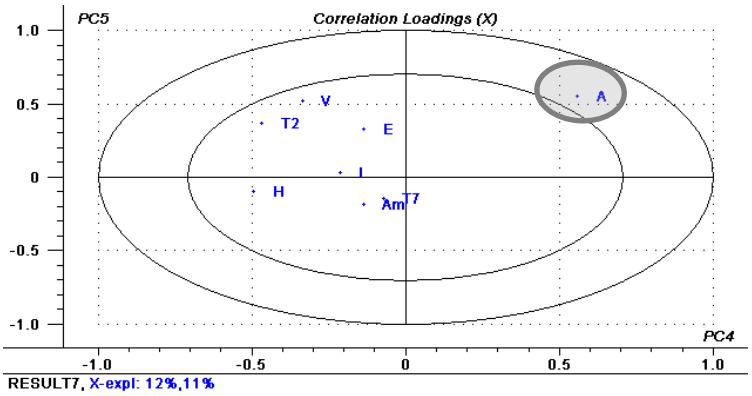

Figure 4-25: Correlation-Loading plot PC4-PC5

Figure 4-26(a) indicates, that higher than average values for A predominantly correspond to blower level ‘1’ and blower level ‘2’. For lower than average values for A no clear interpretation can be given with exception, that blower level ‘1’ seems to occur less frequent. The accumulation of blower level ‘4’ on the negative PC4 axis is probably being induced by higher than average values of H and T2.

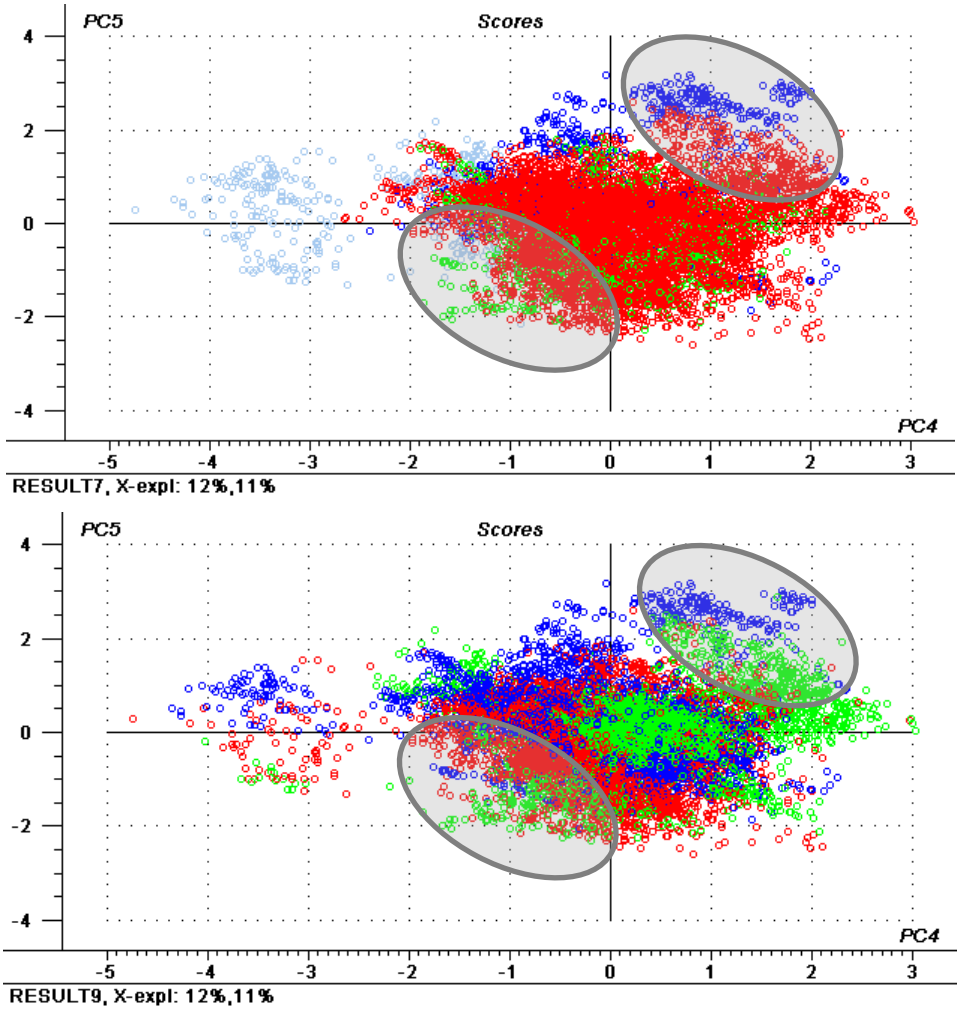

(a)

(b)

Figure 4-26: Score plots PC4-PC5; (a) Blower, (b) Flaps

Figure 4-26(b) shows that higher than average values of A correspond to flap positions ‘breast’ and ‘head’. For lower than average values of A, it appears that flap position ‘breast’ occurs less frequent.

4.6.5 Vehicle speed

V correlates moderately on PC1, PC3 and PC5. Most of V’s variance is described by PC3 and PC5, which explain 50.1% of its variance. This is shown in Figure 4-27. However, it is difficult to interpret the exact influence of V, because variables A and H are explained with similar loadings.

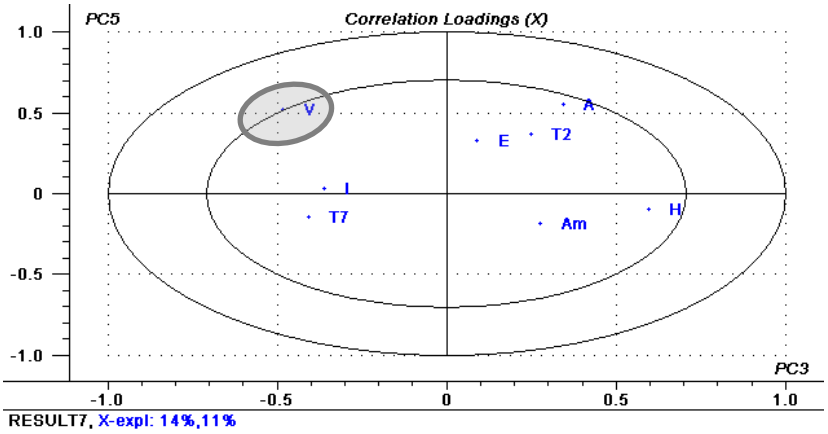

Figure 4-27: Correlation-Loading plot PC3-PC5

In Figure 4-28(a), it is apparent that higher than average values for V predominantly correspond to blower level ‘1’, whereas lower than average values for V seem to be dominated by blower level ‘2’. The overlap of blower level ‘2’ and blower level ‘4’ is being caused by H, which correlates with 35.5% towards PC3. Figure 4-28(b) suggests that for higher than average values of V, flap position ‘breast’ dominates. More detailed interpretations of the flap score plot will be abdicated, because of the moderate loading of the remaining variables.

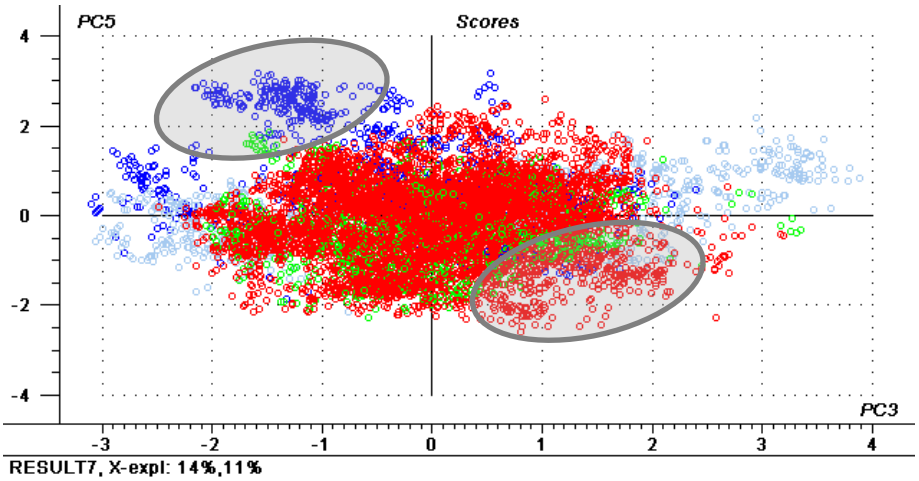

(a)

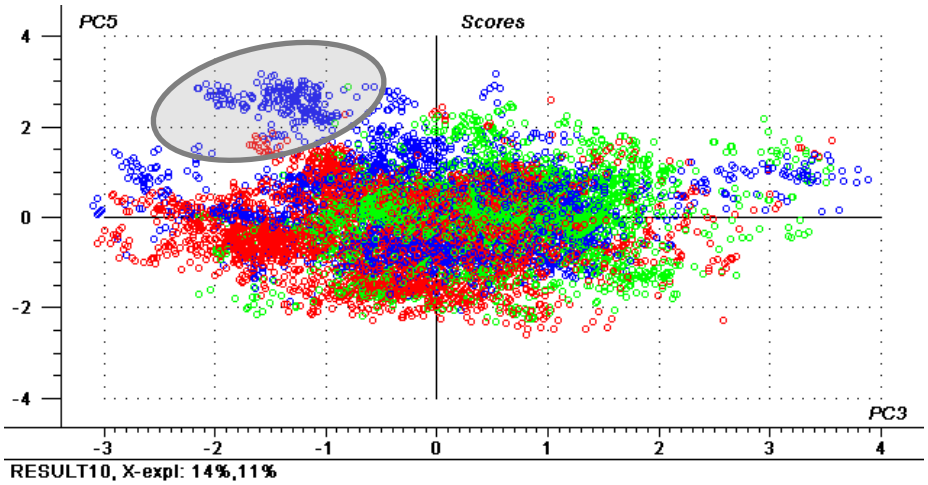

(b)

Figure 4-28: Score plots PC3-PC5; (a) Blower, (b) Flaps

4.6.6 Temperature knob

Blower level and flap position prediction are classification problems due to their discrete domain. In contrary to that, prediction of temperature knob is a regression problem. Figure 4-29 shows the temperature knob in dependence of Am. The ordinate represents the potentiometer setting and is plotted as digits. One digit is thereby equivalent to V = 19mV potentiometer voltage.

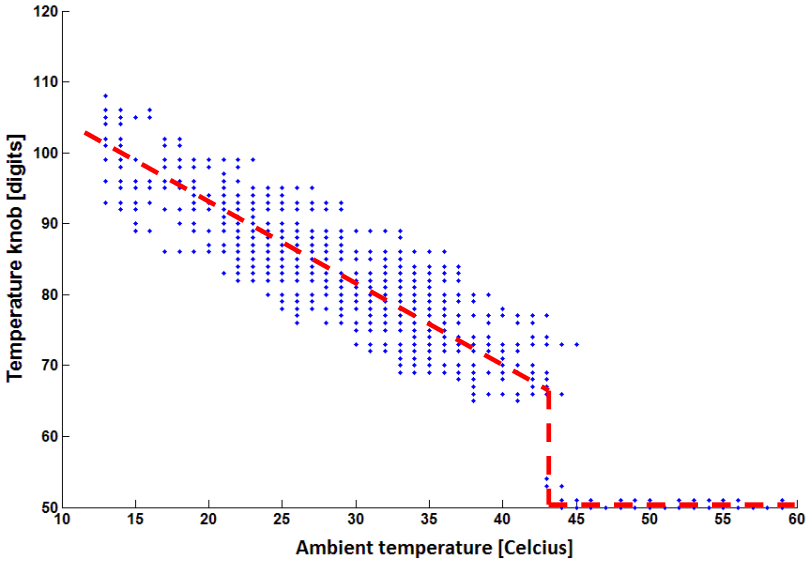

Figure 4-29: Scatter plot temperature knob – Ambient temperature

It is apparent, that up to ambient temperatures of $\vartheta_{Am} < +43°C$, a nearly linear relationship exists. This is confirmed by a negative correlation coefficient of r = -0.853. This means that the higher the ambient temperature, the lower the temperature knob value. For $\vartheta_{Am} \geq +43°C$, the temperature knob value is approximately constant at its lower boundary. This can be considered as a non-linear saturation effect. However, the linear dependency is superimposed by noise with

$\Delta V = \pm 0.2V$. The author suspects that this is caused due to the relative imprecise mechanical transmission ratio from temperature knob to the HVAC ECU's internal potentiometer. For future research, this mechanical transmission should be improved.

It is interesting to note that there seems to be only little functional relationship between the temperature knob and the in-cabin air temperature ϑ_2. This is shown in Figure 4-30.

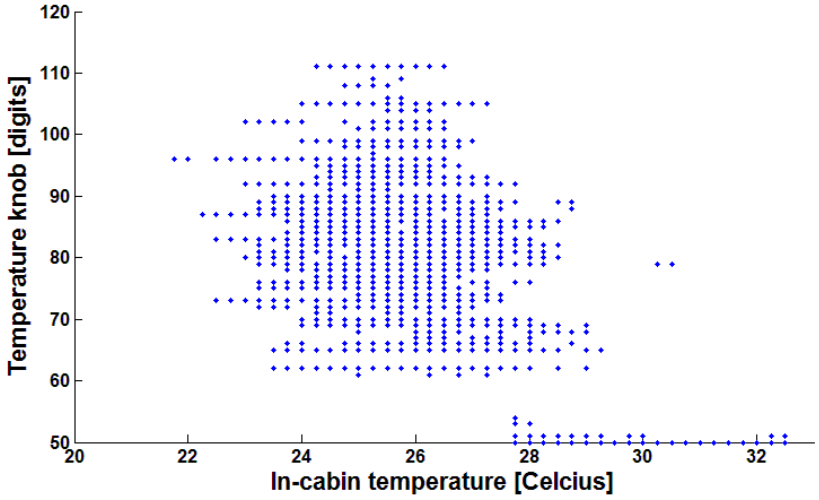

Figure 4-30: Scatter plot temperature knob – In-cabin air temperature

However, it is apparent that a saturation effect occurs for $\vartheta_2 \geq +30℃$. An explanation for the little influence of in-cabin temperature towards temperature knob setting might be justified in the direct influence of ambient temperature to air outlet temperature. Additionally, it might also confirm the ambient temperature's direct influence on head level temperatures, as concluded in Chapter 4.5.2. It is therefore suggested to predict temperature knob setting solely with ambient air temperature.

Methods of artificial intelligence can also be used for regression. However, in this one-dimensional context approximation through a straight line approximation is considered to be sufficient, since no higher level modelling technology will be able to able to remove the noise indicated in Figure 4-29. It is therefore suggested to model the temperature knob as approximation of two straight lines as indicated by the dashed red lines in Figure 4-29.

4.7 Summary

Methods of data mining have been used for data integration, data cleaning, dimensionality reduction, data transformation and have been implemented in Matlab. Principles of multivariate statistics have been applied to discover variable interrelationships and correlations, in order to reduce the dimensionality of the feature space. Special importance has been attached to PCA, a dimensionality reduction and visualization technique, which successively explains maximal

variance. With the application of these methods, the dimension of the input space was reduced from $\mathbb{R}^{20} \rightarrow \mathbb{R}^{8}$. The necessary variables have been identified as:

- Vehicle speed v,
- Relative humidity h,
- Ambient temperature ϑ_{Am},
- In-cabin temperature ϑ_2,
- Dashboard temperature ϑ_7,
- Sun intensity I,
- Sun elevation angle Ψ,
- Sun azimuth angle φ.

The influence of these variables on blower level and flap position has been interpreted with methods of exploratory data analysis. It has been shown, that due to the multidimensional nature of the problem, only little information can be extracted by hand, because the separation of multidimensional hyper-planes probably overstrains human's imagination. In the next chapter, it will be shown that methods of artificial intelligence are capable of coping with this kind of difficulties and perform far superior.

It is been shown that temperature knob setting is predominantly linearly dependent of ambient temperature. However, it has been observed that measurement of temperature set-up values are superimposed by about 0.1V noise. It is assumed that this has been mainly caused by imprecise gear translation but might have been also caused by human fuzziness.

Chapter 5

Modelling and Verification

Modelling aims to represent physical phenomena and processes in a logical and objective way. Scientific models are therefore often based on implementation of mathematical and physical fundamental laws and therefore require certainty, precision and rigor. This classical approach towards modelling is often called hard computing.

Methods discussed in this chapter are often summarized as methods of artificial intelligence and soft-computing. These approaches aim to imitate the intelligence found in nature and are capable of learning from past experience, including pattern recognition and decision making. According to [63], the basic premises for soft computing are:

- The real world is pervasively imprecise and uncertain,
- Precision and certainty carry a cost.

Given an input space $X \subseteq \mathbb{R}^m$ and an output space $Y \subseteq \mathbb{R}^n$, learning can be defined as finding a function *g*, which fulfills

$$\mathbf{y} = g(\mathbf{x}), \tag{61}$$

with $\mathbf{x} \in X$ and $\mathbf{y} \in Y$. In practice there is general neither information about the exact functionality, nor about any underlying distribution available. The only available information might be a training data set T, which contains samples of $\mathbf{x}_i$ and $\mathbf{y}_i$, which have been drawn from the input and output space. The training data set can be mathematically described as

$$T = \{(\boldsymbol{x}_i, \boldsymbol{y}_i) \in X \text{ x } Y\} \; for \; i = 1 \ldots P \; , \tag{62}$$

with P being the total number of available training pairs. With these definitions, machine learning aims to find the function *g* that fulfills equation (61), with use of equation (62). There are various learning methods available today. Some of them have their origins in classical statistical inference. However, classical statistical methods may not always perform well in real world applications, because of their idealized theoretical assumptions [63].

In terms of this research, data has been collected from experimental field research. Assumptions of linear parametric dependency and any predefined underlying probability distribution, can therefore not be guaranteed. Due to a lack of knowledge about the process itself, the author has identified blackbox approaches, like artificial neural networks (ANN) or support vector

machines (SVM), as suitable tools for modelling. Both techniques are non-linear and non-parametric models. ANNs are established methods in AI and many powerful software tools do exist for system development. The author has therefore chosen ANNs for thermal comfort modelling.

5.1 Basics of neural networks

Artificial neural networks are universal function approximates, which are inspired by biological neural networks (NN). They have found wide application in pattern recognition as well as system identification. Human's brain consists of billions of single processing units, so called neurons, which are interconnected to each other and compose a complex and powerful structure. A technical implementation of a single neuron is illustrated in Figure 5-1.

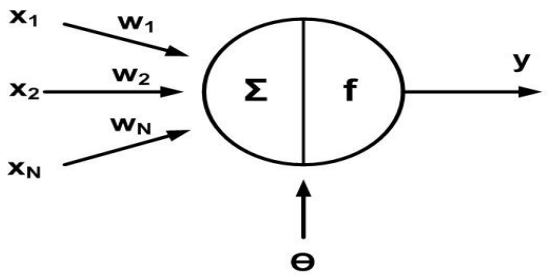

Figure 5-1: Single artificial neural processing unit

Each neuron is capable of processing an input vector $\mathbf{x} \in \mathbb{R}^N$ and outputs a scalar y. The weight vector $\mathbf{w} \in \mathbb{R}^N$ shall thereby imitate biological synapses in NNs, which determine the influence of each x_i on neuron's output y. The weighted summation of the input vector **x** is called 'net' and can be mathematically expressed as

$$net = \mathbf{w}^T \boldsymbol{x} + \Theta = \sum_{i=1}^{N} w_i x_i + \Theta \,. \tag{63}$$

The input signal Θ is a constant, which is often referred to as bias term. Sometimes it is not mentioned explicitly and is incorporated into the input vector **x**. The scalar output signal y can then be expressed as

$$y = f(net) = f\left(\sum_{i=1}^{N} w_i x_i + \Theta\right). \tag{64}$$

The function *f()* is called activation or transfer function. Both nomenclatures will be used interchangeably in this thesis. The activation function can be theoretically any linear or non-linear function. If *f()* is a step function, a neuron as illustrated in Figure 5-1, is called 'perceptron'. A perceptron can be considered as a classificator with linear decision boundary,

making it possible to separate lines and hyper-planes. However, in practice most often non-linear sigmoid or logistic functions are used due to their mathematical properties like monotonicity, continuity and differentiability [102]. Latter property is required for effective learning algorithms. A sigmoid transfer function, which is also used in this research, is given in equation (65).

$$f(x) = \frac{1}{1 + e^{-x}} \tag{65}$$

In practice, neurons are often combined to a network and are arranged in layers as illustrated in Figure 5-2. This allows for solving highly complex classification problems [63].

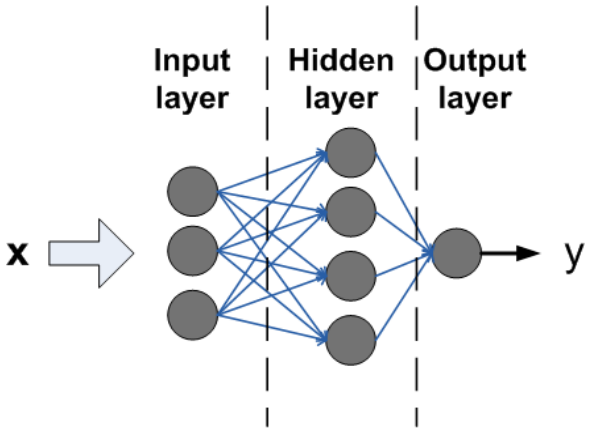

Figure 5-2: Multilayer neural network

The example shows a 3-4-1 ANN with three input neurons, four hidden layer neurons and one output layer neuron. This structure is often called feed-forward neural network (FNN). Sometimes input layers neurons are called nodes, because they just serve as signal distribution units and do not incorporate any signal processing. Similarly to equation (64), the output y_j^n of the jth neuron in the nth layer can be calculated as:

$$y_j^n = f_j^n\left(net_j^n\right) = f_j^n\left(\sum_{i=1}^{N^{n-1}} w_{ji}^n y_i^{n-1} + \Theta_j^n\right), \tag{66}$$

with

$f_j^n()$: Activation function of the jth neuron in layer n,

w_{ji}^n: Weight linking the ith neuron in the (n-1)th layer with the jth neuron in the nth layer,

y_i^{n-1}: Output of the ith neuron in (n-1)th layer,

Θ_j^n: Bias term of the jth neuron in the nth layer,

N^{n-1}: Number of neurons in layer n-1.

Training of an ANN is considered as finding the optimal values for **w** and Θ in equation (66). A suitable measure of performance for the output y_{pk} is the mean square error (MSE).

$$MSE = \frac{1}{2}\sum_{p=1}^{P}\sum_{k=1}^{N}\left(t_{pk} - y_{pk}\right)^2 \quad \textbf{(67)}$$

with

N: Number of output layer neurons,

P: Number of patterns,

t_{pk}: Target value of the k^{th} neuron for the p^{th} pattern.

To reduce the error in the network, equation (67) has to be minimized with respect to the weights and the bias terms in the network. The learning delta for each w can then be calculated as partial derivative of the MSE with respects to the weights w_{ji}^{l} in the network. This is indicated by equation (68).

$$\Delta w_{ji}^{l} = \eta \frac{\partial MSE}{\partial \Delta w_{ji}^{l}}, \quad \textbf{(68)}$$

with η being called learning rate. The solution of equation (68) is mathematically voluminous and will not be presented in this thesis. For details, the reader is referred to literature, e.g. [50], [63]. Additionally, equation (67) shows that equation (68) must be solved sequentially, beginning at the output layer and back-propagating the error to the input of the network.

5.2 Design criteria

When designing a neural network, the engineer has to identify a suitable network structure. Today the amount of possible ANNs is enormous, including highly specific network structures. Today, there are about 50 types of networks available [63]. However, this research will be limited to FNNs, since they are common for pattern analysis problems. The three most important design parameters are sample size, number of hidden layers and number of hidden layer neurons. This will be discussed in the following subsections.

5.2.1 Sample size

The first questions in ANN network design are:

- ‘How many test samples are required to reliably approximate the problem at hand?’
- ‘How many test samples are required to reliably train the ANN at hand?’

A formal answer to these questions cannot be given, since the generalization ability of a neural network predominantly depends on three properties [50]:

- Size of the training set and its quality (expressiveness),
- The architecture of the neural network,
- The complexity of the approximation problem at hand.

Clearly the last factor is not controllable, since when considering an implementation using ANN, the researcher has generally only little knowledge about the process' underlying complexity. The first and the second factor are dependent of each other. However, assuming that the researcher has chosen a suitable neural network structure and an expressive training data set for the problem at hand, [50] suggests equation (69) for determination of the required number of training samples N_s.

$$N_s = O\left(\frac{N_v}{\varepsilon}\right) \tag{69}$$

with:

N_v: Total number of free parameters within the network,

ε: Fraction of classification errors permitted on test data,

O: Order of quantity enclosed in.

For example, with ε = 0.1 (10% error), the number of expressive training samples should be approximately ten times the number of free parameters in the network. The free parameters in a FNN are the number of weights and bias terms. For a k hidden layer FNN, N_v can be calculated according to

$$N_v = N_x(N_{l1} + 1) + \sum_{\substack{i=1 \\ (i+1)\leq k}}^{k} N_{li}(N_{li+1} + 1) + N_{lk}\,(N_o + 1), \tag{70}$$

with

N_x: Number of input nodes,

N_{l1}: Number of first hidden layer neurons,

N_{lk}: Number of k^{th} hidden layer neurons,

N_o: Number of output layer neurons.

It is important to note that equation (71) is an empirical rule, which has proven to perform well in practice. However, its validity can be explained with the theory of bounds on approximation errors. For details, the reader is referred to [50]. No formal exact method is available in literature so far.

5.2.2 Number of hidden layers

An ANN with an arbitrary large number of non-linear hidden layer neurons can approximate any continuous function [63]. This can be shown with the universal approximation theorem for an arbitrary continuous function $f(\mathbf{x})$ [50]:

$$F(\boldsymbol{x}) = \sum_{i=1}^{m_1} \alpha_i \gamma \left(\sum_{j=1}^{m_0} w_{ij} x_i + \mathrm{b}_i \right) \text{ and} \quad \textbf{(71)}$$

$|F(\boldsymbol{x}) - f(\boldsymbol{x})| < \epsilon,$

$F(\boldsymbol{x})$ is therefore an approximation for the continuous function $f(\boldsymbol{x})$.

With:

α_i, w_{ij}, b_i: Constants,

γ: A monotone increasing continuous function,

m_0, m_1: Arbitrary parameters.

Comparison of equation (71) and (64) reveals that equation (71) can be interpreted as an ANN with m_0 input nodes and a single hidden layer with m_1 hidden layer neurons. The output is a scalar and a linear combination of the hidden layer neuron outputs. This theorem shows that a single hidden layer is theoretically sufficient to approximate an arbitrary continuous function $f(\mathbf{x})$. In literature, there is however disagreement if one or two hidden layers should be used in terms of optimal generalization performance. Generalization therefore refers to the network's performance with respect to previously unseen data. There seems to be however consensus that more than two hidden layers are not required [50], [63]. There is currently no sound theory which approach performs better. In terms of this research the author follows the concept of [63], who first recommends trying a network with one hidden layer, before implementing an ANN with two hidden layers.

5.2.3 Number of hidden layer neurons

The number of input and output neurons is generally defined by the dimensionality of the application's input and output space. The number of hidden layer neurons is the most important design parameter, which determines the representational power of the network and its generalization capability [63]. The focus lies thereby on modelling the underlying function of a given input output mapping, whilst filtering out noise and disturbances. Two extreme situations may occur:

- The number of neurons is chosen too small in order to approximate the underlying function (under-fitting),
- The number of neurons is chosen too high what may result in adaption to the data set's noise and disturbances (over-fitting).

This is also known as the variance–bias problem. According to [63], the bias-variance decomposition of MSE can be mathematically expressed as:

$$MSE = \mathbb{E}_T[(y(x;T) - \mathbb{E}[(t|x)])^2] + \mathbb{E}_T[(y(x;T) - \mathbb{E}_T[y(x;T)])^2], \quad \textbf{(72)}$$

with

$\mathbb{E}[y|x]$: Expectation operator of x and y,

$\mathbb{E}_T[y|x]$: Expectation operator of x and y, with respect to the training data set T.

The first term on the right side of equation (72) represents the squared bias, as difference between the expectation of the neural network output and the regression function. The second term quantifies the variance, as the difference between the a specific neural network output and the expected neural network's output with respect to all training patterns. Figure 5-3 shows a graphical interpretation of equation (72).

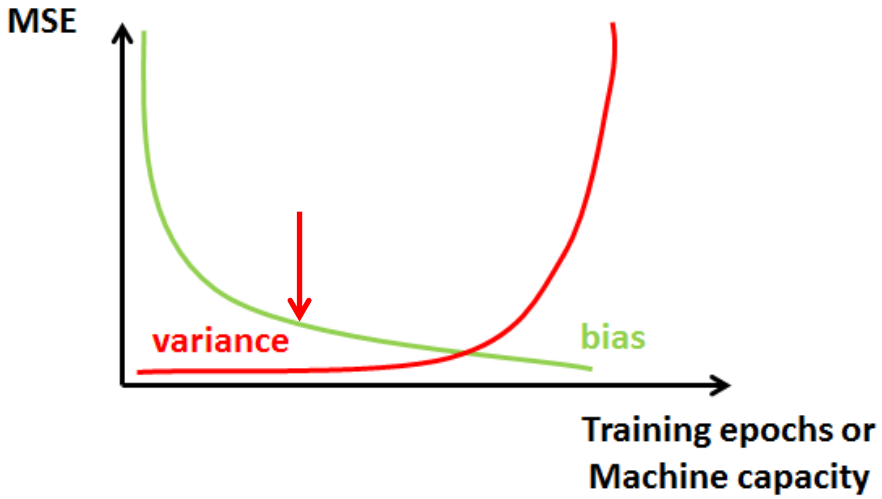

Figure 5-3: Bias Variance

Bias typically decreases with increasing training epochs or with increasing capacity of the learning machine. Variance increases with increasing number of training epochs or machine capacity. The machine's capacity thereby increases with increasing number of hidden layer neurons. According to equation (72), the total error is the sum of bias and variance. In Figure 5-3, the global minimum will be achieved, when both curves meet. This is indicated by the red arrow.

In practice, often an independent validation data set is used in order to monitor the variance. If training error decreases and validation error increases, the network tends to over-fit and adapts to noise and disturbances. This means the network's generalization capability is likely to decrease. At this point, training should be stopped. This is often called cross-validation which is founded on the fact that good performance in training algorithms does not automatically ensure good generalization results. This methodology can also be used to determine the optimal number of hidden layer neurons.

5.3 Application to climate data

In terms of this research, blower level prediction can be described as $\mathbb{R}^8 \rightarrow \mathbb{R}^4$ mapping. The number of input nodes is therefore determined to be eight and the number of output neurons is defined as four. Flap position prediction can be described as $\mathbb{R}^8 \rightarrow \mathbb{R}^3$ mapping, meaning eight input layer nodes but only three output layer neurons.

Since only little a-priori knowledge about blower level and flap position prediction is available, the number of hidden layer neurons must be chosen according to the complexity of the underlying functionality. For training the ANNs about 3000 consistent data samples are available. According to equation (69), this allows for training of networks with a total sum of Nv=300 free parameters with an error probability ε=0.1. With equation (70), the recommended upper bound of hidden layer neurons is determined to be 23 for blower level prediction and 25 for flap position prediction. To determine the number of hidden layer neurons for blower level and flap position prediction, networks with different number of hidden layer neurons have been trained and their performance has been compared. When training an ANN, the weights within the ANN are normally randomly initialized. However, improper initialization of weights may result in infinite training times or stopping at a local minima of performance [63]. Therefore 200 networks have been trained for each hidden layer configuration. The best 150 results for training and validation performance have been taken into account and have been plotted as average in Figure 5-4.

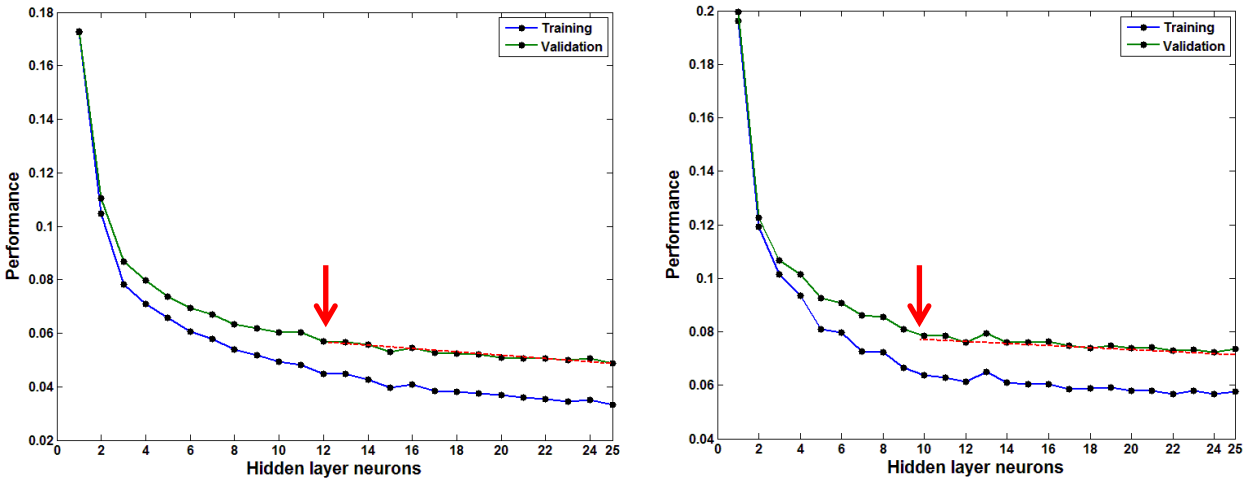

(a) **(b)**

Figure 5-4: Performance plots; (a) Blower level ANN, (b) Flap position prediction ANN

This procedure prevents that poor weights initialization affect the performance plots and additionally provides statistical confidence concerning the results.

Figure 5-4 shows that neither blower level ANNs, nor Flap position ANNs have been over-fitted. It is apparent that the networks' performances initially increases and levels off towards higher numbers of hidden layer neurons. There are no apparent local minima. However, it is also apparent that performance only slowly increases towards high numbers of hidden layer neurons. However, literature suggests to select as few as hidden layer neurons as possible, in order to minimize the number of free parameters within the network [102]. This means trading off precision against cost.

The author therefore adapts Cattel's straight line approach from Chapter 4.3.4.2 to find the optimal number of hidden layer neurons for blower level as well as for flap position prediction. This is indicated by the red lines in Figure 5-4. In Figure 5-4(a), it is apparent that hidden layer neurons 12 to 25 form a more or less straight line, indicating only little further improvements in prediction performance. In Figure 5-4(b), this straight line can be found for hidden layer neurons 10 to 25. The researcher therefore suggests implementing 12 hidden layer neurons for blower level prediction and 10 hidden layer neurons for flap position prediction.

With these findings, the neural network structures have been determined as shown in Figure 5-5.

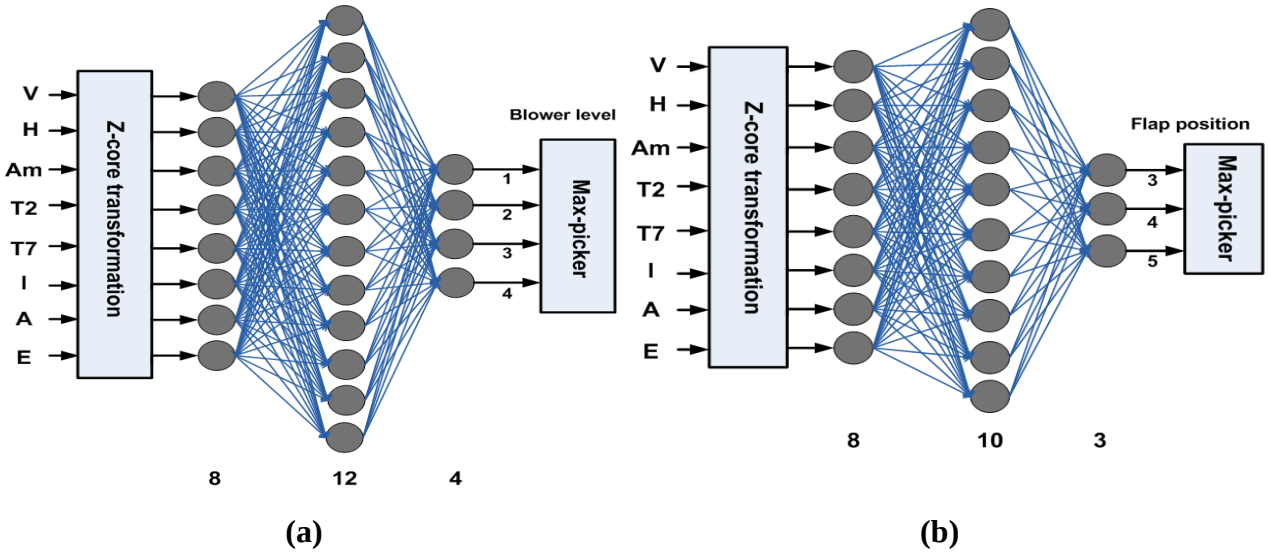

Figure 5-5: Artificial neural network structure; (a) Blower level, (b) Flap position

The total number of free parameters can be determined as N_v=169 for the blower level prediction network in Figure 5-5(a) and as N_v=128 for the flap position prediction network in Figure 5-5(b). According to equation (69), this means that the networks can be efficiently trained with about N_s=1700 for blower level and with about N_s=1300 (good) samples for flap position prediction.

The input variables to both networks have been z-core transformed using equation (56), in order to minimize the bias of one feature over another. In a later design, z-core normalization parameters have to be included into the input layer of the network. This can be implemented as

successive subtraction and division of the z-core parameters. The required parameters are given in appendix A.6. Each output layer is connected to a max-picker element, which provides the following functionality: Given an output vector $\mathbf{y} \in \mathbb{R}^n$, the output can be expressed as

$$y = max(y_1, y_2, \dots, y_n). \quad \textbf{(73)}$$

In terms of this research the available data set consists of each about 3000 samples for training of blower level and flap position ANNs. This data has to be randomly divided into three single datasets for training, validation and testing purposes, as illustrated in Figure 5-6.

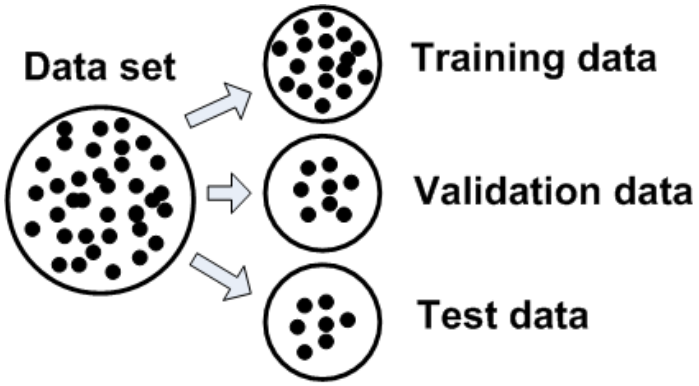

Figure 5-6: Data separation process

The portioning is as follows:

- Training data 65%,
- Validation data 15%,
- Test data 20%.

Validation data is used for stopping training, in order to prevent over-fitting and provides a measure of the generalization capability of the network. Due to a lack of interfacing possibilities to existent HVAC ECUs, no verification in a real vehicle can be implemented at this stage of research. Testing data are therefore being withheld during the training process and are used as independent, not previously seen data for system verification.

5.4 Results

The activation functions in the hidden layer neurons, as well as in the output layer neurons, were chosen to be a sigmoid function like equation (65). The training algorithm was chosen to be the Conjugate gradient descent algorithm, a second order optimization method, which often offers quick convergence. Details about the Conjugate gradient descent algorithm can be found in [50], [63] and [102].

The ANN models in Figure 5-5 have been trained and verified. The results will be presented in the following subsections.

5.4.1 Blower level prediction

The training results for blower level prediction are shown in Figure 5-7(a). It is apparent that best validation performance (BVP) has been reached after 161 training epochs. Training has been cancel at epoch 167, because validation performance has decreased for six successive cycles, meaning the network was tending to over-fit at epoch 161.

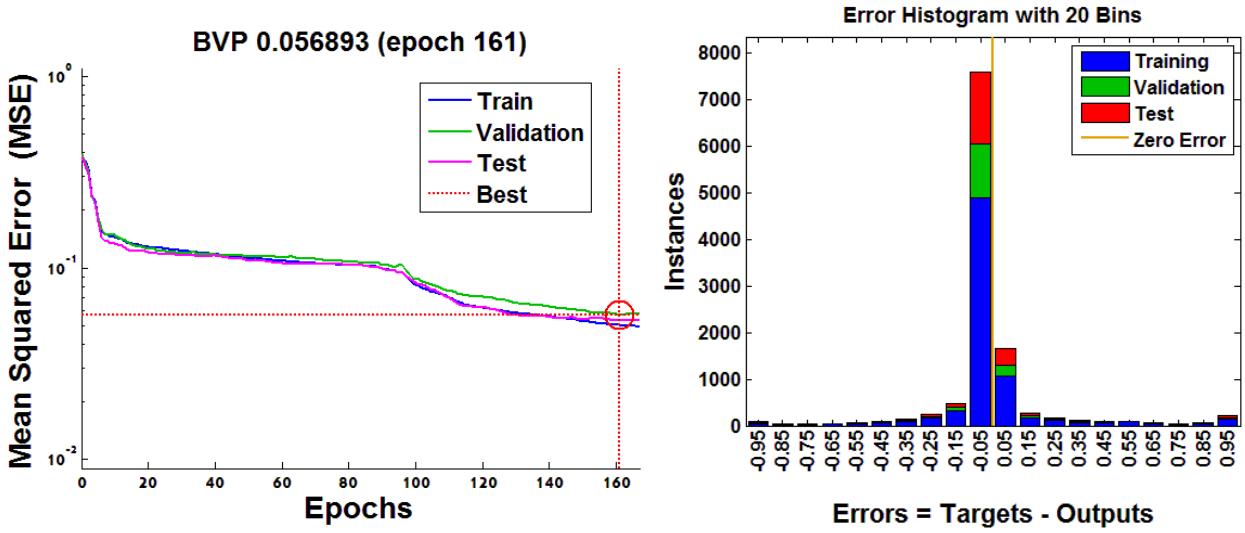

(a) **(b)**

Figure 5-7: Performance plot for blower level prediction; (a) Performance plot; (b) Error histogram

The functional course of test and validation performance in Figure 5-7(a) is similar, which confirms a suitable data separation, as well as a good generalization capability of the network. Since network performance may be dependent on the initial initialization of the weight vectors $\mathbf{w_i}$, the network has been retrained for about 50 times, achieving similar results. The author is therefore confident that a global minimum in the error function has been found. Figure 5-7(b) confirms the good generalization capability and presents an error histogram, divided into 20 bins, which shows the absolute errors between target values and output value for each output layer neuron. The optimal case of zero deviation is indicated by the orange colored line. It is apparent that most of the errors are contained within the interval [-0.05;0]. The number of instances in critical intervals ([-1;-0.5] and [+0.5;+1]), which will lead to misclassification are acceptable low. Figure 5-8 shows the classification results for training, validation and testing. The diagonal cells show the number of cases that were correctly classified and the off diagonal elements show misclassified cases. The blue cell shows the total amount of correctly classified cases.

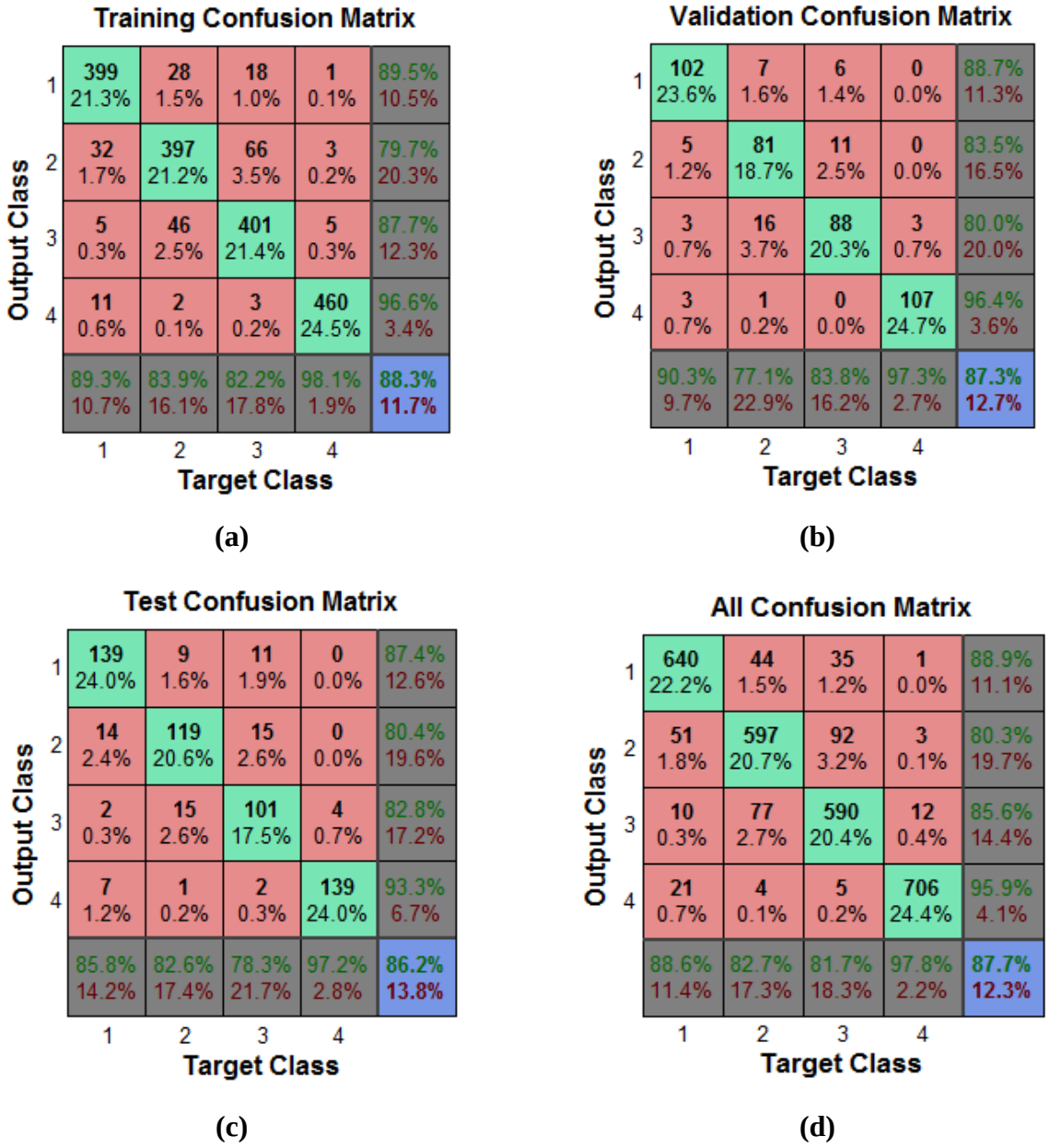

Figure 5-8: Confusion matrix for blower level prediction; (a) Training confusion, (b) Validation confusion, (c) Testing confusion, (d) Overall confusion

Each row shows the classification results with respect to the output class and each column shows the classification results with respect to the target class. Evaluating the overall result from training, validation and testing, which is given in Figure 5-8(d), one can see that a total of 87.7% of the cases were correctly classified. The results for test, validation and training data in Figure 5-8(a), (b) and (c) show similar performance. It is apparent that blower level '1' and blower level '4' have been best classified, suggesting that extreme conditions are well separable. Blower level '1' could be correctly predicted in 88.6%, blower level '2' in 82.7%, blower level '3' in 81.7% and blower level '4' in 97.8% of all cases.

The classification performance between blower level ‘2’ and blower level ‘3’ seems not to be that clear. It is apparent that most cases of misclassification occur in neighboring classes. Figure 5-8 therefore suggests that the operator had more difficulties to uniquely distinguish between blower level ‘2’ and blower level ‘3’ than between extreme situations. There seems to be an estimated 20% overlap between blower level ‘2’ and blower level ‘3’. This tendency is present in the training, validation and testing plots.

There are various possible explanations for these phenomena. One could conclude that humans are fuzzy in evaluation of their thermal environment. This evaluation might also be time and location-variant to some extent. Another possible explanation might be the use of a manual HVAC system, which only allows for setting up a discrete output space. Problems may especially occur when the environmental situations demand an output value in between two discrete output classes. This could result in an increased range of decision fuzziness.

However, it is finally concluded that 87.7% correct overall classification performance is a superior result and offers fairly good prediction results.

5.4.2 Flap position prediction

The training- and validation results of the ANN for flap position prediction are shown in Figure 5-9. Figure 5-9(a) indicates that BVP has been reached after 123 training epochs.

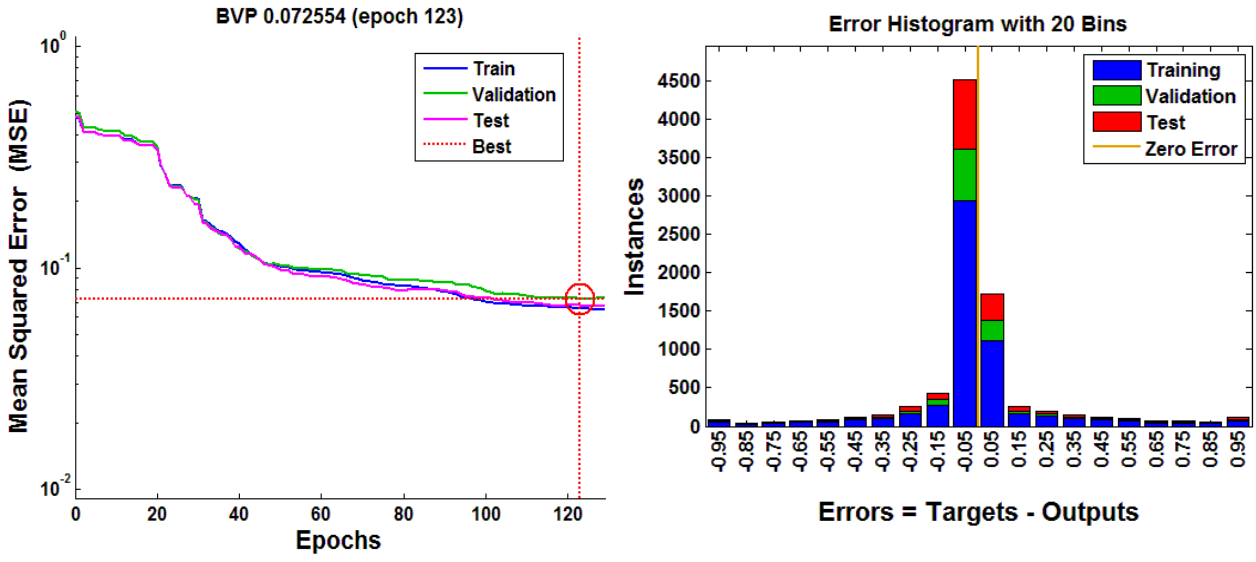

(a) **(b)**

Figure 5-9: Performance plot for flap position prediction; (a) Performance plot; (b) Error histogram

Similarly to blower level prediction, Figure 5-9(a) shows a smooth course of training and validation performance. There are no obvious significant differences in local maxima and

minima which would suggest a poor separation of the data set or over-fitting tendencies. This is confirmed by the error histogram in Figure 5-9(b). It is apparent that most instances are located within the error interval [-0.5;0]. It can be seen that the course of the error envelope decreases slightly slower than for the blower prediction ANN. However, this is not considered as significant, since the number of instances in critical intervals ([-1;-0.5] and [+0.5;+1]) are also comparably low.

Figure 5-10 shows the classification results for training, validation and testing.

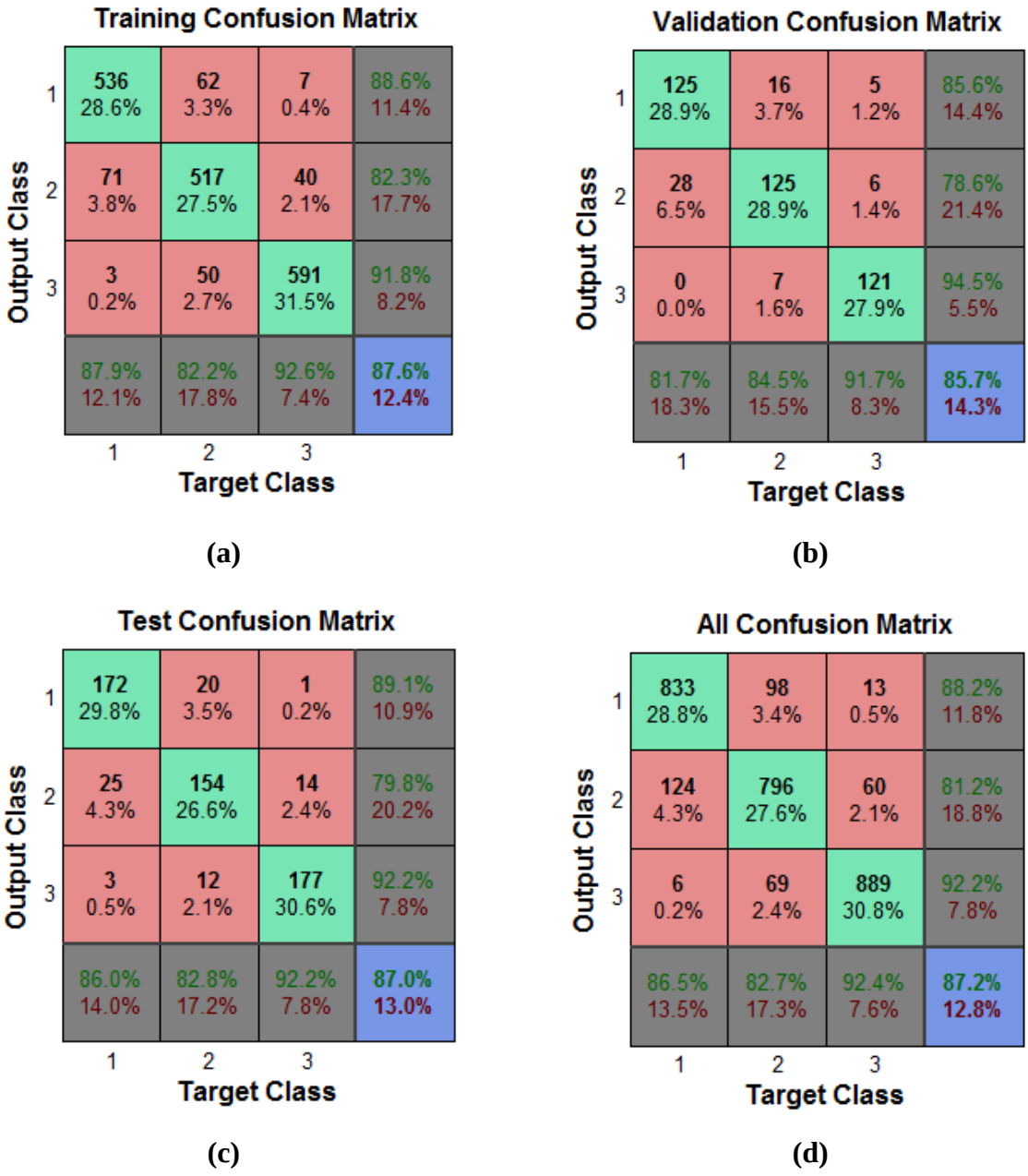

Figure 5-10: Confusion matrix for flap position prediction; (a) Training confusion, (b) Validation confusion, (c) Testing confusion, (d) Overall confusion

Figure 5-10(d) shows the overall classification results. It is apparent that in 87.2% the network is able to produce the correct output. The results for test, validation and training data in Figure 5-10(a), (b), (c) and (d) show each similar performance. Similar to blower level prediction, the extreme values 'breast' and 'head' have been predicted best with 86.5% and 92.4% correct classifications. Flap position 'breast-head' has been correctly classified for 82.7% of all cases. This suggests an overlap between flap positions 'breast' and 'breast head' as well as for flap positions 'breast-head' and head. Possible explanations for these phenomena follow exactly the argumentation of Chapter 5.4.1 and will therefore not be repeated in this context again.

5.4.3 Temperature set-up value

In Chapter 4.6.6, the temperature knob was found to be segmental linear dependent on ambient temperature ϑ_{Am}. According to Figure 4-30, the author suggests to model the temperature knob value T_k with two straight lines. A best fit straight line $y = ax_i + b$ was therefore calculated, so that for each (x_i,y_i)

$$\sum_{i=1}^{N}(y_i - ax_i + b)^2 \rightarrow min, \qquad \textbf{(74)}$$

is fulfilled. The coefficients have been determined for a=-1.061 and b=113. The result is summarized in equation (75).

$$T_k = \begin{cases} -1.061\frac{Am}{°C} + 113 & for \quad Am \leq +43°C \\ +50 & for \quad Am > +43°C \end{cases} \qquad \textbf{(75)}$$

5.5 Summary

This chapter has applied ANN to thermal comfort research in order to predict blower level as well as the heater box's flap position. Research has been conducted to determine the optimal structure of the ANNs. An 8-12-4 FNN was found to be best for blower level prediction and an 8-10-3 FNN for flap position prediction. The networks have both been trained with about 3000 samples, however it was shown that 1700 and 1300 expressive samples should be sufficient to train the blower and the flap network. The term 'expressive' cannot be specified with formal means. In practice, this means that samples have to be collected, which include representative information about the environment. In terms of thermal comfort this means that samples must cover a representative variety of environmental conditions, including moderate as well extreme conditions.

The resulting overall classification performance is about 87% for blower and flap prediction. It has been shown that ANNs are far superior with respect to manual interpretation methods, as presented in Chapter 4.6.

Extreme values for blower level and flap position were predicted best. It was shown that data classes overlap to some extend which might be a result of human fuzziness in thermal comfort evaluation. However it might be also a consequence of the manual HVAC unit, which has been used for this research project.

The ANNs performance has been verified against independent data, which have been randomly chosen from the data set and which have not been used for system training.

It has been shown that it is possible to extract thermal comfort knowledge directly from measurement data. Prior modelling of human's thermo-regularity system and human's response is not necessary. It has also been shown, that it is possible to adapt a technical system to the thermal comfort preferences of an individual.

Temperature knob prediction was found to be primarily dependent on ambient temperature and can be fairly approximated by a stepwise linear function.

Chapter 6

Conclusion and further development

Engineering is a discipline of acquiring and applying scientific knowledge to technical processes, in order to offer solutions for the needs of society. In general, this scientific knowledge incorporates fundamental laws of physics and mathematics, whose interpretations lead to clear results. In terms of thermal comfort control, this approach does not guarantee success. Humans tend to be fuzzy in their decision space and their perception of environment depends on physiological and psychological properties, which might be biased by personal, cultural and ecological expectations. The problems can be summarized as:

- Thermal comfort is subjective and vague,
- Many thermal comfort parameters can only be estimated,
- Thermal comfort control is a multi-dimensional problem and its perception may vary in time and location.

A technical implementation that satisfies everyone is therefore considered to be impossible, although it is manageable to adapt a system to the individual. Knowledge based on more than 40 years of thermal comfort research in residential buildings, can hardly be transferred to the vehicular environment. This is justified due to the extremely inhomogeneous and transient conditions inside the vehicle cabin. However, this did not prevent researchers from applying these methods also to the automotive environment. So far, research in transient environments is still under investigation and generally accepted theories have not been published yet. Automotive industry predominantly adopts physiological and psychological models, in combination with manikins, to assess thermal comfort.

This research project has focused on knowledge extraction from experimental field data and applies strategies of machine learning, in order to predict the passenger's preferences with respect to the HVAC control unit. This methodology bypasses the use and the development of any human psychological and physiological models and aims to directly 'imitate' the user in his/her decision space. This approach is not popular in the scientific world, because it does not add any knowledge towards the better understanding of human's thermo-regularity system and the achieved results might be highly vehicle- and individual specific. However the author opposes, since no mathematical model will be capable of exactly imitating human response, this approach avoids various sources of modelling errors and will deliver the most possible direct and straight-forward implementation of thermal comfort control. To achieve this, a

representative database is required which contains appropriate input-output mappings. Due to the complexity of thermal interactions between the environment and the vehicle, as well as due to psychological reasons, climate chamber tests are not considered to be expressive and field testing is required. Therefore, a novel thermal comfort interface has been developed, that incorporates:

- Interfacing to vehicle ECUs,
- Measuring environmental conditions,
- Measuring vehicle parameters,
- Measuring human response,
- Automatic thermal comfort evaluation using a computer.

The equipment has been installed in a VW Polo in a combination with a prototype manual HVAC unit. Since reliable and consistent data mapping is of great importance for successful system learning, a lot of effort has been put into error recognition mechanisms and consistency algorithms. To make this research as practice-orientated as possible, the direct attachment of sensors to the human body has been abdicated. Sensory devices have been restricted to standard temperature and humidity sensors, which have been installed inside the vehicle cabin. A novel three-dimensional solar sensor has been used in order to measure sun intensity, sun elevation angle as well as sun azimuth angle. It has been noticed that sun angle determination performs poorly at diffuse solar radiation. This effect has been shown to be mainly negatively correlated to sun intensity and can therefore be roughly compensated for. However, high intensity diffuse radiation cannot be accounted for with the present algorithms. The author assumes that diffuse radiation can be completely distinguished with simultaneously considering sun intensity, sun azimuth, sun elevation angle, as well as their variances per observation interval. A learning machine approach could be implemented to distinguish between different daylight situations, meaning a $\mathbb{R}^6 \rightarrow \mathbb{R}^1$ mapping. However, this requires further research.

The influence of mean radiant temperature on thermal comfort perception has been approximated by measuring the dashboard temperature, which has been shown to be thermal comfort relevant.

Air velocity is an implicit function of vehicle speed, blower level and flap position. It is assumed that their effects on thermal comfort perception can be internally revealed by the learning machine.

Human metabolic rate is assumed to be dependent on the traffic situation and has been estimated with vehicle parameters, namely frequency of gas- and brake pedal changes for a given observation interval. These parameters have been mathematically combined to a continuously

adjusted ‘traffic recognition’ function. However, it has turned out that this function is negatively correlated to vehicle speed and can be therefore omitted.

Clothing insulation has been kept constant during all tests. However, it is assumed that basis clothing insulation may inherently vary over the year. For future research, it would be desirable to include this influence by defining an additional variable, accounting for clothing categories. Data in hot to moderate environments have been collected during summer, spring and autumn in Southern Africa. For future research, winter conditions should be included in order to cover the total climatic spectrum. Available testing conditions have accounted for setting up the whole range for blower level. However, flap positions ‘feet’ and ‘head-feet’ have not been observed during data acquisition. This suggests that in moderate climatic conditions, feet are less sensitive to environmental changes than other body parts.

This research has been limited to short-transient and stationary conditions. However, for future research transient conditions, like cooling down or heating up the vehicle cabin, can be included. It has been noticed that in most cases driver and front passenger simultaneously reported different levels of thermal comfort. This might be due to variations in individual comfort perception as well as due to the inhomogeneity of vehicle cabin. Since a single zone HVAC unit has been used for this research, the problem could not be accounted for. To ensure data consistency, only the driver was therefore allowed to change the HVAC settings. To increase the efficiency and to double the amount of data, it is suggested to use a dual zone manual HVAC unit for future testing.

Often, a total thermal satisfaction with the environment cannot be fully established in the vehicle cabin. This is probably caused by various complex and local environmental perturbations. The vehicle’s HVAC unit was often found not being capable of removing all these influences of discomfort simultaneously. However, a kind of relative thermal satisfaction could be established due to removal of the most annoying sources of displeasure. In terms of future improvement, this can be accounted for by independently electronically controlling each air outlet. To achieve that, more actuators have to be installed within the experimental setup. It is noteworthy that such a change would not alter the dimensionality of the data input space for system learning.

During summer testing, seat insulation might additionally affect thermal comfort perception. An affirmative relief could be the integration of seat ventilation systems and their connection to the comfort evaluation system.

Methods of data mining and multivariate statistics have been applied and implemented into Matlab, to reduce the dimensionality of the input space, as well as to ensure data consistency. PCA has been used for exploratory data analysis. The dimensionality of the feature space has been reduced from $\mathbb{R}^{20} \rightarrow \mathbb{R}^{8}$.

The thermal comfort relevant variables have been identified as:

- Ambient temperature,
- Relative humidity,
- Vehicle speed,
- In-cabin air temperature,
- Dashboard temperature,
- Sun intensity,
- Sun azimuth angle,
- Sun elevation angle.

It has been shown that ‘by hand’ interpretation of the variable meanings is difficult, due to the multi-dimensional nature of the problem. A reason for this might be that human’s imagination is restricted to three-dimensional spaces. However, tendencies and possible interpretations have been discussed. It has been concluded to be impossible to extract any exact functional relationship. Visual interpretation is additionally complicated by nonlinear inter-relationships between dependent and independent variables.

To overcome these problems, elements of artificial intelligence have been proposed for classification. Many of those methods are similar in their internal behavior, but do differ in their philosophy of application. Since only little a-priori thermal comfort process knowledge has been available, the author has identified ANNs as a suitable classification and regression framework. ANNs have been therefore implemented to predict blower level and flap position. It is noteworthy, that this kind of problem is universal and any technology, which is capable of distribution-free learning from experimental data, can be used for system implementation. In terms of future research, ANNs might be for example substituted by support vector machines or might be combined with fuzzy logic, in order to account for some human knowledge from Chapter 4.6.

After training, the system’s overall performance to predict blower levels was 87.7%. It has been shown that the percentage of correct prediction for blower levels ‘1’and ‘4’ is 89% and 97.8%, whilst blower levels ‘2’ and ‘3’ are only correctly classified for 82.7% and 81.7% of the cases. Closer investigations have shown that values for blower levels ‘2’ and ‘3’ spread within their neighboring classes. It is therefore apparent, that the test engineer has not been able to clearly distinguish between blower levels ‘2’ and ‘3’ during data acquisition and the classes seem to overlap to some extent. This can be explained due to fuzzy human thermal comfort perception and the use of a manual HVAC unit, which is limited to a discrete output domain. Latter one is especially true for cases, when the desired output lies in between two distinctive output patterns.

If neighboring misclassifications are ignored, the neural network's performance can be improved to about 96%. Further research should therefore especially focus on blower levels '2' and '3'. Implementation of a continuous output domain (PWM control of any actuator) might improve system performance.

Similar conclusions can be found for flap position prediction. The overall correct classification rate is about 87%. Flap positions 'breast' and 'head' are correctly classified for 86.5% and 92.4%, while flap position 'breast-head' only accounts for 83% correct classifications.

The ANNs have been trained with about 3000 training samples. However, it has been shown that 1700 and 1300 expressive samples should be sufficient to train the blower and the flap predictors. The term 'expressive' means in this context, those samples must distinguish from each other and must be representative for a wide range of environmental conditions.

It has been shown that temperature knob setting is highly negatively correlated to ambient temperature. It has been therefore decided to model temperature knob setting using a piecewise straight line approximation.

With the current experimental setup, prediction of blower level and flap position constitutes a pattern recognition problem. Future research could integrate electronic controllers for blower and flap actuators, in order to transform the discrete output space to a continuous domain, resulting in a multidimensional regression problem. This might further increase system performance.

This research has been limited to simulative investigations. The performance of the ANNs has been verified against an independent set of testing data, which has been randomly chosen and has not been used for system training. A practical implementation in the real vehicle and its connection to the vehicle's bus systems has been far beyond the scope of this research. However, in terms of future research such an implementation could be considered.

The goals of this research have been fulfilled and it has been shown that it is possible of directly teaching an intelligent system, using experimental thermal comfort data. The prediction performance is at least comparable to conventional HVAC units, however the development procedure has been considerably simplified. This methodology can be used for HVAC system development and is capable of assisting the application engineer to impress the HVAC ECU with a desired multidimensional characteristic, which is directly extracted from field data. Since it has been shown to be possible to teach a technical system with fuzzy human data, future research could also be extended to HAVC units, which adapt their behavior with respect to the user's inputs during operation.

Bibliography

[1] American Society of Heating, Refrigerating and Air-Conditioning Engineers. ASHRAE handbook of fundamentals: New York: ASHRAE; 2009.

[2] American Society of Heating, Refrigerating and Air-Conditioning Engineers. Thermal environmental conditions for human occupancy. Atlanta, GA: American Society of Heating, Refrigerating and Air-Conditioning Engineers; 2004. (ASHRAE standard).

[3] Arens E, Turner S, Zhang H. Moving Air for Comfort, ASHRAE Journal 2009; 51(25):8-18.

[4] Aroussi A, Aghil S. Characterization of the Flow Field in a Passenger Car Model. Optical Diagnostics in Engineering 2000; 4(1):1-15.

[5] Atmaca I, Kaynakli O, Yigit A. Effects of radiant temperature on thermal comfort. Building and Environment 2007; 42(9):3210–20.

[6] Atthajariyakul S, Leephakpreeda I. Neural computing thermal comfort index for HVAC systems. Energy Conversion and Management 2005; 46(15-16):2553–65.

[7] Baker PJ, Jenkins MD. An Optimized Thermal Design and Development Process for Passenger Compartments of Vehicles. White Paper, Flowmaster Group, 2009.

[8] Becker R, Paciuk M. Thermal comfort in residential buildings - Failure to predict by Standard model. Building and Environment 2009; 44(5):948–60.

[9] Berglund LG. Comfort and humidity. ASHRAE journal 1998; 40(8):35-41

[10] Bhatti MS. Evolution of automotive air conditioning: Riding in comfort: Part II. ASHRAE Journal 1999; 41(9):44-52.

[11] BHTC GmbH, ISOS solar sensor data sheet, 2008, URL: http://www.bhtc.com.

[12] Bohm M, Noren O, Holmer I, et al. Comparison of methods to determine the equivalent temperature in a cab in a climatic chamber. Paper for the CABCLI seminar - EC Cost Contract No SMT4-CT98-6537 (DG12 BRPR), 1999, Dissemination of results from EQUIV - EC Cost Contract No SMT4-CT95-2017.

[13] Bortz J. Statistik für Human- und Sozialwissenschaftler. 6., vollständig überarbeitete und aktualisierte Aufl. Wien: Springer; 2005.

[14] Bronštejn IN. Taschenbuch der Mathematik. 7.ed, Frankfurt am Main: Verlag Harri Deutsch; 2008.

[15] Bureau C, Kampf H, Taxis-Reischl, Traebert A, Mayer E, Schwab R. MARCO – Behr's method to access thermal comfort. In: Proceedings of the 6th Vehicle Thermal Management Systems Conference, May 18-21, 2003, Brighton, UK, Paper: C599/051/2003.

[16] Calvino F, Gennusa ML, Rizzo G, Scaccianoce G. The control of indoor thermal comfort conditions: introducing a fuzzy adaptive controller. Energy and Buildings 2004; 36(2):97–102.

[17] Candas V. The thermal environment and its effects on human. Paper for the CABCLI seminar - EC Cost Contract No SMT4-CT98-6537 (DG12 BRPR), 1999, Dissemination of results from EQUIV - EC Cost Contract No SMT4-CT95-2017.

[18] Charles KE. Fanger's thermal comfort and draught models. Ottawa, Ont: Institute for Research in Construction; 2003. Available from: URL:http://irc.nrc-cnrc.gc.ca/fulltext/rr162. [Accessed 11th June 2008].

[19] Chen K, Jiao Y, Lee ES. Fuzzy adaptive networks in thermal comfort. Applied Mathematics Letters 2006/5; 19(5):420–6.

[20] Chien C-, Jang J-, Chen Y-, Wu S-. 3-D numerical and experimental analysis for airflow within a passenger compartment. Int.J Automot. Technol 2008; 9(4):437–45.

[21] Cisternino M. Thermal climate in cabs and measurement problems, Paper for the CABCLI seminar - EC Cost Contract No SMT4-CT98-6537 (DG12 BRPR), 1999, Dissemination of results from EQUIV - EC Cost Contract No SMT4-CT95-2017.

[22] Continental. Engineered to keep cool – Climate Controls by Continental. [Online]. Available from: www.mediacenter.continental-corporation.com.

[23] Daanen HAM, van der Vliert E, Huang X. Driving performance in cold, warm, and

thermo neutral environments. Applied Ergonomics 2003; 34(6):597-602.

[24] Daly S. Automotive Air Conditioning and Climate control System. Amsterdam: Elsevier; 2006.

[25] Davis L, JR., Sieja T, Matteson R, Dage G, Ames R. Fuzzy logic for vehicle climate control. In: Fuzzy Systems, 1994. IEEE World Congress on Computational Intelligence., Proceedings of the Third IEEE Conference on; 1994. p. 530–4.

[26] de Dear R. Thermal comfort in practice. Indoor Air 2004; 14(s7):32–9.

[27] Deutsches Insitut für Normung e.V. DIN EN ISO 7726:2001. Umgebungsklima-Instrumente zur Messung physikalischer Grössen. Berlin, Beuth Verlag GmbH, 2002.

[28] Deutsches Insitut für Normung e.V. DIN EN ISO 7730:2005. Ergonomie der thermischen Umgebung-Analytische Bestimmung und Interpretation der thermischen Behaglichkeit durch Berechnung des PMV- und des PPD-Indexes und Kriterien der lokalen thermischen Behaglichkeit. Berlin, Beuth Verlag GmbH, 2006.

[29] Deutsches Insitut für Normung e.V. DIN EN ISO 8996:2004. Ergonomie der thermischen Umgebung-Bestimmung des körpereigenen Energieumsatzes. Berlin, Beuth Verlag GmbH, 2005.

[30] Deutsches Insitut für Normung e.V. DIN EN ISO 9886:2004. Ergonomie-Ermittlung der thermischen Beanspruchung durch physiologische Messungen. Berlin, Beuth Verlag GmbH, 2004.

[31] Deutsches Insitut für Normung e.V. DIN EN ISO 9920:2009. Abschätzung der Wärmeisolation und des Verdunstungswiderstandes einer Bekleidungskombination. Berlin, Beuth Verlag GmbH, 2009.

[32] Deutsches Institut fuer Normung e.V., DIN14505, Ergonmomie der thermischen Umgebung – Beurteilung der thermischen Umgebung in Fahrzeugen. Berlin, Beuth Verlag GmbH, 2007.

[33] Devonshire JM, Sayer JR. The effects of infrared-reflective and antireflective glazing on thermal comfort and visual performance: a literature review: Ann Arbor, Mich.:

University of Michigan, Transportation Research Institute; 2002. Available from: URL:http://hdl.handle.net/2027.42/49457. [Accessed 15th June 2008].

[34] Devonshire JM, Sayer, JR. Radiant heat and thermal comfort in vehicles. Human Factors 2005; 47(4):827–39.

[35] Doege K. Behaglichkeitssensor. Luft- und Kaeltetechnik 2002; 38(2): 485-91.

[36] Eilemann A, Kampf H. Comfort-Management. Warrendale, PA: SAE International; 2001.

[37] Fanger PO. Thermal comfort: analysis and applications in environmental engineering. New York: McGraw-Hill; 1972.

[38] Freescale Semiconductor Inc, MC9S12DP512 data-sheet.
URL: http://www.freescale.com.

[39] Furuse K, Komoriya T. Study of passenger's comfort in non-uniform thermal environments of vehicle compartment, JSAE Review 1997; 18(4):411-14.

[40] Gameiro Silva MCD. Measurement of comfort in vehicles. Measurement Science and Technology 2002; 13(6):41-60.

[41] Gielda TP, Hosni MH. Transient Thermal Comfort Predictions for Automotive Environments. Available from:
http://www.grrt.fr/html/travaux/download.php?filename=00gieldahosni.pdf
[Accessed 31th Dec 2009].

[42] Hamdi M, Lachiver G. A fuzzy control system based on the human sensation of thermal comfort. In: Fuzzy Systems Proceedings, 1998. IEEE World Congress on Computational Intelligence., The 1998 IEEE International Conference on; 1998. p. 487–92.

[43] Han J, Kamber M. Data mining: Concepts and techniques. 2nd. Amsterdam ;, Boston, San Francisco CA: Elsevier; Morgan Kaufmann; 2006.

[44] Han T, Huang L, Kelly S, Huizenga C, Hui Z. Virtual Thermal Comfort Engineering. Warrendale, PA: SAE International; 2001.

[45] Han T, Huang L. A Sensitivity Study of Occupant Thermal Comfort in a Cabin Using Virtual Thermal Comfort Engineering. Warrendale, PA: SAE International; 2005.

[46] Han T, Lambert DK, Oberdier LM, Partin DL, Sultan MF. Ultrasonic Air Temperature Sensing for Automatic Climate Control - Sensor Development. Warrendale, PA: SAE International; 2003.

[47] Han T, Lambert DK, Partin DL, Sultan MF. Ultrasonic Air Temperature Sensing for Automatic Climate Control - Vehicle Test. Warrendale, PA: SAE International; 2004.

[48] Hanqing W, Chunhua H, Zhiqiang L, Guangfa T, Yingyun L, Zhiyong W. Dynamic evaluation of thermal comfort environment of air-conditioned buildings. Building and Environment 2006/11; 41(11):1522–9.

[49] Havenith G, Holmér I, Parsons K. Personal factors in thermal comfort assessment: clothing properties and metabolic heat production. Energy and Buildings 2002/7; 34(6):581–91.

[50] Haykin SS. Neural networks and learning machines. 3rd ed. / International. Harlow ; London: Pearson Education; 2009.

[51] Hodder SG, Parsons K. The effects of solar radiation on thermal comfort. International Journal of Biometeorology 2007 Jan; 51(3):233–50.

[52] Holmer I, Nilsson H, Bohm M, et al. Equivalent temperature in vehicles- conclusions and recommendations for standard. Paper for the CABCLI seminar - EC Cost Contract No SMT4-CT98-6537 (DG12 BRPR), 1999, Dissemination of results from EQUIV - EC Cost Contract No SMT4-CT95-2017.

[53] Holmer I, Noren O, Bohm M, Nilsson H. Thermal aspects of vehicle comfort. Applied Human Science 1995; 14(4):159-65.

[54] Honeywell S&C, Data sheet HIH-4000 Integrated Circuitry Humidity sensor, URL: http://www.sensing.honeywell.com.

[55] Humphreys MA, Fergus Nicol J. The validity of ISO-PMV for predicting comfort votes in every-day thermal environments. Energy and Buildings 2002/7; 34(6):667–84.

[56] Izenman A. Modern Multivariate Statistical Techniques. New York, NY: Springer-Verlag New York; Springer e-books; 2008.

[57] Jolliffe IT. Principal component analysis. Second edition. New York: Springer; 2004.

[58] Jong-Uk Bu, Tae-Yoon Kim, In-Sik Kim, Young-Sam Jun, Young-Cho Shim, Sung-Tae Kim. Silicon-based thermal comfort sensing device. Sensors and Actuators A: Physical 1996; 54(1-3):468–71.

[59] Kajino Y, Sugi H, Kawai T, Ito Y, Tateishi M, Samukawa K. Development of Automatic Climate Control with Neural Control. Warrendale, PA: SAE International; 2000.

[60] Kampf H. Die physiologisch geregelte Klimaanlage. ATZ 103, 2001, 802-4.

[61] Karjalainen S. Gender differences in thermal comfort and use of thermostats in everyday thermal environments. Building and Environment 2007/4; 42(4):1594–603.

[62] Kaynakli O, Kilic M. An investigation of thermal comfort inside an automobile during the heating period. Applied Ergonomics 2005/5; 36(3):301–12.

[63] Kecman V. Learning and soft computing: Support vector machines, neural networks, and fuzzy logic models. Cambridge Mass: MIT Press; 2001.

[64] Kessler W. Multivariate Datenanalyse in der Bio- und Prozessanalytik: Mit Beispielen aus der Praxis. Weinheim: Wiley-VCH; 2005.

[65] Kolich M. Predicting automobile seat comfort using a neural network. International Journal of Industrial Ergonomics 2004/4; 33(4):285–93.

[66] Kumar M, Kar IN. Non-linear HVAC computations using least square support vector machines. Energy Conversion and Management 2009/6; 50(6):1411–19.

[67] Liang J, Du R. Design of intelligent comfort control system with human learning and minimum power control strategies. Energy Conversion and Management 2008/4; 49(4):517–28.

[68] Liu W, Lian Z, Zhao B. A neural network evaluation model for individual thermal

comfort. Energy and Buildings 2007/10; 39(10):1115–22.

[69] Lodi CA, Lenzi P, Baietto A, et al. Thermal comfort evaluation through a Matlab-based passenger model integrated into INKA vehicle model. In: Proceedings of the 6th Vehicle Thermal Management Systems Conference, May 18-21, 2003, Brighton, UK, Paper: C599/073/2003.

[70] LumaSense. Thermal comfort. [Online]. Available from: http://lumasense.us [Accessed 1th June 2008].

[71] Luo X, Hou W, Li Y, Wang Z. A fuzzy neural network model for predicting clothing thermal comfort. Computers & Mathematics with Applications 2007/6; 53(12):1840–6.

[72] Lyons P, Arasteh D. Window Performance for Human Thermal Comfort, ASHRAE Trans 1999; 73(2): 4–20.

[73] Maher Hamdi, Gerard Lachiver, Francois Michaud. A new predictive thermal sensation index of human response. Energy and Buildings 1999; 29(2):167–78.

[74] Maria La Gennusa, Antonino Nucara, Gianfranco Rizzo, Gianluca Scaccianoce. The calculation of the mean radiant temperature of a subject exposed to the solar radiation-a generalised algorithm. Building and Environment 2005; 40(3):367–75.

[75] Markov D. Practical Evaluation of Thermal Comfort Parameters. In: Annual International Course: Ventilation and Indoor climate, P. Stankov (ed.), Sofia, 2002:158-70.

[76] Martinho NAG, Silva MCG, Ramos JAE. Evaluation of thermal comfort in a vehicle cabin. Proceedings of the Institution of Mechanical Engineers, Part D: Journal of Automobile Engineering 2004; 218(2):159–66.

[77] Masuda T, Ogawa K, Gyorog T. Klimakomfortmessung im Fahrzeug. In: Dieter Schlenz (ed). PKW Klimatisierung IV, Expert Verlag, 2006, pp. 11-124.

[78] Maxim Integrated Products Inc., Data sheet DS1631 high precision digital thermometer and thermostat, URL: http://www.maxim-ic.com.

[79] Mayer E. Ist die bisherige Zuordnung von PMV und PPD noch richtig? Luft- und

Kaeltetechnik 1998, 34(12): 575-77.

[80] Mayer E. Physik der thermischen Behaglichkeit. Phys. Unserer Zeit 1989; 20(4):97–103.

[81] Mcguffin R, Burke R, Huizenga C, Hui Z, Vlahinos A, Fu G. Human Thermal Comfort Model and Manikin. Warrendale, PA: SAE International; 2002.

[82] Mcguffin R. Modelling of Human Thermal Comfort. Warrendale, PA: SAE International; 2001.

[83] Megri AC, Naqa IE, Haghighat F. A Learning Machine Approach for Predicting Thermal Comfort Indices. International Journal of Ventilation 2005, 3(4):363-76.

[84] Melikov A, Zhou H. Comparison of Methods For Determining t_{eq} Under Well-Defined Conditions. Paper for the CABCLI seminar - EC Cost Contract No SMT4-CT98-6537 (DG12 BRPR), 1999, Dissemination of results from EQUIV - EC Cost Contract No SMT4-CT95-2017.

[85] Mezrhab A, Bouzidi M. Computation of thermal comfort inside a passenger car compartment. Applied Thermal Engineering 2006/10; 26(14-15):1697–704.

[86] Michael A Humphreys, Mary Hancock. Do people like to feel neutral‘?: Exploring the variation of the desired thermal sensation on the ASHRAE scale. Energy and Buildings 2007; 39(7):867–74.

[87] Michalek D, Gehsat C, Trapp R, Bertram T. Hardware-in-the-loop-simulation of a vehicle climate controller with a combined HVAC and passenger compartment model. In: Advanced Intelligent Mechatronics. Proceedings, 2005 IEEE/ASME International Conference on; 2005. pp. 1065–70.

[88] Musat R, Helerea E. Parameters and Models of the Vehicle Thermal Comfort. Acta Universitatis Sapientiae: Electrical and Mechanical Engineering, 2009:215-26.

[89] Naadimuthu G, Liu DM, Lee ES. Application of an adaptive neural fuzzy inference system to thermal comfort and group technology problems. Computers & Mathematics with Applications 2007/12; 54(11-12):1395–402.

[90] Nagel D, Trapp R. Komfort in der Fahrzeugklimatisierung – Der intelligente Solarsensor. ATZ 107; 2005:1106-9.

[91] Nicol JF, Humphreys MA. Adaptive thermal comfort and sustainable thermal standards for buildings. Energy and Buildings 2002/7; 34(6):563–72.

[92] Nilsson H, Holmer I, Bohm M, et al. Definition and theoretical background of the equivalent temperature. Paper for the CABCLI seminar - EC Cost Contract No SMT4-CT98-6537 (DG12 BRPR), 1999, Dissemination of results from EQUIV - EC Cost Contract No SMT4-CT95-2017.

[93] Nilsson HO. Comfort climate evaluation with thermal manikin methods and computer simulation models. Stockholm: Arbetslivsinstitutet; 2004.

[94] Nowotny Sea. Lüftungs- und klimatechnische Gebäudeausrüstung: Grundlagen und Berechnungsmodelle. Wiesbaden: Bauverlag; 1996.

[95] NXP Semiconductors Netherlands B.V. I2C specification sheet, version 2.1, Jan 200. Available from: http://i2c2p.twibright.com/spec/i2c.pdf .
[Accessed 10th Jan 2008].

[96] Olesen BW. Evaluation of the thermal environment in vehicles. Application note, Bruel & Kjaer, Denmark, 1988.

[97] Ormuz K, Muftic O. Main Ambient Factors Influencing Passenger Vehicle Comfort. In: Proceedings of the 2nd International Ergonomics Conference 2004, Oct 21 – 22, Zagreb Croatia, pp. 77-82.

[98] Orosa J. Research on General Thermal Comfort Models. European Journal of Scientific Researc. 2009; 27(2):217-27.

[99] Othman MF, Othman SM. Fuzzy Logic Control for Non Linear Car Air Conditioning. Elektrika Journal of Electrical Engineering 2006; 8(2):38-45.

[100] Parsons KC. The assessment of thermal comfort in vehicles using human subjects. Paper for the CABCLI seminar - EC Cost Contract No SMT4-CT98-6537 (DG12 BRPR), 1999, Dissemination of results from EQUIV - EC Cost Contract No SMT4-

CT95-2017.

[101] Paulke S. Finite element based implementation of Fiala's thermal manikin in THESEUS-FE. In: Proceedings of the 8th Vehicle Thermal Management Systems Conference, May 20-24, 2007, Nottingham UK.

[102] Priddy KL, Keller PE. Artificial neural networks: An introduction. Bellingham, Washington: SPIE Press; 2005.

[103] Prof H. Holdack-Janssen, Grundlagen der Fahrzeugklimatisierung, Lecture notes, Ostfalia University, 2003.

[104] Robert Bosch GmbH, CAN Specification document 1991, Version 2.0.

[105] Rohles FH. Temperature & Temperament. A psychologist looks at comfort. Ashrae Journal 2007; 49(2):14-22.

[106] Ronnlund M, Bohm M, Noren O, et al. Practical considerations from climatic measurements in cabs in field. Paper for the CABCLI seminar - EC Cost Contract No SMT4-CT98-6537 (DG12 BRPR), 1999, Dissemination of results from EQUIV - EC Cost Contract No SMT4-CT95-2017.

[107] Rugh J. Integrated Numerical Modelling Process for Evaluating Automobile Climate Control Systems. Warrendale, PA: SAE International; 2002.

[108] Rugh JP, Bharathan D. Predicting Human Thermal Comfort in Automobiles. Warrendale, PA: SAE International; 2005.

[109] Rugh JP, Farrington RB, Bharathan D. Predicting Human Thermal Comfort in a Transient No uniform Thermal Environment. European Journal of Applied Physiology 2004; 92(6):721-27.

[110] Runkler TA. Methoden und Algorithmen intelligenter Datenanalyse, Wiesbaden: Vieweg+Teubner; 2010.

[111] Saunders B. Automotive climate control based on thermal state estimation. PhD thesis. University of Glasgow; 2002.

[112] Saunders BA, Hunt KJ, McASLAN S, et al. Performance evaluation of TSV and PMV thermal state estimation algorithms programmed in a hand-held device . In: Proceedings of the 6th Vehicle Thermal Management Systems Conference, May 18-21, 2003, Brighton, UK, Paper: C599/080/2003.

[113] Schneider T, Ellinger M, Paulke S, et al. Modernes Thermomanagement am Beispiel der Innenraumklimatisierung. ATZ 2007; 109(2):2-8.

[114] Sedlbauer K, Breuer K, Kaufmann A. Der Mensch in Raeumen – Risiko oder Behaglichkeit. Gesundheits-Ingenieur 2006, 127(4):175-88.

[115] Sedlbauer K, Holm A, Kuenzel HM, Leistner P,Breuer K. Raumklima und Innovation. Eine Aufgabe der Bauphysik. Zeitschrift für Wärmeschutz, Kälteschutz, Schallschutz, Brandschutz 2006; 51(57): 9-16.

[116] Shlens J. A. Tutorial on Principle Component Analysis, Center for neural science, New York University, 2009.

[117] Sola J, Sevilla J. Importance of input data normalization for the application of neural networks to complex industrial problems. IEEE Transactions on Nuclear Science 1997; 44(3):1464–8.

[118] Soleimani-Mohseni M, Thomas B, Fahlén P. Estimation of operative temperature in buildings using artificial neural networks. Energy and Buildings 2006/6; 38(6):635–40.

[119] Stephen EA, Shnathi M, Rajalakshmy P, Parthido MM. Application of Fuzzy Logic in Control of Thermal Comfort, International Journal of Computational and Applied Mathematics 2010; 5(3):289-300.

[120] Strupp NC, Lemke NC, Koehler J, et al. Klimatische Daten und PKW Nutzung (Klimadaten und Nutzungsverhalten zu Auslegung, Versuch und Simulation an Kraftfahrzeug-Kaelte-/Heizanlagen in Europa und den USA). In: DKV-Tagung, Berlin, 2009.

[121] Tabe T, Matsui K, Kakehi T, Ohba M. Automotive climate control. IEEE Control Systems Magazine 1986; 6(5):20–4.

[122] ThermCo, Thermal Comfort in Transient Environments, European Project ThermCo, Contract number: EIE/07/026/S12.466692, University of Denmark, May 2009.

[123] Trygg J, Wold S. Introduction to Statistical Experimental Design - What is it? Why and Where is it Useful? Editorial.

[124] Tse WL, Chan WL. A distributed sensor network for measurement of human thermal comfort feelings. Sensors and Actuators A: Physical 2008 Jun 15; 144(2):394–402.

[125] Ueda M, Yaniguchi Y. The prediction of the passenger's thermal sensation level using a neural network and its application to the automobile HVAC control. In: Systems, Man, and Cybernetics, 1999. IEEE SMC '99 Conference Proceedings. 1999 IEEE International Conference on; 1999. p. 623–34.

[126] van Hoof J. Forty years of Fanger's model of thermal comfort: comfort for all? Indoor Air 2008 Jun; 18(3):182–201.

[127] Volkswagen AG, Air Conditioning in Motor Vehicle, Document number: SSP 208.

[128] Walgama C, Fackrell S, Karimi M, Fartaj A, Rankin GW. Passenger Thermal Comfort in Vehicles - A Review. Proceedings of the Institution of Mechanical Engineers, Part D: Journal of Automobile Engineering 2006; 220(5):543–62.

[129] Weber C, Elshaw M, Mayer NM. Reinforcement learning: Theory and applications. Vienna: I-TECH Education and Pub.; 2008.

[130] Yadollah Farzaneh, Ali A. Tootoonchi. Controlling automobile thermal comfort using optimized fuzzy controller. Applied Thermal Engineering 2008; 28(14-15):1906–17.

[131] Yao R, Li B, Liu J. A theoretical adaptive model of thermal comfort - Adaptive Predicted MeanVote (aPMV). Building and Environment 2009; 44(10):2089–96.

[132] Zhang H, Arens E, Huizenga C, Han T. Thermal sensation and comfort models for non-uniform and transient environments: Part I: Local sensation of individual body parts: 1st International Symposium on Sustainable Healthy Buildings. Building and Environment 2010/2; 45(2):380–8.

[133] Zhang H, Arens E, Huizenga C, Han T. Thermal sensation and comfort models for

non-uniform and transient environments, part II: Local comfort of individual body parts: 1st International Symposium on Sustainable Healthy Buildings. Building and Environment 2010/2; 45(2):389–98.

[134] Zhang H, Arens E, Huizenga C, Han T. Thermal sensation and comfort models for non-uniform and transient environments, part III: Whole-body sensation and comfort: 1st International Symposium on Sustainable Healthy Buildings. Building and Environment 2010/2; 45(2):399–410.

[135] Zhang H, Dai L, Xu G, Li Y, Chen W, Tao W. Studies of air-flow and temperature fields inside a passenger compartment for improving thermal comfort and saving energy. Part I: Test/numerical model and validation. Applied Thermal Engineering 2009/7; 29(10):2022–7.

[136] Zhang Y, Zhao R. Overall thermal sensation, acceptability and comfort. Building and Environment 2008/1; 43(1):44–50.

[137] Zhang Y, Zhao R. Relationship between thermal sensation and comfort in non-uniform and dynamic environments: The 6th International Conference on Indoor Air Quality, Ventilation &Energy Conservation in Buildings (IAQVEC 2007), Sendai, Japan, 28-31 October, 2007. Building and Environment 2009/7; 44(7):1386–91.

[138] Zhao R. Investigation of transient thermal environments: Indoor Air 2005 Conference. Building and Environment 2007/12; 42(12):3926–32.

[139] Zhi HZ, Ying X. The application of artificial neural network in HVAC system. In: Machine Learning and Cybernetics, 2005. Proceedings of 2005 International Conference on; 2005. p. 4800–4.

Appendix

A.1 CAN definitions

This section contains information about the CAN messages which are generated by the thermal comfort acquisition unit.

ID	LNG	Byte		Description	Factor/Offset
$100	**7**	**0**	$00	AC off	1/0
			$10	AC on	
			$FF	No CAN link	
		1	$xx	Blower speed [%]	1/0
			$FF	No CAN link	
		2	$xx	Vehicle speed [km/h]	1/0
			$FF	No CAN link	
		3	$xx	Number of stop/go cycles during the past 150s	1/0
			$FF	No CAN link	
		4	$xx	Engine coolant temperature [ºC]	0.75/-48
			$FF	No CAN link	
		5	$xx	Ambient temperature [ºC]	0.5/-50
			$FF	No CAN link	
		6	$xx	Filtered ambient temperature [ºC]	0.5/-50
			$FF	No CAN link	
$101	**8**	**0**	$xx	Temp1High	0.25/0
			$FF	NC	
		1	$xx	Temp1Low	0.25/0
			$FF	NC	
		2	$xx	Temp2High	0.25/0
			$FF	NC	
		3	$xx	Temp2Low	0.25/0
			$FF	NC	
		4	$xx	Temp3High	0.25/0
			$FF	NC	
		5	$xx	Temp3Low	0.25/0

			$FF	NC	
		6	$xx	Temp4High	0.25/0
			$FF	NC	
		7	$xx	Temp4Low	0.25/0
			$FF	NC	
$102	**8**	**0**	$xx	Temp5High	0.25/0
			$FF	NC	
		1	$xx	Temp5Low	0.25/0
			$FF	NC	
		2	$xx	Temp6High	0.25/0
			$FF	NC	
		3	$xx	Temp6Low	0.25/0
			$FF	NC	
		4	$xx	Temp7High	0.25/0
			$FF	NC	
		5	$xx	Temp7Low	0.25/0
			$FF	NC	
		6	$xx	Temp8High	0.25/0
			$FF	NC	
		7	$xx	Temp8Low	0.25/0
			$FF	NC	
$103	**5**	**0**	$xx	Tempknob	1/0
			$01	Feet	
			$02	Feet-Head	
			$03	Head	
		1	$04	Breast	1/0
			$05	Breast-Head	
			$06	Breast-Feet	
			$07	Error (lower limit exceeded)	
			$08	Error (upper limit exceeded)	
		2	$xx	Humidity	0.63/-25.8
			$FF	NC	
		3	$00	Transient operating mode	1/0
			$01	Stationary operating mode	

		4	$xx	Tempknob deviation	1/0
$104	**6**	**0**	$xx	Sun azimuth angle (high byte)	1/0
			$7F	NC	
		1	$xx	Sun azimuth angle (low byte)	1/0
			$FF	NC	
		2	$xx	Sun elevation angle (high byte)	1/0
			$FF	NC	
		3	$xx	Sun elevation angle (low byte)	1/0
			$FF	NC	
		4	$xx	Sun intensity (high byte)	1/0
			$FF	NC	
		5	$xx	Sun intensity (low byte)	1/0
			$FF	NC	
$105	**6**	**0**	$xx	Speed variation	1/0
			$7F	No CAN link	
		1	$xx	Sun azimuth angle variation	1/0
			$FF	NC	
		2	$xx	Sun elevation angle variation	1/0
			$FF	NC	
		3	$xx	Sun intensity variation	1/0
			$FF	NC	
		4	$xx	Traffic information	1/0
			$FF	No CAN link	
		5	$xx	Total traffic information	1/0
			$FF	No CAN link	
$106	**2**	**0**	$xx	Passenger draught evaluation	1/0
			$FF	NC	
		1	$xx	Passenger comfort evaluation	1/0
			$FF	NC	
$107	**2**	**0**	$xx	Driver draught evaluation	1/0
			$7F	NC	
		1	$xx	Driver comfort evaluation	1/0
			$FF	NC	
$200	**7**	**0**	$00	AC off	1/0

			$10	AC on	
			$FF	No CAN link	
		1	$xx	Blower speed [%]	1/0
			$FF	No CAN link	
		2	$xx	Vehicle speed [km/h]	1/0
			$FF	No CAN link	
		3	$xx	Number of stop/go cycles during the past 150s	1/0
			$FF	No CAN link	
		4	$xx	Engine coolant temperature [ºC]	0.75/-48
			$FF	No CAN link	
		5	$xx	Ambient temperature [ºC]	0.5/-50
			$FF	No CAN link	
		6	$xx	Filtered ambient temperature [ºC]	0.5/-50
			$FF	No CAN link	
$201	**8**	**0**	$xx	Temp1High	0.25/0
			$FF	NC	
		1	$xx	Temp1Low	0.25/0
			$FF	NC	
		2	$xx	Temp2High	0.25/0
			$FF	NC	
		3	$xx	Temp2Low	0.25/0
			$FF	NC	
		4	$xx	Temp3High	0.25/0
			$FF	NC	
		5	$xx	Temp3Low	0.25/0
			$FF	NC	
		6	$xx	Temp4High	0.25/0
			$FF	NC	
		7	$xx	Temp4Low	0.25/0
			$FF	NC	
$202	**8**	**0**	$xx	Temp5High	0.25/0
			$FF	NC	
		1	$xx	Temp5Low	0.25/0
			$FF	NC	

		2	$xx	Temp6High	0.25/0
			$FF	NC	
		3	$xx	Temp6Low	0.25/0
			$FF	NC	
		4	$xx	Temp7High	0.25/0
			$FF	NC	
		5	$xx	Temp7Low	0.25/0
			$FF	NC	
		6	$xx	Temp8High	0.25/0
			$FF	NC	
		7	$xx	Temp8Low	0.25/0
			$FF	NC	
$203	**5**	**0**	$xx	Tempknob	1/0
		1	$01	Feet	1/0
			$02	Feet-Head	
			$03	Head	
			$04	Breast	
			$05	Breast-Head	
			$06	Breast-Feet	
			$07	Error (lower limit exceeded)	
			$08	Error (upper limit exceeded)	
		2	$xx	Humidity	0.63/-25.8
			$FF	NC	
		3	$00	Transient operating mode	1/0
			$01	Stationary operating mode	
		4	$xx	Tempknob deviation	1/0
$204	**6**	**0**	$xx	Sun azimuth angle (high byte)	1/0
			$7F	NC	
		1	$xx	Sun azimuth angle (low byte)	1/0
			$FF	NC	
		2	$xx	Sun elevation angle (high byte)	1/0
			$FF	NC	
		3	$xx	Sun elevation angle (low byte)	1/0
			$FF	NC	

		4	$xx $FF	Sun intensity (high byte) NC	1/0
		5	$xx $FF	Sun intensity (low byte) NC	1/0
$205	**2**	**0**	$xx $FF	Passenger draught evaluation NC	1/0
		1	$xx $FF	Passenger comfort evaluation NC	1/0
$206	**2**	**0**	$xx $7F	Driver draught evaluation NC	1/0
		1	$xx $FF	Driver comfort evaluation NC	1/0

A.2 Bivariate correlation matrix

This section summarizes the bivariate correlation coefficients.

	FAm	V	H	Am	T1	T2	T4	T5	T7	I	E	A	T	IV	EV	AV	VV
FAm	1.000	-0.407	-0.184	0.980	-0.705	0.338	0.694	0.766	0.270	0.437	0.199	0.128	0.164	-0.101	-0.414	-0.305	0.101
V	-0.407	1.000	0.058	-0.439	0.363	-0.030	-0.353	-0.500	-0.027	-0.211	-0.134	-0.116	-0.387	0.069	0.219	0.092	-0.321
H	-0.184	0.058	1.000	-0.176	0.407	0.003	-0.121	-0.338	-0.199	-0.317	-0.181	-0.116	0.034	0.044	0.284	0.226	0.012
Am	0.980	-0.439	-0.176	1.000	-0.701	0.356	0.697	0.767	0.274	0.436	0.197	0.145	0.155	-0.102	-0.414	-0.312	0.101
T1	-0.705	0.363	0.407	-0.701	1.000	-0.007	-0.381	-0.636	-0.243	-0.691	-0.419	-0.038	-0.137	0.074	0.697	0.525	-0.064
T2	0.338	-0.030	0.003	0.356	-0.007	1.000	0.446	0.417	0.316	0.064	-0.069	0.226	0.035	-0.067	0.033	0.047	-0.015
T4	0.694	-0.353	-0.121	0.697	-0.381	0.446	1.000	0.810	0.549	0.315	-0.039	0.133	0.129	-0.106	-0.250	-0.186	0.098
T5	0.766	-0.500	-0.338	0.767	-0.636	0.417	0.810	1.000	0.528	0.480	0.130	0.231	0.189	-0.133	-0.411	-0.265	0.122
T7	0.270	-0.027	-0.199	0.274	-0.243	0.316	0.549	0.528	1.000	0.280	-0.402	0.147	-0.040	-0.093	-0.113	-0.061	-0.010
I	0.437	-0.211	-0.317	0.436	-0.691	0.064	0.315	0.480	0.280	1.000	0.573	-0.066	0.055	-0.156	-0.810	-0.672	0.022
E	0.199	-0.134	-0.181	0.197	-0.419	-0.069	-0.039	0.130	-0.402	0.573	1.000	-0.083	0.119	0.046	-0.741	-0.632	0.030
A	0.128	-0.116	-0.116	0.145	-0.038	0.226	0.133	0.231	0.147	-0.066	-0.083	1.000	0.078	-0.064	0.106	0.148	0.027
T	0.164	-0.387	0.034	0.155	-0.137	0.035	0.129	0.189	-0.040	0.055	0.119	0.078	1.000	-0.017	-0.114	-0.029	0.224
IV	-0.101	0.069	0.044	-0.102	0.074	-0.067	-0.106	-0.133	-0.093	-0.156	0.046	-0.064	-0.017	1.000	0.074	0.042	0.032
EV	-0.414	0.219	0.284	-0.414	0.697	0.033	-0.250	-0.411	-0.113	-0.810	-0.741	0.106	-0.114	0.074	1.000	0.824	-0.048
AV	-0.305	0.092	0.226	-0.312	0.525	0.047	-0.186	-0.265	-0.061	-0.672	-0.632	0.148	-0.029	0.042	0.824	1.000	-0.012
VV	0.101	-0.321	0.012	0.101	-0.064	-0.015	0.098	0.122	-0.010	0.022	0.030	0.027	0.224	0.032	-0.048	-0.012	1.000

A.3 PCA correlation loadings

This chapter contains the PCA correlation loadings which have been used for exploratory data analysis in Chapter 4.

PCA correlation loadings including all variables

Variable	Principle component 1		Principle component 2	
	Correlation Loading	Correlation [%]	Correlation Loading	Correlation [%]
FAm	-0.845	71.403	0.259	6.708
V	0.489	23.912	-0.160	2.560
H	0.378	14.288	0.122	1.488
Am	-0.849	72.080	0.268	7.182
T1	0.844	71.234	0.199	3.960
T2	-0.295	8.703	0.522	27.248
T4	-0.702	49.280	0.505	25.503
T5	-0.858	73.616	0.375	14.063
T7	-0.390	15.210	0.500	25.000
I	-0.753	56.701	-0.409	16.728
E	-0.441	19.448	-0.735	54.023
A	-0.117	1.369	0.389	15.132
Tr	-0.220	4.840	0.066	0.431
IV	0.149	2.220	-0.090	0.816
EV	0.740	54.760	0.581	33.756
AV	0.599	35.880	0.599	35.880
VV	-0.139	1.932	0.077	0.596

Variable	Principle component 3		Principle component 4	
	Correlation Loading	Correlation [%]	Correlation Loading	Correlation [%]
V	-0.620	38.440	0.126	1.588
H	0.278	7.728	0.639	40.832
Am	0.079	0.625	0.222	4.928
T1	0.021	0.044	0.107	1.145
T2	-0.183	3.349	0.289	8.352
T4	-0.072	0.523	0.187	3.497
T5	-0.019	0.035	-0.051	0.255
T7	-0.459	21.068	-0.165	2.723
I	-0.196	3.842	-0.061	0.374
E	0.151	2.280	0.100	0.999
A	0.042	0.173	-0.473	22.373
Tr	0.655	42.903	-0.117	1.369
IV	0.123	1.513	0.305	9.303
EV	0.072	0.513	-0.011	0.012
AV	0.145	2.103	-0.088	0.767
VV	0.593	35.165	-0.171	2.924

Variable	Principle component 5		Principle component 6	
	Correlation Loading	Correlation [%]	Correlation Loading	Correlation [%]
V	0.054	0.287	0.086	0.742
H	-0.315	9.923	0.009	0.008
Am	0.024	0.057	0.106	1.124
T1	-0.092	0.845	0.049	0.238
T2	-0.030	0.088	0.351	12.320
T4	-0.015	0.023	-0.119	1.416
T5	0.049	0.239	-0.023	0.052
T7	0.032	0.099	-0.416	17.306
I	-0.099	0.988	-0.088	0.775
E	0.030	0.089	0.339	11.492
A	0.142	2.016	0.618	38.192
Tr	-0.113	1.277	0.035	0.120
IV	0.904	81.722	-0.057	0.328
EV	0.041	0.170	0.023	0.051
AV	0.042	0.177	0.042	0.174
VV	0.088	0.770	-0.370	13.690

Variable	Principle component 7		Principle component 8	
	Correlation Loading	Correlation [%]	Correlation Loading	Correlation [%]
V	0.164	2.690	-0.045	0.200
H	0.139	1.932	-0.003	0.001
Am	-0.268	7.182	-0.101	1.020
T1	0.255	6.503	-0.021	0.046
T2	0.441	19.448	-0.077	0.593
T4	0.065	0.421	0.023	0.051
T5	-0.009	0.009	0.031	0.093
T7	0.269	7.236	0.181	3.276
I	0.168	2.822	0.030	0.087
E	0.124	1.538	-0.074	0.548
A	0.163	2.657	-0.091	0.836
Tr	0.224	5.018	0.594	35.284
IV	0.088	0.783	0.143	2.045
EV	-0.167	2.789	-0.032	0.104
AV	-0.219	4.796	0.005	0.003
VV	0.340	11.560	-0.548	30.030

Variable	Principle component 9		Principle component 10	
	Correlation Loading	Correlation [%]	Correlation Loading	Correlation [%]
V	0.086	0.732	0.506	25.604
H	-0.471	22.184	0.033	0.111
Am	0.006	0.003	0.167	2.789
T1	0.076	0.576	-0.169	2.856
T2	0.355	12.603	-0.098	0.966
T4	-0.001	0.000	-0.101	1.020
T5	0.036	0.126	-0.132	1.742
T7	-0.195	3.803	0.023	0.053
I	-0.090	0.816	-0.049	0.245
E	0.098	0.956	-0.093	0.859
A	-0.407	16.565	0.058	0.336
Tr	0.147	2.161	0.254	6.452
IV	-0.091	0.832	-0.042	0.175
EV	0.095	0.908	0.019	0.036
AV	0.106	1.124	-0.006	0.004
VV	0.056	0.317	0.173	2.993

PCA correlation loadings removed from FAm, AV and EV

Variable	Principle component 1		Principle component 2	
	Correlation Loading	Correlation [%]	Correlation Loading	Correlation [%]
V	0.542	29.376	-0.154	2.372
H	0.385	14.823	-0.200	4.000
Am	-0.850	72.250	-0.013	0.016
T1	0.779	60.684	-0.400	16.000
T2	-0.393	15.445	-0.520	27.040
T4	-0.788	62.094	-0.374	13.988
T5	-0.931	86.676	-0.162	2.624
T7	-0.502	25.200	-0.579	33.524
I	-0.656	43.034	0.457	20.885
E	-0.265	7.023	0.803	64.481
A	-0.214	4.580	-0.326	10.628
Tr	-0.249	6.200	0.147	2.161
IV	0.174	3.028	0.089	0.798
VV	-0.169	2.856	0.090	0.811

Variable	Principle component 3		Principle component 4	
	Correlation Loading	Correlation [%]	Correlation Loading	Correlation [%]
V	-0.584	34.106	0.062	0.384
H	0.390	15.210	0.396	15.682
Am	0.049	0.238	0.152	2.310
T1	0.175	3.063	-0.001	0.000
T2	-0.020	0.041	0.131	1.716
T4	0.038	0.143	0.227	5.153
T5	0.010	0.011	0.030	0.087
T7	-0.281	7.896	0.059	0.350
I	-0.332	11.022	0.039	0.154
E	-0.079	0.616	0.030	0.089
A	0.133	1.769	-0.631	39.816
Tr	0.651	42.380	-0.122	1.488
IV	0.100	1.000	0.580	33.640
VV	0.612	37.454	0.010	0.010

Variable	Principle component 5		Principle component 6	
	Correlation Loading	Correlation [%]	Correlation Loading	Correlation [%]
V	0.054	0.289	-0.105	1.103
H	-0.403	16.241	-0.314	9.860
Am	-0.042	0.174	-0.157	2.465
T1	-0.043	0.183	-0.103	1.061
T2	0.020	0.039	-0.518	26.832
T4	-0.079	0.630	-0.016	0.026
T5	0.038	0.142	0.005	0.003
T7	0.012	0.014	0.387	14.977
I	-0.131	1.716	0.019	0.037
E	0.043	0.189	-0.393	15.445
A	0.436	19.010	-0.327	10.693
Tr	-0.042	0.176	-0.050	0.253
IV	0.768	58.982	-0.004	0.002
VV	0.092	0.855	0.388	15.054

PCA correlation loadings removed from FAm, AV, EV, T1, T4 and T5

Variable	Principle component 1		Principle component 2	
	Correlation Loading	Correlation [%]	Correlation Loading	Correlation [%]
V	0.616	37.946	-0.187	3.497
H	0.403	16.241	0.024	0.058
Am	-0.785	61.623	-0.135	1.823
T2	-0.359	12.888	-0.552	30.470
T7	-0.356	12.674	-0.720	51.840
I	-0.714	50.980	0.226	5.108
E	-0.409	16.728	0.721	51.984
A	-0.238	5.664	-0.403	16.241
Tr	-0.367	13.469	0.229	5.244
IV	0.216	4.666	0.180	3.240
VV	-0.266	7.076	0.185	3.423

Variable	Principle component 3		Principle component 4	
	Correlation Loading	Correlation [%]	Correlation Loading	Correlation [%]
V	-0.492	24.206	0.095	0.901
H	0.437	19.097	-0.173	2.993
Am	0.005	0.003	0.067	0.449
T2	0.037	0.140	0.236	5.570
T7	-0.140	1.960	-0.070	0.496
I	-0.488	23.814	-0.091	0.825
E	-0.331	10.956	0.174	3.028
A	0.215	4.623	0.329	10.824
Tr	0.574	32.948	-0.051	0.265
IV	0.101	1.020	0.853	72.761
VV	0.561	31.472	-0.019	0.036

Variable	Principle component 5		Principle component 6	
	Correlation Loading	Correlation [%]	Correlation Loading	Correlation [%]
V	0.074	0.549	0.028	0.077
H	0.338	11.424	0.555	30.803
Am	0.090	0.801	0.249	6.200
T2	0.369	13.616	0.360	12.960
T7	-0.423	17.893	0.113	1.277
I	-0.092	0.848	0.127	1.613
E	0.288	8.294	0.021	0.043
A	0.388	15.054	-0.595	35.403
Tr	0.087	0.765	-0.048	0.235
IV	-0.305	9.303	0.234	5.476
VV	-0.423	17.893	-0.048	0.230

PCA correlation loadings removed from Am, AV, EV, T1, T4, T5 and IV

Variable	Principle component 1		Principle component 2	
	Correlation Loading	Correlation [%]	Correlation Loading	Correlation [%]
V	-0.625	39.063	0.155	2.403
H	-0.404	16.322	-0.029	0.085
Am	0.785	61.623	0.164	2.690
T2	0.349	12.180	0.573	32.833
T7	0.338	11.424	0.731	53.436
I	0.712	50.694	-0.226	5.108
E	0.432	18.662	-0.713	50.837
A	0.230	5.290	0.420	17.640
Tr	0.379	14.364	-0.201	4.040
VV	0.281	7.896	-0.153	2.341

Variable	Principle component 3		Principle component 4	
	Correlation Loading	Correlation [%]	Correlation Loading	Correlation [%]
V	-0.494	24.404	0.103	1.061
H	0.449	20.160	0.233	5.429
Am	-0.013	0.018	0.096	0.922
T2	0.007	0.005	0.415	17.223
T7	-0.174	3.028	-0.428	18.318
I	-0.486	23.620	-0.125	1.563
E	-0.316	9.986	0.331	10.956
A	0.195	3.803	0.502	25.200
Tr	0.579	33.524	0.064	0.409
VV	0.560	31.360	-0.395	15.603

Variable	Principle component 5		Principle component 6	
	Correlation Loading	Correlation [%]	Correlation Loading	Correlation [%]
V	0.013	0.016	-0.126	1.588
H	0.618	38.192	-0.052	0.266
Am	0.238	5.664	-0.029	0.082
T2	0.339	11.492	-0.220	4.840
T7	0.075	0.565	0.141	1.988
I	0.134	1.796	0.006	0.004
E	0.015	0.023	-0.138	1.904
A	-0.598	35.760	-0.091	0.830
Tr	-0.021	0.046	0.522	27.248
VV	-0.103	1.061	-0.604	36.482

A.4 Final correlation loadings

This section shows the PCA correlation loadings only containing variables V, H, Am, T2, T7, I, E and A.

Variable	Principle component 1		Principle component 2	
	Correlation Loading	Correlation [%]	Correlation Loading	Correlation [%]
V	-0.485	23.523	-0.239	5.712
H	-0.404	16.322	-0.159	2.528
Am	0.791	62.568	0.033	0.111
T2	0.524	27.458	-0.367	13.469
T7	0.571	32.604	-0.593	35.165
I	0.650	42.250	0.464	21.53
E	0.125	1.563	0.886	78.500
A	0.336	11.290	-0.265	7.023

Variable	Principle component 3		Principle component 4	
	Correlation Loading	Correlation [%]	Correlation Loading	Correlation [%]
V	-0.483	23.329	-0.335	11.223
H	0.596	35.522	-0.495	24.503
Am	0.276	7.618	-0.137	1.877
T2	0.249	6.200	-0.467	21.809
T7	-0.408	16.646	-0.072	0.522
I	-0.362	13.104	-0.214	4.580
E	0.089	0.794	-0.136	1.850
A	0.343	11.765	0.560	31.360

Variable	Principle component 5		Principle component 6	
	Correlation Loading	Correlation [%]	Correlation Loading	Correlation [%]
V	0.517	26.729	-0.012	0.014
H	-0.097	0.949	-0.449	20.160
Am	-0.186	3.460	0.145	2.103
T2	0.365	13.323	0.327	10.693
T7	-0.147	2.161	-0.254	6.452
I	0.034	0.117	-0.361	13.032
E	0.330	10.890	-0.016	0.024
A	0.556	30.914	-0.270	7.290

A.5 Total explained PCA variances

This section shows the explained variance of each principle component with respect to the original data set.

Principle component	Explained variance [%]
PC1	33.97
PC2	15.96
PC3	9.48
PC4	6.26
PC5	5.83
PC6	5.82
PC7	5.01
PC8	4.42
PC9	3.76
PC10	2.97
PC11	2.17
PC12	1.66
PC13	1.00
PC14	0.71
PC15	0.59
PC16	0.39
PC17	0.10

A.6 Z-core parameters

This section shows the z-core parameters required for preprocessing of the neural network inputs.

Variable	$\bar{x}$	σ
V	57.24	36.25
H	33.24	4.5
Am	28.15	8.3
T2	25.66	1.28
T7	28.2	4.8
I	798	275
E	41.46	19.6
A	-25.6	90.36

A.7 Input space domain

Figures A2-A5 show the domain of the input variables. Boxplots have been chosen as method of illustration since they are a convenient way of graphically depicting groups of numerical data. Figure A1 shows how to interpret the boxplots.

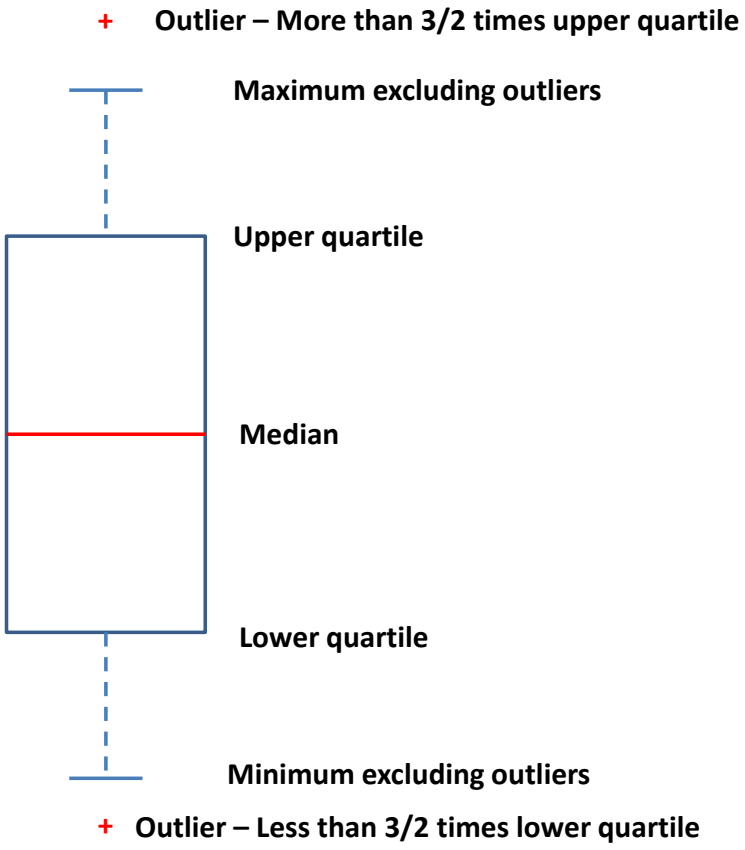

Figure A1: Interpretation of Box plots

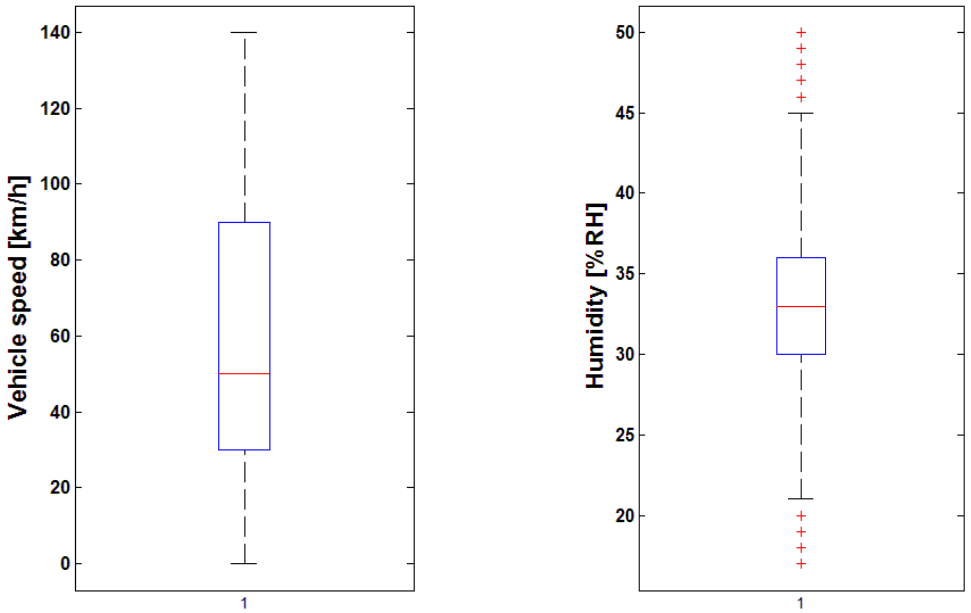

Figure A2: Vehicle speed and humidity

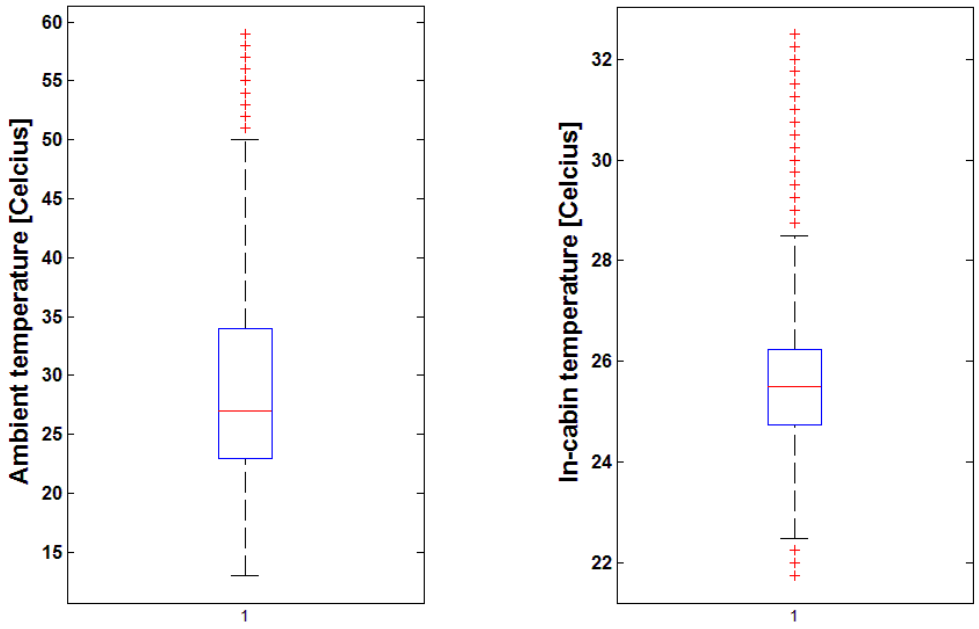

Figure A3: Ambient temperature and In-cabin temperature

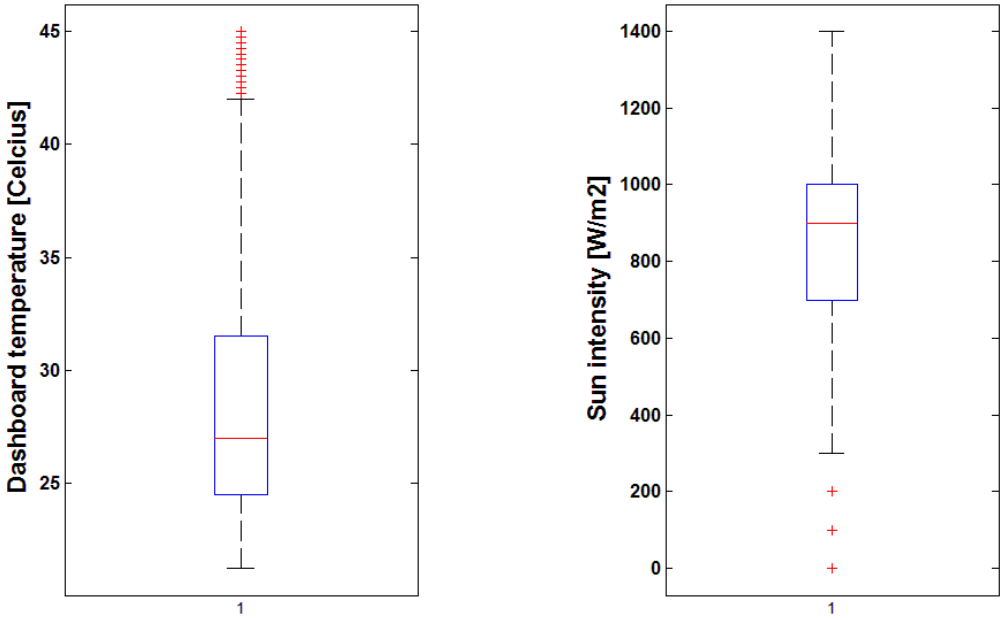

Figure A4: Dashboard temperature and sun intensity

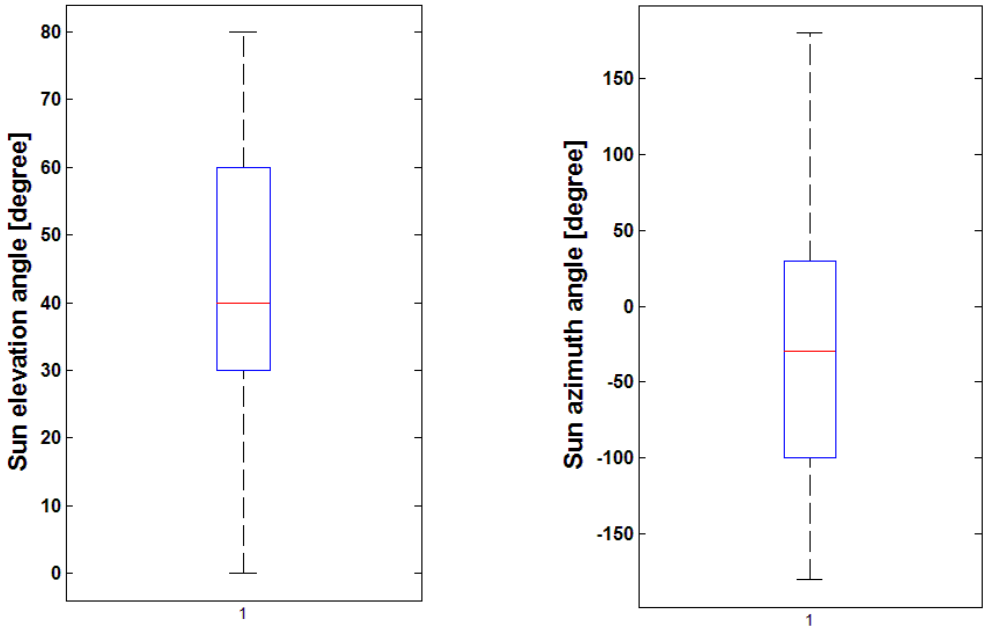

Figure A5: Sun elevation angle and sun azimuth angle

A.8 Proposed publications

The outcome of the research has been submitted for publication in a peer reviewed journal. Two consecutive papers (Part I and Part II) have been generated.

Part I addresses the experimental setup for the research and Part II summarizes the findings from the data mining and modelling process.

Automotive Thermal Comfort Control – A Blackbox Approach
Part I: Comfort Acquisition System Development

J. Kranz*, TI. van Niekerk*, HFG. Holdack-Janssen*, G. Gruhler**

** VWSA-DAAD Chair in Automotive Engineering, Nelson Mandela Metropolitan University, PO 77000 Port Elizabeth 6031, South Africa E-mail: Juergen.Kranz@nmmu.ac.za, Theo.vanNiekerk@nmmu.ac.za, Hinrich.Holdack-Janssen@nmmu.ac.za*
*** Department of Mechatronics, Reutlingen University, Alteburgstrasse 150, 72762 Reutlingen, Germany E-mail: Gerhard.Gruhler@Reutlingen-University.de*

Abstract: Thermal comfort is a very vague and a very subjective term, which depends on physiological and psychological variables. Thermal comfort in transient environments, like an automotive cabin, is far from understood and general accepted theories do not exist. A two part series will investigate the concept of using a blackbox approach for directly associating thermal comfort to field measurements. Part I introduces a novel comfort acquisition tool and its integration into a research vehicle. Data has been collected during spring, autumn and summer conditions in Southern Africa. The successive data mining and learning process will be discussed in Part II.

Keywords: Automotive Thermal Comfort Assessment, Automotive HVAC

1. INTRODUCTION

Mobility has become a substantial part in our society. Since we spend a lot of our available time on the road, we expect the automotive environment to provide similar comfort levels than residential buildings. In terms of thermal comfort this means that the automotive Heating Ventilation and Air Conditioning (HVAC) unit has to maintain in-cabin thermal comfort irrespective of the environment and the driving situation. Thermal comfort is however a very subjective term since its perception to people has enormous variation. This makes it difficult to describe it in terms of clear defined parameters and variables. In 1970, the American Society of Heating, Refrigeration and Air-Conditioning Engineers (ASHRAE) defined thermal comfort as "*That condition of mind which expresses satisfaction with the thermal environment*". This vague definition is still part of thermal comfort standards [1]. To develop and reliably validate thermal comfort models, a comprehensive database is needed which contains information about the thermal environment and its correlation to thermal comfort. Most available thermal comfort models have been developed with data acquired from paper-based questionnaires in climate chambers. Due to the transient and inhomogeneous environments in automotive passenger compartments, climate chamber tests are less expressive and real field testing is required. Due to the enormous difficulties when modeling thermal comfort, this two-part publication investigates the potential of directly learning a technical system with field data without prior thermal comfort modeling. Data is collected from measurement drives and is combined to a database. Methods of data mining are applied aiming to discover functional relationships, to remove inconsistencies and for dimensionality reduction. Elements of artificial intelligence will be used to find the correlation of environmental information to thermal comfort. The structure is shown in Figure 1.

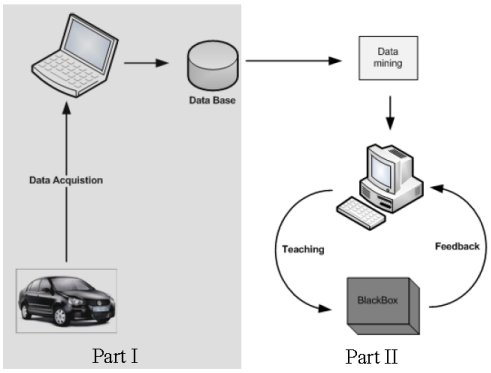

Figure 1: Concept

This first part will discuss the experimental setup and the data acquisition procedure. Data mining and system learning will be referred to in Part II.

2. THERMAL COMFORT PRINCIPLES

In the past decades there has been much effort to model and measure thermal comfort. Research in the 1970s showed that thermal comfort is a function of physical and physiological variables. These variables are air temperature, mean radiant temperature, air velocity, humidity, metabolic rate and clothing insulation [2].
To some extent thermal comfort is an individual state of mind and cannot be explained with physical variables. It has shown to be linked to contextual variables such as local climate, occupants' expectations, available control over the environment and the processes by which the indoor environment is controlled, perceived, experienced,

and interacted with [3]. In general, three conditions must be fulfilled to establish overall thermal comfort [4], [5]:

- Combinations of skin and core temperatures must provide a sensation of thermal neutrality,
- The body must be in thermal equilibrium,
- No occurrence of local discomfort.

Thermal comfort theories in uniform, steady state environments are nowadays widely accepted and have been defined in standards like ISO 7730 or ASHRAE Standard 55P [1], [6]. In non-uniform and transient environments, overall body thermal sensation seems to be a complaint-driven process [7]. The strongest local sensations tend to dominate overall thermal sensation and whole body thermal sensation tends to follow the cooler local body sensations [8]. Assessment of thermal non-uniform environments is difficult due to a lack of general knowledge about the superposition and influence of multiple thermal sources [9]. Comprehensive knowledge and generally accepted theories about thermal comfort in transient, non-stationary environments are not available yet and researchers are still busy with investigations.

3. AUTOMOTIVE THERMAL COMFORT

The automobile cabin can be best classified as an inhomogeneous and transient environment [10]. Thermal comfort predictions in vehicles are very complex due to the inhomogeneity of temperatures and air distribution, high localized air velocities and many radiation sources. Some parameters are not independent from each other and their interrelationship is not known exactly, which complicates an experimental study [11]. Air flow within a passenger compartment is highly asymmetric and of three-dimensional nature [11]-[13]. The ventilation flow from the HVAC unit into the passenger compartment can be affected by many properties, including location of air vents and passenger occupancy [14]. External environmental conditions have a strong influence on the vehicle cabin due to limited insulation material as well as due to a large glazing ratio [12], [13]. Unlike to buildings, the position of a vehicle is not fixed in space and parameters suffer from strong temporal and local variability. Some researchers argue that due to the enormous differences to architectural environments, existent standards and methods can hardly be applied to the automotive environment [4].

4. THERMAL COMFORT ASSESSMENT

Thermal comfort assessment methodologies can be distinguished in subjective, behavioral and objective methods [15].

4.1 Subjective Methods

Subjective methods shall quantify the subject's response to a given environment with use of subjective evaluation scales. These scales are based on psychological continua that are relevant to the phenomenon of interest. Subjective methods are also required for the development and validation of various thermal comfort models and indices. Subjective scales can be distinguished in thermal sensation scales, thermal emotion scales, thermal preference scales, thermal acceptance scales and thermal tolerance scales [15].

Scales must be carefully identified to meet the requirements of the specific application, because the way a scale is represented or handled, may influence the results [15]. Often it is recommended to integrate more than one scale into a questionnaire in order to complement each other [15]. Scales are relatively easy to use because no special instrumentation is needed and the phenomena of interest are directly addressed. A disadvantage is that human sensation of thermal comfort can be an individual state of mind and linguistic terms and semantics of language might be interpreted differently by a panel of test subjects. Human beings vary in their thermal sensitivity, which means the ability to distinguish between different thermal states. A person with a high thermal sensitivity may therefore be able to evaluate a given climate more precisely and with more details than a thermal less sensitive subject.

4.2 Behavioral Methods

Behavioral methods quantify or represent human behavior as response to a given environment. The particular aspect of observed human behavior is assumed to be related to thermal comfort. For example an observed behavioral response to an environment might be a change in clothing or a change in seating. Advantages of behavioral methods include minimum interference with the quantity to be measured and a direct measurement of comfort/discomfort. Disadvantages can be given in terms of difficulties in establishing validity and reliability of the method. For computer based thermal comfort evaluation, the authors however consider behavioral methods as inapplicable.

4.3 Objective Methods

Objective measures aim to quantify the physical or mental condition of a person by the use of instrumentation or with measurements of thermal comfort relevant variables. An advantage of objective measures is that they are often independent from subjective methods and deliver consistent outputs for a given input. However, measurement difficulties may arise. Measured quantities might be influenced by measurement errors and might be superimposed by inferences. In transient and inhomogeneous environments, localized phenomena can affect temperatures and air velocity, making it impossible to measure them accurately [15]. Since thermal comfort is a condition of mind, its correlation to physical variables might not be complete. In buildings, which are considered as stationary and homogeneous environments, it is often sufficient to evaluate the room climate at only one position. Methods and instrumentation for measuring and evaluating thermal environments are defined in ISO 7726 [16]. Due to inhomogeneity of temperature and air

velocity in the vehicle cabin, many sensors would have to be installed inside the vehicle compartment. In order for being able to use thermal comfort indices, measurement values must be accurate and according to their exact definition. Automotive industry predominantly uses the principle of equivalent temperature to assess the thermal environment inside a vehicle compartment [15]. This can be achieved with single heated sensors or with heated manikins. However, none of the methods can exactly simulate the heat exchange of a human body. Different methodologies to determine equivalent temperature may differ up to several degrees Celsius for the same environmental conditions and the differences are known to increase with increasing non-uniformity of the environment [15].

5. SYSTEM REQUIREMENTS

Automotive measurement equipment is required to operate under a variety of environmental conditions. It must be insensitive to shocks, vibrations and it is required to continuously monitor the periphery, in order to prevent corrupt sensor recordings. In terms of thermal comfort evaluation, literature points out that questionnaires are time consuming and may put stress on the test subjects [15]. It is therefore advantageous to use computers for thermal comfort evaluation. This is especially important for automotive thermal comfort evaluation, where subjects are required to evaluate their comfort levels several times per minute, due to the overall transient conditions in the vehicle cabin. All sensor elements must therefore incorporate short response times. Data sources must be synchronized to each other in order to produce consistent data input-output mappings. The measurement equipment must be capable of communicating with the vehicle's bus systems in order to gather thermal comfort relevant vehicle parameters. Additionally, it must be capable of modifying the HVAC control algorithms in order to provide a reliable framework for thermal comfort assessment.

6. SYSTEM DEVELOPMENT

7.1 Measurement variables

The authors emphasize the importance of being consistent with the environmental information measured at the design process of the HVAC unit and within the final product. Measurement of equivalent temperature has been found to be inappropriate for the use in automotive application. This can be justified with technical, economical and ergonomic effects. Disadvantages include weekly calibration requirements, slow sensor response and long recovery times [15]. To make the experimental setup as most as applicable for automotive application, the authors have decided only to incorporate interfacing possibilities for discrete standard sensor elements. Direct attachment of sensors to the human body may influence overall comfort. The authors have therefore decided not to attach any sensor elements at the human body and additional measurements of internal body physiological variables have been abdicated. The relevant thermal comfort variables have been adopted from [2] although it is well known that the exact functional relationship of those variables to thermal comfort is prevalently unknown in transient and inhomogeneous conditions.

Air-temperature

When measuring air temperature, special care must be taken to minimize the influence of radiation from surrounding surfaces [12]. This can be achieved with reducing the emission coefficient of the sensor's surface, reducing the temperature gradient between air and surrounding surfaces, shielding the sensor element against radiation or using air aspirated sensors in order to increase the heat convection between surrounding air and the sensor element [16]. The authors have decided to use a fan-aspirated sensor element to measure mean in-cabin air temperature. Additionally normal unshielded temperature sensors have been installed at feet and head level.

Mean radiant temperature

Mean radiant temperature ϑ_r can be estimated with measurements of surface temperatures. Reference [6] proposes equation (1) for approximation.

$$\vartheta_r^4 = \sum_{i=1}^{N} \vartheta_i^4 F_{p-i} \quad \textbf{(1)}$$

Where:

- ϑ_i: Temperature of surface i,
- $F_{p\text{-}i}$: Angle factor between a person p and surface i;
- N: Number of surfaces surrounding the occupant.

The angle factors $F_{p\text{-}i}$ normally depend on the position and orientation of the person [6]. In practice it is considered to be difficult to determine them and often only surface temperatures are measured instead. In the automotive cabin, the dashboard is the largest continuous part of plastic. Its position close to the windscreen and its colour makes it especially absorbent to radiation. The authors assume that it is the largest radiation source within the vehicle compartment. It is therefore suggested to approximate mean radiant temperature with measurement of only dashboard temperature.

Air velocity

Due to the enormous non-uniformity of air distribution and the variety of possible air-flow patterns inside the vehicle cabin, the authors consider it as impossible to measure air velocity with one, or more single discrete sensors, at all comfort relevant positions. It is assumed, that air velocity v_a and the air distribution inside the vehicle cabin is a function of mainly

- Vehicle speed v_v,
- Air distribution flap position f,
- Blower load b.

This dependence can be mathematically expressed as

$$v_a = f(v_v, f, b). \quad (2)$$

It is assumed that the unknown function *f(·)* in equation (2) can be approximated by the blackbox.

Humidity
For human heat exchange with the environment, only absolute humidity is of relevance [16]. Vapour pressure can be considered as constant within the vehicle cabin [15]. Humidity h is considered to have only a minor influence on thermal comfort and a 10% increase in humidity is equivalent to only $\Delta\vartheta$=0.3°C rise in air temperature [17]. At low air temperatures, thermal sensation can be even considered as independent of humidity [18]. However, humidity is a contributing factor towards indirect comfort influences like skin moisture, tactile sensation of fabrics, health and air quality. The authors therefore suggest including measurements of relative humidity for thermal comfort determination.

Metabolic rate
ISO 8996 provides measurement methodologies for human metabolic rate [19]. These methods are extensive and are hardly applicable to the automotive environment. In case of vehicular application, it is assumed that human internal activity M is predominantly linked to the driving or traffic situation and can be expressed as:

$$M = f(T_r, v, \sigma_v) \quad (3)$$

with

T_r:	An empirical function quantifying the traffic load,
v:	Vehicle speed,
σ_v:	Standard deviation of vehicle speed.

According to the authors research, a good indicator for the traffic situation is the number of alternating changes in gas and brake pedal for a given observation interval. The empirical function T_r can therefore be expressed as:

$$T_r[n] = \sum_{k=1}^{k=N} T[n-k] \quad (4)$$
$$T[n-k] = 0 \; for \; (n-k) < 0$$

with:

T[n]:	Number of brake gas pedal changes for period n,
N:	Total observation interval.

Equation (4) determines the number of subsequent alternations of gas and brake pedal and therefore indicates the traffic situation. It is assumed that stop-and-go situations put more stress on the driver than driving on a highway with constant speed.

Clothing insulation
Measurement of clothing insulation is extremely difficult and is commonly done with heated manikins [20]. In this research, it is assumed that subjects have consistent clothing habits while driving a car. It is considered as implausible, that a person chooses different clothing insulations for thermally identical environments. However, it must be considered that basic clothing insulation may vary during the year.

Solar load
Solar load has significant influence on thermal comfort in a vehicle compartment. It is estimated, that 50% of the HVAC unit's cooling load in recirculation mode is due to solar heat gain [21]. Sun radiation may project complex patterns on the human body which require local cooling [22]. It is therefore suggested to use a novel three-dimensional solar sensor which is capable of determining the azimuth angle φ, the elevation angle ψ as well as the solar intensity I. This is illustrated in Figure 2.

Figure 2: Solar angle definitions

7.2 Automotive testing procedures

Established test procedures for automotive HVAC units can be divided into three categories [10]:

- Transient conditions,
- Short-transient conditions,
- Stationary conditions.

Transient conditions refer to heating up and cooling down of the passenger compartment under extreme environmental conditions. An example may be a cooling down process of a passenger vehicle, which has been previously soaking in the sun. Short-transient testing conditions aim to simulate small variations of interior and exterior climate. An example may be a change in cabin set-temperature, ambient temperature, vehicle speed or sun load. Short-transient conditions consolidate the overwhelming majority of conditions in every-day driving situations. Stationary conditions rarely occur in automobiles. Steady-state conditions may be present in a truck cabin during the sleeping period of the driver [10]. The measurement equipment must be able to distinguish between all these conditions, in order for being able to draw the correct conclusions concerning thermal comfort.

7.3 Experimental setup.

Sensor elements have been installed in a research vehicle. The sensor positions are shown in Figure 3. Temperature measurement locations are indicated by ϑ_i, humidity by h and the solar properties by I, ψ and φ.

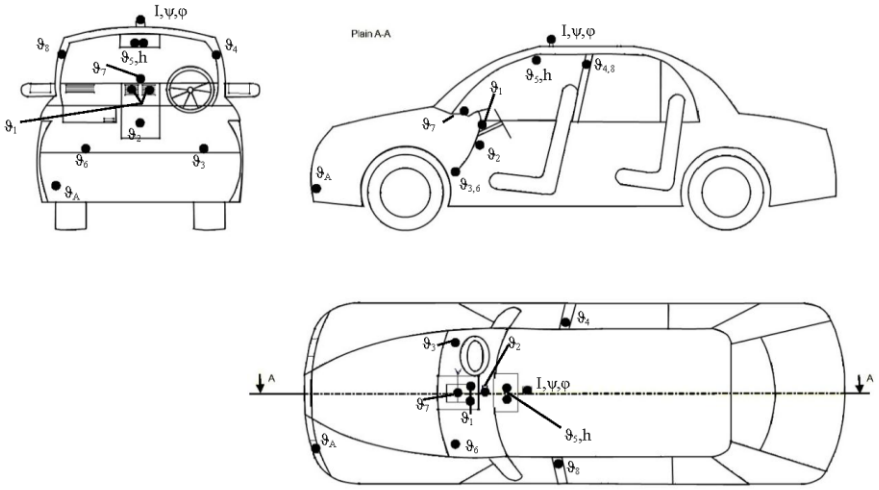

Figure 3: Sensor installment locations

7.4 Sampling rate

Choosing an appropriate sampling time t_s is of great importance for thermal comfort assessment. If the sampling rate is chosen too low, transient conditions will not be detected. This may result in a loss of valuable information. On the other hand, if sampling rate is chosen too high, a hypersensitivity to transients and distortions may occur. This can influence system stability and may result in an overload of data. Literature reveals different sampling rates for similar concepts. Reference [23] analyses the airflow in a vehicle compartment with 72 temperature sensors and choses a sampling rate of 0.2 Hz. Similar research has been conducted by [24], which selects a sampling rate of 0.1 Hz. This is confirmed by [15] who recommends t_s=10s for heating up and cooling down measurements in a vehicle cabin. To determine an optimal sampling rate for thermal comfort evaluation, experiments in a car have been conducted. Sampling rate should be as low as possible, but high enough for being able to detect the most transient source influencing thermal comfort. This most transient source was determined to be the sun. Subjects were placed in a pre-conditioned vehicle, which has been initially parked in the shadow. It was taken care that the subjects felt comfortable inside the car before the test started. Thereafter, the vehicle was directly exposed to sun radiation with an intensity of I=1000 W/m^2. It was ensured, that some body parts were directly exposed to sun radiation. The subjects were asked to report any occurrence of discomfort immediately and that time was measured. It was paid attention, that during the tests similar body parts were radiated and the subjects wore similar clothing. The subjects reported discomfort after periods ranging from 5s<t<15s. The differences in response times can be explained with individual differences of thermal sensitivity. According to these results the mean sampling time has been averaged as t_s=10s.

7.5 Human thermal comfort evaluation

The transient environment in an automobile requires frequent periodical thermal comfort evaluation. These intervals are equivalent to the sampling rate, meaning that subjects are required to evaluate their environment every ten seconds. This would probably overstrain the subjects. Secondly from a driver's point of view, it is considered to be irresponsible and unpractical to demand filling questionnaires with a frequency of 0.1 Hz during road testing. It is therefore required to develop an evaluation system which can be used intuitively during driving without reducing the driver's ability to focus on traffic situations. As a rule of thumb, evaluation scales should be as detailed as necessary but as simple as possible. Both effects are of opposite nature and a trade-off must be found. Too detailed evaluation scales might exceed the subject's thermal sensitivity and might result in inconsistent data. The authors have decided to implement two methodologies to evaluate the thermal environment in an automobile:

- Direct electronic thermal comfort evaluation using a thermal preference scale in combination with a draught preference scale,
- Indirect evaluation of thermal comfort using the HVAC controller's setup parameters.

The second approach avoids direct thermal comfort evaluation and assumes that the occupant interacts with the HVAC controls in such a way, that thermal comfort will always be maintained inside the vehicle cabin. According to the magnitude of change, it is possible to estimate the degree of comfort or discomfort.

7.6 Hardware design

A 16-bit HCS12 MCU was used as computing unit for the thermal comfort acquisition system. The experimental setup incorporates:

- One fan aspirated sensor element for measurement of in-cabin air temperature,
- Two I^2C channels, each capable of connecting up to 16 digital DS1631 thermostats,
- A Klimabus-interface for the three-dimensional ISOS solar sensor,
- An interface for the HIH 4000 humidity sensor,
- A connection to the Climate ECU for tabbing analogue signals like temperature knob and air distribution flap position,
- A HMI consisting of a 248x128 dot matrix display and two 4-way joysticks for thermal comfort and draught evaluation,
- A high-speed Controller Area Network (CAN) connection to the vehicle's powertrain bus, in order to obtain vehicle parameters,
- A low-speed CAN connection to the vehicle's comfort CAN to connecting to the HVAC ECU in order to set up control parameters.

A simplified block diagram is shown in Figure 4.

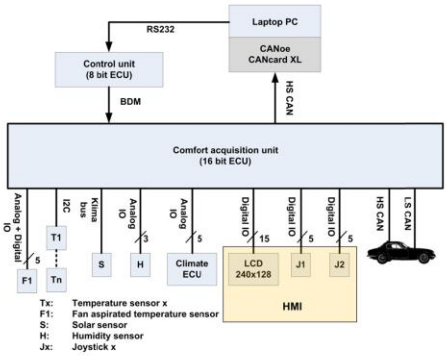

Figure 4: System structure

All sensor sources are being synchronized and are sent to a PC via CAN link and will be stored on a laptop PC. Vector CANoe® is used as data acquisition tool. The comfort acquisition unit is controlled by an eight bit ECU which allows for in-system programming and customization. Figure 4 shows the visual interface.

Label 2 in Figure 4 displays the solar information as well as its statistical properties. Label 3 shows the temperature measurements. Label 4 displays vehicle parameters and label 5 shows the flap position and the blower level.

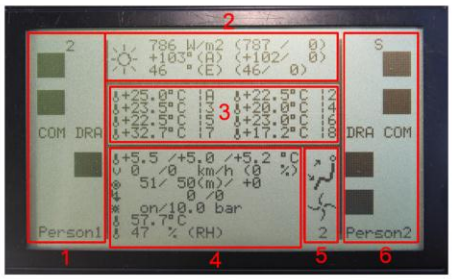

Figure 5: LCD

Label 1 and label 6 refer to comfort and draught evaluation for driver and front passenger. The coding of the scales is shown in Figure 6.

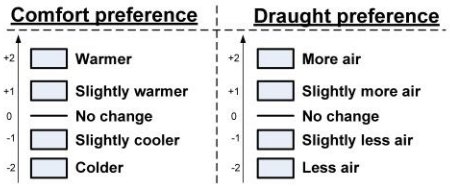

Figure 6: Comfort and draught scale

Thermal comfort and draught preference for driver and front passenger can be setup with joysticks which have been incorporated into the vehicle's control panel. This is shown in Figure 7.

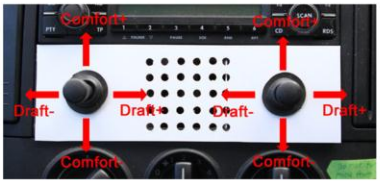

Figure 7: HMI

7.7 Software structure

Figure 8 shows the software structure of the main program.

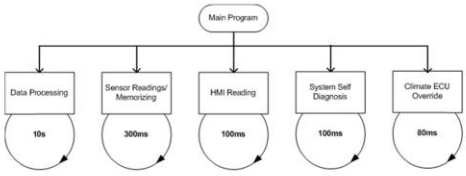

Figure 8: Software main loop

The main software loop consists of five parallel concurrent tasks. The authors have decided to use a manual HVAC unit in order to prevent complications regarding human thermal comfort assessment and HVAC control adjustments. Although manual HVAC units are not able to autonomously control the interior cabin climate, they still influence it indirectly due to control of cooling parameters. Because of permanent changes in environmental conditions and driving situations, the required cooling load is adjusted continuously. This mainly affects the set-up value of the evaporator temperature. However, this research requires a constant evaporator temperature, irrespective of the mode of operation and irrespective of changing environmental conditions. The HVAC control unit must therefore be limited in its functionality and scope of operation. This is achieved by periodically accessing its firmware and forcing it into a special engineering operating mode during testing, which allows for individual set-up of various control parameters. Since this process is essential in terms of providing consistent measurement conditions, it was assigned with the highest priority. It can therefore not be interrupted by any process, but can interrupt all other processes. In order to prevent corrupt data acquisition due to failure of previously recognized periphery, hardware must be monitored periodically. This is done with a frequency of 10Hz. Any detected failure will result in an immediate stop of data acquisition and will produce an error message on the LCD, in combination with an acoustic alarm signal. The HMI is sampled with a frequency of 10Hz in order to ensure immediate response to any user input. Comfort and draught sensations cannot be evaluated simultaneously and must therefore be done sequentially. If software detects a change in any direction of driver and passenger joysticks, the appropriate CAN message is temporarily deactivated from the CAN map. This prevents sampling of comfort and draught values in between or during user inputs. The corresponding CAN message is activated again shortly after user interaction. This is done when no joystick change is detected for at least two seconds. This time span is optically displayed with two blue LEDs on the LCD, for driver and front passenger respectively. This methodology additionally allows for easy correction of accidentally wrong entered data.

Information of all sensors and the CAN parameters are read and synchronized every 300ms and are stored in internal memory. Data is being statistically processed every ten seconds. For each continuous variable, the mean and coefficient of variation is determined. Discrete variables are processed considering their cumulative sums. Solar information is transformed to spherical coordinates and for each measurement interval the resultant solar parameters are calculated.

7. CONCLUSIONS

Thermal comfort assessment in the automotive environment is considered to be difficult due to the transient and inhomogeneous environment. This paper has introduced a novel thermal comfort acquisition interface which has been used to create a database, which contains mappings of environmental parameters and corresponding HVAC control output. The thermal comfort acquisition system takes into account various environmental parameters, vehicle information, as well as data from a three-dimensional solar sensor. Thermal comfort evaluation for driver and front passenger, as well as draught level evaluation, can be done via two separate four-way joysticks. Dependent of the application, thermal comfort can alternatively be estimated with knowledge of the user's interaction with the HVAC ECU. Data acquisition has been conducted in moderate to hot environments during spring, autumn and summer conditions in Southern Africa, over a total distance of 20.000 km.

8. REFERENCES

[1] Thermal Environmental Conditions for Human Occupancy, ASHRAE Standard 55-2004, 2004

[2] Fanger, P. O., *Thermal comfort analysis and applications in environmental engineering.* New York: McGraw-Hill, 1972, 1970.

[3] R. Becker and M. Paciuk, "Thermal comfort in residential buildings - Failure to predict by Standard model," *Building and Environment*, vol. 44, no. 5, pp. 948–960.

[4] Devonshire and M, J., *The effects of infrared-reflective and antireflective glazing on thermal comfort and visual performance: a literature review: Deep Blue at the University of Michigan:* University of Michigan, Ann Arbor, Transportation Research Institute, 2007. http://deepblue.lib.umich.edu/handle/2027.42/49457 (accessed February 22, 2011).

[5] Markov D. "Practical Evaluation of Thermal Comfort Parameters". In: *Annual International Course: Ventilation and Indoor climate*, P. Stankov (ed.), Sofia, 2002:158-70.

[6] Deutsches Insitut für Normung e.V. DIN EN ISO 7730:2005. Ergonomie der thermischen Umgebung-Analytische Bestimmung und Interpretation der thermischen Behaglichkeit durch Berechnung des PMV- und des PPD-Indexes und Kriterien der lokalen thermischen Behaglichkeit. Berlin, Beuth Verlag GmbH, 2006.

[7] Zhang, H., Arens, E., Huizenga, C., and Han, T., "Thermal sensation and comfort models for non-uniform and transient environments, part III: Whole-body sensation and comfort," *Building and Environment*, vol. 45, no. 2, pp. 399–410, 2010.

[8] Gielda TP, Hosni MH. Transient Thermal Comfort Predictions for Automotive Environments. Available from: http://www.grrt.fr/html/travaux/download.php?filename=00gieldahosni.pdf (accessed February 19, 2010).

[9] Dear, R. de, "Thermal comfort in practice," *Indoor Air*, vol. 14, no. s7, pp. 32–39, 2004.

[10] Cisternino M. Thermal climate in cabs and measurement problems, Paper for the CABCLI seminar - EC Cost Contract No SMT4-CT98-6537 (DG12 BRPR), 1999, Dissemination of results from EQUIV - EC Cost Contract No SMT4-CT95-2017.

[11] Han, T. and Huang, L., *A Sensitivity Study of Occupant Thermal Comfort in a Cabin Using Virtual Thermal Comfort Engineering.* Warrendale, PA: SAE International, 2005.

[12] Silva, M. C. G. d., "Measurements of comfort in vehicles," *Meas. Sci. Technol*, vol. 13, no. 6, pp. R41, 2002.

[13] Ormuz K, Muftic O. "Main Ambient Factors Influencing Passenger Vehicle Comfort". In: *Proceedings of the 2nd International Ergonomics Conference 2004*, Oct 21 – 22, Zagreb Croatia, pp. 77-82.

[14] Aroussi A, Aghil S. "Characterization of the Flow Field in a Passenger Car Model. Optical" *Diagnostics in Engineering 2000*; vol 4, no 1, pp.1-15.

[15] Deutsches Institut fuer Normung e.V., DIN14505, Ergonmomie der thermischen Umgebung – Beurteilung der thermischen Umgebung in Fahrzeugen. Berlin, Beuth Verlag GmbH, 2007.

[16] Deutsches Insitut für Normung e.V. DIN EN ISO 7726:2001. Umgebungsklima-Instrumente zur Messung physikalischer Grössen. Berlin, Beuth Verlag GmbH, 2002.

[17] Olesen BW. Evaluation of the thermal environment in vehicles. Application note, Bruel & Kjaer, Denmark, 1988.

[18] Sedlbauer, K., "Raumklima und Innovation. Eine Aufgabe der Bauphysik," *Wksb. Zeitschrift für Wärmeschutz, Kälteschutz, Schallschutz, Brandschutz*, vol. 51, no. Nr.57, pp. 9–16, 2006.

[19] Deutsches Insitut für Normung e.V. DIN EN ISO 8996:2004. Ergonomie der thermischen Umgebung-Bestimmung des körpereigenen Energieumsatzes. Berlin, Beuth Verlag GmbH, 2005.

[20] Deutsches Insitut für Normung e.V. DIN EN ISO 9920:2009. Abschätzung der Wärmeisolation und des Verdunstungswiderstandes einer Bekleidungskombination. Berlin, Beuth Verlag GmbH, 2009.

[21] Walgama, C., Fackrell, S., Karimi, M., Fartaj, A., and Rankin, G. W., "Passenger Thermal Comfort in Vehicles - A Review," *Proceedings of the Institution of Mechanical Engineers, Part D: Journal of Automobile Engineering*, vol. 220, no. 5, pp. 543–562, 2006.

[22] J Kranz, "Intelligent thermal comfort control", PhD thesis, Nelson Mandela Metropolitan University, 2011.

[23] Chien, C.-H., Jang, J.-Y., Chen, Y.-H., and Wu, S.-C., "3-D numerical and experimental analysis for airflow within a passenger compartment," *Int.J Automot. Technol*, vol. 9, no. 4, pp. 437–445, 2008.

[24] Zhang, H., Dai, L., Xu, G., Li, Y., Chen, W., and Tao, W.-Q., "Studies of air-flow and temperature fields inside a passenger compartment for improving thermal comfort and saving energy. Part I: Test/numerical model and validation," *Applied Thermal Engineering*, vol. 29, no. 10, pp. 2022–2027, 2009.

Automotive Thermal Comfort Control – A Blackbox Approach
Part II: Data Mining and System Learning

J. Kranz*, TI. van Niekerk*, HFG. Holdack-Janssen*, G. Gruhler**

** VWSA-DAAD Chair in Automotive Engineering, Nelson Mandela Metropolitan University, PO 77000 Port Elizabeth 6031, South Africa E-mail: Juergen.Kranz@nmmu.ac.za, Theo.vanNiekerk@nmmu.ac.za, Hinrich.Holdack-Janssen@nmmu.ac.za*
*** Department of Mechatronics, Reutlingen University, Alteburgstrasse 150, 72762 Reutlingen, Germany E-mail: Gerhard.Gruhler@Reutlingen-University.de*

Abstract: Thermal comfort is a very vague and a very subjective term, which depends on physiological and psychological variables. Thermal comfort in transient environments, like an automotive cabin, is far from understood and general accepted theories do not exist. A two part series will investigate the concept of using a blackbox approach for directly associating thermal comfort to field measurements. Part I introduces a novel thermal comfort acquisition system, which allows for electronic thermal comfort acquisition as well as determination of HVAC parameter set-up. Part II immediately follows Part I and deals with the data mining and modelling process. Artificial intelligence is used to predict blower level, air blend position and in-cabin temperature. The results are promising and it is concluded that methods of artificial intelligence can be used as a powerful tool during the development process of vehicle HVAC ECUs and have great potential for time and cost reduction.

Keywords: Automotive Thermal Comfort, Neural Networks

1. INTRODUCTION

This two-part publication investigates the potential of directly learning a technical system from field thermal comfort measurements. A comprehensive database containing environmental information and thermal comfort correlations has been collected through measurements in a real vehicle for moderate to hot environments in Southern Africa, over a total distance of 20.000km. The experimental setup has been described in the first part of this publication. Part II deals with methods of data mining and the modelling process. Data mining is used to discover functional relationships within the database, to remove inconsistencies and to reduce the dimensionality of the input domain. Methods of artificial intelligence are used to implement a learning machine, capable of autonomously learning input-output mappings. The structure is shown in Figure 1 again.

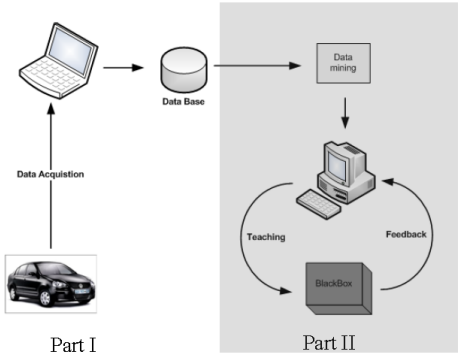

Figure 1: Concept

2. THERMAL COMFORT MODELS

Thermal comfort modeling basically started in the 1960s mainly for the use in military and aerospace application. As a consequence, oodles of thermal comfort models have been developed and published in the past decades and an overview is extremely in transparent. The most valuable and best understood thermal comfort model has been developed by P.O. Fanger in 1970 and is called Predicted Mean Vote (PMV). This model is based on the promise that thermal comfort is present at body thermal equilibrium and assumes skin temperatures being in narrow limits [1]. The PMV model is eligible for uniform and steady state environments and is still the state of art of current thermal comfort standards. However, due to the transient and inhomogeneous conditions in a vehicle compartment, its use in automotive applications is not recommended [2]. Automotive industry predominantly uses thermal comfort models in the development process of automotive HVAC units in order to reduce costs arising from vehicle test involving subjects. An up to date overview of thermal comfort models in automotive environment is given in [3], [4]. Generally thermal comfort models aim to simulate human's internal physiological and psychological response. This is an error prone process since human's internal system behavior is not fully understood yet. The authors propose a different approach and assume that thermal comfort is dependent of some measurable environmental variables and is linked to thermal comfort through an unknown function in some statistical sense. In other words, the issue can also be addressed as an approximation problem in a multidimensional feature space. Artificial intelligence is

predominantly used in fields of research, where it is difficult to obtain exact mathematical knowledge about a process or when knowledge is even unavailable. Many approaches using methods of artificial intelligence have been proposed in literature with respect to thermal comfort. On the one hand this may be justified with the fuzzy definition of thermal comfort and on the other hand due to the enormous difficulties in measuring and assessing thermal comfort. A lot of effort has been done in approximating Fanger's PMV model using fuzzy logic and neural networks e.g. in [5]-[9]. However, little research is so far available about learning an intelligent structure with direct mappings of environmental field data and HVAC parameter outputs.

3. DATA MINING

Data mining has emerged during the 1980s and is considered as an ensemble of tools and methods for knowledge extraction from large amounts of data. Data mining is a multidisciplinary field including database technology, artificial intelligence, machine learning, statistics, pattern recognition, knowledge-based systems, knowledge acquisition, information retrieval, high-performance computing and data visualization [10]. Measurement equipment has been installed at characteristic locations within the vehicle cabin. Data from test drives have been conducted over a distance of 20.000km in Southern Africa during spring, summer and autumn at moderate to hot environmental conditions. The experimental setup has been described in Part I.

2.1 Data pre-processing

Real world data tend to be incomplete, noisy and inconsistent. In this paper, data cleaning refers to smoothing out of noise, removal of disturbances and inconsistencies. The authors' research only considers steady state and short transient conditions. Transient measurement vectors have been deleted upfront. Latter ones may occur during the initial heating up or cooling down phase of a vehicle. Human beings are fuzzy in their decision space. When measuring human response for a given thermal environment, inconsistencies may occur. However, from a technical point of view, a unique mapping of input and output vector is essential for a successful learning strategy. Given two sets X and Y, this requirement can be written with equation (1):

$$R \subseteq X \times Y, \quad \forall x \in X, \quad \forall y_1, y_2 \in Y, \\ (x, y_1) \in R \ \wedge (x, y_2) \in R \ \Rightarrow \ y_1 = y_2. \tag{1}$$

Determination of solar parameters implies sensor exposure to direct sun light. The authors discovered that in terms of measurement of solar angles, diffuse radiation cannot be handled by the available solar sensor. Research has however shown that the sun intensity I can be used as a first approximation to distinguish between reliable and erroneous solar angular information. However, this correlation might not be complete, because there may also be diffuse radiation with high radiation levels. According to the authors' investigations, sun radiation level I < 300 W/m^2 seemed to be appropriate as lower boundary and has only little influence on human's thermal comfort sensation. In these cases, knowledge of the exact sun position is not necessary, which however results in missing values for the solar angles. Similar situations might occur when re-transformation from Spherical to Cartesian coordinates is undefined. This is especially true when the sun is in zenith relative to the vehicle. There are various methods available to handle missing data [10]. In terms of this research, it seems to be straightforward to output an error constant when solar angles can't be measured or converted. Rounding and summarizing equivalent samples can be considered as a technique for data reduction. A high resolution of sensory information is not needed for thermal comfort research. The variable's accuracy was therefore reduced to:

- Temperatures: $\Delta\vartheta = \pm 0.5°C$,
- Vehicle speed: $\Delta v = \pm$ 10km/h,
- Sun Intensity: $\Delta I = \pm$ 100W/m2,
- Solar Angles: $\Delta\Psi$, $\Delta\varphi = \pm 10°$,
- Humidity: $\Delta h = \pm 5\%$ RH,
- Variances: $\Delta\sigma_i = \pm$ 10%.

2.2 Feature selection

Pareto's principles states that only 20% of the data accounts for 80% of the information. An appropriate method for feature selection and for discovering functional relationships is correlation analysis. With large data sets the number of available data pairs increases dramatically, which makes an overview extremely in-transparent. Especially for large data sets, it is therefore often desirable to have a method that transforms variables into a new feature space, in order to facilitate visualization of their properties. Such a methodology is principle component analysis (PCA). PCA is a statistical technique of multivariate data analysis, which is often used for data visualization and dimensionality reduction. It is also known as Karhunen-Loève transform or Hotelling transform [11], [12]. PCA is based on the assumption that salient information in a given feature space lies in those features which have the largest variance. PCA aims to linearly transform the original data matrix $\mathbf{X}$ into a new data matrix $\mathbf{Y}$. Given a matrix $\mathbf{X}$ with $\mathbf{X} \in \mathbb{R}^{m \times n}$, this rotational operation can be defined as

$$\boldsymbol{Y} = \boldsymbol{PX}, \tag{2}$$

where $\mathbf{P}$ is an orthonormal matrix, which maximizes the variance of $\mathbf{Y}$ and minimizes its co-variance. PCA has been applied to the data set using the software packages Mathworks Matlab® and CAMO Unscrambler®. Table 1 shows the explained percentage of variance for each principle component (PC).

Table 1: Explained variances

Principle component	Explained variance [%]
PC1	33.9
PC2	49.9
PC3	59.3
PC4	65.6
PC5	71.4
PC6	77.2
PC7	82.2
PC8	86.7
PC9	90.4
PC10	93.4
PC11	95.5
PC12	97.2
PC13	98.2
PC14	98.9
PC15	99.5
PC16	99.9
PC17	100.0

It is apparent, that the data set contains high redundancy. The first ten PCs already account for 93.4% of the data set's total variance. PC11 to PC17 only explain 6.6% of the remaining variance and can be therefore considered as noise. Figure 2 shows the corresponding Scree plot.

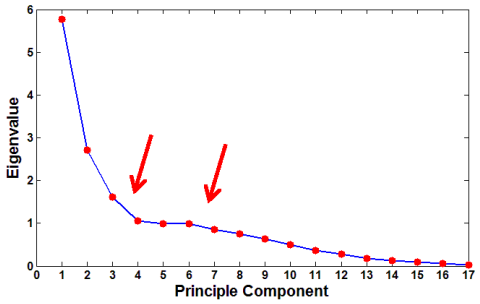

Figure 2: Scree plot

There is one distinctive „elbow" between PC3 and PC4. A second „elbow", with a less gradient occurs between PC6 and PC7. The scree criterion would therefore suggest keeping three or four factors [13]. The eigenvalues for PC4 and PC5 are 1.063 and 0.988 respectively. According to the Kaiser-Guttman criterion, only PC1 to PC4 would be relevant. Table 1 shows that the first three components account for about 59.3% of the dataset's variance. If PC4 is added, 65.6% variance can be explained. Considering the second „elbow" in Figure 2, six components should be retained, accounting for a total explained variance of 77.2%. This interpretation is fairly confirmed by Cattel's straight line approximation. The authors therefore recommend considering six PCs for further processing.

Table 2 shows the PCA variable loadings of the first six PCs.

Table 2: PCA correlation loadings for all variables

	Principle component					
	PC1	PC2	PC3	PC4	PC5	PC6
ϑ_F	-0.85	0.26	0.07	0.22	0.03	0.10
v	0.49	-0.16	-0.62	0.13	0.05	0.09
h	0.38	0.12	0.28	0.64	-0.32	0.01
ϑ_A	-0.85	0.27	0.08	0.22	0.02	0.11
ϑ_1	0.84	0.20	0.02	0.11	-0.09	0.05
ϑ_2	-0.30	0.52	-0.18	0.29	-0.03	0.35
ϑ_4	-0.70	0.51	-0.07	0.19	-0.02	-0.12
ϑ_5	-0.86	0.38	-0.02	-0.05	0.05	-0.02
ϑ_7	-0.39	0.50	-0.46	-0.17	0.03	-0.42
I	-0.75	-0.41	-0.20	-0.06	-0.10	-0.09
φ	-0.44	-0.74	0.15	0.10	0.03	0.34
ψ	-0.12	0.39	0.04	-0.47	0.14	0.62
T	-0.22	0.07	0.66	-0.12	-0.11	0.04
σ_I	0.15	-0.09	0.12	0.31	0.90	-0.06
σ_E	0.74	0.58	0.07	-0.01	0.04	0.02
σ_A	0.60	0.60	0.15	-0.09	0.04	0.04
σ_V	-0.14	0.08	0.59	-0.17	0.09	-0.37

The meaning of the variables is given in Table 3.

Table 3: Variable meanings

Symbol	Meaning
ϑ_F	Filtered ambient temperature
v	Vehicle speed
h	Relative humidity
ϑ_A	Ambient temperature
ϑ_1	Air outlet temperature
ϑ_2	In-cabin air temperature
ϑ_4	Driver head temperature
ϑ_5	Cabin roof temperature
ϑ_7	Dashboard temperature
I	Sun intensity
φ	Sun azimuth angle
ψ	Sun elevation angle
T	Empirical traffic function
σ_I	Standard deviation of sun intensity
σ_E	Standard deviation of sun elevation angle
σ_A	Standard deviation of sun azimuth angle
σ_V	Standard deviation of vehicle speed

The correlation loadings for ϑ_F and ϑ_A on PC1 to PC6 suggest that these variables are very similar. The correlation-loadings also suggest that variables σ_E, and σ_A are highly negatively correlated to I and ψ. Correlation loadings for variables σ_E, σ_A and I are in opposite direction with exception of PC4. However, the influence of PC4 is not significant, since it only contributes 0.3% towards I, 0.01% towards σ_E and 0.77% towards σ_A. A score plot shows that samples with higher than average values for σ_E and σ_A and lower than average values for I are linearly separable from the rest of the data cloud. The researchers assume that these samples contain diffuse solar radiation levels. These variables contain redundant information and variables σ_A and σ_E can be removed from the data set. Table 4 shows the correlation loadings for a PCA recalculated without the influence of variables ϑ_F, σ_A and σ_E. It is apparent that the variables ϑ_A, ϑ_4 and ϑ_5 share similar variance with PC1 (72.2%, 62.1%, 86.7%) but only moderately differ on PC2 (0.0%, 14%, 2.6%). The researchers assume that they are similar in effect. However, the correlation loadings only indicate some rough similarity but no clear redundancy.

Table 4: PCA correlation loadings removed from ϑ_F, σ_A, σ_V

	Principle component					
	PC1	**PC2**	**PC3**	**PC4**	**PC5**	**PC6**
v	0.54	-0.15	-0.58	0.06	0.05	-0.11
h	0.39	-0.20	0.39	0.40	-0.40	-0.31
ϑ_A	-0.85	-0.01	0.05	0.15	-0.04	-0.16
ϑ_1	0.78	-0.40	0.18	0.00	-0.04	-0.10
ϑ_2	-0.39	-0.52	-0.02	0.13	0.02	-0.52
ϑ_4	-0.79	-0.37	0.04	0.23	-0.08	-0.02
ϑ_5	-0.93	-0.16	0.01	0.03	0.04	0.01
ϑ_7	-0.50	-0.58	-0.28	0.06	0.01	0.39
I	-0.66	0.46	-0.33	0.04	-0.13	0.02
φ	-0.27	0.80	-0.08	0.03	0.04	-0.39
ψ	-0.21	-0.33	0.13	-0.63	0.44	-0.33
T	-0.25	0.15	0.65	-0.12	-0.04	-0.05
σ_I	0.17	0.09	0.10	0.58	0.77	0.00
σ_v	-0.17	0.09	0.61	0.01	0.09	0.39

In Figure 3, the variables ϑ_A, ϑ_4 and ϑ_5 are plotted in dependence of all samples. It is obvious, that ϑ_4 and ϑ_5 fairly share the same tendency and follow the course of ϑ_A.

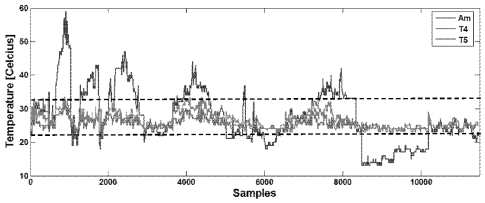

Figure 3:

ϑ_4 and ϑ_5 specify the temperature at head and roof level. The head area is especially sensitive to climatic extremities. The clear influence of ϑ_A towards ϑ_4 and ϑ_5 is an amazing insight, which suggests that thermal comfort perception inside the vehicle cabin is considerably influenced by the ambient temperature, even if the cabin interior is air-conditioned and decoupled from the exterior environment. In this context, it shall be mentioned, that temperature sensors ϑ_4 and ϑ_5 have not been shielded against radiation. The research vehicle's black colour might have intensified radiation effect. However, it is apparent, that this dependency is not linear. Figure 3 suggests that there seems to be a saturation effect in ϑ_4 and ϑ_5 towards lower and higher values of ϑ_A. This is indicated by the dashed lines. These non-linear saturation effects may limit the expressiveness of the bivariate correlation coefficient and the PCA results and might also be the reason why ϑ_A, ϑ_4 and ϑ_5 share most of their common variance on PC1, but distinguish on PC2. For this research, linear correlation is not a necessary requirement. Methods of artificial intelligence are capable of theoretically realizing any non-linear mapping. Therefore, ϑ_4 and ϑ_5 can be considered to be redundant to ϑ_A and can be removed from the dataset. Most of the data acquisition was done on sunny days with low values for σ_I. The available database does not contain the necessary number of samples allowing for statistical expressiveness of σ_I. The variable σ_I is therefore not covered by the further course of investigations and further data acquisition, especially on cloudy days, is considered as advantageous. Table 4 reveals that 76.7% of ϑ_1's variance is explained by PC1 and PC2. The authors assume that ϑ_1 might be highly negatively correlated to ϑ_A. However, ϑ_A is not correlated to PC2, while PC2 adds additional 16% variance towards ϑ_1. Figure 4 shows a scatter plot of ϑ_A and ϑ_1. For ϑ_A<+36°C, ϑ_A and ϑ_1 are fairly negatively linearly correlated. This is indicated by the red line on the left-hand side of the plot. For ϑ_A>+36°C, ϑ_1 seems to be fairly positively linearly correlated to ambient temperatures

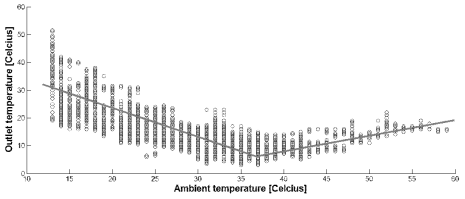

Figure 4:

An explanation of this effect might be that for increasing ambient temperatures the required cooling load must increase, in order to maintain in-cabin comfort levels. This means, that the air outlet temperature must decrease. At a certain point, when the available cooling power is exhausted, or the maximum setup point of the HVAC unit has been reached, a further increase in ambient temperature forces the outlet temperature to rise as well. With a reasonable degree of accuracy, ϑ_1 can therefore be removed from the dataset, because its information can be described with variable ϑ_A. Table 5 shows the correlation loadings of the data set removed by the influence of variables σ_I, ϑ_1, ϑ_4 and ϑ_5.

Table 5: PCA correlation loadings removed from σ_I, ϑ_1, ϑ_4 and ϑ_5

	Principle components					
	PC1	**PC2**	**PC3**	**PC4**	**PC5**	**PC6**
v	-0.63	0.16	-0.49	0.10	0.01	-0.13
h	-0.40	-0.03	0.45	0.23	0.62	-0.05
ϑ_A	0.79	0.16	-0.01	0.10	0.24	-0.03
ϑ_2	0.35	0.57	0.01	0.42	0.34	-0.22
ϑ_7	0.34	0.73	-0.17	-0.43	0.08	0.14
I	0.71	-0.23	-0.49	-0.13	0.13	0.01
ψ	0.43	-0.71	-0.32	0.33	0.02	-0.14
φ	0.23	0.42	0.20	0.50	-0.60	-0.09
T	0.38	-0.20	0.58	0.06	-0.02	0.52
σ_v	0.28	-0.15	0.56	-0.40	-0.10	-0.60

Vehicle speed is largely explained by PC1 (39.1%) and PC3 (24.4%). The remaining loadings are insignificant. The first three components explain 41.59% of σ_v's and 51.9% of T's total variance. It is apparent, that on the first three factors, v is in opposite direction of σ_v and T. For a first approximation, the author therefore suggests omitting the variables T and σ_v from the dataset, since a large proportion of their common variance is negatively correlated. There is a logical explanation for these findings. When the vehicle speed is high, the vehicle is most probably driving on a highway. Changes in vehicle speed and variations of gas and brake pedal activity

probably occur less frequent. At low vehicle speed, the vehicle is most likely driving under urban traffic conditions. Therefore changes in speed, due to acceleration and deceleration, may occur more frequently. Differences on higher factors can be explained with the memory effect of variable T.

4. MODELLING

The environmental climate inside the vehicle cabin is mainly controlled by the blower level, flap positions and the temperature setup. The available data base for this research has been collected from test drives. Assumptions of linear parametric dependency and any predefined underlying probability distribution, can therefore not be guaranteed. The authors have identified non-linear and non-parametric models as suitable implementation. Due to a lack of knowledge about the process itself, a blackbox approach has been chosen and an exemplary implementation using like artificial neural networks (ANN) is shown.

3.1 Artificial neural networks

Artificial neural networks consist of many single processing units which are typically arranged in layers. These processing units are called neurons. The schematic of a neuron is shown in Figure 5.

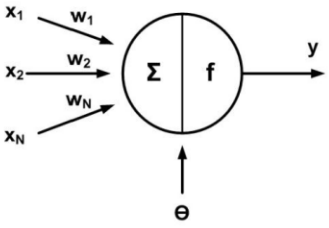

Figure 5: Neural processing unit

Each neuron is capable of processing an input vector $\mathbf{x} \in \mathbb{R}^N$ and outputs a scalar y. The weight vector $\mathbf{w} \in \mathbb{R}^N$ shall thereby imitate biological synapses in NNs, which determine the influence of each x_i on the neuron's output y. The weighted summation of the input vector **x** is called 'net' and can be mathematically expressed as

$$net = \mathbf{w}^T\boldsymbol{x} + \Theta = \sum_{i=1}^{N} w_i x_i + \Theta\,. \tag{3}$$

The input signal Θ is a constant, which is often referred to as bias term. Sometimes it is not mentioned explicitly and is incorporated into the input vector **x**. The scalar output signal y can then be expressed as

$$y = f(net) = f\left(\sum_{i=1}^{N} w_i x_i + \Theta\right). \tag{4}$$

The function *f(·)* is called activation or transfer function. The activation function can be theoretically any linear or non-linear function. However, in practice often non-linear sigmoid or logistic functions are used due to their mathematical properties like monotonicity, continuity and differentiability. Latter property is required for effective learning algorithms. A sigmoid transfer function, which is also used in this research, is given in equation (5).

$$f(x) = \frac{1}{1 + e^{-x}} \tag{5}$$

3.2 Network design

When designing a neural network, the engineer has to identify a suitable network structure. Today the amount of possible ANNs is enormous, including highly specific network structures. Today, there are about 50 types of networks available [14]. However, modelling will be limited to FNNs, since they are common for pattern analysis problems. The three most important design parameters are sample size, number of hidden layers and number of hidden layer neurons. The generalization capability of a neural network predominantly depends on three properties [15]:

- Size of the training set and its expressiveness,
- The architecture of the neural network,
- The complexity of the approximation problem.

The last factor is hardly controllable, since when considering an implementation using ANN, the researcher has generally only little knowledge about the process' underlying complexity. The first and the second factor are dependent of each other. However, assuming that the researcher has chosen a suitable neural network structure and an expressive training data set for the problem at hand, [15] suggests equation (6) for determination of the required number of training samples N_s.

$$N_s = O\left(\frac{N_v}{\varepsilon}\right) \tag{6}$$

With:

N_v:	Total number of free parameters within the network,
ε:	Fraction of classification errors permitted on test data,
$\mathbf{O}(\cdot)$:	Order of quantity enclosed in.

The free parameters in a FNN are the number of weights and bias terms. A FNN with an arbitrary large number of non-linear hidden layer neurons can approximate any continuous function [14], [15]. In literature, there is however disagreement if one or two hidden layers should be used in terms of optimal generalization performance. Generalization therefore refers to the network's performance with respect to previously unseen data. There seems to be however consensus that more than two hidden layers are not required. There is currently no sound theory which approach performs better. In terms of this research the authors follow the concept of [14], who first recommends trying a network with one hidden layer, before implementing an ANN with two hidden layers.
Blower level prediction can be described as $\mathbb{R}^8 \rightarrow \mathbb{R}^4$ mapping. The number of input nodes is therefore

determined to be eight and the number of output neurons is defined as four. Flap position prediction can be described as $\mathbb{R}^8 \rightarrow \mathbb{R}^3$ mapping, meaning eight input layer nodes but only three output layer neurons. Since only little a-priori knowledge about blower level and flap position prediction is available, the number of hidden layer neurons must be chosen according to the complexity of the underlying functionality. For training the ANNs, about 3000 consistent data samples have been available. According to equation (6), this allows for training of networks with a total sum of Nv=300 free parameters with an error probability ε=0.1. The recommended upper bound of hidden layer neurons is thereby determined to be 23 for blower level prediction and 25 for flap position prediction. To determine the number of hidden layer neurons for blower level and flap position prediction, networks with different numbers of hidden layer neurons have been trained and their performance has been compared. When training a FNN, the weights within the network are randomly initialized. However, improper initialization of weights may result in infinite training times or stopping at a local minima of performance.

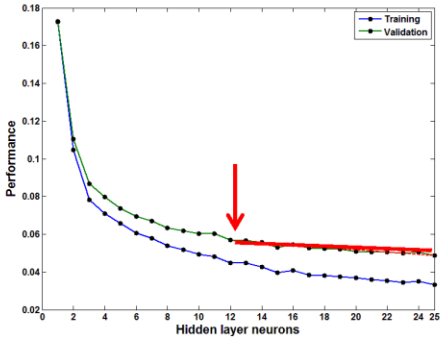

Figure 6: Blower networks performance

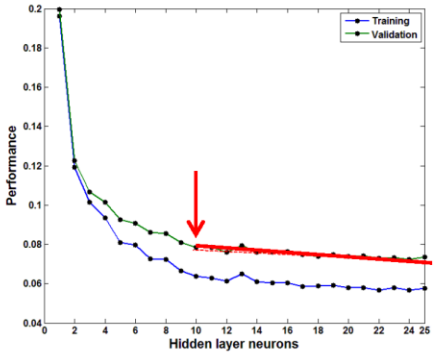

Figure 7: Flap networks performance

Therefore 200 networks have been trained for each hidden layer configuration. The best 150 results for training and validation performance have been taken into account and have been plotted as average in Figure 6 for blower level prediction and in Figure 7 for flap position prediction. This procedure prevents that poor weights initialization affect the performance plots and additionally provides statistical confidence concerning the results. It is apparent that the networks' performances initially increases and levels off towards higher numbers of hidden layer neurons. There are no apparent local minima. However, it is also apparent that mean square error only slowly decreases towards high numbers of hidden layer neurons. Literature suggests to select as few as hidden layer neurons as possible, in order to minimize the number of free parameters within the network, meaning a trade-off between precision and cost [16]. In Figure 6 it is apparent that hidden layer neurons 12 to 25 form a more or less straight line, indicating only little further improvements in prediction performance. In Figure 7, this straight line can be found for hidden layer neurons 10 to 25. The researcher therefore suggests implementing 12 hidden layer neurons for blower level prediction and 10 hidden layer neurons for flap position prediction. With these findings, the neural network structures have been determined as shown in Figure 8 and Figure 9.

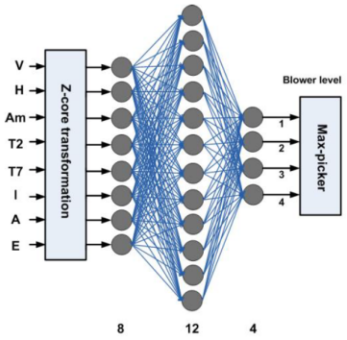

Figure 8: Blower level network structure

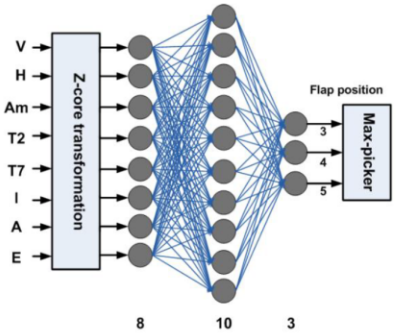

Figure 9: Flap position network structure

The input variables to both networks have been z-core transformed using equation in order to minimize the bias

of one feature over another. A max-picker functionality has been implemented for unique classification results. The total number of free parameters can be determined as N_v=169 for the blower level prediction network in (a) and as N_v=128 for the flap position prediction network in (b). According to equation (6), this means that the networks can be efficiently trained with about N_s=1700 for blower level and with about N_s=1300 (good) samples for flap position prediction.

3.3 Training

The neural networks have been trained using the Conjugate gradient descent algorithm for training. The data set has been divided into 65% training data, 15% validation data and 20% testing data. Training data was used for system learning and validation data was used as cross validation for preventing the network from over-fitting. The networks have been finally tested with the randomized and previously unseen test data. The testing results for blower level prediction are shown in Table 6.

Table 6: Confusion matrix for blower level prediction

Test data	Blower level				Identified
	L1	L2	L3	L4	[%]
L1	139	9	11	0	87.4
L2	14	119	15	0	80.4
L3	2	15	101	4	82.8
L4	7	1	2	139	93.3
Correctly classified [%]	85.5	82.6	78.3	97.2	86.2

It is apparent that a total of 86.2% of the test cases were correctly classified. The results for validation and training data are given in [17] and show similar performance. It is apparent that blower level „1" and blower level „4" have been best classified, suggesting that extreme conditions are well separable. Blower level „1" could be correctly predicted in 85.5%, blower level „2" in 82.6%, blower level „3" in 78.3% and blower level „4" in 97.2% of all cases. The classification performance between blower level „2" and blower level „3" seems not to be that clear. It is apparent that most cases of misclassification occur in neighboring classes. Table 6 therefore suggests that the operator had more difficulties to uniquely distinguish between blower level „2" and blower level „3" than between extreme situations. There seems to be an estimated 20% overlap between blower level „2" and blower level „3". This tendency is present in the training, validation and testing plots. There are various possible explanations for these phenomena. One could conclude that humans are fuzzy in evaluation of their thermal environment. This evaluation might also be time and location-variant to some extent. Another possible explanation might be the use of a manual HVAC system, which only allows for setting up a discrete output space. Problems may especially occur when the environmental situations demand an output value in between two discrete output classes. This could result in an increased range of decision fuzziness. The verification results with previously unseen data for flap position prediction are shown in Table 7.

Table 7: Confusion matrix for flap position prediction

Test data	Flap position			Identified
	P1	P2	P3	[%]
P1	172	20	1	89.1
P2	25	154	14	79.8
P3	3	12	177	92.2
Correctly classified [%]	86.0	82.8	92.2	87.0

It is apparent that in 87% the network is able to produce the correct output. Similar to blower level prediction, the extreme values „breast" (P1) and „head" (P3) have been predicted best with 86 % and 92.2% correct classifications. Flap position „breast-head" (P2) has been correctly classified for 82.8% of all cases. This suggests an overlap between flap positions „breast" and „breast head" as well as for flap positions „breast-head" and head. Possible explanations for these phenomena follow exactly the argumentation of blower prediction network.

3.5 Temperature reference modelling

The data mining process revealed that temperature knob setting is fairly segmental linear dependent on ambient temperature ϑ_A. This is shown in Figure 10. The authors suggest to model temperature reference value T_k with two straight lines, which have been added in Figure 10.

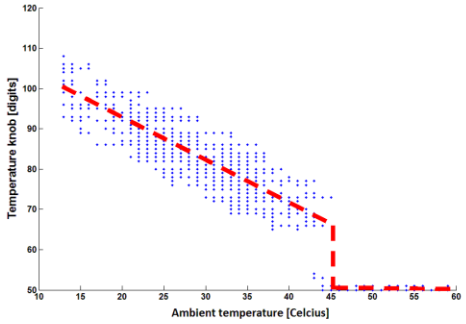

Figure 10: Temperature knob

A best fit straight line $y = ax_i + b$ was therefore determined, so that for each (x_i,y_i)

$$\sum_{i=1}^{N}(y_i - ax_i + b)^2 \rightarrow min, \quad \textbf{(7)}$$

is fulfilled. The coefficients have been calculated as

- a=-1.061,
- b=113.

The result is summarized in equation (8).

$$T_k = \begin{cases} -1.061\frac{Am}{°C} + 113 & for \quad Am \leq +43°C \\ +50 & for \quad Am > +43°C \end{cases} \quad \textbf{(8)}$$

5. CONCLUSIONS

Methods of data mining have been used for data integration, data cleaning, dimensionality reduction, data transformation and have been implemented in Matlab. Principles of multivariate statistics have been applied to discover variable interrelationships and correlations, in order to reduce the dimensionality of the feature space. Special importance has been attached to PCA, a dimensionality reduction and visualization technique, which successively explains maximal variance. The dimension of the input space was reduced from $\mathbb{R}^{17}$ to $\mathbb{R}^{8}$. The necessary variables have been identified as vehicle speed, relative humidity, ambient temperature, in-cabin temperature, dashboard temperature, sun intensity, sun elevation angle and sun azimuth angle. ANNs have been applied to thermal comfort research in order to predict blower level as well as the heater box's air distribution flap position. Research has been conducted to determine the optimal structure of the ANNs. An 8-12-4 FNN was found for blower level prediction and an 8-10-3 FNN for flap position prediction. The networks have both been trained with about 3000 samples, however it was shown that 1700 and 1300 expressive samples should be sufficient to train the blower and the flap network respectively. The term expressive cannot be specified with formal means. In practice, this means that samples have to be collected, which include representative information about the environment. In terms of thermal comfort this means that samples must cover a representative variety of environmental conditions, including moderate as well extreme conditions. The resulting overall testing classification performance is about 87% for blower and flap prediction. Extreme values for blower level and flap position were predicted best. It was shown that data classes overlap to some extend which might be a result of human fuzziness in thermal comfort evaluation. However it might be also a consequence of the manual HVAC unit, which has been used for this research project. The ANNs performance has been verified against independent data, which have been randomly chosen from the data set and which have not been used for system training. It has been shown that it is possible to extract thermal comfort knowledge directly from measurement data. Prior modeling of human's thermo-regularity system and human's response is not necessary. It has therefore also been shown, that it is possible to adapt a technical system to the thermal comfort preferences of an individual. Temperature knob prediction was found to be primarily dependent on ambient temperature and can be fairly approximated by a stepwise linear function.

6. REFERENCES

[1] Fanger, P. O., *Thermal comfort analysis and applications in environmental engineering.* New York: McGraw-Hill, 1972, 1970.

[2] Deutsches Institut fuer Normung e.V., DIN14505, Ergonmomie der thermischen Umgebung – Beurteilung der thermischen Umgebung in Fahrzeugen. Berlin, Beuth Verlag GmbH, 2007.

[3] Walgama, C., Fackrell, S., Karimi, M., Fartaj, A., and Rankin, G. W., "Passenger Thermal Comfort in Vehicles - A Review," *Proceedings of the Institution of Mechanical Engineers, Part D: Journal of Automobile Engineering*, vol. 220, no. 5, pp. 543–562, 2006.

[4] Alahmer, A., Mayyas, A., Mayyas, A. A., Omar, M., and Shan, D., "Vehicular thermal comfort models; a comprehensive review," *Applied Thermal Engineering*, vol. 31, no. 6-7, pp. 995–1002, 2011.

[5] Farzaneh, Y. and Tootoonchi, A., "Controlling automobile thermal comfort using optimized fuzzy controller," *Applied Thermal Engineering*, vol. 28, no. 14-15, pp. 1906–1917, 2008.

[6] Calvino, F., "The control of indoor thermal comfort conditions: introducing a fuzzy adaptive controller," *Energy and Buildings*, vol. 36, no. 2, pp. 97–102, 2004.

[7] Hamdi, M., "A new predictive thermal sensation index of human response," *Energy and Buildings*, vol. 29, no. 2, pp. 167–178, 1999.

[8] Zhi-Hua Zhou and Ying Xia, *The application of artificial neural network in HVAC system:* IEEE, 2005.

[9] Liang, J. and Du, R., "Design of intelligent comfort control system with human learning and minimum power control strategies," *Energy Conversion and Management*, vol. 49, no. 4, pp. 517–528, 2008.

[10] Kamber, M. and Pei, J., *Data Mining: Concepts and Techniques, Second Edition (The Morgan Kaufmann Series in Data Management Systems),* 2nd ed. Morgan Kaufmann, 2006.

[11] Bortz, J., *Statistik: für Human- und Sozialwissenschaftler (Springer-Lehrbuch) (German Edition),* 6th ed. Springer, 2005.

[12] Izenman, A. J., *Modern multivariate statistical techniques: Regression, classification, and manifold learning.* Springer texts in statistics. New York, London: Springer, 2008.

[13] Jolliffe, I. T., *Principal component analysis,* 2nd. Springer series in statistics. New York: Springer, 2002.

[14] Kecman, V., *Learning and soft computing: Support vector machines, neural networks, and fuzzy logic models.* Complex adaptive systems. Cambridge Mass: MIT Press, 2001.

[15] Haykin, S. S., *Neural networks and learning machines,* 3rd. New York: Prentice Hall, 2009.

[16] Priddy, K. L. and Keller, P. E., *Artificial neural networks: An introduction.* Tutorial texts in optical engineering TT 68. Bellingham Wash: SPIE Press, 2005.

[17] J Kranz, "Intelligent thermal comfort control", PhD thesis, Nelson Mandela Metropolitan University, 2011.